UNIVERSITY OF SOUTHAMPTON

FACULTY OF ENGINEERING, SCIENCE AND MATHEMATICS

School of Ocean and Earth Science

Trace Elements in Marine Biogenic Carbonates: Analysis and Application to Past Ocean Chemistry

by

Mervyn John Greaves

Thesis for the degree of Doctor of Philosophy

March 2008

UNIVERSITY OF SOUTHAMPTON

ABSTRACT

FACULTY OF ENGINEERING, SCIENCE AND MATHEMATICS

SCHOOL OF OCEAN AND EARTH SCIENCE

Doctor of Philosophy

TRACE ELEMENTS IN MARINE BIOGENIC CARBONATES: ANALYSIS AND APPLICATION TO PAST OCEAN CHEMISTRY

by Mervyn John Greaves

Trace elements in marine biogenic carbonates may be used as proxies for past ocean chemistry provided that there is an established relationship between the trace element proxy and a parameter of interest, this relationship is preserved within biogenic carbonate, and the trace element can be determined sufficiently accurately. Successful application of any trace element proxy requires both development of the analytical methodology to ensure accurate data with the necessary sensitivity, and an understanding of the relationship between proxy and seawater chemistry.

Herein I develop methods for the determination of Mg/Ca, Sr/Ca and Cd/Ca in planktonic foraminiferal calcite, using inductively coupled plasma optical emission spectrophotometry and isotope dilution thermal ionisation mass spectrometry, and propose a potential reference material for Mg/Ca in foraminiferal calcite. The developed techniques are applied to an investigation of the Mg/Ca temperature proxy over Chatham Rise in the Southwest Pacific Ocean and a calibration study of the partition coefficient, D_{Cd}, for cadmium incorporation into planktonic foraminifera.

Comparisons of planktonic foraminiferal Mg/Ca, shell weight and oxygen isotope records from sites north and south of the Subtropical Front on Chatham Rise, demonstrate the effects of hydrography, foraminiferal habitat and dissolution as controls on Mg/Ca. Determinations of Cd/Ca in seven species of planktonic foraminifera confirm that the dominant controls on Cd/Ca are foraminiferal habitat and hydrography, with only a minor influence of post depositional dissolution. The major uncertainty in determination of D_{Cd} from core top samples comes from uncertainty in estimation of the depth distribution and seasons of calcification of planktonic foraminifera.

CONTENTS

Figures page

Chapter 1

Chapter 2

Chapter 3

Chapter 4

Tables page

Chapter 6

DECLARATION OF AUTHORSHIP

I, **Mervyn John Greaves** declare that the thesis entitled

Trace Elements in Marine Biogenic Carbonates: Analysis and Application to Past Ocean Chemistry

and the work presented in the thesis are both my own, and have been generated by me as the result of my own original research. I confirm that:

- this work was done wholly or mainly while in candidature for a research degree at this University;
- where any part of this thesis has previously been submitted for a degree or any other qualification at this University or any other institution, this has been clearly stated;
- where I have consulted the published work of others, this is always clearly attributed;
- where I have quoted from the work of others, the source is always given. With the exception of such quotations, this thesis is entirely my own work;
- I have acknowledged all main sources of help;
- where the thesis is based on work done by myself jointly with others, I have made clear exactly what was done by others and what I have contributed myself;
- parts of this work have been published as:

Rickaby, R.E.M., M.J, Greaves, & H.Elderfield, Cd in planktonic and benthic foraminiferal shells determined by thermal ionisation mass spectrometry. *Geochim. Cosmochim. Acta* **64**, 1229-1236, 2000.

de Villiers, S., M. Greaves & H. Elderfield, An intensity ratio method for the accurate determination of Mg/Ca and Sr/Ca of marine carbonates by ICP-AES, *Geochem. Geophys. Geosyst.* **3**, 2001GC000169, 2002.

Barker, S., M. Greaves & H. Elderfield. A study of cleaning procedures used for foraminiferal Mg/Ca paleothermometry, *Geochem. Geophys. Geosyst.*, **4**, 9, 10.1029/2003GC000559, 2003.

Greaves, M., S. Barker, C. Daunt & H. Elderfield, Accuracy, standardisation and interlaboratory calibration standards for foraminiferal Mg/Ca thermometry, *Geochem. Geophys. Geosyst.,* **6,** Q02D13, doi:10.1029/2004GC000790, 2005.

Signed: ……..

Date:…….

Acknowledgements

I would like to thank my supervisors at Southampton, Peter Statham and Paul Wilson for all of their help and advice during the preparation of this thesis. Also, I wish to express my thanks to Eelco Rohling as chairman of the PhD advisory panel.

Harry Elderfield has supported me with help and advice during this project and for many years previously. Many friends provided helpful discussions both at the outset and in the progress of this work. In particular, Stephen Barker, Frank Bassinot, Ian Hall, Heather Johnstone, Nick McCave, Katharina Pahnke, Alex Pietrowski, Aradhna Tripati, Ros Rickaby, Jimin Yu and Rainer Zahn provided help at various stages in this project, gave stimulating discussions, or read drafts of chapters as writing progressed.

I am grateful for the support of all my current colleagues at Cambridge, Linda Booth, Caroline Daunt, Salima Souanef-Ureta, Patrizia Ferretti, Babette Hoogakker, Greta-Bjork Kristjansdottir, Luke Skinner, Jason Day, Hazel Chapman, Mike Bickle, Albert Galy, Caroline Dawber, David Thornalley and Adam Scrivner. Also to past colleagues, especially the many now at Southampton, who always expressed support and encouragement when we met socially or at conferences, including Pallavi Anand, Matthew Cooper, Brian Dickie, Chris German, Hilary and Paul Kennedy, Gary Klinkhammer, Carrie Lear, Rachael James, Rachel Mills, Martin Palmer and Martin Sinha.

Finally, thank you to Kathleen, Vanessa and Rosie for all the help, encouragement and patience while I was writing this thesis.

Abbreviations and acronyms

AABW	Antarctic Bottom Water
AAIW	Antarctic Intermediate Water
AAS	Atomic Absorption Spectrophotometry
ACC	Antarctic Circumpolar Current
AFZ	Azores Frontal Zone
amu	Atomic Mass Unit
APF	Antarctic Polar Front
APNAP	Actuomicropaleontology Paleoceanography North Atlantic Project
CCD	Charge Coupled Device
CDW	Circumpolar Deep Water
DWBC	Deep Western Boundary Current
GF-AAS	Graphite Furnace Atomic Absorption Spectrophotometry
ICPMS	Inductively Coupled Plasma Mass Spectrometry
ICP-OES	Inductively Coupled Plasma Optical Emission Spectrophotometry
ID-TIMS	Isotope Dilution - Thermal Ionisation Mass Spectrometry
ka	Age in kilo years
mcd	composite depth of ODP cores in metres
µg/g	Micro grams per gram
mmol/mol	Millimoles per Mole
n	Number of determinations
NAC	North Atlantic Current
ODP	Ocean Drilling Project
PCR	Polymerase Chain Reaction
PDB	Pee Dee Belemnite
PFA	Teflon perfluoroalkoxy
pg	picograms
PP	Polypropylene
ppb	Parts per Billion
ppm	Parts per Million
PS	Polystyrene
r.s.d.	Relative Standard Deviation

SAF	Subantarctic Front
SAW	Subantarctic Surface Water
s.d.	Standard Deviation
SF	Subarctic Front
SMOW	Standard Mean Ocean Water
SST	Sea Surface Temperature
STF	Subtropical Front
STW	Subtropical Surface Water
TIMS	Thermal Ionisation Mass Spectrometry
WOCE	World Ocean Circulation Experiment

Chapter 1

Introduction

1.1 Background

Studies of past ocean chemistry are important to the understanding of long term change in the ocean-climate system. An understanding of climate change in the geological past allows modern climate models to be tested and permits the refinement of predictions of future climate change. Proxies are therefore required to trace important variables such as temperature, salinity, nutrient distributions and ocean circulation in order to enable reconstruction of the past oceanic environment [see review of Henderson, 2002].

Biogenic carbonates in marine sediments hold records of both surface and deepwater oceanic chemistry contained within planktonic and benthic foraminifera. Continuous records spanning hundreds of thousands of years are available from drilled ocean cores, but with resolution usually limited to >1000 years by deep ocean sedimentation rates and bioturbation. In contrast, massive corals contain very high resolution, annual or seasonal, records of surface water chemistry but these rarely span time periods in excess of a few hundred years.

The oxygen isotopic compositions of foraminifera have been used since the work of Emiliani [1955] to trace combined past ocean temperatures and ice volume. However, reliable trace element records from foraminifera have only been available since the early 1980s; following the development of procedures for cleaning foraminifera shells of sedimentary contamination and trace element-rich coatings [Boyle, 1981; Boyle and Keigwin, 1985].

Trace elements in marine biogenic carbonates may be used as proxies for past ocean chemistry provided that a number of conditions are fulfilled: 1) There is an established relationship between the trace element proxy and a parameter of interest. 2) This

relationship is preserved within the biogenic carbonate after burial. 3) The trace element can be determined at the precision and accuracy necessary to produce reliable data. Thus, the relationship between Cd and P in the oceans has enabled Cd/Ca in foraminifera to be used as a proxy for deepwater phosphate and deep ocean circulation [Boyle, 1981, 1988, 1992]. The relationship between Ba and alkalinity permits the use of Ba/Ca ratios as a proxy for alkalinity [Lea and Boyle 1989, 1990; Lea 1993, 1995]. Zn/Ca ratios combined with Cd/Ca may be used as proxy for deep water carbonate ion concentration [Marchitto *et al.,* 2000], and U/Ca ratios in benthic foraminifera provide a record of past seawater uranium concentrations, a possible indicator of the extent of anoxic or low-oxygen bottom waters [Russell *et al.,* 1994]. The isotopic composition of boron, $\delta^{11}B$, [Palmer and Pearson, 2003] and B/Ca ratios in planktonic foraminifera [Yu *et al.,* 2007] may be used as proxies for surface seawater pH, while B/Ca ratios in benthic foraminifera have been shown to reflect deep water carbonate saturation state [Yu and Elderfield, 2007].

There are caveats and conditions associated with the use of all trace metal ratio proxies. Reconstruction of surface ocean phosphate utilisation from Cd/Ca in planktonic foraminiferal calcite is complicated by a perceived temperature dependence [Rickaby and Elderfield, 1999] and by non-linearity of the cadmium:phosphate relationship in surface waters [Elderfield and Rickaby, 2000]. Work by Rubin *et al*. [2003] demonstrates that Ba and alkalinity cycles in the ocean are not directly coupled and therefore the use of Ba/Ca as proxy for alkalinity must be less straightforward than previously thought. Correlation between U/Ca & Mg/Ca in planktonic foraminiferal calcite suggests a temperature component in the U/Ca signal which may be significantly larger than variations due to changes in the extent of anoxic or suboxic sediments, complicating the use of U/Ca ratios as an indicator of past seawater uranium [Russell *et al.,* 1996].

Tracers of nutrient distributions in past oceans provide information on changes in the transport and mixing of ocean waters and on processes controlling oceanic carbon dioxide concentrations. The combination of $\delta^{13}C$ and Cd/Ca has been particularly effective [Boyle, 1992]. Both proxies are recorded in the shells of planktonic and benthic foraminifera revealing chemical contrasts between the surface and deep oceans,

yet differences in behaviour (in particular the effect of air-sea exchange on $\delta^{13}C$) lead to discrepancies in their palaeoceanographic distributions [e.g., Boyle, 1988].

The observation that foraminiferal shell weight decreases on the seafloor by dissolution in proportion to the degree of undersaturation with respect to $CaCO_3$ [Lohmann; 1995], allows the mass of individual planktonic foraminifera within a narrow size fraction to be used as a proxy for carbonate ion concentration ($[CO_3^{2-}]$) in the deep ocean. Foraminiferal shell weight possesses none of the analytical difficulties of trace metal determinations and has the major advantage of simplicity of use. Thus, planktonic foraminiferal shell weight has been used as an indicator of past bottom water $[CO_3^{2-}]$ [Broecker and Clark; 2001a, 2001b]. However, the calcification process in marine calcifying organisms is influenced by seawater $[CO_3^{2-}]$, as demonstrated in laboratory culturing experiments. These show shell weight variation as a consequence of $[CO_3^{2-}]$ control [Spero *et al*., 1997, Bijma *et al*., 1999]. Using several species of planktonic foraminifera taken from North Atlantic core tops, Barker and Elderfield [2002] demonstrated initial shell weight variation with surface water $[CO_3^{2-}]$. Barker and Elderfield [2002] also showed initial shell weight variation on glacial to interglacial timescales. Glacial aged shells were shown to be heavier than interglacial shells. This result was attributed to higher surface ocean $[CO_3^{2-}]$ in glacial times in line with lower atmospheric CO_2. Therefore, planktonic foraminiferal shell weight reflects a composite signal from the effect of seafloor dissolution that is a function of bottom water $[CO_3^{2-}]$, superimposed on initial shell weight variability, a consequence of variations in surface ocean $[CO_3^{2-}]$.

Reliable estimates of palaeotemperature are fundamental to understanding the ocean-climate system in the geological past. Faunal abundances and the oxygen isotopic composition ($\delta^{18}O$) of foraminiferal calcite have been used extensively to reconstruct past ocean temperatures. During recent years Mg/Ca in foraminiferal calcite has been developed as a palaeotracer of ocean temperature [Nurnberg *et al*., 1996; Hastings *et al*., 1998; Lea *et al*., 1999, 2000; Elderfield and Ganssen, 2000; Mashiotta *et al*., 1999; Rosenthal *et al*., 2000; Dekens *et al*., 2002; Barker *et al*., 2005]. Magnesium/calcium ratios in foraminiferal calcite show a temperature dependence due to the partitioning of Mg during calcification and can be used, where calibrations are available, to calculate

the calcification temperatures of foraminifera. As an independent palaeotemperature proxy, Mg/Ca ratios provide important additional information to $\delta^{18}O$ in foraminiferal calcite. The latter reflects both the water temperature and seawater $\delta^{18}O$, itself an indicator of global ice-volume and salinity. One of the potential advantages of the method is that paired measurement of Mg/Ca and $\delta^{18}O$ on the same foraminiferal samples permits $\delta^{18}O_{seawater}$ to be calculated from $\delta^{18}O_{carbonate}$ using the palaeotemperature equation [Mashiotta *et al.,* 1999, Lear *et al.,* 2000].

Mg/Ca follows an exponential relationship with temperature, as predicted for thermodynamic control [Mucci, 1987; Oomori et al., 1987], but with sensitivity approximately 3 times greater than would be expected from equilibrium thermodynamics [Lea *et al*., 1999]. Temperature calibrations of the form:

$$Mg/Ca = A \exp (B \times T)$$

where T is temperature in ^{o}C, have been produced for planktonic foraminifera from culture [Nurnberg *et al.,* 1996; Lea et al., 1999; Mashiotta et al., 1999], core tops [Elderfield and Ganssen, 2000; Lea et al., 2000; Dekens et al., 2002] and sediment traps [Anand et al., 2003]. There is general agreement that the exponential constant $B \approx 0.1$, equivalent to a ~10 % change in Mg/Ca per ^{o}C, with values for the pre-exponent A (the Mg/Ca intercept at $T = 0^{o}C$) varying between species [Anand *et al*., 2003].

Temperature calibration of benthic foraminiferal Mg/Ca is less clear, with calibrations indicating a much larger degree of inter-species variability than for planktonic species [Rosenthal *et al*., 1997b; Lear *et al*., 2002; Martin *et al*., 2002; Skinner *et al*., 2003] and a significant carbonate ion influence on Mg/Ca at cold deep sea temperatures [Elderfield *et al*., 2006].

Post-depositional dissolution affects foraminiferal Mg/Ca because partial dissolution of high Mg calcite produces lower Mg/Ca ratios [Brown and Elderfield, 1996]. Dissolution is depth-dependent and a function of the bottom water carbonate ion concentration [Rosenthal *et al*., 2000; Dekens *et al*., 2002; Regenberg *et al*., 2006] reducing Mg/Ca at the same time as decreasing foraminiferal shell weight. Hence, a combination of foraminiferal shell weight and Mg/Ca ratios enabled Rosenthal and

Lohmann [2002] to produce dissolution-corrected Mg/Ca calibrations for the planktonic species, *Globigerinoides ruber* and *Globigerinoides sacculifer*.

Sr/Ca in foraminifera has been proposed as a tracer of seawater chemistry but with evidence of only a minor palaeotemperature signal [Lea *et al.,* 1999; Martin *et al.,* 1999; Stoll *et al.,* 1999; Elderfield *et al.,* 2000, 2002; Lear *et al.,* 2003; Mortyn *et al.,* 2005]. In contrast, Sr/Ca in coral aragonite shows a strong correlation with temperature [Beck *et al.,* 1992; de Villiers *et al.,* 1994, 1995; McCulloch *et al.,* 1994; Shen *et al.,* 1996]. Mitsuguchi, *et al.*, [1996] studied Mg/Ca thermometry in coral skeletons and showed a variation of Mg/Ca ratio with temperature approximately four times greater than that of Sr/Ca, but in the opposite direction; increasing Mg/Ca with temperature being accompanied by a corresponding decrease in Sr/Ca.

The strontium isotopic composition ($^{87}Sr/^{86}Sr$) of marine biogenic carbonates is an important tracer of long term variations in ocean chemistry [Palmer and Elderfield, 1985]. As a radiogenic tracer with a long half life ($t_{1/2} = 5 \times 10^{11}$ years for decay of $^{87}Rb \rightarrow {}^{86}Sr + \beta^-$) the strontium isotopic composition of seawater records inputs to the oceans, not outputs and, because of the long oceanic residence time of Sr (~4 million years) compared to the mixing time of the oceans (~1000 years), oceanic $^{87}Sr/^{86}Sr$ is uniform at any one time [Hess *et at.,* 1986]. The seawater Sr isotope record reflects long term changes in input flux resulting from mountain uplift and the weathering of limestones and silicate rocks [Hodell *et al.,* 1989, 1990]. Strontium isotope stratigraphy was reviewed by Hodell [1994], who discussed the variations in the $^{87}Sr/^{86}Sr$ of seawater during the Cenozoic and illustrated the finer levels of structure in the seawater curve over progressively shorter timescales ranging from 500 to 0.5 million years. However, measurable changes in seawater $^{87}Sr/^{86}Sr$ on glacial/interglacial time scales are unlikely and would require massive increases in weathering fluxes. Henderson *et al.* [1994] constrained the glacial/interglacial variation in $^{87}Sr/^{86}Sr$ to a maximum amplitude of 6 to 9 ppm which, nevertheless, would correspond to a ~30% change in the Sr riverine flux. High precision $^{87}Sr/^{86}Sr$ measurements in corals have proved valuable for investigation of atoll chronology and sea level history associated with atoll formation [Ohde *et al.,* 2002].

The successful application of any trace element proxy requires development both of the analytical methodology, to ensure accurate data with the necessary sensitivity and resolution, and knowledge of the relationship between the proxy and parameter of interest in seawater. Understanding how trace element proxies are incorporated into living biogenic carbonates is equally important. Depth and temperature habitats, together with the season when organisms calcify and incorporate trace elements, or other proxies, all affect the signal recorded and need to be understood to permit reliable interpretation of past ocean chemistry.

1.2 Trace elements in marine biogenic carbonates.

The trace element composition of marine biogenic carbonates is illustrated in Figure 1.1 showing the range of trace metal concentrations found in foraminifera. Foraminiferal calcite is composed of extremely pure (~99%) $CaCO_3$ with four minor elements Na, Mg, Sr and F comprising most of the remaining ~1%, these elements being present at abundances greater than 10^{-3} mol/mol Ca [Lea, 1999]. The remaining trace metals are present at extremely low abundances between ~10^{-4} to 10^{-9} mol/mol Ca (Figure 1.1). In comparison, coral aragonite contains Mg at concentrations similar to those found in foraminiferal calcite but contains almost an order of magnitude greater Sr, ~ 0.8% by weight. Other trace elements are present in aragonitic coral at similar or lower abundances than in foraminiferal calcite.

The analytical issues involved in the determination of trace metals in biogenic carbonates are clearly demonstrated by the relative abundances shown in Figure 1.1. Trace metals must be determined in the presence of orders of magnitude greater Ca, with potential contamination from high concentrations of these elements within sediments and in ferro-manganese coatings on foraminifera tests. Any method for the determination of trace metals or radiogenic isotopes must have the precision and accuracy appropriate to the range of concentrations or to the isotopic range involved. For example, Mg/Ca ratios in foraminifera vary with temperature by typically 9 % per ºC [Anand *et al.,* 2003] and values within a suite of samples may range over a factor of ~2. Therefore, in many cases analytical methods precise and accurate to ~ 2 % are appropriate for Mg/Ca

determinations. In contrast, Sr/Ca in aragonitic coral varies by only ~ 0.7 % per ºC and covers a total range of ~ 10 % [e.g. Beck *et al.*, 1992]. Consequently, much higher precision, better than 0.2 %, is required to produce meaningful results. Determinations of the extremely low concentrations of trace metals such as Ba, Cd & Zn in biogenic carbonates are complicated by their low abundances and much higher concentrations in potential contaminants. Trace metal clean procedures, combined with sensitive detection methods, are essential for successful determinations. In addition, trace element determinations present particular analytical problems which are often specific to individual trace metals.

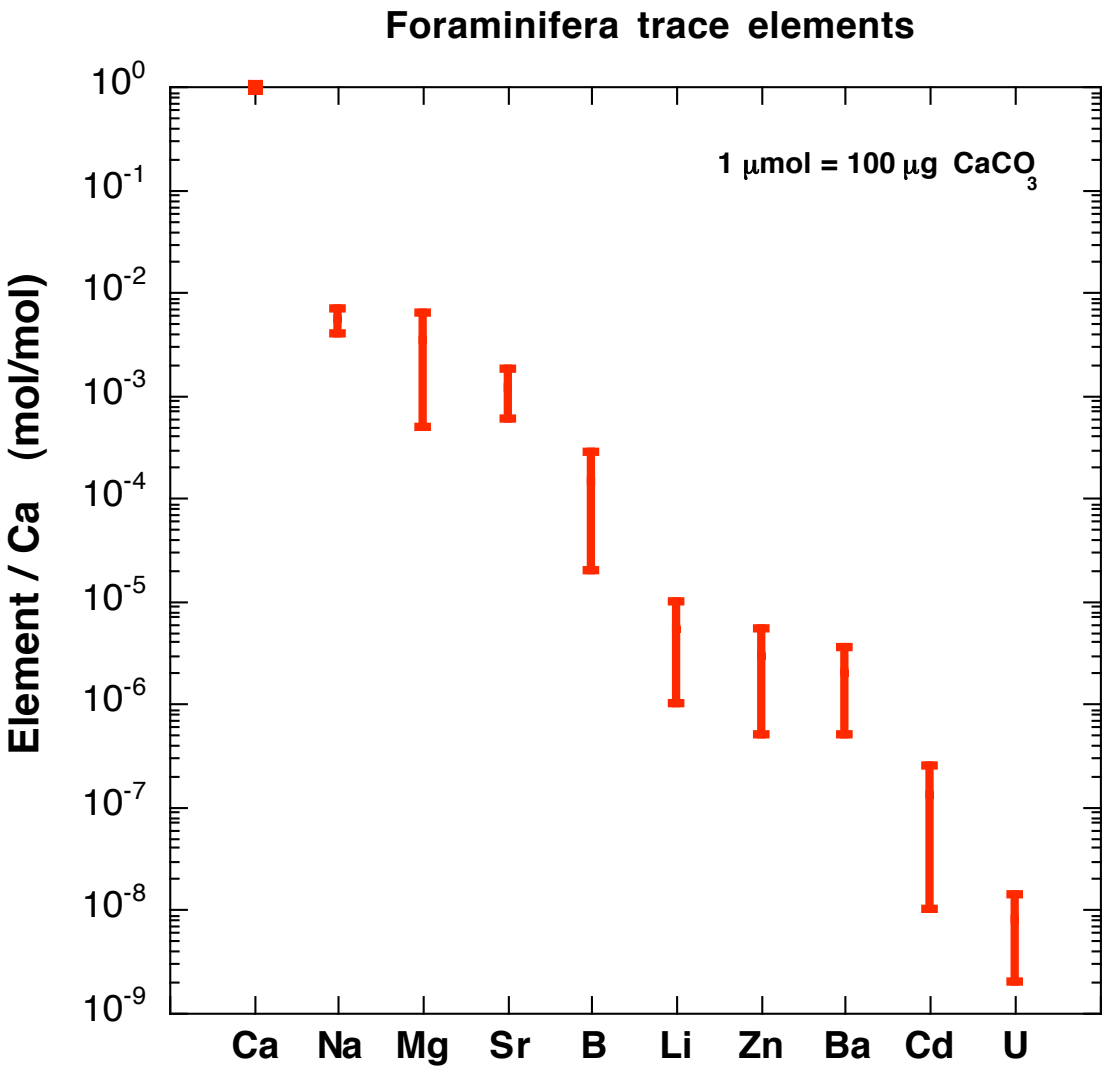

Figure 1.1 Trace elements in foraminiferal calcite (100 µg $CaCO_3$ = 1 µmol)

The application of proxies to studies of past ocean chemistry requires both understanding of the systematics and limitations of the proxies, and development of appropriate analytical methodology to produce data with the accuracy, sensitivity and resolution necessary to permit reliable interpretation. The aims of the research described in this thesis are both to develop methods for the determination of trace elements in marine biogenic carbonates, and to apply these methods to specific palaeoceanographic problems.

1.3 Objectives and outline of the dissertation

This dissertation is composed of seven chapters spanning work on both method development and palaeoceanographic interpretation. The main body of the dissertation is presented in Chapters 2 to 6, as summarised in the concluding Chapter 7. The objectives of this dissertation are to develop techniques of appropriate sensitivity and accuracy for the determination of trace metal proxies in marine biogenic carbonates (Chapters 2, 3 and 5), and to apply the developed methods to specific palaeoceanographic problems (Chapters 4 and 6). These objectives are detailed as follows:-

- Chapter 2: To present an inductively coupled plasma optical emission spectrophotometry (ICP-OES) method for the determination of Mg/Ca and Sr/Ca ratios in foraminiferal calcite, by application of an intensity ratio technique to overcome matrix effects. To develop and apply cleaning and analytical procedures for Mg/Ca & Sr/Ca determinations in foraminiferal calcite. To assess the effect of the analytical blank on Mg/Ca and Sr/Ca ratios and the implications for Mg/Ca temperature calculations.

- Chapter 3: To document accurately prepared standard solutions for verification of the method developed in Chapter 2, over a range of Mg/Ca and Sr/Ca ratios. To investigate solid carbonate materials as potential standards for interlaboratory calibration.

- Chapter 4: To report a downcore Mg/Ca and Sr/Ca record for the last 440 kyr from ODP Site 1123, on Chatham Rise in the Southwest Pacific, for the planktonic foraminifera species *Globigerina bulloides*. To assess the implications of down-core variations in Mg/Ca from this record for glacial and interglacial seawater temperatures. To interpret the planktonic Mg/Ca and $\delta^{18}O$ records relative to the hydrography of the water masses influencing the site. To investigate the *G. bulloides* shell weight and $\delta^{18}O$ records as a composite signal from dissolution-related weight loss superimposed on initial shell weight variability.

- Chapter 5: To outline a recently developed isotope dilution - thermal ionisation mass spectrometry (ID-TIMS) method for the determination of Cd in foraminiferal calcite. To optimise chemical and mass spectrometric procedures to produce reliable measurements of Cd/Ca ratios in planktonic foraminifera. This chapter describes method development work performed in collaboration with Rosalind Rickaby, published in Rickaby et al. [2000], and subsequent developments to this method which are applied in Chapter 6.

- Chapter 6: To investigate the use of planktonic foraminiferal Cd/Ca as a palaeoceanographic tracer for surface water nutrients. To examine processes influencing the incorporation of cadmium into planktonic foraminiferal calcite, with reference to foraminiferal habitat, hydrography and the effects of dissolution, as controls on Cd/Ca of planktonic foraminifera. To determine the partition coefficient D_{Cd} for the incorporation of cadmium into a number of species of planktonic foraminifera. To assess the temperature dependence of D_{Cd} using multiple species of planktonic foraminifera taken from a North Atlantic core-top transect.

Chapter 2

Instrumental methods and analytical procedures for the determination of Mg/Ca and Sr/Ca ratios in foraminiferal calcite

2.1 Introduction

The applications of Mg/Ca and Sr/Ca ratios as palaeoceanographic proxies in biogenic carbonates have advanced significantly during recent years. The temperature dependence of foraminiferal Mg/Ca led to its development as an ocean temperature proxy [Nurnberg *et al*., 1996; Hastings *et al*., 1998; Lea *et al*., 1999, 2000; Elderfield and Ganssen, 2000; Mashiotta *et al*., 1999; Rosenthal *et al*., 2000; Dekens *et al*., 2002; Barker *et al*., 2005]. Measurements of foraminiferal Sr/Ca have been used to investigate the Sr/Ca ratio of seawater and to examine the relationship between inputs to the oceans from rivers, hydrothermal processes, and from carbonate dissolution and diagenesis [Graham *et al*., 1982; Martin *et al*., 1999; Stoll *et al*., 1999; Elderfield *et al*., 2000; Shen *et al*., 2001].

Development of reliable analytical methodology for their determination is prerequisite to the interpretation of Mg/Ca and Sr/Ca ratio measurements in biogenic carbonates. The variation with temperature of Mg/Ca in foraminiferal calcite, increasing exponentially by ~ 9 % per ºC [Anand *et al*., 2003], from < 0.5 mmol/mol to > 5.0 mmol/mol over the temperature range 0 to 30 ºC, implies that a measurement precision and accuracy of ~ 2 % is adequate for temperature estimation. However, a consequence of the exponential relationship is that, in order to ensure the accuracy of calculated temperatures, the relative measurement precision, expressed as a percentage of the measured ratio, must be maintained across the range of Mg/Ca ratios from low to high values. This is contrary to the usual situation in analytical methods, where relative

measurement precision becomes worse with decreasing values [Horwitz; 1982], and has important implications for temperature calculations from the low Mg/Ca ratios found in benthic and planktonic foraminifera occuring in cold waters.

Sr/Ca ratios in foraminifera typically are between 1.2 mmol/mol and 1.6 mmol/mol, varying downcore by < 8 % over a glacial-interglacial cycle [Martin *et al.,* 1999; Elderfield *et al.,* 2000; Shen *et al.,* 2001]. Aragonitic coral contains higher Sr/Ca, in the range 8 to 10 mmol/mol, but with a temperature variation of only ~ 0.7 % per ^{o}C [Beck *et al.,* 1992]. Hence, high precision measurements are necessary to produce useful Sr/Ca data.

The quality of results obtained from any analytical determination depends both on the precision and accuracy of the instrumental method, and on the analytical procedures employed. An instrumental technique may be the limiting factor in the accuracy of a determination but, more often, the accuracy is governed by the sampling and chemical procedures and by the analytical blank introduced during these procedures. It is therefore essential to assess data quality over a complete analytical method and to minimise errors as appropriate for each stage.

Chapter 2 is divided into sections reflecting the development of instrumental methods and analytical procedures for the accurate determination of Mg/Ca and Sr/Ca ratios in foraminiferal calcite. Section 2.2 describes instrumental method development by inductively coupled plasma optical emission spectrophotometry (ICP-OES). The cleaning procedures required for Mg/Ca and Sr/Ca determinations in foraminifera are discussed in section 2.3, with particular relevance to the samples analysed in Chapter 4. Section 2.4 covers factors affecting data quality and the efficiency of the cleaning procedure. The effect of the analytical blank on Mg/Ca and Sr/Ca ratios and implications for temperature determinations are assessed in section 2.5.

2.2 Determination of Mg/Ca and Sr/Ca in foraminiferal calcite by simultaneous ICP-OES

This section summarises my contribution to the development work for the intensity ratio calibration method published by de Villiers, Greaves and Elderfield [2002]. The developed method is compared with other ICP-OES procedures for the determination of Mg/Ca and Sr/Ca ratios in foraminiferal calcite [Green *et al*. 2003; Wara *et al*. 2003].

Instrumental methods used for the determination of Mg/Ca and Sr/Ca ratios in biogenic carbonates include flame atomic absorption spectrophotometry (AAS) [Boyle, 1981; Brown and Elderfield, 1996; Russell, 1996], graphite furnace atomic absorption spectrophotometry (GF-AAS) [Boyle, 1981; Brown and Elderfield, 1996], isotope dilution - thermal ionisation mass spectrometry (ID-TIMS) for Sr/Ca determination in corals [Beck *et al*., 1992; McCulloch *et* al., 1994; de Villiers *et* al., 1994, 1995, Swart *et al*., 2002] and in foraminifera [Elderfield *et al*., 1996], and inductively coupled plasma mass spectrometry (ICPMS) [Lea & Martin, 1996; Rosenthal *et al*., 1999].

Inductively coupled plasma optical emission spectrophotometry (ICP-OES), alternatively named inductively coupled plasma atomic emission spectrophotometry (ICP-AES), is well suited to the determination of Mg/Ca and Sr/Ca ratios in biogenic carbonates. Mg and Sr are present as minor constituents in foraminiferal calcite, 2 to 3 orders of magnitude less abundant than Ca [Chapter 1, Figure 1.1]. Their abundances relative to Ca give concentrations in solution, from an appropriate initial weight of calcite, comfortably within the working range of ICP-OES. Foraminifera samples of 0.1 – 0.3 mg typically produce solution concentrations in the range; Ca 50 – 200 ppm, Mg 0.05 – 0.15 ppm and Sr 0.1 – 0.2 ppm when dissolved in 250 – 500 µl after cleaning.

ICP-OES instruments may be configured to view the plasma either axially or radially, axial detection giving greater sensitivity although radial view is less subject to matrix effects within the plasma [Brenner & Zander, 2000]. The major advantage of ICP-OES compared to other techniques is its ability to measure all analytes simultaneously. In addition to the obvious benefit of speed of analysis, simultaneous detection cancels out time dependent effects within the instrument, particularly those caused by fluctuations

in the plasma, producing excellent short term precisions for element ratio determinations. For example, Schrag [1999] obtained better than 0.2% precision (relative standard deviation) for Sr/Ca determinations over a range of Ca concentrations.

2.2.1 Instrument and operating conditions

A Varian Vista, axial configuration, echelle type spectrophotometer was used for this work. The instrument contains a charged coupled device (CCD) detector with 70,000 pixels arranged to match the two dimensional image from the echelle optics, giving simultaneous coverage of wavelengths in the range 167 to 785 nm. The CCD detector has anti-blooming protection on every pixel, so that if an intense signal saturates a pixel, excess electrons drain into a gutter rather than into nearby pixels, allowing simultaneous measurement of trace elements in the presence of concentrated analytes.

The sample introduction system for carbonate analyses comprised a low flow glass concentric nebulizer (Glass Expansion, Micromist) with a low volume glass cyclonic spraychamber (Glass Expansion, Cinnabar) and a peristaltic pump to regulate sample uptake. Sample volumes in the range 250 – 500 µl required an analysis time of approximately 2 minutes. Typical operating conditions and the range of relevant parameters are shown in Table 2.1.

Parameter	**Details**	**Setting**
RF Power:		1.2 - 1.3 kW
Plasma gas flow:		15 L/min
Auxiliary gas flow:		0.75 or 1.5 L/min
Nebuliser gas flow:		0.7 - 1.1 L/min
Nebuliser:	Glass Expansion, Micromist	0.2 - 0.4 ml/min uptake
Spraychamber:	Glass expansion, Cinnabar Cyclonic	
Pump tubing:	orange/green	0.38 mm I.D
Pump rate:	~0.17 mL/min	15 r.p.m.
Measurement:	Replicates, integration time	6, 5 s.

Table 2.1 Instrument operating conditions

2.2.2 Emission lines, sensitivities and matrix effects

Wavelengths of emission lines and their relative sensitivities are listed in Table 2.2. In addition to data for Ca, Mg and Sr, Table 2.2 shows emission lines for elements monitored to check the efficiency of the cleaning procedure (see section 2.4). The most sensitive Ca lines give signals too intense for Ca determination at ppm levels by Axial ICP-OES but are included in Table 2.2 as potential interferences on other element lines. Measured intensities for a particular element concentration and sample uptake are a function of the individual excitation energies, as expressed by the relative sensitivities in Table 2.2, the RF generator voltage and hence temperature of the plasma, and the nebuliser gas flow.

Argon gas flow rates are an important control on line intensities, the nebuliser gas flow being the most critical. The effect of varying the nebuliser gas flow differs between emission lines but, in general, lower flow gives higher signal intensity while higher flow improves the signal to background ratio. Compromise conditions must be sought for high precision element ratio measurements. The ionic/atomic line intensity ratio of the Mg II 280.270 nm/Mg I 285.213 nm lines has been used as a measure of plasma robustness when optimising operating conditions [Mermet; 1991] with higher ratios indicating more robust plasmas. Higher ratios are obtained at higher RF power and lower nebulizer flow. However, this parameter is influenced by other factors, including individual instrument characteristics and the suppression of ionic line intensities by high concentrations of easily ionisable elements such as Ca and Na [Brenner and Zander; 2000].

High concentrations of calcium cause high background signals on other element lines, particularly evident for Al at 396.152 nm (Table 2.2). Calcium also shows a self-matrix effect which has been postulated as a dominant cause of line curvature in calibration graphs [Ramsey *et al.,* 1987]; decreasing sensitivity with increasing calcium concentration is observed for both calcium and trace element lines. The magnitude depends on the excitation energy of individual lines, those with the highest excitation energy being most affected and hence showing the greatest calibration curvature. This observation implies that the use of lower sensitivity lines will be preferable when determining element/Ca ratios. The large number of emission lines for Ca together with

its high concentration give a wide selection of potentially useful lines (Table 2.2), but lower concentrations allow a choice of fewer lines for Mg and Sr determinations.

Element	Type[a]	Wavelength (nm)	Sensitivity[b]	Order
Ca	II	396.847	3862750	1
Ca	II	393.366	1930472	2
Ca	I	422.673	128727	3
Ca	II	317.933	29986	4
Ca	II	315.887	14590	5
Ca	II	373.690	6125	6
Ca	II	183.944	1629	9
Ca	II	211.276	580	10
Mg	II	279.553	1290270	1
Mg	II	280.270	464735	2
Mg	I	285.213	82150	3
Sr	II	407.771	3869250	1
Sr	II	421.552	2481390	2
Sr	II	216.596	11165	3
Al	II	167.019	910	1
Al	I	396.152	32702	2
Fe	II	238.204	41015	1
K	I	766.491	22436	1
Mn	II	257.610	222170	1
Na	I	589.592	61215	1
Si	I	251.611	49839	1
Ti	II	336.122	153944	1

a) Type I atomic, Type II ionic emission lines.
b) Relative sensitivities of the lines - typical intensity expected from 5 ppm of element in solution (Data fromVarian instrument setup file)

Table 2.2 Emission lines and relative sensitivities

The effect of the Ca matrix on sensitivities of Ca, Mg and Sr emission lines was investigated using dilutions of a mixed standard solution containing Mg/Ca = 5.13 mmol/mol, Sr/Ca = 2.09 mmol/mol (preparation details are given in Chapter 3) over a

Ca concentration range from 10 – 220 ppm. Relative sensitivities, expressed as the background corrected signal intensity normalised to the intensity obtained at 60 ppm Ca are shown in Figure 2.1. There is clear evidence of calcium self-absorption with the most sensitive Ca 422.673 nm line showing a ~20% drop in sensitivity over the 10 – 220 ppm concentration range, compared to ~ 5% decrease in sensitivity for the Ca 211.276 nm line and ~7% and ~8% respectively for Ca 315.887 and 317.933 nm lines. Similarly for magnesium, the least sensitive Mg 285.213 nm line showed the least matrix effect whereas the 279.553 nm and 280.270 nm lines each showed ~10% decrease in sensitivity. All three Sr lines showed a noticeable matrix effect with ~ 6 % decrease in sensitivity for the 216.596 nm line compared to ~10% for the more sensitive lines. For each element Type II ion lines behaved in a similar manner whereas Type I atomic lines showed different trends, suggesting that the matrix effect is different between the two line types. However, the largest decrease in sensitivity was observed for the Type I Ca 422.673 nm line and the smallest for the Type I Mg 285.213 nm line, implying a complicated relationship between line type, sensitivity and matrix.

The Ca 315.887 nm line was chosen for element ratio calculations, as a compromise between sensitivity and matrix effect, the Ca 211.276 line would be an alternative for all except the smallest samples. The Mg 285.213 nm line was selected for Mg/Ca calculations in foraminiferal calcite and the Sr 421.552 nm line for Sr/Ca, the Sr 216.596 nm line being available for the higher Sr concentrations in corals.

The consequence of the Ca matrix effect when calculating element/Ca ratios depends on the curvature of individual concentration calibrations and on how closely sample concentrations match those of calibration standards. Sample and calibration solutions will never match exactly and matrix effects within multielement calibration standards may be different from those in sample solutions [Ramsey and Coles; 1992]. The use of internal standards added to both calibration and sample solutions has been proposed, mainly as a method of correcting for signal instability but could also be applied to matrix effects [Walsh; 1992]. However, no internal standard can exactly match the behaviour of other analytes in the plasma and normalisation of signal intensities to an internal standard would cancel when element ratios are calculated. Matrix effects may be minimised by sample dilution, a technique used by Green *et al*. [2003] for Mg/Ca

and Sr/Ca determinations in foraminiferal calcite. Here, an alternative technique is employed to determine Mg/Ca and Sr/Ca ratios directly from signal intensity ratios.

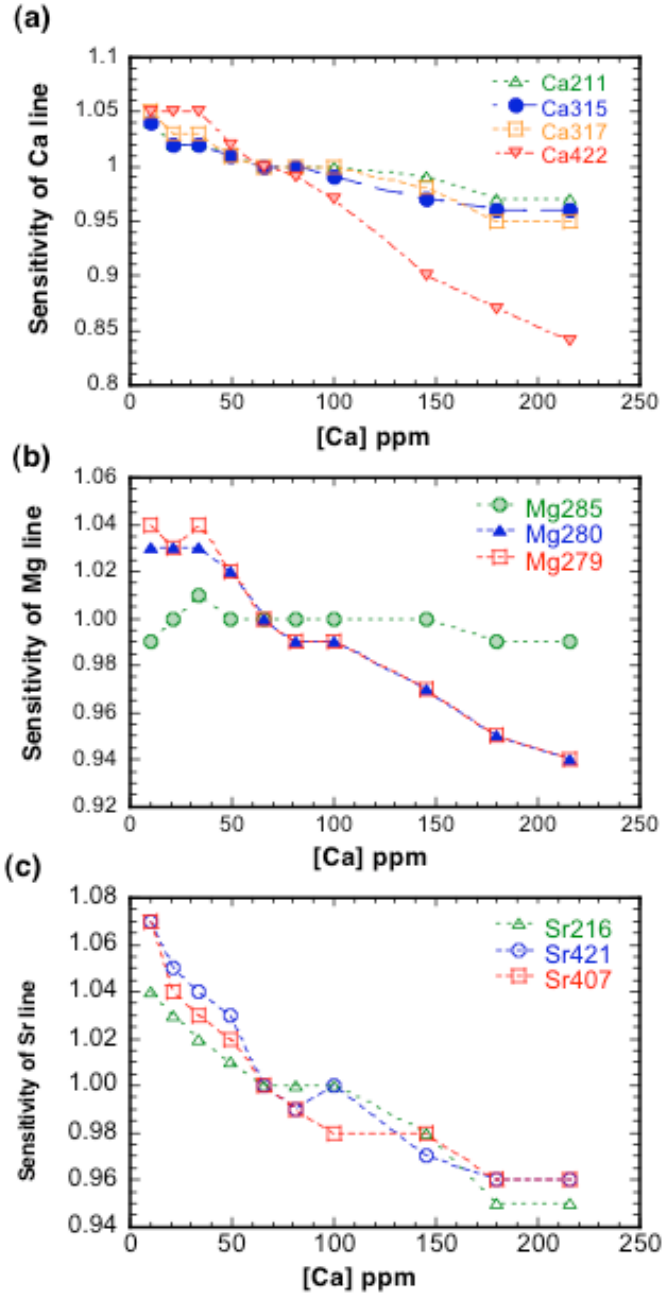

Figure 2.1 Relative sensitivities of emission lines as a function of Ca concentration, for solutions with Mg/Ca = 5.13 mmol/mol and Sr/Ca = 2.09 mmol/mol. (a) Sensitivity of Ca lines, normalized to the value at 60 ppm (µg/g). Absolute sensitivities in order: Ca211 < Ca315 < Ca317 < Ca422. (b) Sensitivity of Mg lines (normalized to the value at 60 ppm Ca). Absolute sensitivity increases in the order:Mg285 < Mg280 < Mg279. (c) Sensitivity of Sr lines (normalized to the value at 60 ppm Ca). Absolute sensitivity increases in the order: Sr216 < Sr421 < Sr407. (reproduced from de Villiers *et al*. 2002)

2.2.3 Intensity ratio calibration

The calculation of element/Ca ratios from individual concentration measurements is necessary when elements are determined separately, but where a multielement instrumental technique is employed it is possible to determine ratios directly from signal intensities, avoiding errors introduced during concentration calibrations. Simultaneous ratio determinations, by definition include an internal standard, Ca, the major element to which others are normalised, making the addition of separate internal standards redundant if Ca concentrations are similar. Thus, instead of conventional concentration calibrations where standards with constant Mg/Ca and Sr/Ca ratios are used for calibration over a range of concentrations, a suite of standards were prepared containing a range of Mg/Ca and Sr/Ca ratios. Details of the preparation of these standards are given Chapter 3. Standards and samples were diluted to similar Ca concentrations; a simple and effective means of matrix matching when the composition is dominated by a single element, as in the case of foraminiferal calcite where Ca represents ~99% of the matrix.

Calibration involves the regression of intensity ratios for the selected lines, in this case Mg285/Ca315 and Sr421/Ca315, against the Mg/Ca and Sr/Ca mole ratios of the standard solutions to produce linear calibration graphs at a constant Ca concentration (Figure 2.2). This procedure overcomes both the Ca matrix effect and other problems associated with using traditional concentration standards. Element ratios remain constant over time, unless contamination occurs; thus errors arising from the evaporation of concentration standards are eliminated and, because the element ratios of the samples are calculated directly, there is no propagation of the errors associated with individual concentration calibrations. Additionally, accurately prepared element ratio standards minimise errors in regression lines where procedures assume that all the errors are in the y-values (intensity ratios) and the x-values (standards) are error free [Miller and Miller, 1993].

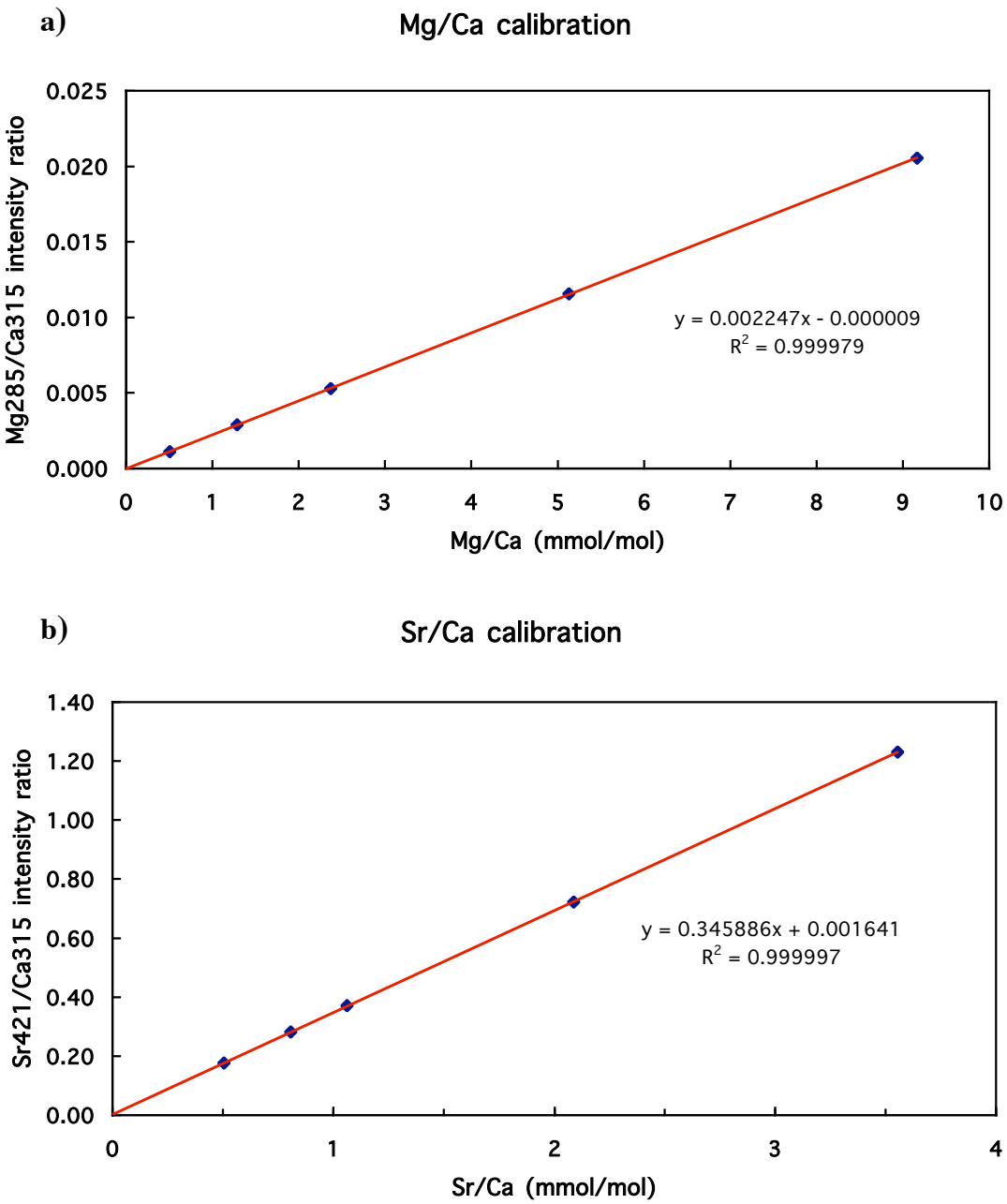

Figure 2.2 Intensity ratio calibrations for standard solutions with [Ca] = 60 µg/g a) Mg/Ca, b) Sr/Ca

It was shown by de Villiers *et al*. [2002] that the slopes of intensity ratio calibration graphs varied significantly with Ca concentration, by ~4% for Mg/Ca and ~2% for Sr/Ca over the range 20 – 100 ppm Ca. This resulted in the need to constrain [Ca] within a narrow working range, between approximately 45 and 70 ppm when using a calibration at 60 ppm Ca. In comparison, Wara *et al*. [2003], using a Perkin-Elmer Optima 4300 DV ICP-OES with a radially viewed plasma, found no significant differences between slopes of Sr/Ca regression lines, and only a ~1.2% difference between slopes of Mg/Ca regression lines, over a working range of ~0.6 – 2.4 mM Ca

(20 – 100 ppm). This may partly reflect the different instruments used, their different plasma characteristics and the effect of radial compared to axial view.

Subsequently, it was found when using the Varian Vista Axial ICP-OES that the nebuliser and gas flow have a strong control on the slopes of intensity ratio regression lines. De Villiers *et al*. [2002] used a 0.4 ml/min nominal sample consumption nebuliser fed through orange/green pump tubing (0.38 mm ID) producing an actual sample consumption of ~ 170 µl/min., and tuned the instrument to obtain maximum Ca and Mg signal intensity at a nebuliser gas flow of 0.65 l/min. This nebuliser was later replaced with a 0.2 ml/min nominal nebuliser, fed through the same internal diameter pump tubing at ~ 170 µl/min sample consumption. On tuning the instrument a higher nebuliser gas flow was selected. This gave reduced signal intensities but at the same time improved the signal to background ratio; i.e. proportionately greater reductions occured in background intensity than in signal intensity. The reduction in signal intensity varied between emission lines but the intensity of the Ca 315.887 nm line decreased more than intensities of the Mg 285.213 nm and Sr 421.552 nm lines. The result was both an increase in the slopes of intensity ratio calibration graphs and less variation between the slopes at different Ca concentrations. Using a nebuliser gas flow up to 1.05 l/min, adjusted to suit the individual nebuliser, gave an increase in slope of intensity ratio calibration graphs by factors of 2.0 - 2.5 for Mg/Ca and 2.5 - 3.0 for Sr/Ca. The higher nebuliser gas flow reduced the differences between slopes of Mg/Ca calibration graphs to <0.5% over a Ca concentration range of 60 – 100 ppm and ~ 1.2% over 30 – 100 ppm Ca, comparable to those found by Wara *et al*. [2003]. Differences between the slopes of Sr/Ca calibrations remained ~2 % over the 30 – 100 ppm Ca concentration range.

2.2.4 Short term and long term instrumental precision

Precision may be assessed as repeatability of measured values for a single solution during an analytical run and also, on longer timescales, as reproducibility between analytical runs [IUPAC, 1998]. Repeatability of Mg/Ca and Sr/Ca determinations better than 0.5% (r.s.d), determinated by replicate analyses of a standard solution during a run, are routinely achieved by simultaneous ICP-OES [Schrag, 1999; de Villiers *et al*., 2002; Green *et al*., 2003; Wara *et al*., 2003].

Within run and between run Mg/Ca and Sr/Ca measurement precisions were determined by repeat analyses of a consistency standard (Solution Q), prepared by dilution of calibration standard CL 1 (see Chapter 3) to 60 μg/g Ca. This solution (Mg/Ca = 5.130 mmol/mol, Sr/Ca = 2.088 mmol/mol) is run routinely approximately once every 5 samples during every analytical run. The number of replicates varies according to the length of run with an average of 15 on a typical day (min 3, max 44). During the six year period from May 2001 to April 2007 an average daily repeatabilty of 0.27 % r.s.d. (Figure 2.3) was obtained for Mg/Ca and 0.32 % r.s.d for Sr/Ca over a total of 234 analytical runs. The long term reproducibility over this period was; Mg/Ca = 5.134 +/- 0.018 (s.d.) mmol/mol (0.35% r.s.d), Sr/Ca = 2.094 +/- 0.008 (s.d.) mmol/mol (0.40% r.s.d) on 234 runs, confirming the reproducibilities obtained during the initial 16 runs by de Villiers *et al*. [2002].

The daily averages plotted in Figure 2.3 are uncorrected for the effects of instrumental drift. Daily results may be used to correct for instrumental drift during a run but this has not been required, repeatability > 0.5 % has occured on only 10 occasions for Mg/Ca and 23 occasions for Sr/Ca out of the 234 runs during this period. Application of a within run drift correction improves within run repeatability to ~0.1 % for Mg/Ca and ~0.2 % for Sr/Ca [de Villiers *et al*., 2002] and would be appropriate where higher precisions are required, such as for Sr/Ca determinations in coral aragonite.

The long term reproducibility reflects differences between daily calibrations and applies to comparison of results obtained on different days. A long term correction could be applied by normalising the daily batch run average to the true ratio. This is only necessary where the daily batch run average deviates significantly from the long term mean. The worst Mg/Ca reproducibilities (11/07/01 and 01/02/04, Figure 2.3) were respectively 1.1% below and 1.5% above the true value, well within the reproducibility obtained for replicate analyses of foraminiferal Mg/Ca [Barker *et al*., 2003; Wara *et al*., 2003] and foraminifera results have not been routinely normalised to those for a consistency standard. Where higher accuracy is required, such as for the analyses of carbonate standards (Chapter 3), results may be normalised to the daily batch average of the consistency standard.

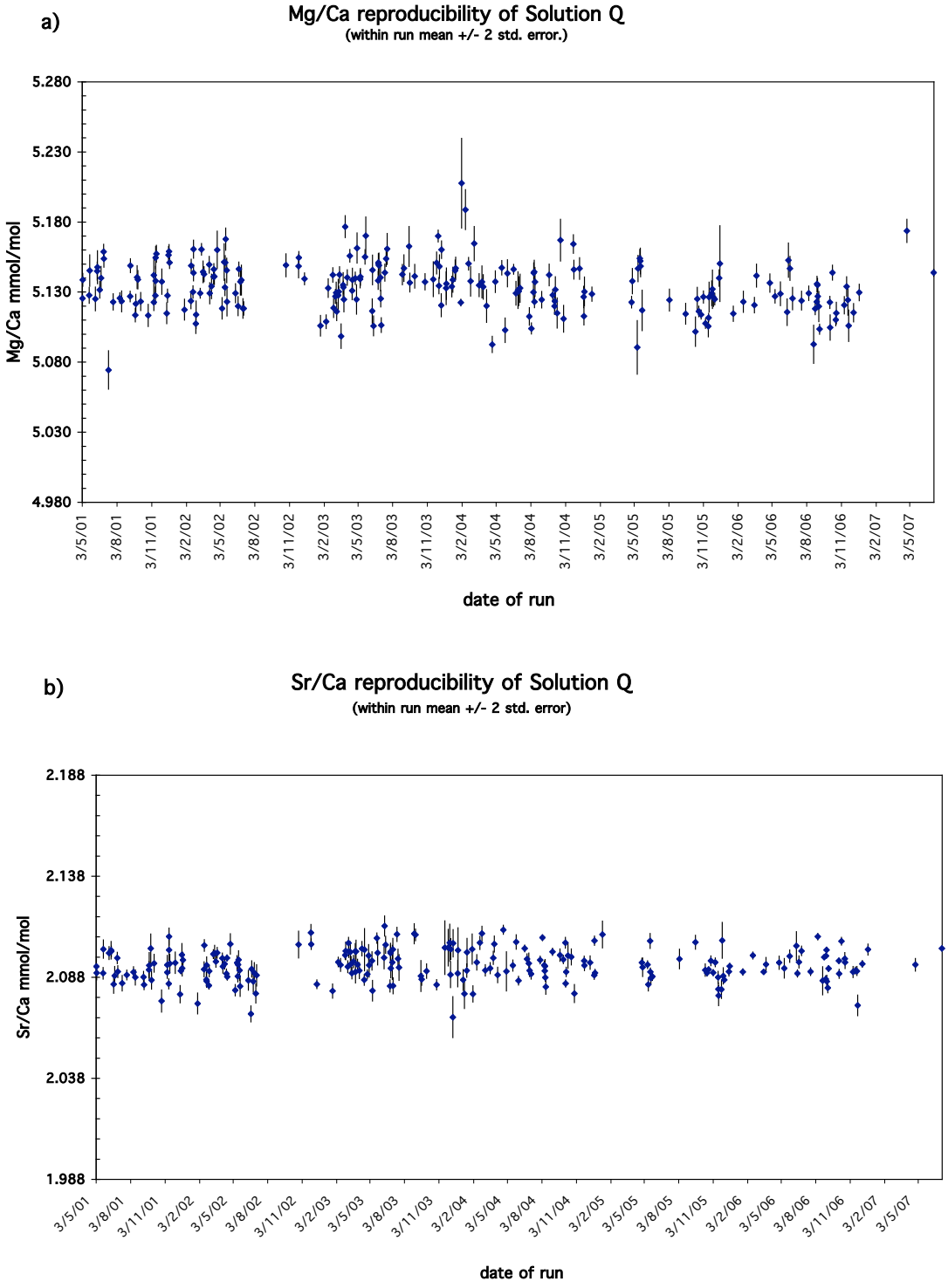

Figure 2.3 Analyses of laboratory consistency standard (Solution Q) on 234 days during the six year period May 2001 to April 2006, a) Mg/Ca, b) Sr/Ca. Error bars are the daily within run 2 σ_m (standard error is used to allow for different numbers of analyses in each run).

A second consistency standard, Solution R (Mg/Ca = 1.289 mmol/mol, Sr/Ca = 0.808 mmol/mol, [Ca] = 100 μg/g) was prepared in addition to Solution Q to be run during analyses of the foraminifera samples presented in Chapter 4. This standard contains Mg/Ca more similar to values found for *Globogerina bulloides* in these samples. On average 6 replicates (min 2, max 21) were measured for this standard in addition to Solution Q during a days run. Reproducibility of Solution R is plotted in Figure 2.4.

During the period from December 2002 to April 2007 an average daily repeatabilty of 0.27 % r.s.d. (Figure 2.4) was obtained for Mg/Ca and 0.28 % r.s.d for Sr/Ca over 67 analytical runs, showing that within run repeatability is maintained at the lower Mg/Ca and Sr/Ca ratios of this standard. The reproducibility obtained over this period for Solution R is: Mg/Ca = 1.286 +/- 0.006 (s.d.) mmol/mol (0.46 % r.s.d), Sr/Ca = 0.810 +/- 0.003 (s.d.) mmol/mol (0.36 % r.s.d) on 67 runs, demonstrating that reproducibility is equally good for both consistency standards. Neither a within run drift correction nor a between run normalisation were applied to the results in Figure 2.4.

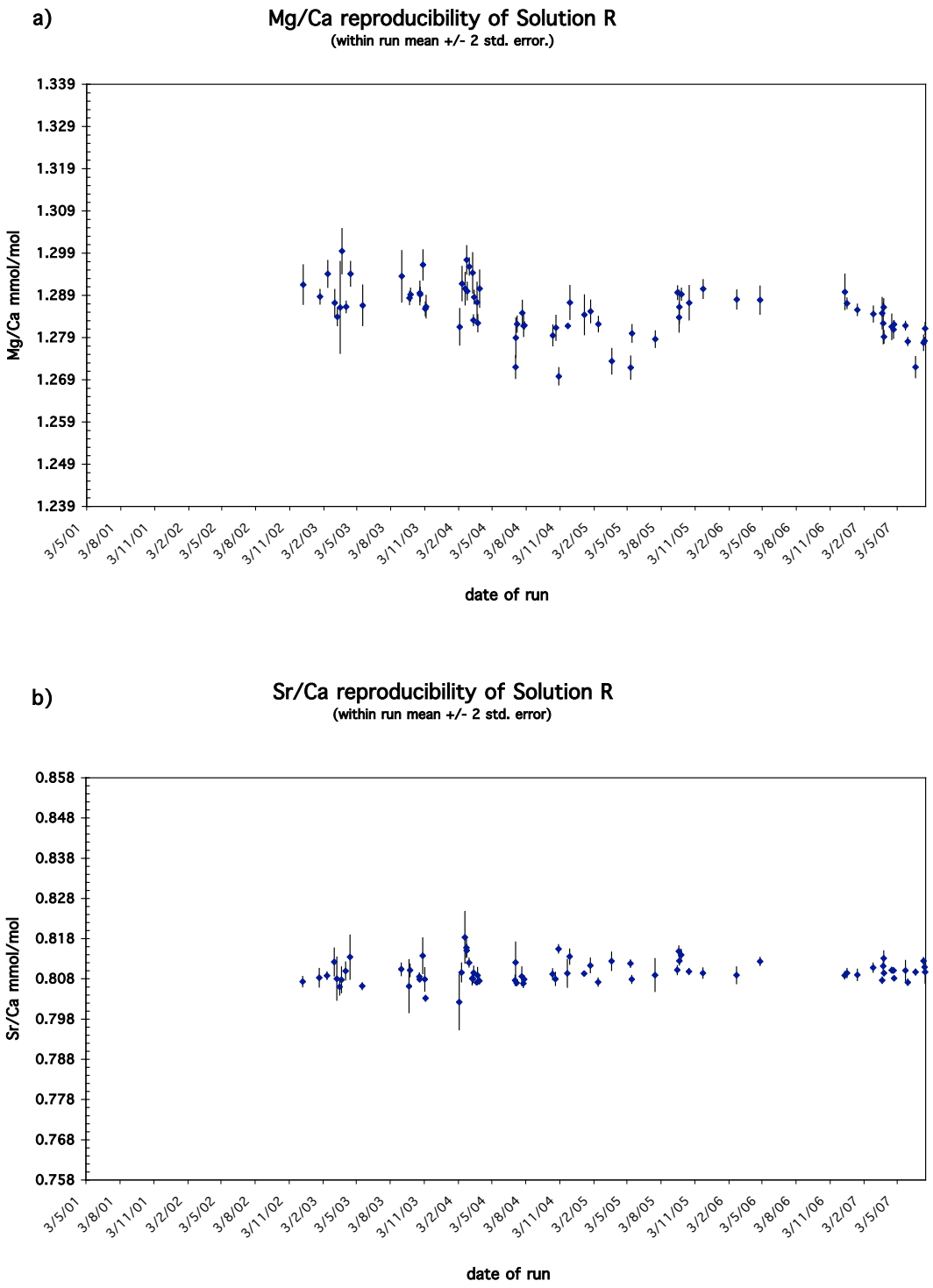

Figure 2.4 Analyses of laboratory consistency standard (Solution R) on 67 days during the period May 2001 to April 2007, a) Mg/Ca, b) Sr/Ca. Error bars are the daily within run 2 σ_m (standard error is used to allow for different numbers of analyses in each run)

2.3 Cleaning procedures for Mg/Ca and Sr/Ca determinations

Sample preparation techniques for Mg/Ca and Sr/Ca determination have evolved from the method developed for Cd/Ca determination by Boyle [1981] and Boyle and Keigwin [1985] and modified by Rosenthal *et al*. [1997a]. Crushed samples are ultrasonicated in distilled water and methanol to remove clays, followed by removal of trace metal enriched ferromanganese oxide coatings by reductive cleaning with hydrazine (NH_2NH_2) in a hot citric acid / ammonia buffer solution, and oxidative removal of organic matter with hot alkali buffered H_2O_2 solution. A series of leaching steps with dilute nitric acid are then used to remove adsorbed contaminants and any manganese carbonate coating before sample dissolution.

The higher abundances of Mg and Sr in comparison with Cd in foraminiferal calcite (Mg/Ca and Sr/Ca ratios are of the order 10^{-3} – 10^{-2} mol/mol compared to Cd/Ca of 10^{-8} – 10^{-7} mol/mol (see Chapter 1, Figure 1.1) imply that the rigorous cleaning schemes and trace metal contamination precautions required for Cd determination should not be necessary for Mg and Sr. Consequently, cleaning procedures for Mg/Ca and Sr/Ca determination have differed between laboratories, possibly depending on the requirements for the determination of other trace elements in foraminiferal calcite as much as on those for Mg and Sr. For example, Brown and Elderfield [1996] washed samples with water and methanol then leached with 1M ammonium chloride to remove exchangeable Sr. Rathburn and de Deckker [1997] cleaned benthic foraminifera samples by ultrasonication in water and alcohol. Rosenthal et al [1997b] employed ultrasonication in distilled water followed by a dilute acid leach. Elderfield and Ganssen [2000], Elderfield *et al*. [2000] and Lear et al [2000] used a scaled down version of Boyle and Keigwin's [1985] Cd/Ca method, omitting the reductive cleaning step on the assumption that Mg and Sr concentrations are negligible in any ferromanganese coatings. In contrast, Mashiotta *et al*. [1999] and Martin *et al*. [1999] used the complete Cd/Ca reductive cleaning procedure plus the chelation step required for the analysis of Ba/Ca [Lea and Boyle, 1991] to permit multiple element determination of a suite of trace metals in the same samples; their full procedure consisting of clay removal, reductive cleaning, oxidative cleaning, chelation and dilute acid leaching before sample dissolution.

2.3.1 Initial cleaning procedure.

Initially, the method described by Elderfield *et al*. [2000] was employed in this project. Typically 10 - 20 individuals were picked from the 300-355 μm size fraction or, for *Uvigerina peregrina,* the 250-300 μm fraction where insufficient specimens were available in the larger fraction. The foram tests were viewed under a microscope while gently crushed between glass plates to ensure all the chambers were opened, ultrasonicated three times in water and twice in methanol to remove clays, followed by hot alkaline oxidative cleaning to remove organic matter, and a single short (30s) leach with 0.001M HNO_3 before dissolution in 400μl 0.075M HNO_3.

2.3.2 Comparison between non-reductive and reductive (Cd/Ca) cleaning.

Different results produced by different cleaning procedures can be readily demonstrated. Multiple species of planktonic foraminifera from core top samples previously analyzed for Mg/Ca and Sr/Ca [Elderfield and Ganssen, 2000; Elderfield *et al*., 2000] were cleaned for Cd/Ca determination using Boyle and Keigwin's [1985] method as modified by Rosenthal *et al*. [1997a]; the Cd/Ca results are presented in Chapter 6. Mg/Ca and Sr/Ca results obtained after cleaning for Cd are compared to those obtained using the Mg cleaning method of Elderfield *et al*. [2000] in Figure 2.5.

Systematic offsets in Mg/Ca results were obtained between the two methods (Fig. 2.5a), significantly greater than expected from natural heterogeneity [Barker, 2002]. The Cd/Ca cleaning procedure, including the reductive cleaning step, gave on average 16% lower Mg/Ca ratios than the Elderfield and Ganssen [2000] procedure. The largest offsets, calculated as the difference in slope between the best fit line through the data and the 1:1 line, were observed for *N. pachyderma* (25%) and *G. bulloides* (23%) whereas differences in results for *G. sacculifer* (2%) and *G. inflata* (8%) were close to those which may be expected from natural variability. These differences could be due to a greater efficiency in removal of contaminant phases by reductive cleaning [Martin and Lea; 2002], but could also be a result of partial dissolution of carbonate by the more corrosive reagents used. In contrast, almost all of the scatter in Sr/Ca (Fig 2.5b), except for a few results for *G. hirsuta,* lies within the range expected from natural variability.

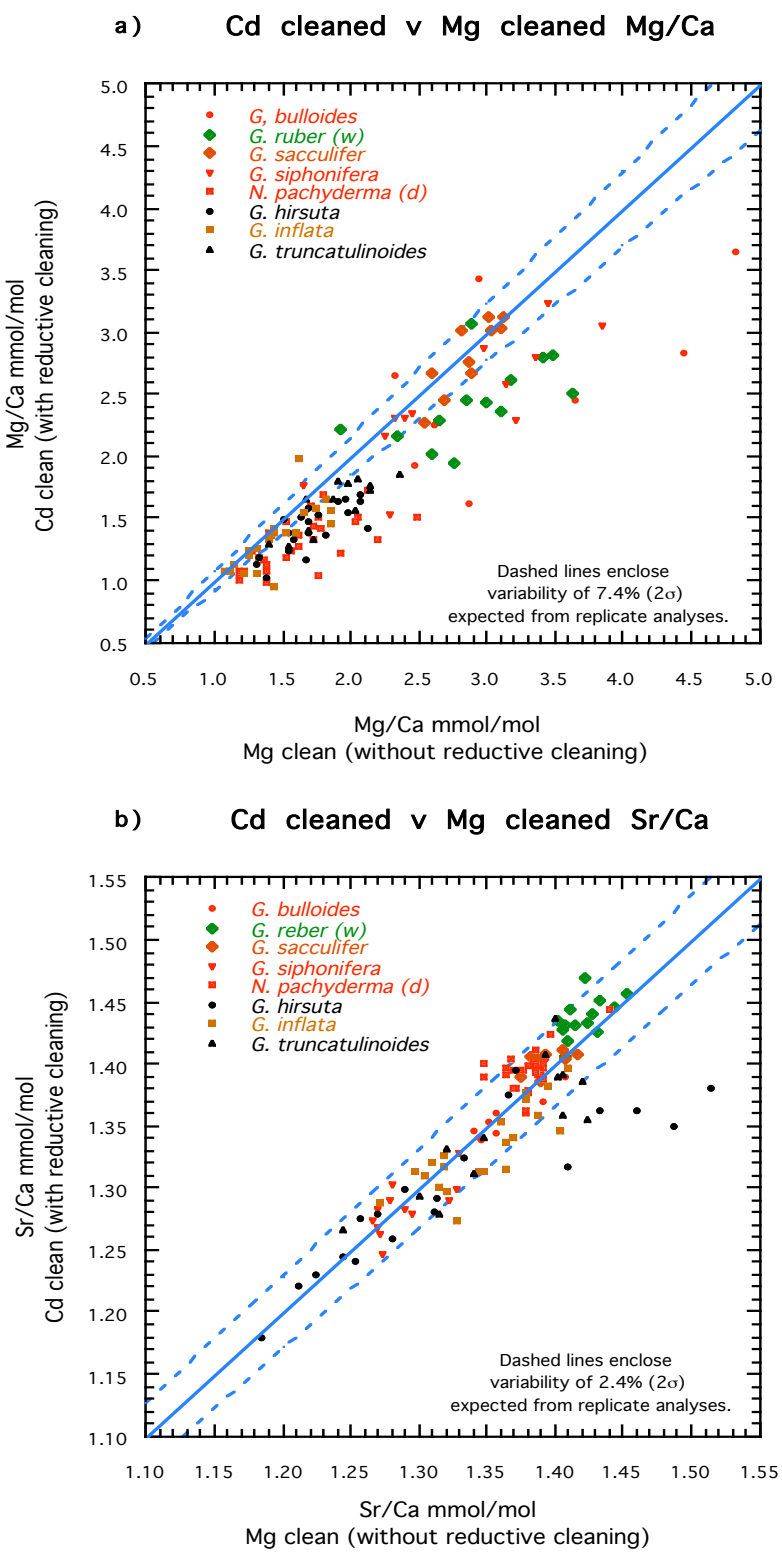

Figure 2.5 Comparison of (a) Mg/Ca and (b) Sr/Ca results obtained on multiple species of planktonic foraminifera from two cleaning procedures. The dashed lines represent scatter around the 1:1 line which may be expected from natural variability.

2.3.3 Improved Mg/Ca cleaning procedure.

A detailed investigation of the Mg/Ca cleaning procedure was performed by Barker [2002], who demonstrated that of the cleaning steps used in Mg/Ca and Sr/Ca determination, clay removal has by far the largest effect on the final Mg/Ca composition obtained. Clays in the form of illite, kaolinite, montmorillonite and chlorite contain from 1 – 10 % Mg by weight [Deer et al., 1992] and are present as fine (< 2 μm) material in a significant proportion of marine sediment [Riley and Chester, 1971]. The high concentrations of Mg in clays make them serious contaminants in foraminiferal Mg/Ca determination. A residue after cleaning of 1μg of clay containing 1% Mg would add 10ng Mg to the analysis solution, sufficient to cause significant contamination in many cases, particularly where samples are small and have low Mg/Ca ratios. For example, a 200 μg foraminifera sample with Mg/Ca of 1 mmol/mol contains ~ 50 ng Mg and contamination from residual clay as above would increase Mg/Ca by 20%. The potential for contamination from clays is also species dependent. Species such as *G. bulloides* with thin walled tests and comparatively large chambers tend to suffer much more from clay contamination than those with denser, closed shells, such as the benthic genus *Uvigerina*. Thus, during this work it was found that while the basic cleaning procedure of Elderfield *et al*. [2000], described above, produced adequate results for Mg/Ca from *Uvigerina spp*. the method was unable to clean the planktonic species *G. bulloides* sufficiently well to give meaningful data.

Modifications to the method of Elderfield *et al*. [2000] to give more reproducible Mg/Ca results for foraminifera susceptible to clay contamination were developed by Barker [2002] and are described in Barker *et al*. [2003]. The principal modification is a much more efficient clay removal stage. Samples are ultrasonicated five times in water, with further repetitions as necessary, instead of the previous three times. The volume of water required for clay separation by ultrasonication has been optimised, and samples are treated individually when removing suspended clays, instead of in batches, with a minimal settling technique employed to ensure maximum efficiency of clay removal. An additional step was added to the method to remove coarse grained silicates which are occasionally present, and are not separated in suspension with fine clays. Before dissolution, the samples are carefully examined under a microscope, employing a light

and dark background in turn, and any apparently non-carbonate particles are removed manually. During subsequent method development it was found that centrifugation of samples after dissolution effectively removed any remaining particles not picked out in the manual silicate removal step. Centrifugation improved data quality even in situations where residual particles were thought to be insignificant and it was therefore included routinely in the cleaning procedure. The improved method is described in detail in Appendix 1 and was used for repeat analyses of *G. bulloides* from ODP Site 1123 and all subsequent analyses.

A reductive cleaning step was not included in the method because the lower Mg/Ca ratios found after reductive cleaning (section 2.3.2) were thought more likely to be the result of shell dissolution by the corrosive reagents used, rather than from removal of a Mn-Fe oxide coating. Available evidence from Mn nodules and micro-nodules [de Lange *et al.*, 1992; Pattan, 1993] and from Mn carbonates in marine sediments [Pedersen and Price, 1982] indicates that these materials contain insufficient Mg to represent a significant source of contamination in foraminiferal Mg/Ca determinations, both containing Mg/Mn of approximately 0.1 mol/mol. Mn/Ca ratios in foraminifera after cleaning, without removal of Mn phases, are of the order of 0.1 mmol/mol (Fig. 2.6c) which suggests a contribution to Mg/Ca of ~0.01 mmol/mol or ~1% for a typical sample. Additional element ratios (Mn/Ca, Al/Ca, Fe/Ca etc) were measured to monitor potential oxide and silicate contamination, as described in section 2.4.

2.4 Assessing data quality and cleaning efficiency

Accuracy of foraminiferal Mg/Ca and Sr/Ca determination is constrained by the accuracy of the instrument calibration, by Mg contamination from non-carbonate phases not removed in the cleaning process and by the analytical blank of the procedure. Standard solutions for instrument calibration were prepared with element ratios known accurately to better than 0.1% (see Chapter 3) and instrumental accuracy was therefore equivalent to the ICP-OES measurement precision. In practice, the accuracy of foraminiferal Mg/Ca determination is limited by Mg contamination from residual non-carbonate phases and the analytical blank, whereas contamination from these sources has less effect on Sr/Ca ratios.

The efficiency of the cleaning procedure was monitored during analyses by simultaneously measuring other elements to indicate the presence of either an oxide coating (Fe, Mn) or residual silicate material (Al, Fe, initially; K, Na, Si, Ti added later).

Fe and Mn each have sensitive, Type II ionic, emission lines (Table 2.2) and are readily determined by ICP-OES. High Mn/Ca indicates the presence of either an authigenic Mn-Fe oxide coating or a Mn-rich carbonate [Boyle,1981;1983] whereas high Fe/Ca may be from either a Mn-Fe oxide coating or residual silicate material. The Mn/Fe ratio is an aid to distinguishing between these two sources, ranging from low values, ~ 0.05 mol/mol for silicate to 1 -10 mol/mol for Mn-Fe oxide coatings.

An element with an unequivocal source, such as Al, Si or Ti, would be an ideal indicator of aluminosilicate contamination. ICP-OES is not a sensitive technique for the determination of Al (Table 2.2), with a detection limit of ~0.13 mmol/mol found for Al/Ca at $[Ca^{2+}]$ = 60 μg/g when using the 396.152 nm line. Si has similar low sensitivity and additionally suffers from high background counts from Si within the sample introduction system. Titanium is a more sensitive element for determination by ICP-OES, using the 336.122 nm ionic emission line but, in practice, Ti seldom is observed above the detection limit of 0.001 μg/g and its presence serves to confirm contamination shown by other indicators, Al & Fe. The alkali metals K & Na may indicate aluminosilicate contamination, but these elements also have low sensitivity for determination by ICP-OES using atomic emission lines.

Figure 2.6 shows the effect of clay contamination on Mg/Ca ratios for the two species analysed and the cleaning procedures used. Contamination of the measured Mg/Ca ratios of *G. bulloides* by silicate material when using the initial basic cleaning procedure is demonstrated by the high Al/Ca and Fe/Ca ratios obtained, (Fig 2.6a,b). In contrast, the improved cleaning procedure of Barker et al. [2003], as detailed in Appendix 1, in most cases reduced Al concentrations to below detection for determination by ICP-OES (Fig. 2.6a). Similarly, Fe/Ca ratios were reduced to <0.2mmol/mol (Fig 2.6b). The association of Fe in this case with silicate contamination rather than with the presence of an Fe-Mn oxide coating is demonstrated by the Mn/Ca ratios (Fig 2.6c) which remained at a similar level when either cleaning procedure was employed. The thicker

shelled benthic species *Uvigerina peregrina* is much less prone to contamination than *G. bulloides* and low Al/Ca and Fe/Ca ratios were generally obtained when using the initial basic cleaning procedure.

Na/Ca ratios in planktonic foraminifera are expected to be in the range 4 – 7 mmol/mol [Lea, 1999]. The majority of *G. bulloides* analysed (Fig. 2.6d) have Na/Ca within this range but, high values occur which may be a consequence of silicate contamination and these can be used to eliminate suspect high Mg/Ca results.

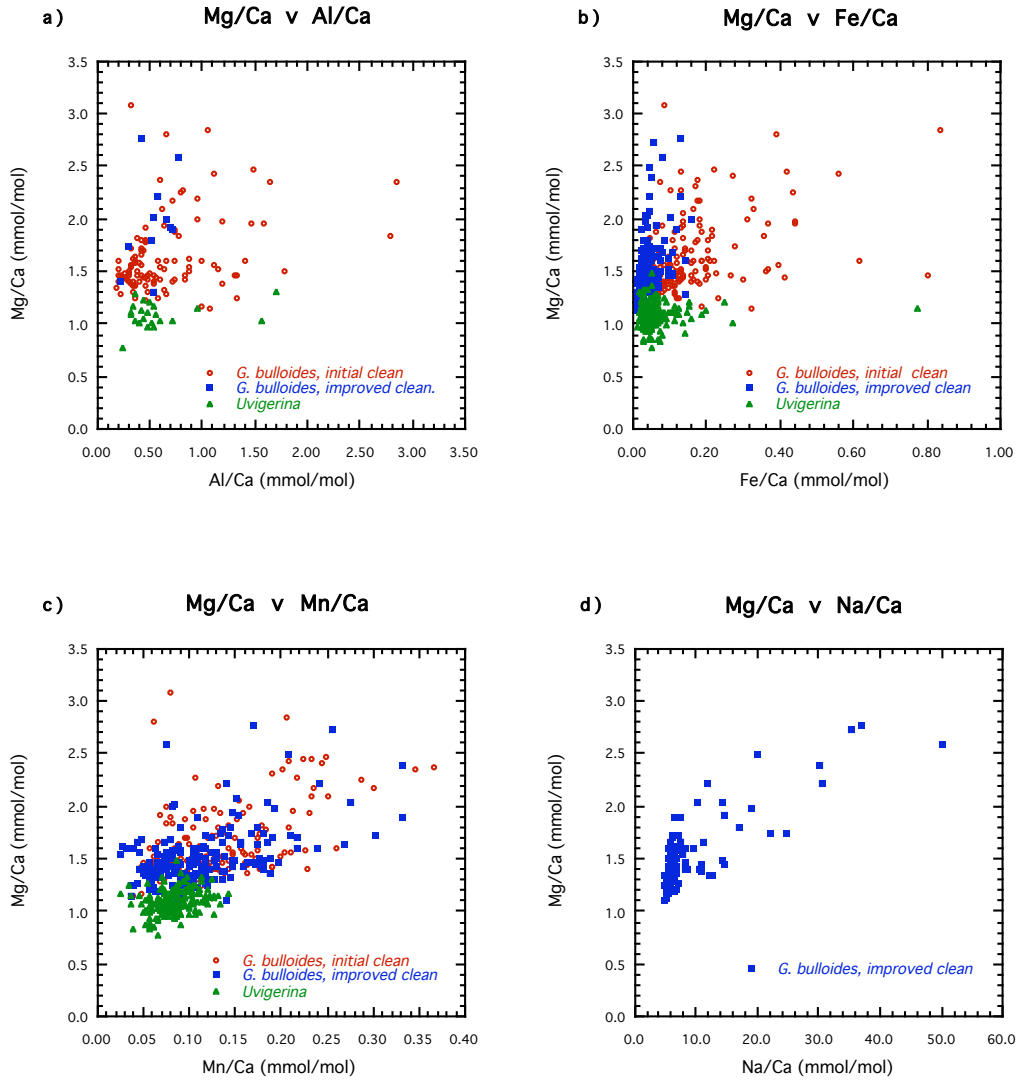

Figure 2.6 Measured Mg/Ca in *G. bulloides* and *U. peregrina* from ODP site 1123 versus a) Al/Ca, b) Fe/Ca, c) Mn/Ca, d) Na/Ca for two cleaning procedures. Samples cleaned by the procedure of Elderfield et al (2000), *G. bulloides* (red circles), *Uvigerina* (green triangles) and by the procedure of Barker et al (2003), *G. bulloides* (blue squares).

In principle, knowledge of the contaminant composition would permit correction of measured Mg/Ca ratios [Barker, 2002; Barker *et al*. 2003], an estimate of the correction being given by, for example, the ratio of Fe/Mg of the contaminant phase to the measured sample Fe/Mg. If the Fe/Mg of the contaminant phase were 1 mol/mol and all of the Fe could be attributed to that phase, a sample Fe/Mg ratio of 0.1 mol/mol would indicate that Mg/Ca was 10% high. Uncertainty in estimating the composition of the contaminant phase is likely to produce large errors but, in appropriate circumstances where the Fe/Mg ratio of the contaminant can be reliably determined a correction to Mg/Ca ratios may be applied [Lea *et al*., 2005]. In this work, measured Al/Ca, Al/Mg, Fe/Ca and Fe/Mg ratios were used for the rejection of potentially contaminated sample Mg/Ca. The criteria used to reject Mg/Ca data as potentially contaminated by Mg from clays or silicate minerals were; measured Al/Ca > 0.4 mmol/mol, or Al/Mg > 0.2 mol/mol, Fe/Ca > 0.1 mmol/mol or Fe/Mg > 0.1 mol/mol, or Si significantly greater than background. High Na/Ca ratios (> 10 mol/mol) also were used as an indicator of suspect Mg/Ca data.

2.5 The analytical blank and implications for Mg/Ca determination in foraminiferal calcite.

The analytical blank and its effect on the results is an important parameter in all determinations. Although magnesium is not present at the extremely low concentrations of cadmium and other trace elements in foraminiferal calcite, Mg is particularly susceptible to contamination because of its high natural abundance. The presence of Mg in potential contaminants, including water, reagents and apparatus, makes the analytical blank a limiting factor in foraminiferal Mg/Ca determination.

Figure 2.7 shows measured Mg/Ca and Sr/Ca ratios for *G. bulloides* from ODP site 1123 (41° 47.15'S, 171° 29.94'W) plotted against calcium concentrations of the measurement solutions. Increasing Mg/Ca ratios with decreasing calcium concentrations below approximately 20 ppm are clearly visible and there is some concentration below which Mg/Ca data become unreliable. In contrast, Sr/Ca ratios remain unaffected to much lower calcium concentrations (< 3 ppm) and then decrease

with decreasing calcium concentrations. A minimum Ca concentration, typically ~10 ppm, has been used as a criterion for Mg/Ca data rejection [e.g Lear *et al*., 2000; Wara *et al*., 2003] but the relationship between measured Mg/Ca ratios and Ca concentration has not been investigated in detail.

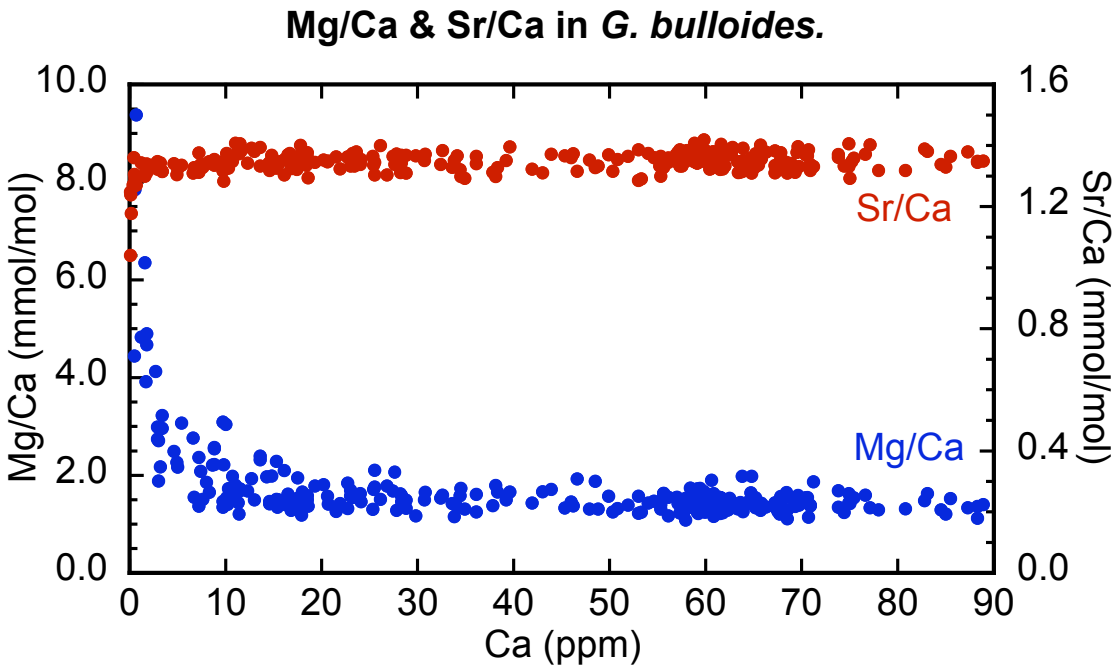

Figure 2.7 Measured Mg/Ca and Sr/Ca ratios for *G. bulloides* from ODP site 1123 versus Ca concentration (µg/g) of the analysis solution.

2.5.1 Source of the analytical blank

Procedure blanks for Ca, Mg and Sr, determined during the course of this work by processing the routinely used polypropylene vials (Eppendorf, Safe-Lock, 0.5ml) through the foram cleaning procedure of Barker *et al*. [2003], are shown in Table 2.3 together with calculated Mg/Ca and Sr/Ca ratios for the blank. Average blank contributions of 0.002 ppm Mg and 0.03 ppm Ca were obtained, equivalent to Mg/Ca >300 mmol/mol. The calculations contain large errors but the general picture is clear, the effect of the analytical blank on Mg/Ca ratios may be considerable; a sample with Mg/Ca in the range 1 – 5 mmol/mol could be subject to an analytical blank with Mg/Ca >>100 mmol/mol, whereas for Sr/Ca the ratio of the analytical blank is of the same order of magnitude as Sr/Ca of samples and consequently has a much smaller effect.

	Ca (ppm)	Mg (ppm)	Sr (ppm)	Mg/Ca (mmol/mol)	Sr/Ca (mmol/mol)
Max	0.20	0.0080	0.00062	1700	10.15
Min	0.00	0.0002	-0.00001	31	-0.34
Mean	0.03	0.0021	0.00010	314	2.03
std dev	0.04	0.0015	0.00014	340	2.02
n	31	31	31	31	31

Table 2.3 Procedure blanks obtained using conventional polypropylene vials.

Since the 1970's the manufacture of polypropylene, high density polyethylene and other poly-olefins has involved the use of $MgCl_2$ supported Ziegler-Natta catalysts in the polymerisation process [Masuda *et al.,* 1997; Mulhaupt; 1999]. Therefore, polypropylene poses a serious risk as a source of magnesium contamination. The magnitude of any contamination will depend on the amount of magnesium retained within the polymer structure and whether this is removed from the polymer surface by acid cleaning, or is continually leached from within the polymer during use, even after acid cleaning.

A number of observations suggest that Mg is leached from polypropylene vials over time. Polypropylene vials are routinely trace metal cleaned before use by soaking overnight in ~1.5M HNO_3 (Appendix 1). Nevertheless, repeat analyses of a series of sample solutions after storage for more than a few hours, in most cases produced higher Mg/Ca ratios than the initial determinations. Wara *et al.,* [2003] employed a more rigorous cleaning procedure but "found possible Mg contamination from plastic ware at low solution concentrations of Ca and Mg and for any prolonged storage (greater than a few hours)".

The leaching of Mg from sample vials was investigated using a number of vial types and cleaning procedures. Four vial types were examined; conventional polypropylene (PP), thin walled polypropylene RNASE-DNASE free PCR tubes (PCR), polystyrene (PS) and teflon (PFA). Details are given in Table 2.4.

material	abbreviation	manufacturer	details	code
polypropylene	PP	Eppendorf	Safe-Lock tubes, 0.5ml	0030 121.023
polypropylene	PCR	Treff Lab	PCR tubes, 0.5ml, thin walled, RNASE-DNASE free	96.9216.9.01
polystyrene	PS	Robbins Scientific	1.0ml tubes with polyethylene caps.	1010-00-0
Teflon PFA	PFA	Savillex	0.5ml microcentrifuge vials and caps	7245

Table 2.4 Details of vials tested.

Sample dissolution acid (500µl 0.075M HNO_3) was added to each of the four types of vials, after cleaning by a number of different procedures, then analysed for Mg following various storage times. The results are shown in Table 2.5 and confirm that Mg is leached from acid cleaned polypropylene vials over time. The Mg concentrations obtained from conventional polypropylene vials were sufficent to account for much of the analytical blank shown in Table 2.3. The increase in Mg concentration with time, regardless of cleaning procedure, demonstrates this effect is not a surface trace metal contamination but must be the result of leaching of Mg out of polypropylene. Thin wall polypropylene vials showed a reduced effect compared to conventional polypropylene whereas polystyrene and PFA were, as expected, noticeably cleaner.

Cleaning procedure	when analysed	Mg ppb	s.d.	no. vials
Polypropylene (Eppendorf Safe-Lock, 0.5 ml)				
Not cleaned	immediately	17		1
1 x 10% HNO3, soaked overnight.	immediately	0.18	0.01	3
(usual procedure).	after ~ 90 mins	0.21	0.01	3
	after 24 hours	1.06	0.47	5
1 x 50% HCl, overnight.	immediately	0.42	0.11	3
1 x 50% HCl, overnight followed by	after ~ 20 hours	0.55	0.16	5
1 x 10% HNO3, overnight.	after 1 week	1.90		1
2 x 10% HNO3, overnight	immediately	0.04	0.01	3
dried between stages.	after ~20 hours	0.61	0.08	5
	after 1 week	1.20		1
Polypropylene (TreffLab, thin wall, 0.5 ml)				
1 x 10% HNO3, overnight.	after ~90 mins	0.05	0.07	5
(usual procedure)	after 24 hours	0.26	0.14	5
	after 1 week	0.42	0.12	5
Polystyrene (Robbins, 1 ml)				
1 x 10% HNO3, overnight.	after ~3 hours	-0.02	0.02	5
(usual procedure)	after 24 hours	0.00	0.04	5
	after 25 days	0.08	0.10	5
PFA, (Savillex, 0.5 ml)				
1 x 50% HNO3, warm, overnight.	after ~ 20 hours	0.16	0.11	5

Table 2.5 Investigation of the source of the Mg blank.

2.5.2 Mg/Ca ratios and the analytical blank

The implications of the analytical blank for Mg/Ca ratios were modelled by calculating mixing hyperbolae between a series of Mg concentrations (0.0005, 0.001 & 0.002 ppm) and a hypothetical sample with Mg/Ca = 1.3 mmol/mol (Figure 2.8). The shapes of the curves closely resemble the trend of Mg/Ca in Figure 2.7 and demonstrate that the

analytical blank is a limiting factor for low Mg/Ca ratios when measured at low calcium concentrations. The line showing a 10% increase in Mg/Ca, equivalent to calculated temperatures too high by ~1°C is also shown, intercepting the mixing lines at ~ 6.5 ppm, 13 ppm and 26 ppm Ca respectively.

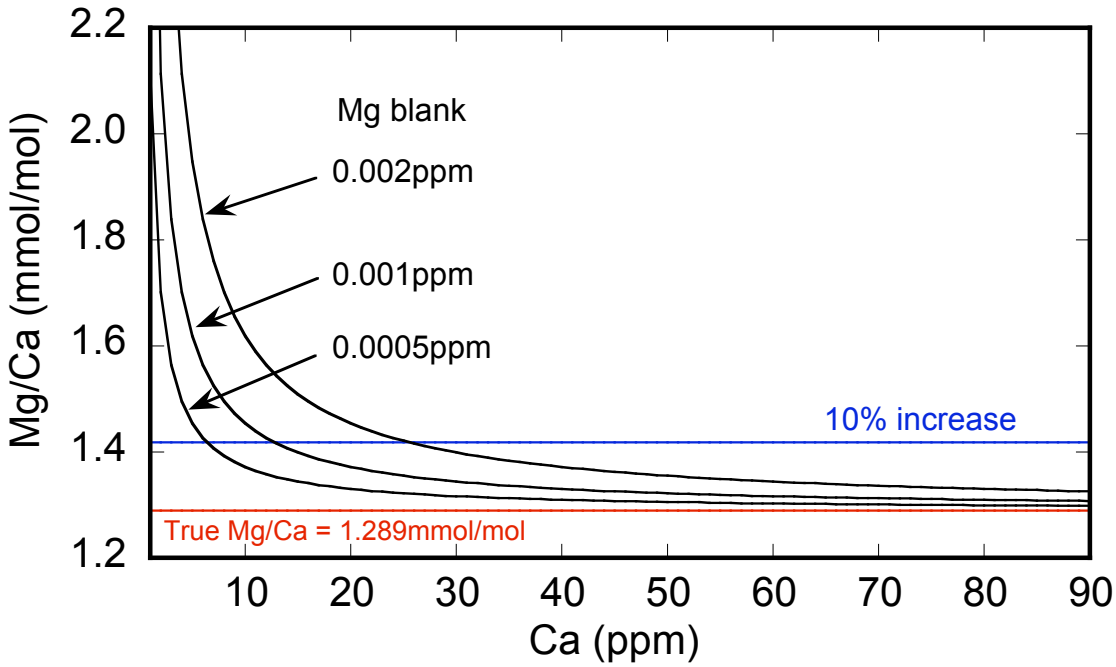

Figure 2.8 Calculated mixing curves for Mg blank contamination of a sample containing Mg/Ca =1.289 mmol/mol. The line showing a 10% increase in Mg/Ca, equivalent to calculated temperatures too high by ~1°C is also shown.

Contamination from the Mg blank on measured Mg/Ca ratios was investigated over a range of Ca concentrations. Polypropylene and polystyrene vials (Table 2.4) were cleaned by soaking overnight in cold 1.5M HNO_3 (the usual cleaning procedure, Appendix 1) whereas teflon vials were cleaned more rigorously by soaking overnight in warm (40 - 50°C) 8M HNO_3. Aliquots of a standard solution (Mg/Ca =1.289 mmol/mol, Sr/Ca = 0.808 mmol/mol) were pipetted into a series of each type of vial (50 of PP, PS and PCR, 20 of PFA) and diluted to 500µl with 0.075M HNO_3 to give Ca concentrations in the range 0 - 100 ppm. The vials were sonicated and mixed to mimic the sample dissolution procedure as closely as possible.

Concentrations were determined by ICP-OES commencing approximately five hours after filling the vials and taking three hours to run the series. The instrument was calibrated with dilutions prepared in 30ml LDPE bottles from the same concentrated standard, using 0.075M HNO_3 dissolution acid as the calibration blank. Hence, the standards and "samples" were matrix matched as closely as possible. Vials were run in sequence of increasing concentration to minimise differences from solutions of similar concentration standing for different lengths of time, starting with the lowest concentration in each vial type and running all vials of that concentration then moving to the next higher concentration. A determination consumed ~250µl solution and after running the vials were capped and stored overnight. The analyses were repeated the next day, starting approximately 24 hours after initial preparation and consuming the remaining 250µl solution.

The Mg/Ca ratios measured from all four types of vials on the day of solution preparation are shown in Figure 2.9a, overlain with the mixing hyperbolae from Figure 2.8. The effect of the Mg blank is noticeable below ~ 25 ppm Ca in all four types of vial. Figure 2.9b shows the results for the samples when re-analysed after 24 hours. The increase in Mg/Ca ratios compared to Figure 2.9a confirms increasing blank contamination on storage.

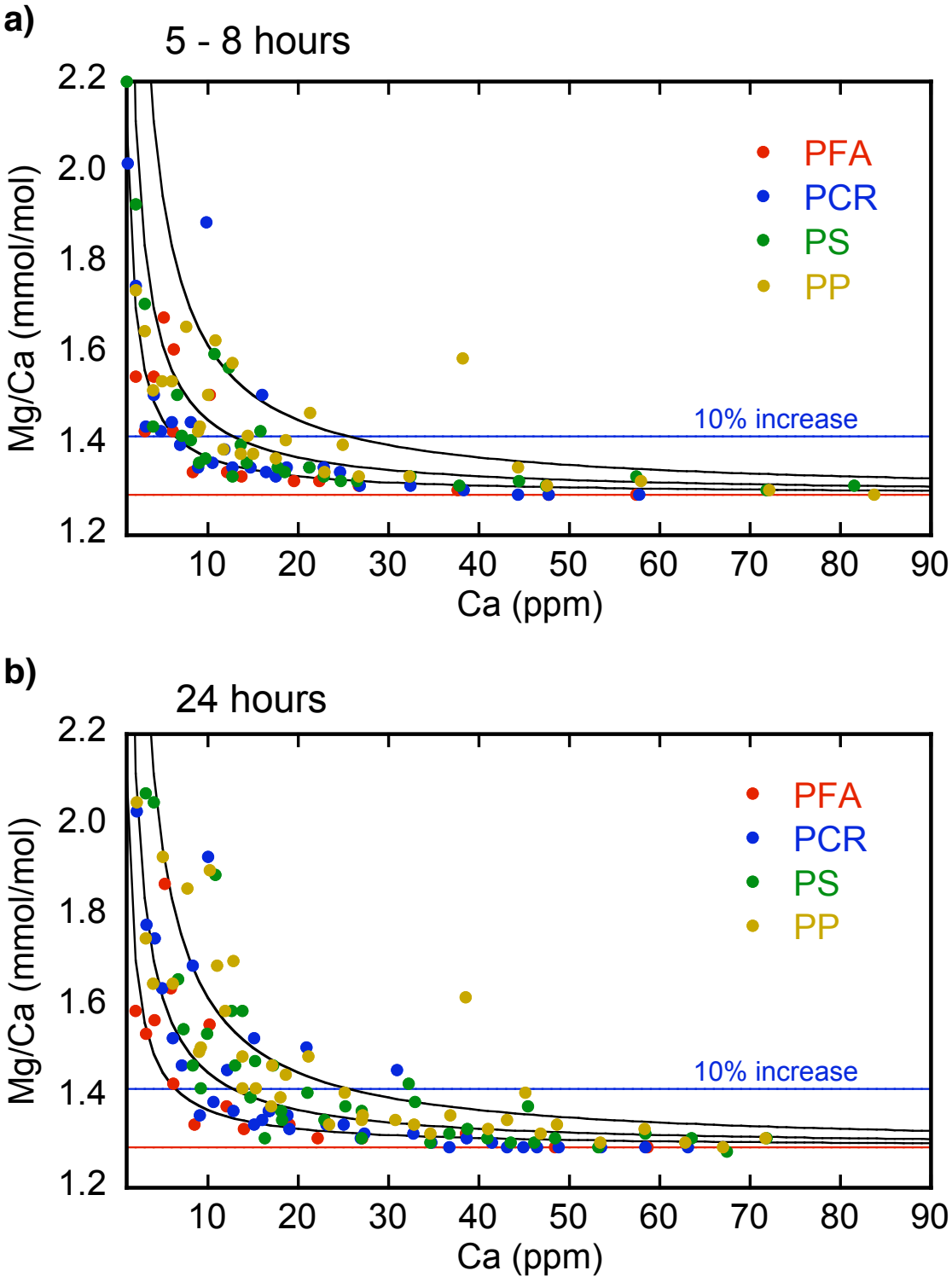

Figure 2.9 The effect of the analytical blank on Mg/Ca ratios. a) after 5 to 8 hours, b) after 24 hours.

The different types of vial are compared in Figure 2.10a-d with in each case solid symbols representing analyses after 5-8 hours and open symbols analyses after 24 hours. PFA vials (Figure 2.10a) showed the least effect from blank contamination which, for Ca concentrations greater than ~12 ppm, remains below 5% with only small

increases in Mg/Ca ratio on storage overnight. The Mg blank contribution from thin walled polypropylene PCR type vials (Figure 2.10b) for analyses after 5 – 8 hours closely follows the 0.0005 ppm Mg mixing hyperbola, with a few outliers. Storage for 24 hours produced more outliers in the 10 – 30 ppm Ca concentration range but, at higher concentrations the results agree with the initial values. Results for polystyrene (PS) vials (Figure 2.10c) show a larger effect from the Mg blank, particularly on storage, and conventional polypropylene vials (Figure 2.10d) are noticeably worse, with higher Mg blank contribution and more scatter, both after 5 – 8 hours and when repeated after 24 hours.

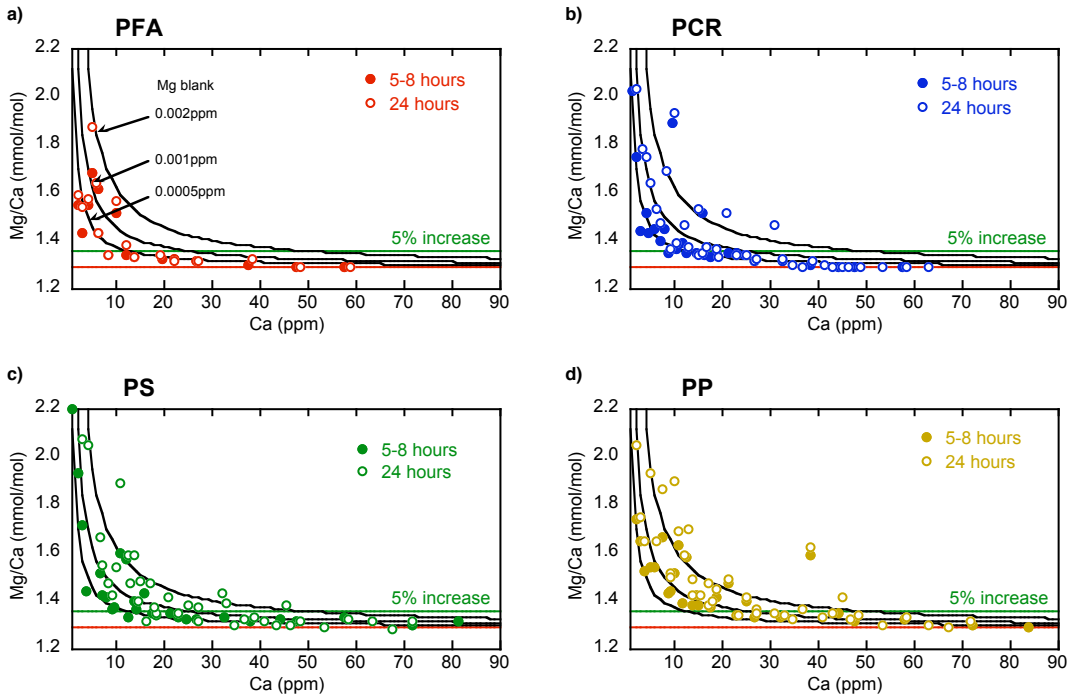

Figure 2.10 Contribution to the analytical blank over time periods of 5 – 8 hours (solid symbols) and 24 hours (open symbols) from different vial types: a) Teflon PFA vials, b) thin walled polypropylene RNASE-DNASE free PCR tubes, c) polystyrene (PS) vials, d) conventional polypropylene (PP) vials.

Teflon (PFA) vials gave the lowest blank contribution of those tested but cost would prohibit their use for all except the most critical applications. Polystyrene (PS) was expected to be a cleaner material for trace metal determinations than polypropylene [Moody and Lindstrom, 1977] but this was not confirmed for Mg in this study when samples were re-analysed after 24 hours. This may reflect the difficulty of sample

handling when using vials with separate caps. The thin walled (PCR) vials were the cleanest of the disposable vials and the foram cleaning procedure [Appendix 1] was amended to include sample transfer to these vials immediately before the dilute acid leach, conventional polypropylene vials being retained during the earlier stages because of their ability to withstand the high temperatures during oxidative cleaning. The thin walled (PCR) vials are manufactured from polypropylene and it remains unclear from these experiments whether their lower blank contribution was because they contained less Mg from the manufacturing process, or because the cleaning procedure was more efficient at removing Mg from the thinner walls. Additional experiments would be required to determine whether there are significant differences in the Mg blank contribution between vial types from different manufacturers and, indeed, between different batches of vials from the same manufacturer.

Procedure blanks obtained following the inclusion of thin walled polypropylene (and occasionally polystyrene) vials in the method are shown in Table 2.6, giving a 4 fold improvement in the Mg blank and 2 fold improvements in Ca and Sr blanks compared to the use of conventional polypropylene vials (Table 2.3).

	Ca (ppm)	Mg (ppm)	Sr (ppm)	Mg/Ca (mmol/mol)	Sr/Ca (mmol/mol)
Max	0.082	0.0027	0.00021	3942	49.72
Min	0.000	0.0001	0.00001	-75	0.54
Mean	0.017	0.00055	0.000051	213	3.72
std dev	0.019	0.00057	0.000047	712	9.24
n	30	30	30	30	30

Table 2.6 Procedure blanks using thin-walled polypropylene and polystyrene vials.

Regardless of the blank contribution and materials used, it is important that the effect of the analytical blank is assessed and taken into consideration when interpreting results. Figure 2.11 shows calculated mixing curves for three concentrations of Mg when applied to sample Mg/Ca ratios over the range 0.5 to 7.5 mmol/mol and demonstrates the need to optimise the sample/blank ratio according to the samples analysed.

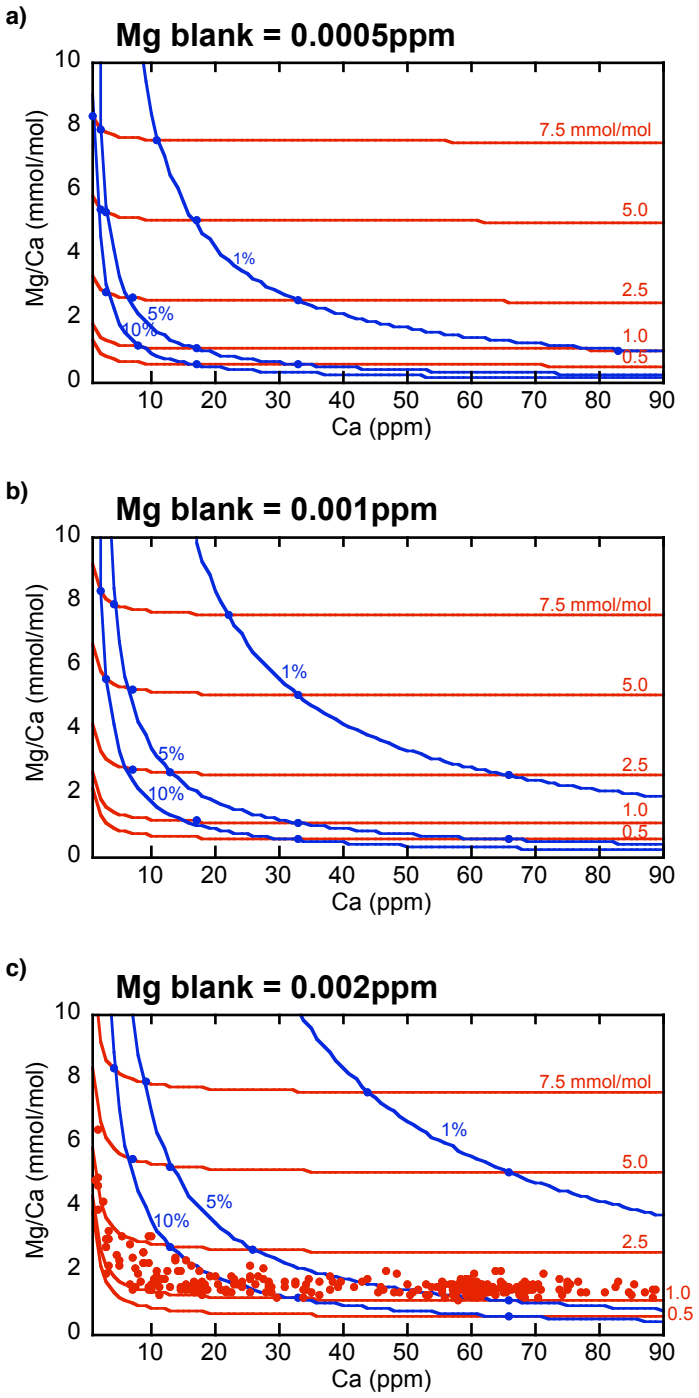

Figure 2.11 Calculated mixing curves for Mg/Ca in the range 0.5 – 7.5 mmol/mol and the effect of the analytical blank on measured ratios for an Mg blank of: a) 0.0005 ppm, b) 0.001 ppm, c) 0.002 ppm.

The analytical blank is unlikely to present significant problems in the determination of high Mg/Ca ratios (> ~2.5mmol/mol) except at very low solution concentrations or where very accurate determinations are required, as demonstrated by the lines indicating 1% blank contribution in Figure 2.11a-c. Measured Mg/Ca ratios for *G.*

bulloides from ODP site 1123 (Figure 2.7) obtained using conventional polypropylene vials are also plotted in Figure 2.11c. When working at low Mg/Ca ratios the analytical blank becomes a limiting factor, and its effect is particularly important because of the shallow slope of Mg/Ca temperature calibration curves at low temperatures. It is therefore very important to determine the analytical blank and use appropriate solution concentrations to ensure accurate results. In this work, for the samples shown in Figure 2.11c (discussed in Chapter 4), analyses with [Ca] < 40 ppm in solution were rejected as potentially unreliable because of the low Mg/Ca ratios involved.

2.6 Summary

Methods have been developed and optimised for the efficient cleaning of foraminiferal calcite and the determination of Mg/Ca and Sr/Ca ratios by ICP-OES.

A procedure to determine Mg/Ca and Sr/Ca element ratios by calibrating measured intensity ratios of emission lines against element ratios of standard solutions at constant Ca concentration was developed [de Villiers, Greaves and Elderfield 2002]. The Ca matrix effect on sensitivities of Ca, Mg and Sr emission lines was investigated and the instrument optimised to produce robust intensity ratio calibrations. Long term precision of the method, determined by routine analyses of consistency standards over a six year period, was shown to be better than 0.5% (r.s.d.) without requiring normalisation of results, either for within run instrumental drift correction or to correct for calibration differences between separate runs.

Cleaning procedures for the determination of Mg/Ca and Sr/Ca ratios in foraminiferal calcite were investigated, leading to the method published by Barker, Greaves and Elderfield [2003]. Subsequent development has concentrated on assessing the efficiency of cleaning to ensure reliable data. A significant influence on Mg/Ca ratios from the analytical blank was traced to contamination from Mg in polypropylene. The effect of the analytical blank on Mg/Ca ratios was modelled, showing that for low Mg/Ca ratios, or for determinations at low concentration, the analytical blank is the limiting factor to obtaining accurate results.

Chapter 3

Accuracy, standardisation and interlaboratory calibration standards for foraminiferal Mg/Ca thermometry

3.1 Introduction

The material presented in this chapter is published as :
Greaves, M., S. Barker, C. Daunt and H. Elderfield, Accuracy, standardisation and interlaboratory calibration standards for foraminiferal Mg/Ca thermometry. *Geochemistry, Geophysics, Geosystems* 6, Q02D13, doi:10.1029/2004GC000790, 2005.

Reliable estimates of marine palaeotemperature are crucial to understanding the ocean-climate system in the geological past. Magnesium/calcium ratios in foraminiferal calcite show a temperature dependence due to the partitioning of Mg during calcification and, during recent years, Mg/Ca ratios in foraminiferal calcite have become established as a palaeotracer of ocean temperature [Nurnberg *et al.*, 1996; Hastings *et al.,* 1998; Lea *et al.,* 1999, 2000; Elderfield and Ganssen, 2000; Mashiotta *et al.,* 1999; Rosenthal *et al.,* 2000; Dekens *et al.*, 2002].

As foraminiferal Mg/Ca ratios are now routinely analysed as indicators of past ocean temperatures, comparability of measurements between laboratories has become an important issue. A recent inter-laboratory calibration study by Rosenthal *et al.* [2004] evaluated the reproducibility of results within and between laboratories, both for the analyses of foraminiferal samples and of synthetic standard solutions. The study demonstrated that for analyses of synthetic standard solutions, within laboratory instrumental precisions better than 0.5% were usually obtained for both Mg/Ca and Sr/Ca measurements, but inter-laboratory precisions (r.s.d.) were significantly worse

(up to 3.4 % and 1.8 % respectively). Inter-laboratory precision of about 8 % obtained for the measurement of Mg/Ca in foraminifera reflected a combination of inter-laboratory instrumental precision and the effect of different cleaning methods used by different laboratories.

It is clear that a number of analytical issues remain. A central conclusion made by Rosenthal *et al.* [2004] highlighted the need for good instrumental intercalibration standards. Synthetic standard solutions are valuable but there are analytical issues in the preparation of accurate element ratio standards and, when distributed between laboratories, the risk always remains that solutions have not retained their initial composition by the time they are analysed. A solid intercalibration standard would overcome some of these problems, although such a material would itself first need to be calibrated by the community.

In this paper, we address the requirements for and the preparation of accurate analytical standards, and investigate solid reference materials which could be developed for use as robust intercalibration standards.

3.2 Standard solutions for Mg/Ca & Sr/Ca calibration

Standard solutions with accurately known element concentrations and ratios are essential for instrument calibration and for the investigation of matrix effects. The significantly worse inter-laboratory precisions, compared to within laboratory precisions, obtained for analyses of circulated standard solutions as reported by Rosenthal *et al.* [2004], could be a result of differences between calibration standards used by laboratories, or because the circulated standard solutions had become contaminated in the interval between their preparation and analyses, or a combination of both.

In most cases, calibration standards are prepared by mixing single element standard solutions to give the required element ratio. The accuracy of the element ratio obtained depends on the errors introduced by the preparation procedure, corrections for inter-element contamination and, crucially, the accuracy of the single element standards.

Typically, commercial single element standard solutions are certified to +/- 0.5% of the quoted concentration but, usually, this applies to the batch prepared by the manufacturer and not to the individual bottle. Concentration errors in single element standards propagate into mixed element standard solutions as systematic errors on the calculated ratios. In order to ensure that concentrations of single element standard solutions were more accurately known before preparing mixtures, we prepared single element standards starting from primary solid materials, as described by Moody *et al.,* [1988]. Mixed standard solutions prepared from these are used routinely in this laboratory for Mg/Ca & Sr/Ca determinations by ICP-OES following the method of de Villiers *et al.,* [2002]. Standard solution preparation was described briefly by de Villiers *et al.,* [2002]; more details are included here.

Calibration solutions were prepared gravimetrically starting from high purity $CaCO_3$ (NIST SRM 915a), $SrCO_3$ (NIST SRM 987) and Mg metal rod (Newmet Koch, purity 99.9+ %) following the criteria recommended by Moody *et al.,* [1988]. Before dissolution the carbonate standards were dried to constant weight at 110°C and the Mg metal rod was etched with ~0.1M HNO_3 (and microscopically examined) to remove any oxide coating, then dried under vacuum. The standards were weighed in Pt crucibles and the weights corrected for air buoyancy and the certified assay purity. Single element concentrated standards were prepared in 1 litre Teflon FEP (fluorinated ethylene propylene) bottles, cleaned by soaking overnight in hot 50% HNO_3 then rinsed and dried before use. The carbonate standards were rinsed into the bottles with water, covered with water and dissolved by the slow addition of nitric acid; this procedure prevents powder loss from static and sample loss from effervescence on dissolution. Ultrapure water and nitric acid (quartz distilled) were used throughout. Similarly, the Mg rod was transferred to an FEP bottle, covered with water and dissolved by slow addition of nitric acid. After dissolution the standards were made up with water and acidified to give an acid concentration of ~0.1M HNO_3. Concentrations of the other two elements in each standard solution were measured by ICP-OES. Mg and Sr concentrations in the Ca standard solution were in agreement with concentrations calculated from the NIST 915a certified values, and contributions for these two elements were included in the error propagation calculations when preparing subsequent mixtures. Measurement of the Ca and Sr concentrations in the Mg standard solution,

and Ca and Mg concentrations in the Sr standard solution confirmed that their contributions would be negligible in the subsequent mixed standard solutions and no corrections were applied.

Standard	Mg/Ca (mmol/mol)	Estimated error (mmol/mol)	(%)	Sr/Ca (mmol/mol)	Estimated error (mmol/mol)	(%)	[Ca] (μg/g)
CL 2	0.5059	0.0003	0.06	0.5057	0.0002	0.04	1801
CL 9	0.9083	0.0007	0.07	0.7023	0.0005	0.07	830
CL 3	1.289	0.001	0.05	0.8083	0.0003	0.04	1047
CL 4	2.374	0.001	0.04	1.0633	0.0004	0.04	1002
CL 7	4.048	0.003	0.07	1.615	0.001	0.06	881
CL 1	5.130	0.002	0.03	2.088	0.001	0.03	2088
CL 8	7.509	0.005	0.06	2.835	0.002	0.06	926
CL 5	9.162	0.005	0.06	3.554	0.002	0.06	924
CL 6	18.43	0.01	0.06	7.337	0.004	0.06	891

Table 3.1 Mg/Ca and Sr/Ca mixed standard solutions

Mixed standard solutions were prepared containing Mg/Ca and Sr/Ca ratios covering the range observed in foraminiferal calcite. All solutions were prepared gravimetrically in FEP bottles using ultrapure reagents to give solutions in ~0.1M HNO_3. Estimated errors on the Mg/Ca and Sr/Ca ratios were calculated by propagation of the weighing errors and the concentration uncertainties of the single element primary standards [Miller and Miller, 1993] to produce a series of concentrated standard solutions each with Mg/Ca and Sr/Ca ratios known accurately to better than 0.1%. Details of the concentrated mixed standards are given in Table 3.1. Aliquots of these standard solutions for interlaboratory calibration, to complement the standard solutions previously circulated by Rosenthal *et al.* [2004], can be provided on request. On the other hand, it would be preferable to have appropriate solid standards for use as reference material by laboratories.

3.3 Intercalibration standard

Synthetic standard solutions are not ideal for inter-laboratory calibration because of the difficulty of ensuring their integrity over time. The risk always remains that solutions on analysis have not retained their prepared composition because of either evaporation or contamination during transport and storage. Evaporation, which affects element concentrations equally, is only a minor problem for element ratio standards, whereas contamination affects individual elements unequally and has serious consequences for element ratios. Plastics such as polypropylene and high density polyethylene, manufactured catalytically using a polymerisation procedure involving $MgCl_2$ supported Ziegler-Natta catalysts [Masuda *et al.,* 1997], represent an obvious contamination risk for Mg/Ca standard solutions. The potential for contamination is minimised by circulating concentrated standard solutions in acid cleaned plastic bottles, but there will always be uncertainty in the integrity of small volumes of standard solutions over time. An ideal reference material for interlaboratory calibration would be a solid standard with well characterised Mg/Ca (and Sr/Ca) ratios, similar to typical foraminifera calcite. This would circumvent the potential problems inherent in the circulation of liquid standards. A series of three reference standards, covering the range of Mg/Ca ratios in foraminifera, would enable analysts to check the sensitivity and linearity of their techniques across the range.

Requirements for any solid standard are:- 1) that it has Mg/Ca (and Sr/Ca) within the range of foraminifera samples; 2) it is homogeneous, both within and between batch samples; 3) it has a matrix of pure calcite with no contribution to Mg/Ca and Sr/Ca ratios from other mineral phases; 4) it is readily available in a form suitable for use.

We have investigated commercial reference materials to see whether existing carbonate standards could be used as reference materials for Mg/Ca in foraminiferal calcite. Table 3.2 lists element concentrations and calculated Mg/Ca and other element ratios for a selection of certified reference materials (CRMs). In general, the Mg concentrations of available calcite and limestone certified reference materials are too high to match foraminiferal calcite, and these materials contain significant Al, Fe, Si and Ti from other mineral phases. (Table 3.2).

CRM	Certified	Quoted element concentrations (wt. %)							
	by:	Ca	Mg	Sr	Al	Fe	Mn	Si	Ti
IPT 35	IPT	38.5	0.42	0.034	0.064	0.049	0.01	0.93	0.008
ECRM 701-1	ECISS	37.7	0.36	-	0.29	0.73	0.02	0.93	0.018
SRM 1C	NIST	35.9	0.25	0.025	0.34	0.19	0.02	3.20	0.042
VS W10/2	ICRM	39.9	0.19	-	0.003	-	-	0.02	-
CM 1767	CMSI	39.4	0.14	-	0.03	0.06	-	0.21	-
ECRM 752-1	BAS	39.6	0.093	0.016	0.033	0.016	0.01	0.33	0.005
UN AK	IMRM	39.2	0.066	0.237	0.029	0.045	-	0.30	-
BAM RS3	BAM	40.0	0.018	0.017	<0.001	<0.001	-	-	-
		Calculated ratios (mmol/mol)							
	Material	**Mg/Ca**	**Sr/Ca**		**Al/Ca**	**Fe/Ca**	**Mn/Ca**	**Si/Ca**	**Ti/Ca**
IPT 35	calcitic limestone	18.1	0.40		2.5	0.9	0.18	34.3	0.17
ECRM 701-1	calcite	15.8	-		11.4	13.9	0.43	35.2	0.40
SRM 1C	argillaceous limestone	11.6	0.32		14.2	3.8	0.39	126.9	0.98
VS W10/2	limestone	8.0	-		0.1	-	-	0.8	-
CM 1767	limestone	6.1	-		1.0	1.0	-	7.6	-
ECRM 752-1	limestone	3.9	0.19		1.2	0.3	0.15	11.9	0.12
UN AK	aragonite	2.8	2.76		1.1	0.8	-	10.9	-
BAM RS3	calcite	0.8	0.20		<0.02	<0.01	-	-	-

IPT - Insituto do Pesquisas Tech. do Estado de Sao Paulo, Brazil.
ECISS - European Committee for Iron and Steel Standardisation.
NIST - National Institute of Standards and Technology, USA.
ICRM - Institute for Certified Reference Materials, Russia
CMSI - China Metallurgical Standardization Research Institute, Beijing
BAS - Bureau of Analysed Samples Ltd, Newnham Hall, Middlesborough, UK.
IMRM - Institute of Mineral Raw Materials, Czech Republic
BAM - Bundesanstalt fur Materialforschung und-prufung, Germany

Table 3.2 Certified Reference Materials

Among the certified reference materials listed in Table 3.2 one standard closely meeting the requirements for foraminiferal calcite is ECRM 752-1 (alternative name BCS-CRM 393), a limestone CRM issued by the Bureau of Analysed Samples Ltd. UK. The calculated Mg/Ca ratio of ECRM 752-1 is 3.9 mmol/mol, within the range of typical planktonic foraminifera samples. Calculated Al/Ca, Fe/Ca, Si/Ca and Ti/Ca ratios, indicating the presence of contaminant silicate minerals and associated non-carbonate Mg, are low, although higher than observed in cleaned foraminifera [Barker *et al.*, 2003]. The certified element concentrations of ECRM 752-1 are insufficiently precise

to permit direct use as a foraminiferal Mg/Ca CRM; propagation of the concentration errors produces a 6.8 % (r.s.d.) error on the calculated Mg/Ca ratio. However, if this material is sufficiently homogeneous it has potential as an Mg/Ca consistency standard for use within and between laboratories.

ECRM 752-1 was prepared from a Derbyshire, UK, limestone and is supplied as a powder, ground to pass a 75 μm sieve. Enquiries of the manufacturer confirmed that this material was prepared in a single batch, but is packed according to demand with individual bottles labelled with a packing lot number (Bureau of Analysed Samples, pers. comm.). Determination of its Mg/Ca homogeneity, both within the calcium carbonate, and the contribution from accessory mineral phases, is necessary in order to assess its suitability as a reference material for foraminiferal Mg/Ca. We performed homogeneity tests on two separate bottles of ECRM 752-1, taken from the same packing lot number, 0973, using sample weights in the range 0.1 mg to 1000 mg.

3.3.1 Analytical methods

Replicate aliquots of 10, 50,100, 250, 500 and 1000 mg were weighed from each of two 100g bottles of ECRM 752-1 into acid cleaned (10% HNO_3, overnight) and dried low density polyethylene (LDPE) bottles. Samples were dissolved in 0.075M HNO_3 in line with foraminiferal sample preparation. No sample treatment was employed before dissolution. Dissolution volumes were maintained in proportion to sample weights to give constant $[Ca^{2+}]$ of ~ 400 μg/g. (i.e. 10 mg in 10 ml, 50 mg in 50 ml etc). In the case of smaller sample sizes, 1.0 and 0.1 mg, replicate aliquots were weighed into acid cleaned polypropylene microcentrifuge tubes and dissolved in 1ml or 0.5 ml 0.075M HNO_3 respectively. The powder dissolved easily, with no particles visible to the naked eye remaining and solutions were analysed both with and without centrifugation. 0.5ml aliquots were centrifuged using an Eppendorf model 5415 C microcentrifuge (10 mins. >= 6000 rpm). Between six and twelve replicate weighings were analysed after centrifugation at each weight, but not all samples were analysed without centrifuging. Solutions were diluted to $[Ca^{2+}]$ = 60 μg/g and element ratios determined by ICP-OES using a Varian Vista Axial instrument following the procedure of de Villiers *et al,* [2002]. The analytical and instrumental conditions are summarised in Table 3.3.

Sample wt. (mg)	0.075M HNO_3 (ml)	Dissolution vessel	[Ca] (μg/g)
1000	1000	1000 ml LDPE bottle	400
500	500	500 ml LDPE bottle	400
250	250	250 ml LDPE bottle	400
100	100	125 ml LDPE bottle	400
50	50	60 ml LDPE bottle	400
10	10	15 ml LDPE bottle	400
1	1	1.5 ml PP microcentrifuge tube	400
0.1	0.5	0.5 ml PP microcentrifuge tube	80
All solutions diluted to constant Ca concentration for analysis:			60
Instrument		Varian Vista Simultaneous ICP-OES	
Category		**Parameter**	**Setting**
Plasma:		Configuration	Axial
		RF Power	1.2 kW
		Plasma gas flow	15 L/min
		Auxiliary gas flow	1.5 L/min
		Nebuliser gas flow	1.0 L/min
Nebuliser		Glass Expansion, Micromist	0.2 ml/min
Spraychamber		Glass expansion, Cinnabar Cyclonic	
Measurement		Integration time	5 s
		Replicates	6

LDPE – low density polyethylene, PP – polypropylene

Table 3.3 Analytical and Instrumental Conditions

Solutions were always analysed (both with or without centrifugation) on the same day as samples were dissolved, although the entire experiment was performed over a number of days. The instrument was calibrated using the standard solutions described in Section 3.2. Dilution of samples and standard solutions to constant [Ca] permits instrument calibration using the intensity ratio method, with a Ca concentration of 60 μg/g chosen. [de Villiers *et al,* 2002]. Within run precisions of 0.3% or better were

obtained for replicate Mg/Ca determinations of a solution (Q5) containing [Ca^{2+}] = 60 µg/g, Mg/Ca = 5.130 mmol/mol, Sr/Ca = 2.088 mmol/mol and no correction was applied for instrument drift during a run. Daily instrument calibration differences produced mean values for solution Q5 ranging from –0.73% to + 0.30 % of its expected Mg/Ca ratio and results were normalised to the Mg/Ca ratio for solution Q5 to account for this variation.

3.3.2 Results

The Mg/Ca and other element ratios measured in material from the two bottles of ECRM 752-1, using sample weights in the range 10 – 1000 mg, are summarized in Table 3.4. The mean Mg/Ca ratios and standard deviations obtained for each set of analyses, including those using smaller sample weights down to 0.1 mg, are plotted against sample weight in Figure 3.1a.

Results after centrifuging agree well, both within and between the two bottles analysed, over the range of sample weights from 10 mg to 1000 mg and confirm the homogeneity of Mg/Ca within the readily soluble carbonate material. Inhomogeneity would be indicated by increasing scatter in the data with decreasing sample size but this was not observed, the standard deviations for the sets of analyses remaining similar over the five orders of magnitude weight range (Figure 3.1a). However, higher Mg/Ca ratios were consistently measured for the smallest sample weights. Small samples, 1.0 and 0.1 mg, were dissolved in polypropylene microcentrifuge tubes and it is likely that sufficient Mg was extracted from the polypropylene to produce these higher Mg/Ca ratios. An addition of < 0.5 ng Mg to 0.1 mg sample would be required to increase its Mg/Ca ratio from 3.75 mmol/mol, the average for all samples weighing from 10 to 1000 mg, to 3.77 mmol/mol, the average for 0.1 mg. This contribution is within the range of Mg blank values measured in this laboratory for polypropylene microcentrifuge tubes (Eppendorf SafeLok) after acid cleaning.

	mmol/mol						
	Mg/Ca	**Sr/Ca**	**Al/Ca**	**Fe/Ca**	**Mn/Ca**	**Si/Ca**	**Ti/Ca**
	Not Centrifuged						
Bottle 1							
Mean	3.849	0.189	0.97	0.210	0.143	1.34	0.025
s.d.	0.034	0.002	0.19	0.029	0.006	0.37	0.010
r.s.d. (%)	0.87	1.29	19.5	13.7	4.2	27.8	40.3
on	34	34	34	34	34	19	34
Bottle 2							
Mean	3.810	0.182	0.74	0.174	0.143	1.08	0.015
s.d.	0.013	0.010	0.17	0.017	0.005	0.22	0.005
r.s.d. (%)	0.35	5.25	22.6	9.7	3.7	20.2	33.9
on	34	34	34	34	34	34	34
	Centrifuged						
Bottle 1							
Mean	3.749	0.189	n.d.	0.076	0.140	n.d.	n.d.
s.d.	0.018	0.004		0.007	0.004		
r.s.d. (%)	0.47	1.92		9.21	2.83		
on	59	59		59	59		
Bottle 2							
Mean	3.750	0.186	n.d.	0.075	0.141	n.d.	n.d.
s.d.	0.012	0.008		0.003	0.004		
r.s.d. (%)	0.33	4.47		4.5	3.1		
on	59	59		59	59		
Detection limit			0.13	0.024	0.006	0.049	0.007

Table 3.4 includes all results obtained using sample weights from 10 – 1000 mg, but excludes results obtained using smaller sample weights. n.d. – below detection

Table 3.4 ECRM 752-1, average element ratios obtained using sample weights in the range 10 – 1000 mg.

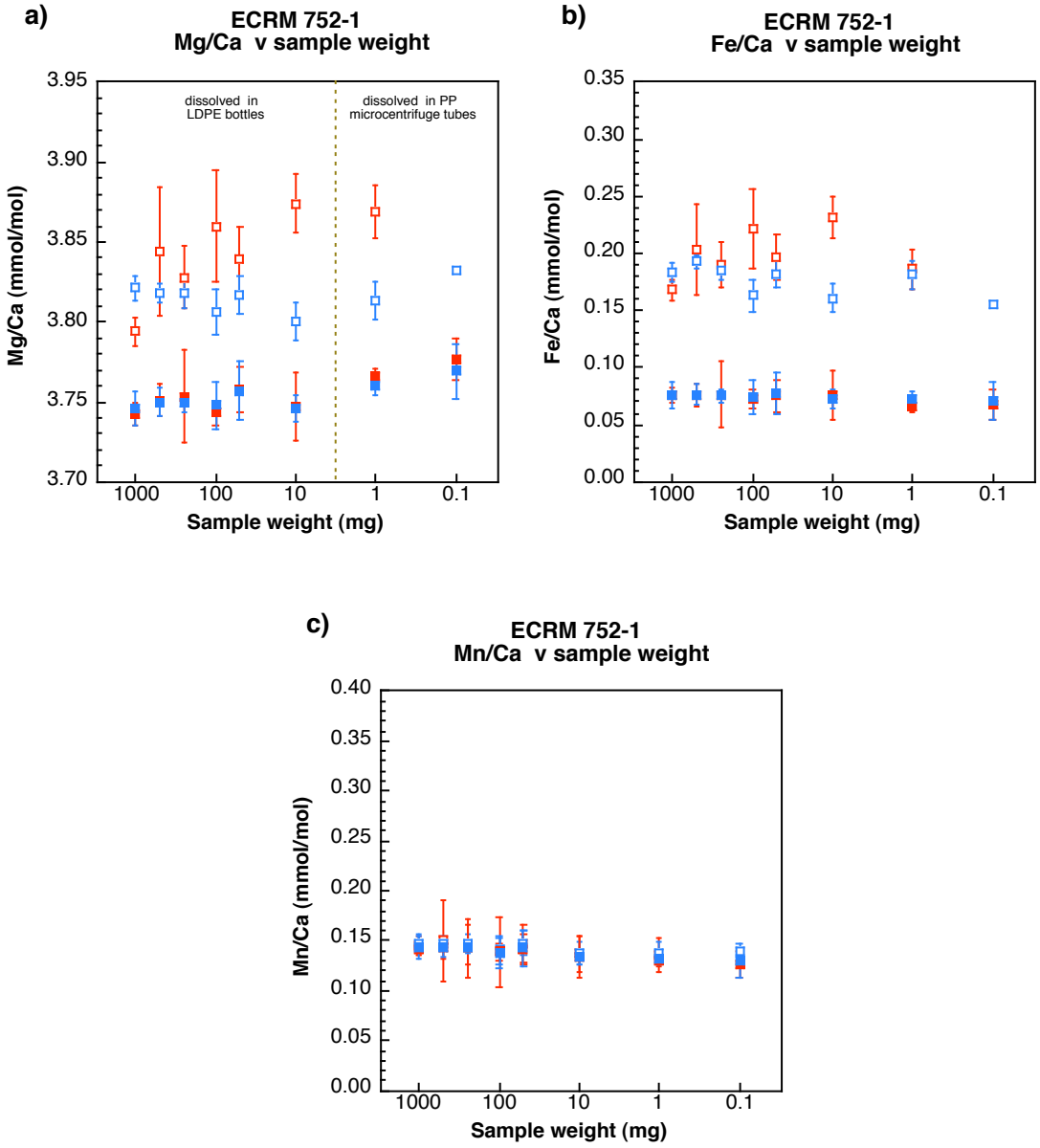

Figure 3.1 Homogeneity of ECRM 752-1, measured element ratios v sample weight: a) Mg/Ca; b) Fe/Ca; c) Mn/Ca.
Open symbols – not centrifuged. Solid symbols – centrifuged after dissolution. Red – 1st bottle, blue – 2nd bottle.

The differences between results for centrifuged and non-centrifuged samples clearly demonstrate the effect of suspended insoluble material, carried through the nebuliser into the plasma torch, on Mg/Ca ratios. Non-centrifuged samples contain higher and more variable Mg/Ca (Table 3.4, Figure 3.1a) consistent with higher Fe/Ca (Figure 3.1b), demonstrating the presence of other mineral phases in this material. Fe/Ca falls to consistent but non-zero values on centrifugation (Figure 3.1b, 3.2a), suggesting that

Fe is associated both with the readily soluble carbonate and with the insoluble suspended material. In contrast, Mn/Ca ratios (Figure 3.1c) show very little difference between centrifuged and non-centrifuged determinations. Results for Al/Ca, Si/Ca and Ti/Ca (Table 3.4) show the presence of these elements in the suspended material. When analysed after centrifuging, concentrations of these elements fall close to detection limits by ICP-OES. Detection limits, estimated as three times the standard deviation of the blank were, Al, 0.005 μg/g, Fe, 0.002 μg/g, Mn, 0.001 μg/g, Si, 0.002 μg/g, Ti, 0.001 μg/g, giving element ratio detection limits at $[Ca^{2+}]$ = 60 μg/g of Al/Ca, 0.126 mmol/mol, Fe/Ca, 0.024 mmol/mol, Mn/Ca, 0.006 mmol/mol, Si/Ca, 0.049 mmol/mol, Ti/Ca, 0.007 mmol/mol. As element concentrations approach the detection limits, calculated element ratios become unreliable because of the domination of the intensity signal by baseline noise and any interferences on the measured wavelengths. We therefore used intensity data for these elements to demonstrate the effect on Mg/Ca from non-carbonate phases. Figure 3.2b shows Mg/Ca plotted against Al intensity, after correction of the Al intensity signal at 396.15 nm for the contribution from 60 ppm Ca in solution. The correlation between Mg/Ca and Al indicates aluminosilicate minerals and also shows differences between the two bottles. Similarly, a plot of Mg/Ca against Si (Figure 3.2c), after subtraction of the Si intensity of the acid blank, clearly demonstrates the effect of un-dissolved silicate phases on Mg/Ca determinations. The close correlation of Al with Si (Figure 3.2d) reinforces this conclusion. The contaminant silicate material must have remained mainly in suspended form to permit centrifugation to lower the Mg/Ca and minor element ratios, but its contribution to the dissolved phase depends on its mineralogy, the acid used and the time interval between the addition of acid and removal of the dissolved phase after centrifuging. The reproducibility of Mg/Ca and Fe/Ca after centifuging (Figure 3.1a, 3.1b) implies that any dissolution of contaminant silicate minerals was also reproducible under the conditions used. More detailed experiments would be necessary to quantify the contribution from suspended silicate minerals to the dissolved phase under different conditions.

Measurements of the Sr/Ca ratio (Table 3.4) of this material confirmed the calculated ratio of 0.19 mmol/mol (Table 3.2), much lower than Sr/Ca of 1.0 – 1.5 mmol/mol typically found in foraminiferal calcite.

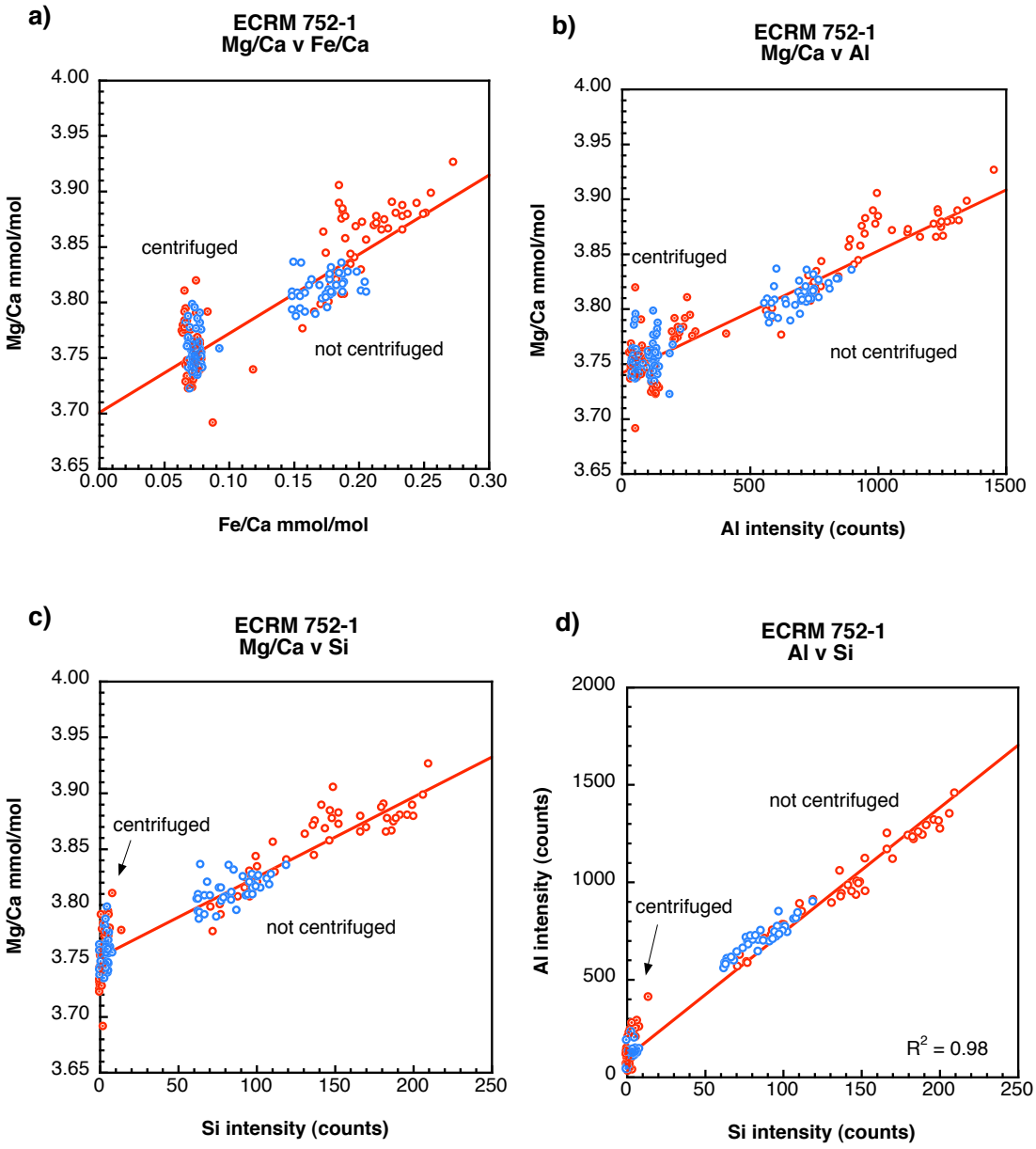

Figure 3.2 The effect on Mg/Ca of the contribution from insoluble alumino-silicate minerals: a) Mg/Ca v Fe/Ca; b) Mg/Ca v Al; c) Mg/Ca v Si; d) Al v Si. Open symbols – not centrifuged. Partially filled symbols – centrifuged after dissolution. Red – 1st bottle, blue – 2nd bottle.

Mean measured Mg/Ca ratios of 3.849 mmol/mol (0.034 s.d., 0.87% r.s.d.) and 3.810 mmol/mol (0.013 s.d., 0.35% r.s.d.,) were obtained for 34 determinations from each of the two bottles of ECRM 752-1 when analysed without centrifugation. The differences in Mg/Ca within and between the two bottles being a result of the contribution of Mg from undissolved aluminosilicate minerals. In comparison, where samples were

centrifuged after dissolution, average values of Mg/Ca = 3.749 mmol/mol (0.018 s.d., 0.48% r.s.d.) and 3.750 mmol/mol (0.012 s.d., 0.32% r.s.d.,) were obtained on 59 determinations from each of the two bottles of ECRM 752-1 tested.

Measurement precisions more than an order of magnitude better than those calculated from the reference analysis certificate reflect partly the improved precision of modern methods, but also the use in this study of a single technique applied to two bottles of material taken from the same packing lot. Investigation of many bottles from more than one packing lot would be expected to give worse reproducibility. However, it is clear from this study (see Figure 3.2) that the major contribution to inhomogeneity within this material is from contaminant silicate minerals; not visible to the naked eye but visible microscopically as small particles within the powder. Homogeneity of the readily soluble calcite material across many bottles may therefore not be significantly different from that established using the two bottles tested in this study. The dissolution protocol employed is important, the primary objective being to check instrumental calibrations. It is obviously necessary for laboratories to record a batch number and, if discrepancies are found, it would be a simple exercise for collaborating laboratories to exchange material. It is preferable to dissolve a sample weight in the range 10 – 100 mg to give a high Ca concentration and analyse an aliquot, rather than dissolving a sample weight more typical of foraminifera analyses, in order to minimise the effect of the Mg blank from dissolution vials (Figure 3.1a).

3.4 Conclusions

Errors involved in the preparation of accurate calibration standards for Mg/Ca and Sr/Ca determinations in foraminiferal calcite represent a significant contribution to inter-laboratory analytical precision. To minimise systematic errors in the preparation of mixed standards we prepared initial single element standard solutions starting from primary solid standards. However, the use of standard solutions for inter-laboratory calibration is not ideal because of the difficulty of maintaining the integrity of small volumes of liquid standards.

We have investigated commercial reference materials to determine whether there are existing carbonate standards of appropriate composition which could be used as reference materials for Mg/Ca determinations in foraminiferal calcite. In the absence of a pure calcium carbonate standard certified for Mg/Ca, we propose that ECRM 752-1, a limestone CRM containing Mg/Ca within the range of typical planktonic foraminifera, is a suitable solid standard for interlaboratory calibration. Two bottles of this material, from the same packing lot number, were tested for homogeneity with respect to their Mg/Ca ratio. The presence of minor alumino-silicate mineral phases affected the homogeneity of the bulk material but, after removal of these phases by centrifugation the average results for the two bottles tested (Table 3.4) showed that this material is homogenous within the precision of daily instrumental Mg/Ca determinations over a range of sample weights from 10 - 1000 mg, with Mg/Ca = 3.75 mmol/mol (0.015 s.d., 0.41% r.s.d.) on 118 determinations from the two bottles. This reproducibility is equivalent to an estimated error in Mg/Ca temperature calculation of +/- 0.1 ^{o}C. The reproducibility of Mg/Ca ratios confirms the potential of the ECRM 752-1 standard as a reference material for Mg/Ca determinations in foraminiferal calcite, provided that care is taken to remove undissolved contaminant silicate phases before analysis.

We chose to investigate ECRM 752-1 because of its Mg/Ca ratio within the mid-range of planktonic foraminifera and its ready availability. Investigation of other reference materials (Table 2) are necessary to determine how their suitability compares to ECRM 752-1.

Chapter 4

Inferring climate variability from records of planktonic foraminiferal Mg/Ca, oxygen isotopes and shell weight in the Southern Ocean

4.1 Introduction

One of the controlling factors in the Earth's climate system is the exchange of heat between the Southern Ocean and the three major ocean basins. Approximately half of the water that replenishes the abyssal ocean originates in the Southern Ocean. This water is rapidly mixed with deep water originating in the Atlantic Ocean by the Antarctic Circumpolar Current, and northward transfer of deep water from the Southern Ocean into the Pacific and Indian Oceans is a major component of global thermohaline circulation [Broecker, 2004]. In the surface ocean, heat transfer from the equator to the pole is controlled by the locations of the major oceanic fronts, the Subtropical Front, Subantarctic Front and Antarctic Polar Front. Palaeoceanographic studies of water mass variability and the migration of oceanic fronts over glacial-interglacial cycles are critical to understanding glacial-interglacial climate change.

The Southwest Pacific Ocean east of New Zealand is a region where bathymetry exercises a strong influence on the locations of both surface ocean fronts and deep ocean currents. The Subtropical Front, Subantarctic Front and Antarctic Polar Front all occur in this region which is also the primary gateway for deep ocean circulation into the Pacific Ocean, the Deep Western Boundary Current through the Southwest Pacific Ocean providing 40% of the flux of cold bottom water into the major ocean basins [Carter *et al*.,1999].

This chapter uses records of planktonic foraminiferal Mg/Ca, oxygen isotopes and shell weight to investigate the palaeoeanographic history of this region and the applicability

of the Mg/Ca temperature proxy. Temperature is the dominant control on foraminiferal Mg/Ca although species habitat, the season and depth of calcification, and the effect of dissolution are all important and can bias paleoceanographic reconstructions. In order to investigate the relative importance of these controls on Mg/Ca, records are compared from three sites at different water depths in a transect across the Subtropical Front (ODP Site 1123, CHAT 16K and MD97-2120) in the Southwest Pacific Ocean (Figure 4.1). Core locations are described in Section 4.1.2 and detailed in Table 4.1.

Mg/Ca and $\delta^{18}O$ ratios of *Globogerina bulloides* from ODP Site 1123, north of the Subtropical Front on Chatham Rise, were measured to reconstruct changes in sea surface temperature and seawater oxygen isotopic composition ($\delta^{18}O_w$) over the past 440,000 years. These results are compared to a 340,000 year Mg/Ca record published by Pahnke *et al*. [2003] from site MD97-2120, located south of the Subtropical Front. Over glacial Terminations I and II, at both sites and also at site CHAT 16K, detailed Mg/Ca, $\delta^{18}O$ and shell weight records were obtained from two narrow size fractions (250-300 μm and 300-355 μm) of *Globigerina bulloides* and *Globorotalia inflata*. Combining these data permitted investigation into the effects of hydrography, foraminiferal habitat and dissolution susceptibility as controls on Mg/Ca.

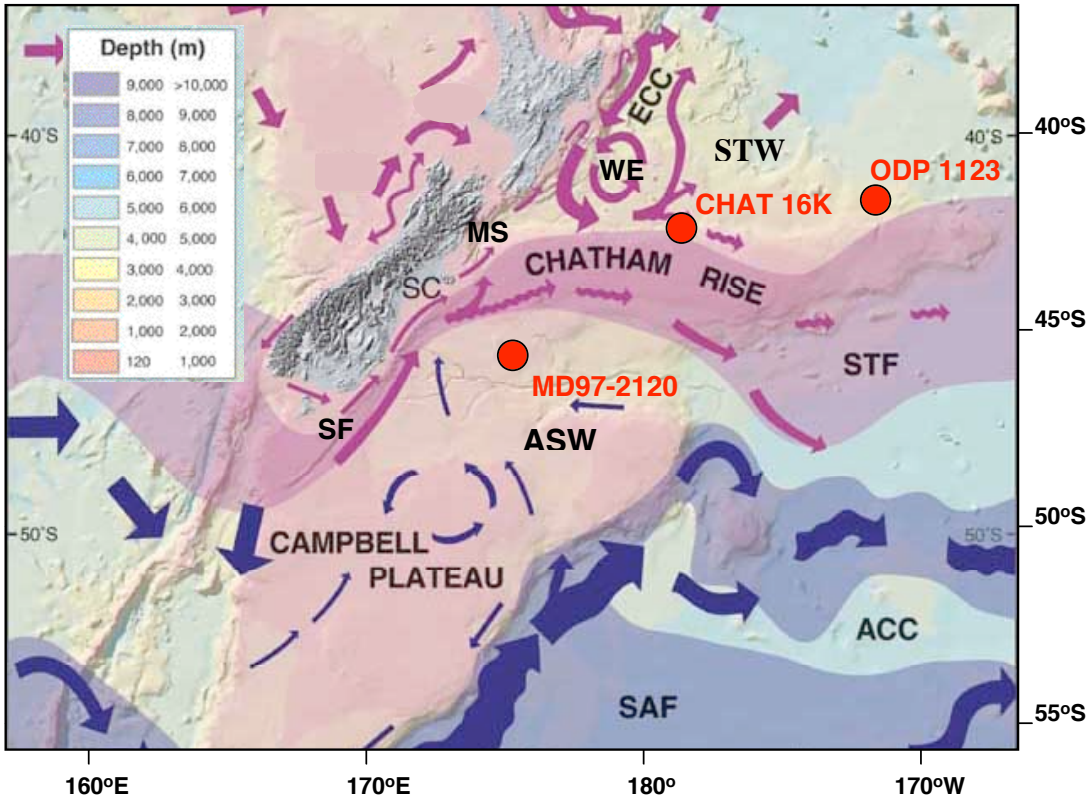

ECC	East Cape Current	STF	Subtropical Front
WE	Wairarapa Eddy	SAF	Subantarctic Front
MS	Mernoo Saddle	ACC	Antarctic Circumpolar Current
SC	Southland Current	SF	Southland Front
ASW	Australian Subantarctic Water	STW	Subtropical Water

Figure 4.1 Modern hydrography and bathymetry East of New Zealand (after Carter 2001; Carter *et al*., 1998) with locations of cores indicated.

4.1.1 Influence of hydrography

The presence of three fronts south and east of New Zealand results in strong regional gradients in sea-surface temperature. The Subtropical Front separates comparatively warm saline Subtropical Water to the north from colder, fresher Australian Subantarctic water to the south (Figure 4.1). The warm, surface, East Cape Current flows south past New Zealand N. Island then turns east along the north side of the Subtropical Front, with the Wairarapa Eddy, a permanent warm core eddy, lying north of Chatham Rise to the east of New Zealand N. Island [Roemmich and Sutton, 1998; Sutton, 2001]. The cold Southland Current flows northeast along the east coast of New Zealand S. Island and splits into two on reaching Chatham Rise, a minor portion flowing through the Mernoo Saddle where a depth of 580 m separates Chatham Rise from the continental

slope, the remainder flowing east along Chatham Rise on the south side of the Subtropical Front [Heath, 1981]. Chatham Rise extends at a water depth of ~ 400 m for over 1000 km at latitude 44° S towards the Chatham Islands. East of Chatham Rise the East Coast Current and the Southland Current merge into the South Pacific Current. The Subtropical Front lies along the crest of Chatham Rise, approximately following the 15 °C surface isotherm in summer and the 10 °C surface isotherm in winter [Heath, 1981; 1985]. Seasonally, the Suptropical Front may move over Chatham Rise by up to 2° of latitude, between ~44°S in spring and ~42°S in late summer and autumn [Chiswell, 1994; 2002].

The contrasting surface water properties north and south of the Subtropical Front are clearly illustrated by a meridional salinity section for the southwest Pacific Ocean (Figure 4.2). This shows also the influence of Antarctic Intermediate Water at sites MD97-2120 and CHAT 16 compared to Lower Circumpolar Deep Water influencing ODP Site1123. The deep western boundary current, at depths below ~ 2000 m, flows northwestward over ODP Site 1123, after passing through the Valerie Passage at the eastern end of Chatham Rise [Carter *et al.,* 2004a].

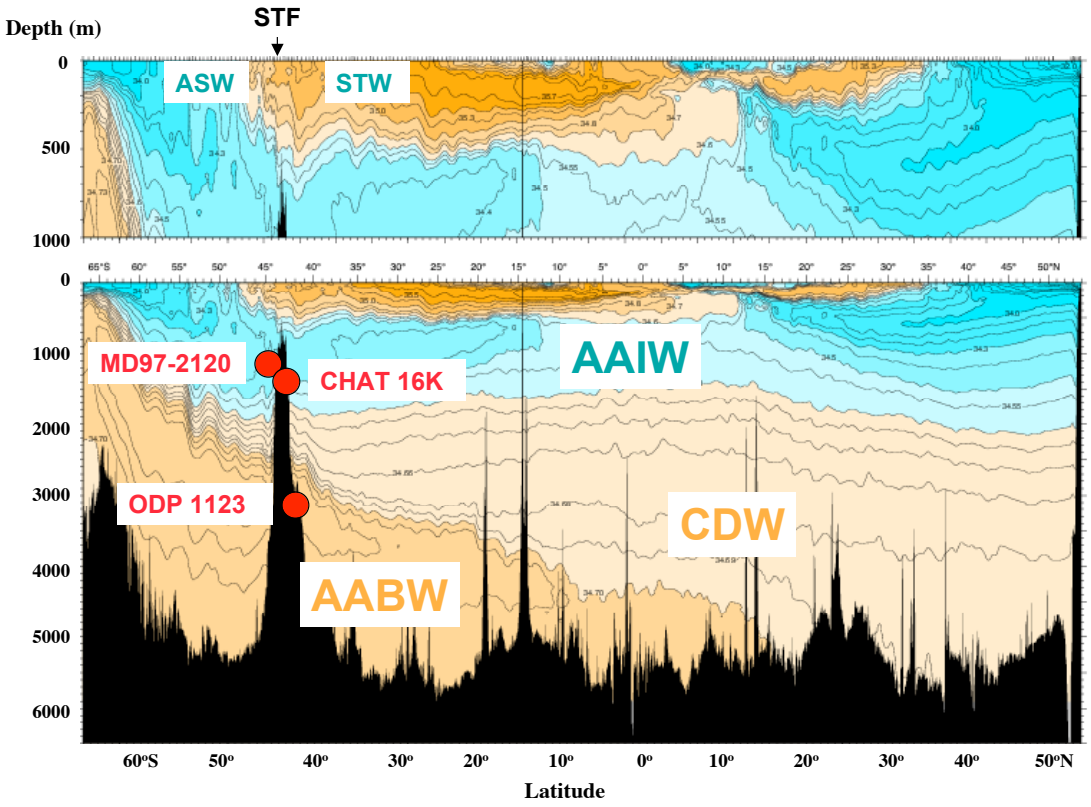

STF Subtropical Front
STW Subtropical Water
CDW Circumpolar Deep Water
ASW Australian Subantarctic Water
AAIW Antarctic Intermediate water
AABW Antarctic Bottom Water

Figure 4.2 World Ocean Circulation Experiment meridional salinity transect in the southwest Pacific, WOCE line P15, 165°W

There is substantial evidence that, during glacial periods, the Subtropical Front east of New Zealand remained aligned to the topography of Chatham Rise [Fenner *et al.*, 1992; Nelson *et al.*, 1993; Weaver *et al.*, 1998; Sikes *et al.*, 2002; Fenner and Di Stefano, 2004; Scott & Hall, 2004] whereas in the open ocean it may migrate through as much as 6° of latitude [Howard and Prell, 1992]. Close to New Zealand S. Island the Subtropical Front extends to the south west as the Southland Front (Figure 4.1) which, paradoxically, may have migrated southeasterly during glacial periods [Carter *et al.*, 2004b; Wilson *et al.*, 2005].

The effect of glacial northward shift of the Subantarctic Front, if the Subtropical Front remained in the same location, would be an increased temperature gradient between the two fronts. Stronger glacial cooling on the southern side of the Subtropical Front would

have resulted in greater temperature differences between sites located north and south of the Subtropical Front (Figure 4.1).

Southward migration of the Subtropical Front during the warm interglacial Marine Isotope Stages 11 and 5.5 was documented by Wilson *et al*. [2005]. The consequence of migration of the Subtropical Front south of site MD97-2120 would have been higher surface water temperatures over this site and a reduced interglacial temperature gradient between site MD97-2120 and the more northerly sites (Figure 4.1).

The hydrography of the Southwest Pacific Ocean has a significant influence on modern foraminiferal abundances, both regionally and seasonally [Weaver *et al*., 1997; King and Howard, 2001]. In a study of seasonal foraminifera fluxes, King and Howard [2001] demonstrated the close association between foraminiferal assemblages and water masses north and south of Chatham Rise, and revealed differences in both the composition and timing of foraminiferal productivity between water masses. Results from sediment traps located north and south of Chatham Rise show highly seasonal flux patterns, with the inference that sedimentary records also must reflect seasonal fluxes. King and Howard [2001] observed distinctly different foraminiferal compositions north and south of Chatham Rise, *Globorotalia inflata* being dominant over *Globigerina bulloides* and *Neogloboquadrina pachyderma(*d) in the warmer Subtropical Water north of Chatham Rise, whereas in Subantarctic Water south of Chatham Rise the assemblage is dominated by *G. bulloides*. Additionally, these authors found different seasonal patterns in foraminifera fluxes north and south of Chatham Rise. The major foraminifera flux at the site south of Chatham Rise occurred in September, during Austral spring, whereas the flux continued through spring, summer and autumn at the site north of Chatham Rise.

The foraminifera abundances observed in sediment traps by King and Howard [2001] are reflected in modern sediments, with a Transitional assemblage dominated by *G. inflata* found in core top samples north of the Subtropical Front and a Subpolar assemblage dominated by *G. bulloides* occuring south of the Subtropical Front [Weaver *et al*., 1997]. Over longer timescales, foraminiferal abundances in downcore records from sites north and south of the present day Subtropical Front show glacial to

interglacial variation. Faunas north of the Subtropical Front are dominated by *N. pachyderma(*d), *G. inflata* and *G. bulloides* during both glacial and interglacial periods. South of the Subtropical Front, glacial faunas are strongly dominated by *N. pachyderma(*s) whereas during interglacials *N. pachyderma(*d), *G. bulloides* and *G. inflata* become more abundant [Schaefer *et al.,* 2005, Wilson *et al.,* 2005]. The coretop and downcore foraminiferal assemblages confirm that modern conditions are recorded and provide evidence for glacial to interglacial sea surface temperature changes.

4.1.2 Locations of cores

ODP Leg 181 Site 1123 (41° 47.15'S, 171° 29.94'W) is located 410 km northeast of the Chatham Islands, on the deep northeastern slopes of Chatham Rise (Figure 4.1) at a water depth of 3290 m [Carter *et al*., 1999]. The site lies beneath the southwest Pacific deep western boundary current within Lower Circumpolar Deep Water (Figure 4.2). This northernmost site in the transect is characterized by February sea surface temperature of 18ºC, a strong thermocline and a mixed layer depth of ~50 m and surface salinity of 35.1, compared to August sea surface temperature of 12ºC, no thermocline and surface salinity of 34.8 (Figure 4.3). Nearby core CHAT 1K at station S924 (41° 35'S, 171° 30.0'W), a short kasten core collected in the vicinity of ODP site 1123 [Weaver *et al*.,1998; Lean and McCave, 1998] was used to provide coretop samples not recovered at ODP Site 1123.

Site MD 97-2120 is located south of the Subtropical Front (45° 32.06'S, 174° 55.85'E) at a water depth of 1210m [Pahnke *et al.,* 2003], close to the location of DSDP Site 594, within the depth range of Antarctic Intermediate Water (Figure 4.2). In contrast to ODP Site 1123 this southernmost site of the transect experiences February sea surface temperature of 14ºC, August sea surface temperature of 8ºC and surface water salinities close to 34.4 throughout the year (Figure 4.3). Similar to ODP Site1123, thermal stratification over site MD97-2120 is greatest during February, with a mixed layer depth < 50 m, but minimal in August.

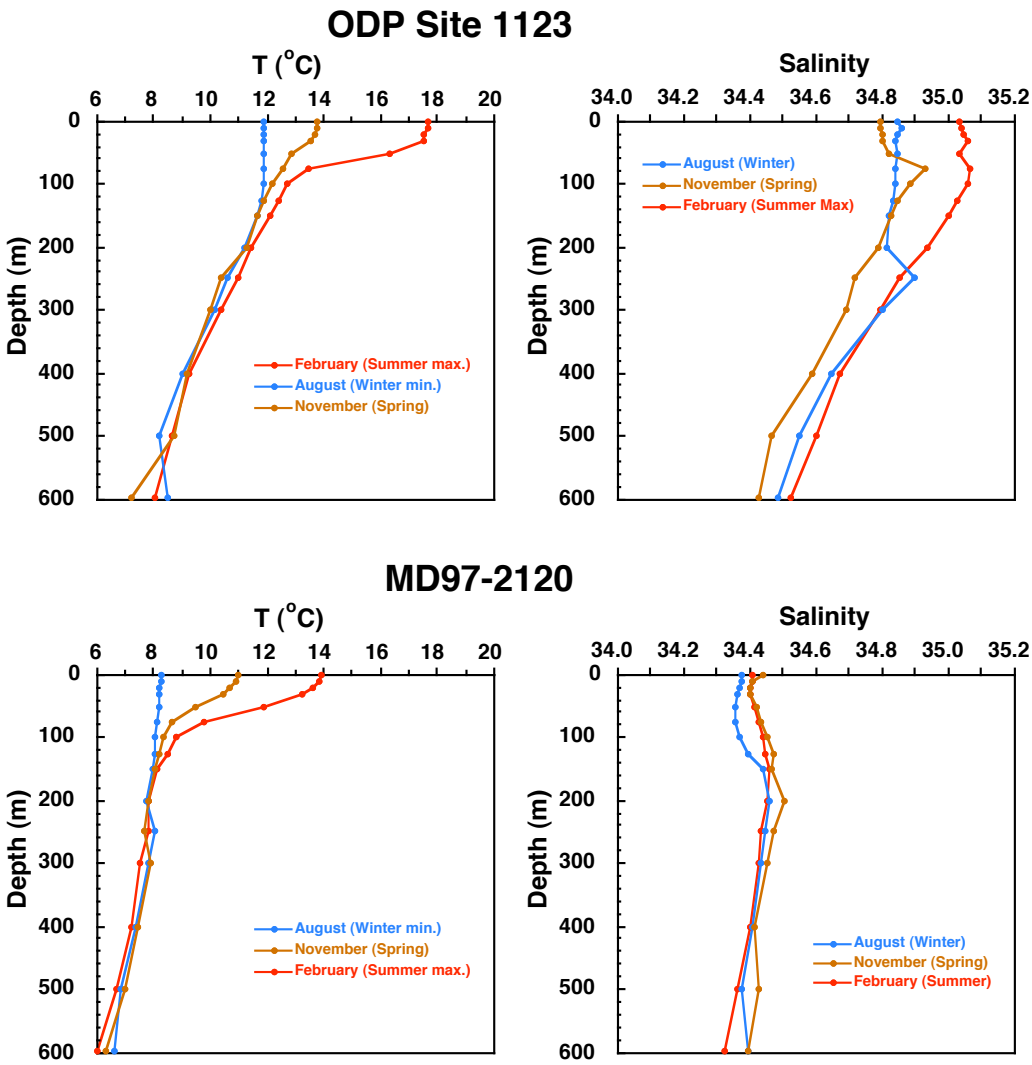

Figure 4.3 Seasonal temperature and salinity profiles for ODP Site 1123 and MD97-2120, north and south of Chatham Rise (Data from World Ocean Atlas 2001, Conkright *et al.*, [2002])

CHAT 16K (42° 23.0'S, 178° 29.9'W) lies north of the Subtropical Front close to the position of ODP Site 1125 and is the same location as core R657 studied by Weaver *et al.*, [1997; 1998] and Sikes *et al.*, [2002]. Modern surface water hydrography over this site is similar to hydrography over ODP Site1123. The shallower depth of CHAT 16K (1408m) compared to ODP Site1123 (3290m) should assist in distinguishing the effects of dissolution and hydrographic signals on foraminifera shell chemistry at the three sites.

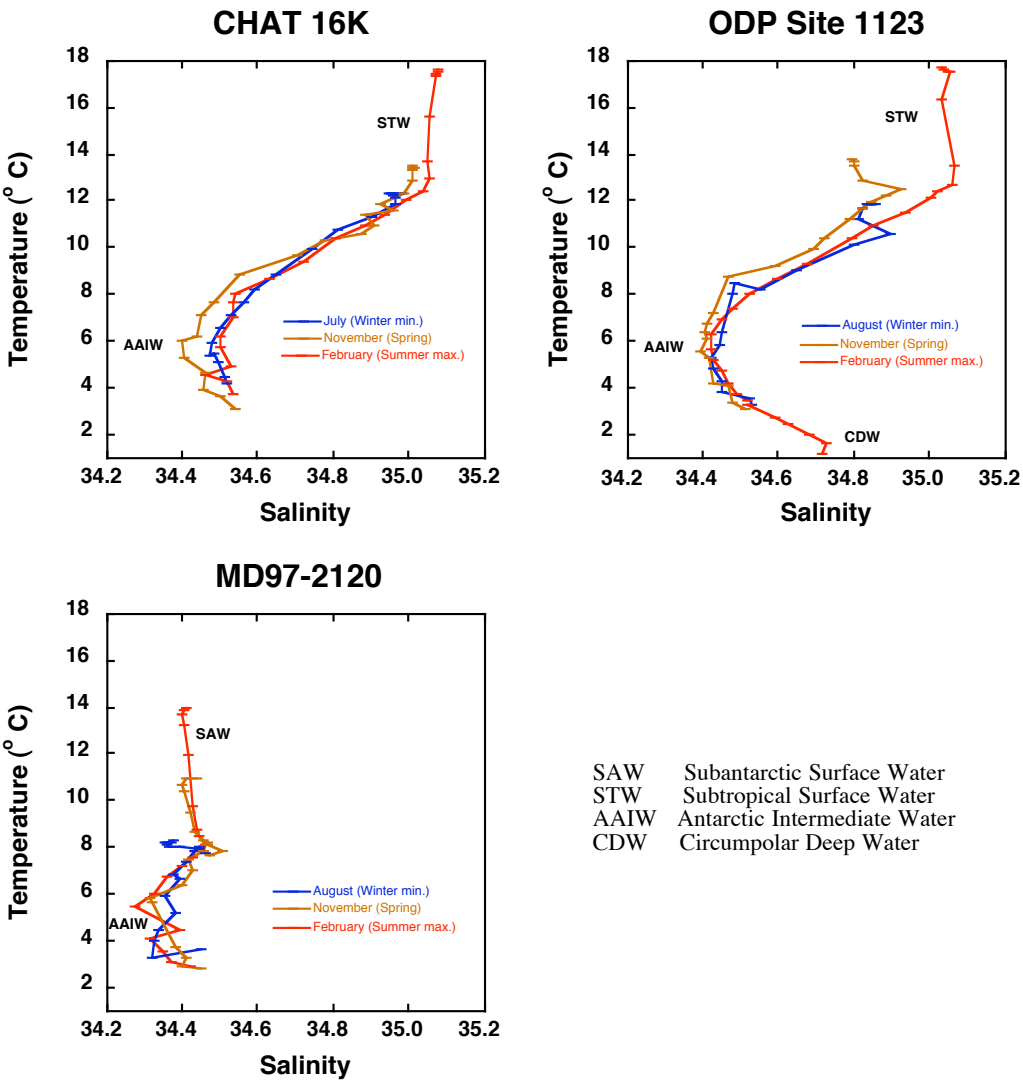

Figure 4.4 Temperature versus salinity at the three study sites. (Data from World Ocean Atlas 2001, monthly analyzed data from surface to 1500m, annual below 1500m. [Conkright *et al.*, 2002])

Plots of temperature versus salinity (Figure 4.4) clearly identify the water masses over the three sites. Site MD97-2120 lies within the core of Antarctic Intermediate Water with a bottom water salinity of 34.4 influencing this site at a depth of 1210 m. Over sites CHAT 16K and ODP Site1123 the core of Antarctic Intermediate Water, with a salinity minimum of ~34.4 and a temperature of ~6 °C, occurs at a water depth of approximately 1000 m (Figure 4.2). Circumpolar Deep Water is identified in Figure 4.4 over ODP Site1123 and its influence can be seen in the bottom water over CHAT 16K. A mixture of Antarctic Intermediate Water and Circumpolar Deep Water gives a bottom water salinity of 34.6 over CHAT 16K at a depth of 1408 m.

Details of the core locations, water depths, surface and deep water masses influencing the sites are summarised in Table 4.1.

Site	Latitude	Longitude	Depth (m)	Water masses Surface, deep
ODP 1123	41° 47.2'S	171° 29.9'W	3290	STW, CDW
CHAT 1K	41° 35.0'S	171° 30.0'W	3556	STW, CDW
CHAT 16K	42° 23.0'S	178° 29.9'W	1408	STW, AAIW, CDW
MD97-2120	45° 32.1'S	174° 55.8'E	1210	SAW, AAIW

STW Subtropical Surface Water
SAW Subantarctic SurfaceWater
AAIW Antarctic Intermediate Water
CDW Circumpolar Deep Water

Table 4.1 Locations of cores

4.1.3 Age models

A detailed age scale for core MD97-2120 was established by Pahnke *et al.,* [2003] using accelerator mass spectrometry ^{14}C dating over the interval 0 to 35 thousand years (ka). In the interval 40 – 72 ka these authors established the age scale by correlation of the benthic $\delta^{18}O$ record with that of core MD95-2042 in the northeast Atlantic [Shackleton *et al.,* 2000] and from 105 to 340 ka by correlation of the Mg/Ca derived sea surface temperature record with the Antarctic Vostok δD temperature record [Shackleton, 2000]. The age model yields sedimentation rates for core MD97-2120 between 15.5 cm kyr^{-1} during glacials and 6 cm kyr^{-1} during interglacials [Pahnke *et al.,* 2003].

The age model for ODP site 1123 is based on that constructed by Hall *et al.,* [2001] and refined between 0 and 340,000 years by tuning the benthic *Uvigerina spp*. $\delta^{18}O$ record to that for site MD97-2120 [F. Bassinot, pers. comm.]. The tuned age model gives sedimentation rates for ODP Site1123 during the period 0 to 340,000 years ranging from 1.7 to 5.9 cm kyr^{-1} (Figure 4.5), compared to between 2.1 and 5.1 cm kyr^{-1} calculated from the original age model [Hall *et al.,* [2001] and an age of ~6000 years for the top of the recovered core. The age model for core CHAT 1K used to provide recent Holocene samples was taken from Lean and McCave [1998].

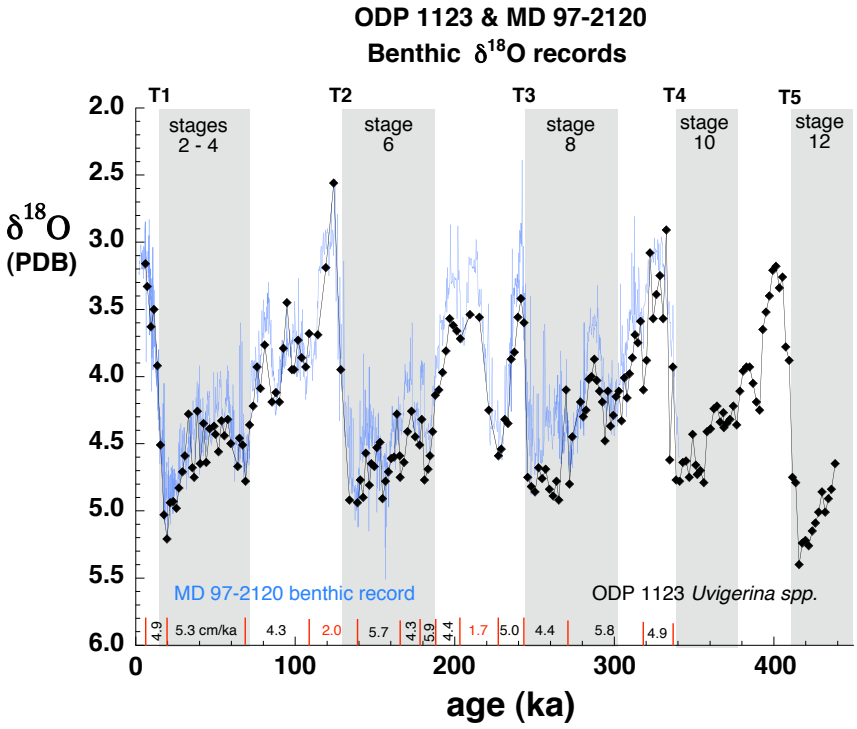

Figure 4.5 Age model for ODP Site 1123 tuned to MD97-2120
Red lines show age tie points, with calculated sedimentation rates.

The CHAT 16K age model was constructed from the benthic *Uvigerina spp.* $\delta^{18}O$ data [I.N. McCave, pers. comm.] giving sediment accumulation rates between 0.6 cm kyr^{-1} and 3.5 cm kyr^{-1}, the slowest of the three sites. The benthic *Uvigerina spp.* $\delta^{18}O$ records for CHAT 16K and ODP Site 1123 are compared in Figure 4.6.

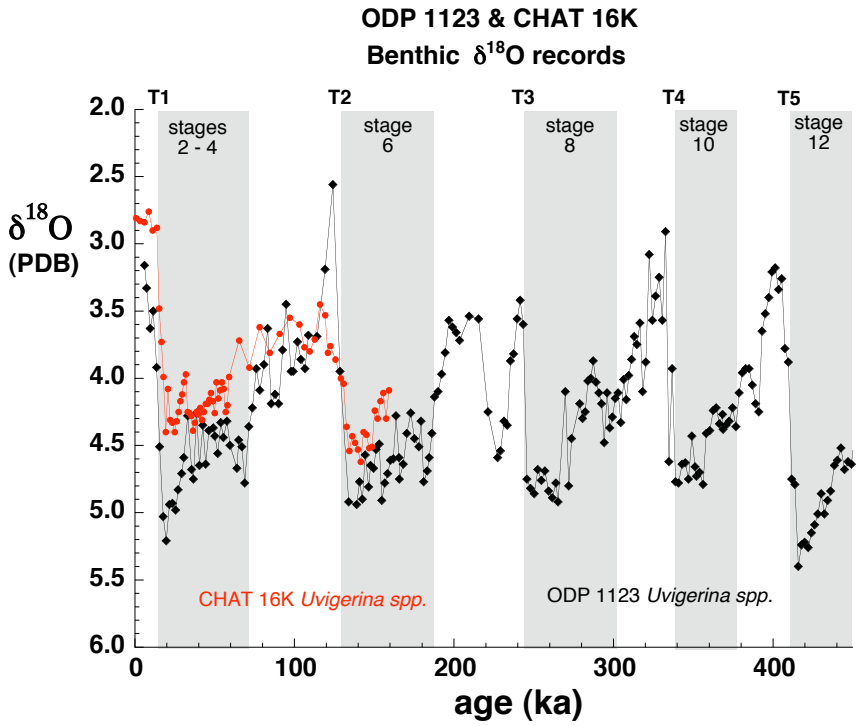

Figure 4.6 Benthic oxygen isotope records and age models at ODP Site 1123 and CHAT 16K. (ODP 1123 age model tuned to MD 97-2120 [F. Bassinot, pers. comm.] CHAT 16K age model from I.N. McCave).

4.2 Materials and methods

4.2.1 Sampling

Samples extending over the past 440 thousand years were taken from the top 18.2 m at ODP Site 1123. Initially, 199 samples of ~ 2 cm sediment thickness were taken at 10 cm intervals, with an average time resolution of ~ 2,200 years. Later, the core was re-sampled, again taking ~ 2 cm samples at 10 cm intervals but positioned between the original samples. This gave an additional 141 samples and improved the sampling interval to ~5 cm with an average time resolution of ~ 1,300 years. Foraminifera tests of *Globigerina bulloides* were picked from the 250-300 μm and 300-355 μm, and *Globorotalia inflata* from the 300-355 μm, size fractions of the washed sediment.. Details of samples taken are tabulated with the results in Appendix 2.

Core CHAT 1K, a 3.57 m kasten core used to provide coretop samples to supplement the ODP Site 1123 record, was sampled at 1 cm intervals to a depth of 10cm over the time interval from 0 to 6000 years, and at 4 cm intervals deeper in the core [Lean and McCave, 1998].

The 3.03 metre long core CHAT 16K was sliced at 1 cm intervals and *G. bulloides* and *G. inflata* were picked from the 250-300 μm and 300-355 μm size fractions of the washed sediment in the same manner as for ODP Site 1123. Mg/Ca and Sr/Ca ratios were determined on 50 samples over the time interval from 0 – 32.4 ka, covering glacial/interglacial Termination 1 with an average resolution of ~700 years. A further 20 samples were analysed over the interval 100 – 158 ka, covering glacial/interglacial Termination 2, at a resolution ranging from 1,800 to 3,200 years.

4.2.2 Analytical methods

Cleaning procedures and instrumental methods for foraminiferal Mg/Ca and Sr/Ca determination are discussed in detail in Chapter 2. A brief summary is given here. Analyses of *G. bulloides* and *G. inflata* were performed using between 20 and 70 individuals picked from the 300-355 μm or 250-300 μm size fraction, weighed on a 7 decimal place microbalance (0.1μg resolution) then crushed and split into two fractions to permit paired trace element and stable isotope analyses. Samples were cleaned following the procedure detailed in Appendix 1. Element ratios were determined by ICP-OES [de Villiers *et al.,* 2002] as described in Chapter 2.

The efficiency of the cleaning procedure was monitored during analyses by simultaneously measuring Al, Fe, Mn, Na, Si and Ti [see Chapter 2]. The criteria used to reject Mg/Ca data as potentially contaminated by Mg from clays or silicate minerals [Barker *et al.,* 2003] were; measured Al/Ca > 0.4 mmol/mol or Al/Mg > 0.2 mol/mol, Fe/Ca > 0.1 mmol/mol or Fe/Mg > 0.1 mol/mol, or Si intensity significantly greater than background. High Na/Ca (>10 mmol/mol) or Ti greater than its detection limit of 0.001 μg/g provided additional indication of suspect determinations.

At low solution concentrations and for low Mg/Ca ratios the analytical blank is the limiting factor to obtaining accurate results. Its effect is particularly important because of the shallow slope of Mg/Ca temperature calibration curves at low temperatures. Therefore, analyses with [Ca] < 40 ppm in solution were rejected as potentially unreliable because of the low Mg/Ca ratios involved. Detailed discussion of the Mg analytical blank and its effect on Mg/Ca ratios is given in Chapter 2.

4.3 A 440,000 year *Globigerina bulloides* Mg/Ca, shell weight and $\delta^{18}O$ record from ODP Site 1123

The downcore planktonic *G. bulloides* (300-355 μm) Mg/Ca, shell weight and $\delta^{18}O$ records from ODP Site 1123 are shown in Figure 4.7; glacial stages are shaded for clarity and glacial-interglacial terminations T1 through T5 are indicated. There were insufficient *G. bulloides* available for analyses in two sections of the core, from 300-330 ka and 370-410 ka during interglacial stages 9 and 11. The implications of this observation are discussed in detail in Section 4.5. The planktonic $\delta^{18}O$ record (Fig. 4.7c) shows surface water features in addition to the dominant 100,000 year cycle observed in the benthic *Uvigerina spp*. record (Figure 4.6).

Mg/Ca ratios lie in the range 1.12 – 2.49 mmol/mol (Fig. 4.7a), giving a temperature range of 7.5 ºC between minimum glacial temperature of 8.0 ºC and maximum interglacial temperature of 15.5 ºC using the *G. bulloides* temperature calibration of Mashiotta *et al*. [1999]. The anticipated large temperature changes over glacial Terminations 1 and 2 are not seen in this Mg/Ca record although a prominent temperature increase is visible at Termination 3.

The *G. bulloides* shell weight record (Fig. 4.7b) is closely correlated with $\delta^{18}O$ and displays a large range, from 9 μg to 28 μg for the average weight of individuals picked from the 300-355 μm size fraction. Typically 30 individuals were weighed, the number depending on availability and ranging from a minimum of 8 to a maximum of 60. Only 13 of the data points in Figure 4.7b are from samples of < 20 individuals. Heavier shell weights are observed in glacial periods and the lighter, interglacial, specimens must

reflect thinner wall thickness within the same size fraction. Interglacial specimens are less abundant than glacial, with very few individuals found in stages 9 and 11. The correlation of shell weight with $\delta^{18}O$ (Figure 4.8) suggests that shell weights in stages 9 and 11, if they had been available, would have been no heavier, and perhaps lighter, than those obtained for interglacial stages 5 and 7. The lack of specimens found in stages 9 and 11 is presumably a function of low initial weights and dissolution of thin fragile individuals.

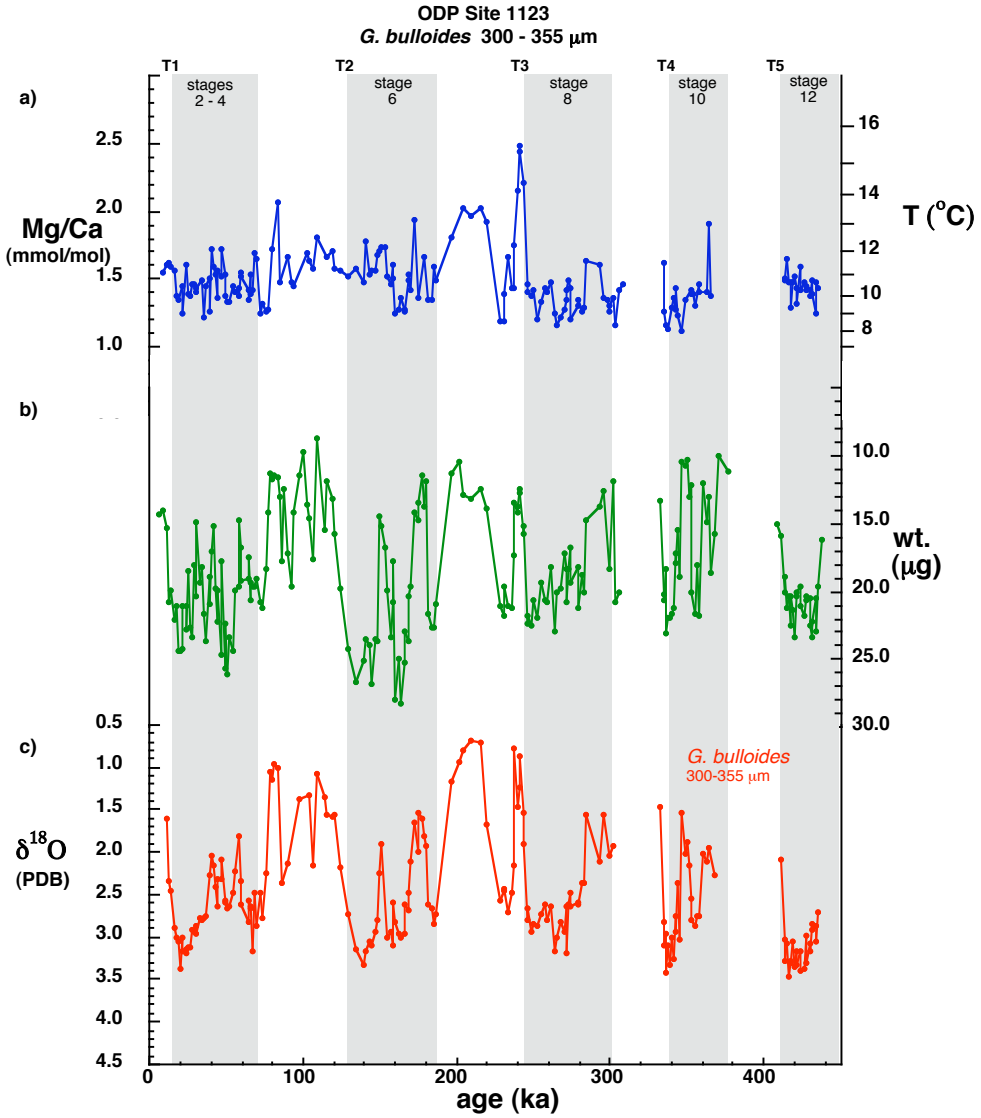

Figure 4.7 Records of a) Mg/Ca (with temperature scale using the equation of Mashiotta *et al.*, [1999]), b) average shell weight, c) $\delta^{18}O$ of *G. bulloides* (300-355 µm) at ODP Site 1123.

The shell weight record has analytical implications for Mg/Ca determinations because lighter, interglacial, specimens would be expected to have higher Mg/Ca ratios, but fewer individuals, with thin fragile shells, were available for analysis. Sample loss during the cleaning procedure was considerable for light (< 15 μg) specimens, and Mg/Ca data were examined critically, as described in section 4.2.2, to ensure results were not biased towards high Mg/Ca by the analytical procedure.

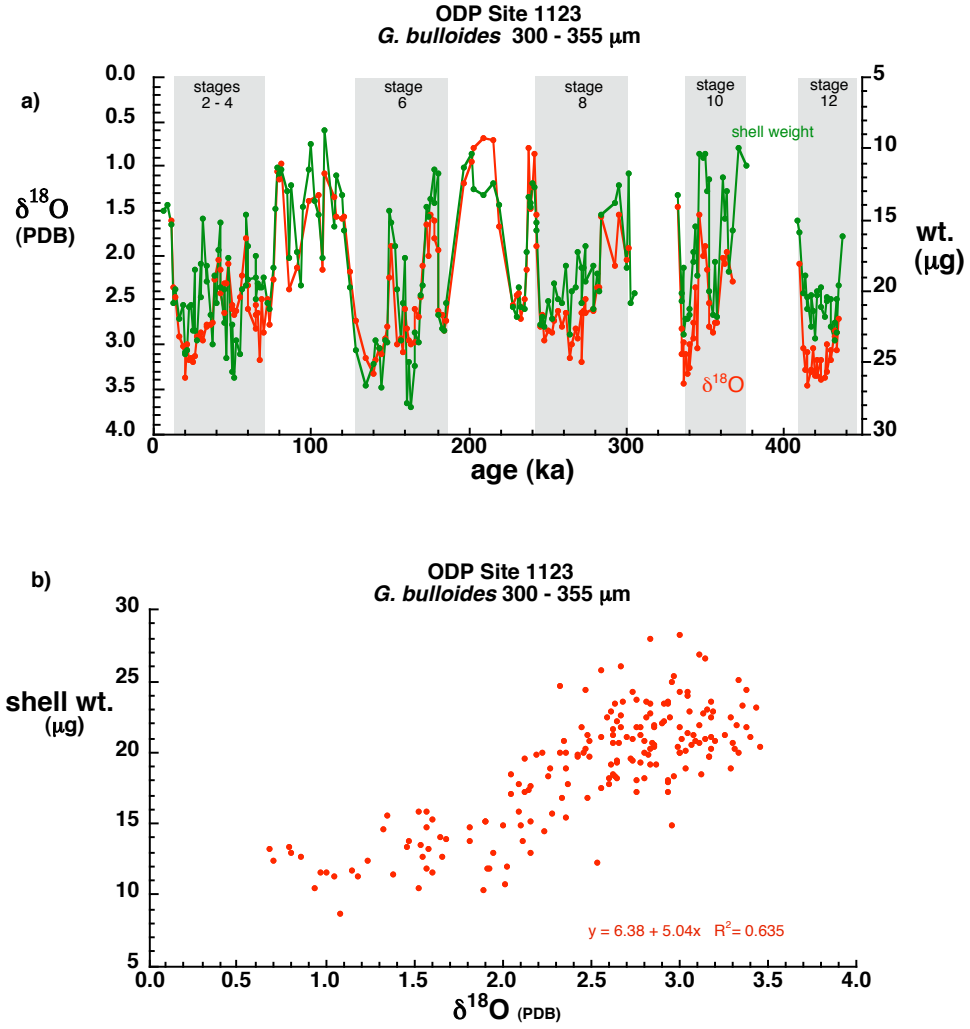

Figure 4.8 Correlation of G. *bulloides* shell weight and $\delta^{18}O$ at ODP Site 1123

4.3.1 Comparison of ODP Site 1123 and MD 97– 2120 *G. bulloides* Mg/Ca, shell weight and $\delta^{18}O$ records.

In Figure 4.9, the *G. bulloides* Mg/Ca, shell weight and $\delta^{18}O$ records from ODP Site 1123 are compared to records from the shallower site (MD97-2120) located south of the Subtropical Front. Mg/Ca and $\delta^{18}O$ data for *G. bulloides* (250-300 μm) at site MD97-2120 are from Pahnke *et al.,* [2003]. The shell weight record for MD97-2120 is courtesy of K. Pahnke [pers. comm.]. Mg/Ca data for the two records (Fig. 4.9a) are directly comparable because they were generated in the same laboratory, using the same cleaning procedure, ICP-OES instrument and calibration standards. Therefore, observed differences between the records can only be attributed to analytical issues if these arise from significant day to day instrumental differences [see Chapter 2]. Artefacts could possibly be introduced from the cleaning of foraminifera by different analysts but, unless there is a significant dependence of Mg/Ca data on individual analytical performance, the differences observed between the two records must be a product of the size fractions of the species, their habitats and seasons of calcification, and the hydrography and preservation at the respective sites.

Significant differences are observed between the records obtained from the *G. bulloides* 250-300 μm and 300-355 μm size fractions at these locations north and south of the Subtropical Front. The higher resolution $\delta^{18}O$ record at site MD97-2120 (Fig 4.9c) follows similar trends to the record from ODP site 1123 but many of the features seen in the ODP site 1123 record are less prominent, a consequence of the different surface water masses over the two sites. During interglacial stages 5 and 7, lower $\delta^{18}O$ values are observed at ODP Site 1123 than at site MD97-2120.

The Mg/Ca record at site MD97-2120 (Fig 4.9a) is similar to the record from ODP Site 1123 in some sections, but also shows features not seen in the ODP Site 1123 record. During glacial periods the MD97-2120 record generally shows lower Mg/Ca than found at ODP Site 1123 whereas during interglacials the records are more similar, as observed during the recent section of stage 5 and through stage 7. The excursion at Termination 3 is matched closely in both records. However, the MD97-2120 record clearly displays temperature changes at glacial Terminations 1 and 2 not seen in the ODP Site 1123

record and also contains data for interglacial stage 9 where *G. bulloides* were absent at ODP Site 1123.

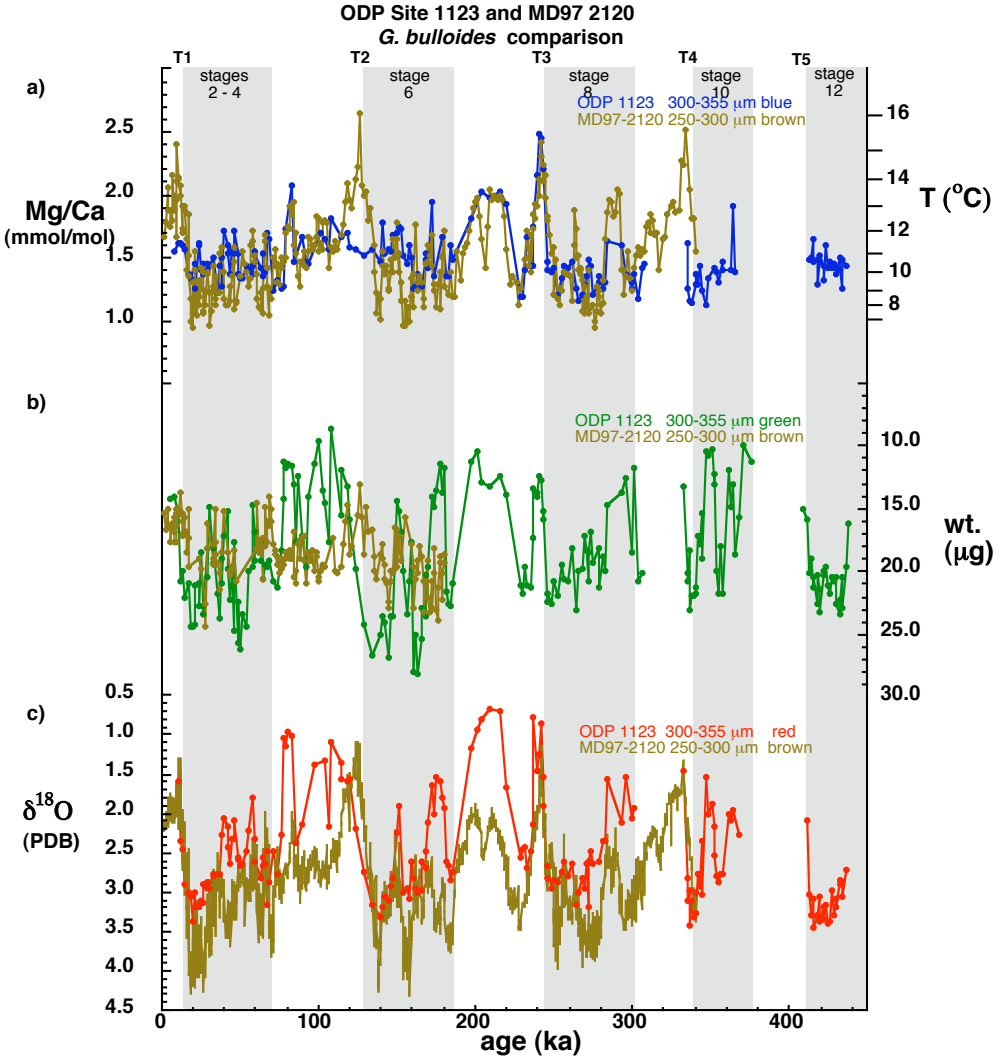

Figure 4.9 Comparison of *G. bulloides* records at ODP Site 1123 and MD97 2120 a) Mg/Ca (temperature scale using the equation of Mashiotta *et al.*, [1999]), b) average shell weight, c) $\delta^{18}O$

The 250-300 µm *G. bulloides* shell weight record from MD97-2120 (Fig. 4.9b) shows heavier shell weights in glacials than interglacials, but with a narrower range than observed in the 300-355 µm *G. bulloides* record from ODP Site1123. Average weights of the 250-300 µm fraction at MD97-2120 range from 13 – 24 µg compared to 8 – 28 µg for the 300-355 µm fraction at ODP Site 1123. In glacial periods, the 300-355 µm *G. bulloides* at ODP Site 1123 are, as expected, heavier than the 250-300 µm size fraction of *G. bulloides* at MD97-2120 but, during interglacial stages 1 and 5 the

smaller *G. bulloides* from site MD97-2120 are heavier than the larger *G. bulloides* from ODP Site 1123. The largest change in weight, almost a factor of two, occurs across Termination 2, but this is much smaller than seen across Termination 2 for the 300-355 μm *G. bulloides* size fraction at ODP Site 1123. The MD97-2120 shell weight and $\delta^{18}O$ records each follow similar trends (Fig. 4.10a) but the close correlation between shell weight and $\delta^{18}O$ found at ODP Site 1123 is not seen (Fig 4.10b).

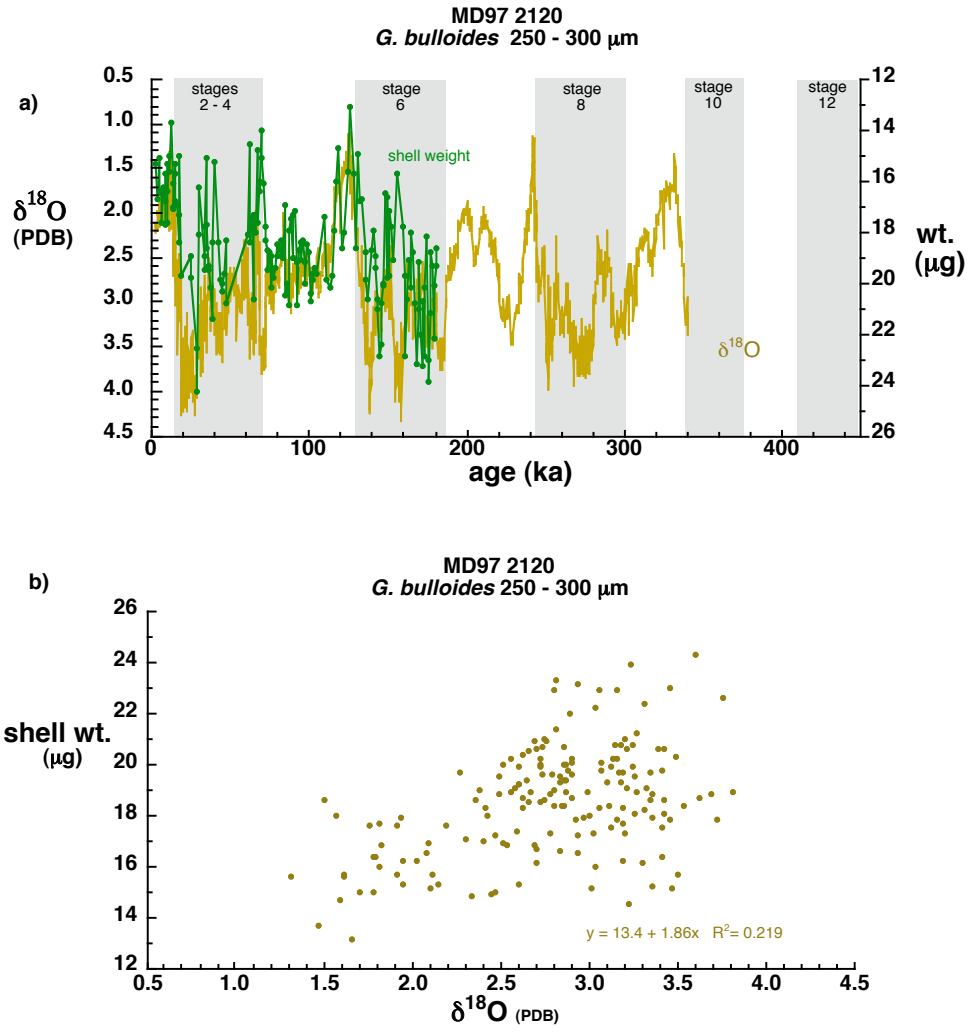

Figure 4.10 G. *bulloides* shell weight and $\delta^{18}O$ at Site MD97-2120

The differences observed between the Mg/Ca, shell weight and $\delta^{18}O$ records for *G. bulloides* at the two sites reflect hydrographic differences north and south of the Subtropical Front. However, complications in comparing the two sets of records are introduced by the different size fractions used and the different water depths of the sites.

Different calcification depths, seasons of calcification and water column stratification may be represented in the records at the two sites. The records must also have been modified by dissolution, a process further complicated if different size fractions have different susceptibilities to dissolution.

4.4 *G. bulloides* and *G. inflata* records from two size fractions across Terminations 1 and 2 at ODP Site 1123, MD 97-2120 and CHAT 16K

In order to differentiate between the influences of habitat, hydrography and dissolution, detailed Mg/Ca, shell weight and $\delta^{18}O$ records were obtained from both the 250-300 μm and 300-355 μm size fractions of *G. bulloides* over Termination 1 and Termination 2 at ODP Site1123, MD97-2120 and CHAT 16K. In addition, records were obtained for the deeper dwelling species *G. inflata* at ODP Site 1123 and CHAT 16K and samples from site CHAT 1K (Table 4.1) were analysed to provide coretop data to supplement the ODP Site1123 records.

Records of Mg/Ca, shell weight and $\delta^{18}O$ shown in Figures 4.11, 4.12 and 4.13 have been plotted in two ways to facilitate comparisons between the three sites and the species studied. The results are discussed first with reference to the sites (plots a to c), then compared between species and size fraction (plots d to f).

4.4.1 Comparisons of records between sites.

Large glacial to interglacial transitions are seen in the Mg/Ca records across both Termination 1 and Termination 2 at site MD97-2120 (Fig. 4.11a). The two *G. bulloides* size fractions display almost identical Mg/Ca ratios, suggesting similar calcification temperatures and preservation histories for the two populations. In contrast, at ODP Site1123 (Fig. 4.11c) changes are observed in the 250-300 μm *G. bulloides* Mg/Ca record across Terminations 1 and 2 which are not seen in the 300-355 μm record. Consistent with its deeper habitat, *G. inflata* records lower Mg/Ca and corresponding temperatures than *G. bulloides*, with a sharp increase observed across Termination 1.

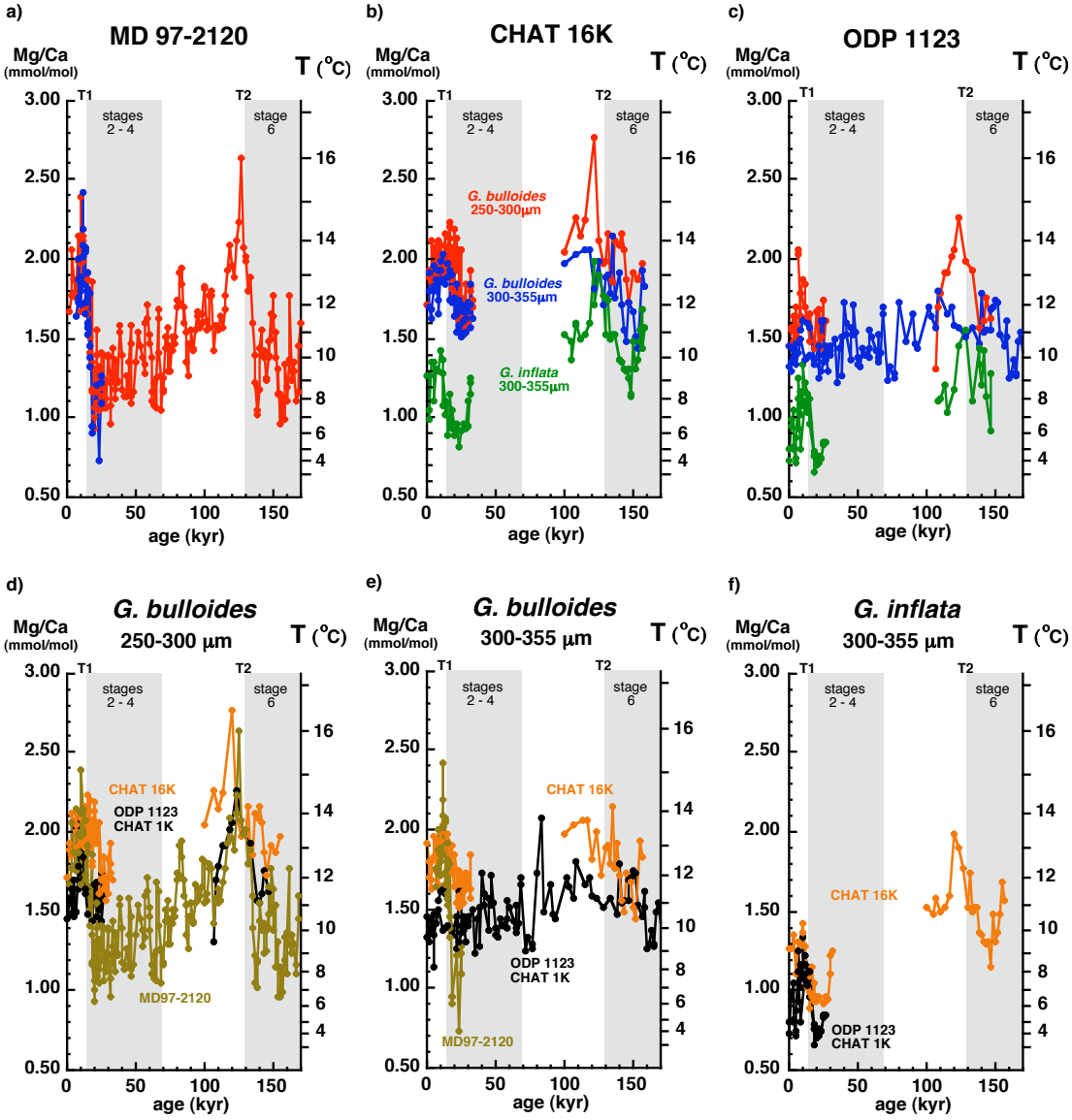

a) MD97-2120, b) CHAT 16K, c) ODP Site1123, CHAT1K
G. bulloides - 250-300 µm (red), 300-355 µm (blue), *G. inflata* (green)

d) *G. bulloides* 250-300 µm, e) *G. bulloides* 300-355 µm, f) *G. inflata* 300-355
ODP 1123, CHAT 1K (black), CHAT 16K (orange), MD97-2120 (brown)

Temperature scale, Mashiotta *et al.* [1999].

Figure 4.11 Mg/Ca records across Termination 1 and Termination 2

At CHAT 16K, Mg/Ca ratios of the 250-300 µm *G. bulloides* are consistently higher than in the larger size fraction (Fig. 4.11b), indicative of calcification in warmer water. This could reflect a deeper habitat for the larger *G. bulloides,* or be a consequence of seasonal differences in calcification, or may indicate that individuals reach maturity

earlier in warmer years. Over Termination 1, Mg/Ca ratios of *G. inflata* are consistent with a deeper habitat for this species but, over Termination 2 the *G. inflata* and *G. bulloides* records are more similar to one another. This may reflect hydrographic differences or differences in *G. inflata* habitat between the two intervals.

The *G. bulloides* shell weight records at site MD97-2120 (Fig. 4.12a) show some variation in the 250-300 μm size fraction, but the 300-355 μm record is more striking. A significant decrease in shell weight, from 28 to 19 μg, is observed in the 300-355 μm fraction across Termination 1 but, after a sharp minimum, shell weights increase during the Holocene to a maximum of 29 μg for the most recent samples.

The shell weight records from CHAT 16K (Fig. 4.12b) show large differences between the size fractions of *G bulloides* with features similar to those observed at ODP Site 1123. The *G. inflata* record from this site contains the largest range in weight of the species and sites studied.

At ODP Site 1123 (Fig. 4.12c) the *G. bulloides* 250-300 μm shell weights range from 8 to 13 μg across Termination 1 with a slightly narrower range across Termination 2, from a minimum interglacial weight of 8 μg to a maximum glacial weight of ~12 μg. This is in marked contrast to the large weight range shown by 300-355 μm *G. bulloides*, 14 to 24 μg across Termination 1 and 9 to 27 μg across Termination 2. During interglacial stage 5, the 300-355 μm *G. bulloides* shell weights become so light that the 300-355 μm and 250–300 μm records coincide.

The $\delta^{18}O$ records at site MD97-2120 for the two size fractions of *G. bulloides* (Fig. 4.13a) have almost identical $\delta^{18}O$ values across Termination 1, with $\delta^{18}O$ and Mg/Ca (Fig. 4.11a) records following similar trends downcore.

At ODP Site 1123 the $\delta^{18}O$ records show significant offsets between the two *G. bulloides* size fractions (Fig. 4.13c). Across both terminations, 250-300 μm *G. bulloides* $\delta^{18}O$ are lighter than 300-355 μm. Increasing *G. bulloides* $\delta^{18}O$ with shell size has been observed previously, in culture studies and in fossil *G. bulloides* from Chatham Rise [Spero and Lea; 1996]. The 300-355 μm record closely follows shell weight, but the 250-300 μm $\delta^{18}O$ record shows more pronounced changes than shell

weight (Fig. 4.12c). *G. inflata* $\delta^{18}O$ follow the trends of the *G. bulloides* records, with heavier $\delta^{18}O$ over Termination 1, consistent with a deeper habitat but, over Termination 2, *G. inflata* $\delta^{18}O$ are lighter than in the 300–355 μm *G. bulloides* size fraction.

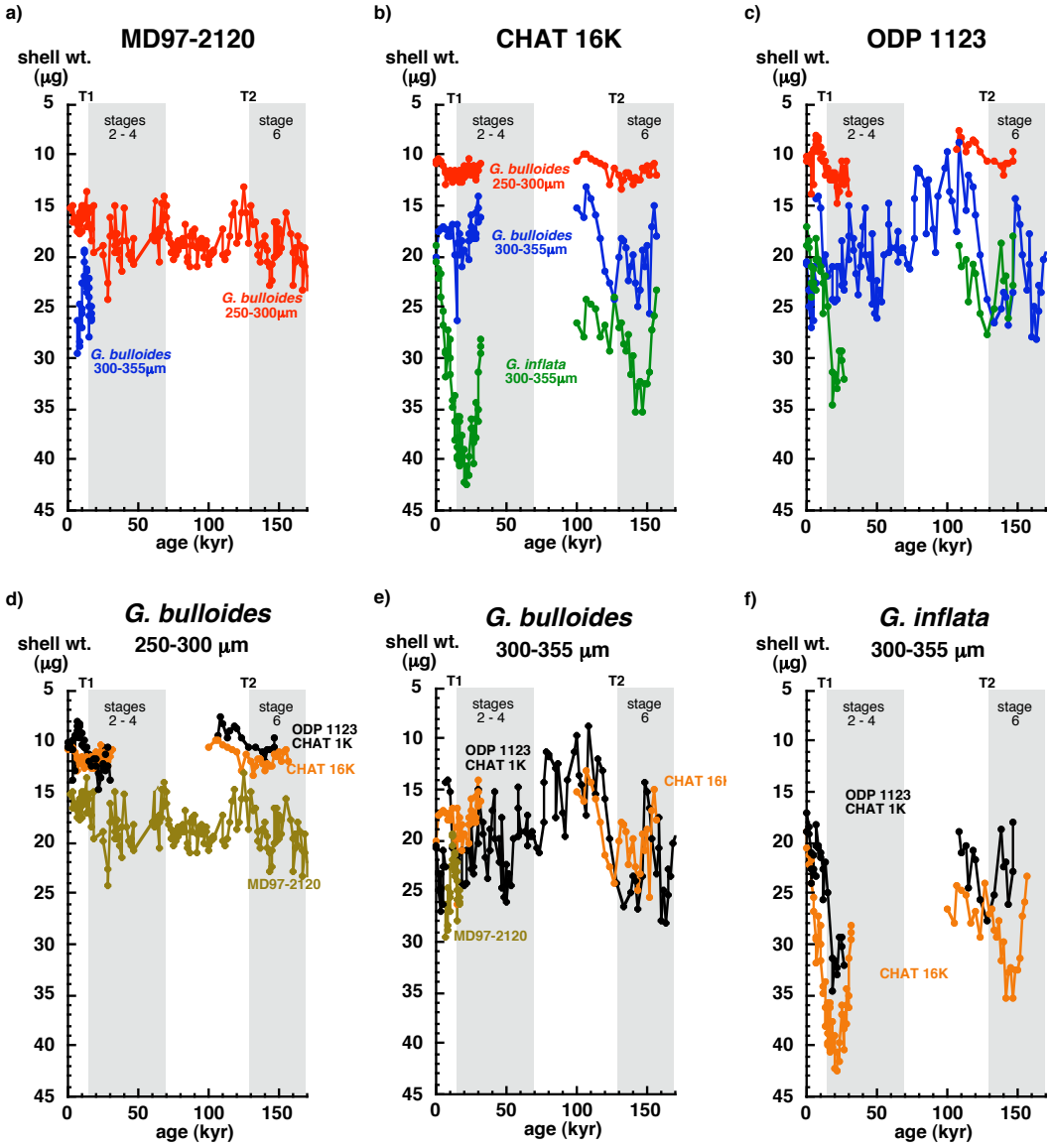

a) MD97-2120, b) CHAT 16K, c) ODP Site1123, CHAT1K
G. bulloides - 250-300 μm (red), 300-355 μm (blue), *G. inflata* (green)

d) *G. bulloides* 250-300 μm, e) *G. bulloides* 300-355 μm, f) *G. inflata* 300-355
ODP 1123, CHAT 1K (black), CHAT 16K (orange), MD97-2120 (brown)

Figure 4.12 Shell weight records across Termination 1 and Termination 2

The *G. bulloides* 250-300 μm record at CHAT 16K (Fig. 4.13b) also shows lighter $\delta^{18}O$ than the 300-355 μm record. Calcite $\delta^{18}O$ of the two size fractions converge during interglacials and diverge during glacials. *G. inflata* $\delta^{18}O$ are close to *G. bulloides* 300-355 μm over Termination 2, but are offset over Termination 1, as at ODP Site 1123 and as observed in the Mg/Ca records (Fig. 4.11b).

4.4.2 Comparisons of records between species and size fractions.

Comparison between species and size fractions shows that Mg/Ca in 250-300 μm *G. bulloides* (Fig. 4.11d) is higher at CHAT 16K, by 0.1 – 0.3 mmol/mol, than corresponding results from ODP Site 1123. This may be an effect of differences in carbonate dissolution between the depths of CHAT 16K (1408m) and ODP Site 1123 (3290m). However, the 250-300 μm *G. bulloides* records at ODP Site 1123 and MD97-2120 are remarkably similar, particularly across Termination 2, suggesting that the dominant signal is hydrographic and/or ecological. Offsets in the timing of features in the CHAT 16K record, for example close to Termination 2, may be a consequence of imperfect age models (Figure 4.6).

Larger differences are observed between *G. bulloides* 300-355 μm Mg/Ca records (Fig. 4.11e) than between the 250-300 μm size fraction records (Fig. 4.11d). Mg/Ca ratios at CHAT 16K are higher than corresponding values at ODP Site1123 by 0.2 – 0.4 mmol/mol, except during glacial stage 6. Across Termination 1, a much larger increase in Mg/Ca is recorded at Site MD97-2120 than at either of the other sites. Mg/Ca range from 0.9 to 2.4 mmol/mol across Termination 1 at site MD97-2120, equivalent to a temperature increase of ~9 ºC.

The *G. inflata* Mg/Ca records (Fig. 4.11f) show similar features over Termination 1 at ODP Site 1123 and CHAT 16K but, during glacial stage 2 Mg/Ca ratios at CHAT 16K are higher by 0.1 - 0.2 mmol/mol than at ODP Site 1123. Both records, especially CHAT 16K, show significantly higher Mg/Ca ratios over Termination 2 than over Termination 1.

Comparison of shell weights by size fraction shows that 250-300 µm *G. bulloides* (Fig. 4.12d) are heavier at CHAT 16K than at ODP Site 1123 and cover a narrower range, from 10 to 13 µg, the records converging in glacial and diverging in interglacials. Shell weights in the 250-300 µm *G. bulloides* record from Site MD97-2120 are consistently heavier (by up to a factor of two) than at ODP Site 1123 and CHAT 16K.

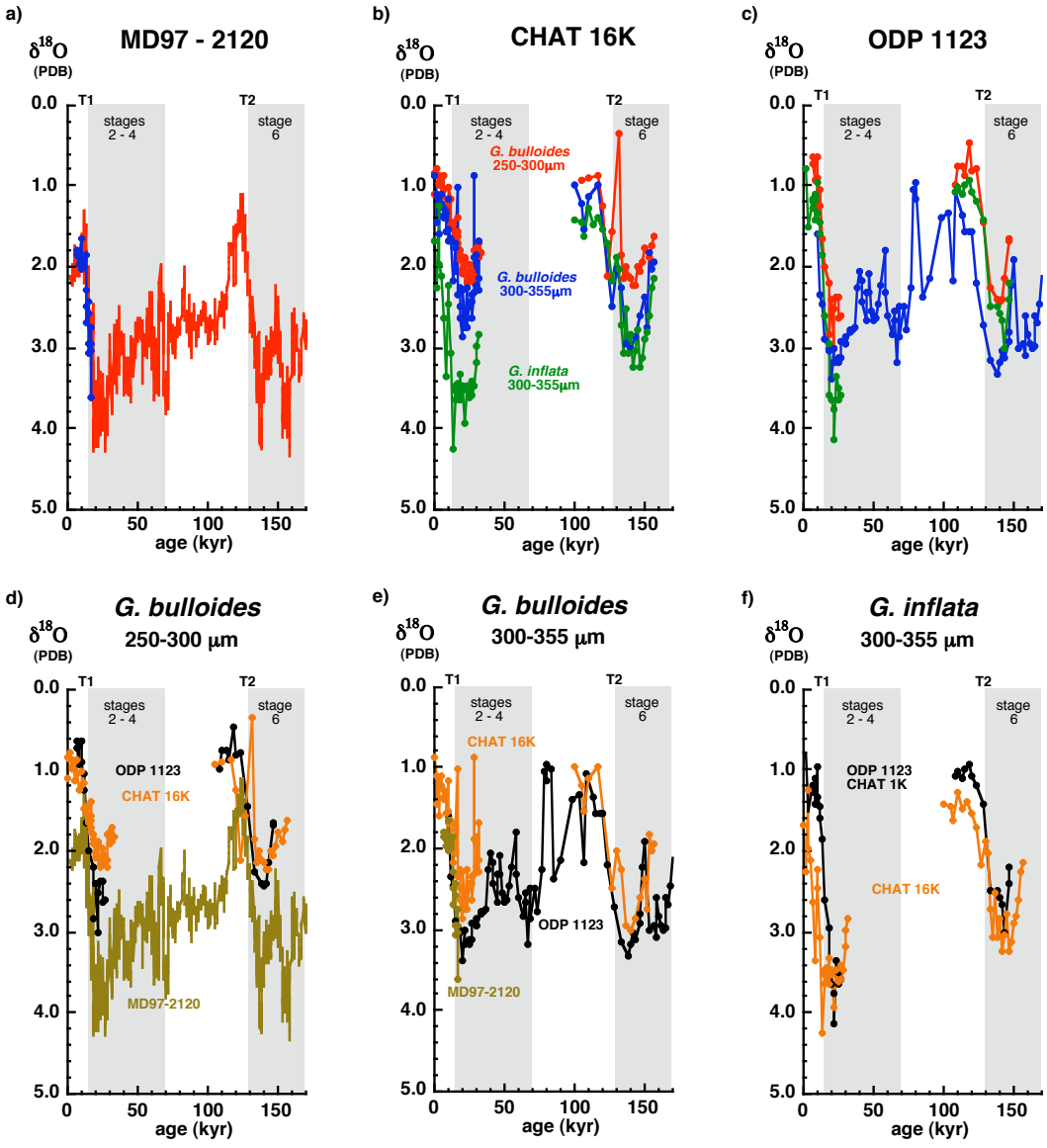

a) MD97-2120, b) CHAT 16K, c) ODP Site1123, CHAT1K
G. bulloides - 250-300 µm (red), 300-355 µm (blue), *G. inflata* (green)

d) *G. bulloides* 250-300 µm, e) *G. bulloides* 300-355 µm, f) *G. inflata* 300-355
ODP 1123, CHAT 1K (black), CHAT 16K (orange), MD97-2120 (brown)

Fig 4.13 $\delta^{18}O$ (V-PDB) records across Terminations 1 and 2

The 300-355 μm *G. bulloides* records over Termination 1 (Fig. 4.12e) show similar trends at CHAT 16K and ODP Site 1123 during stage 2, with maximum weights recorded just before the Termination, but shell weights are lighter at CHAT 16K than at ODP Site 1123, opposite to what would be expected from depth-dependent dissolution. After Termination 1, shell weights decrease to a minimum of 14 μg at ODP Site 1123 but at CHAT 16K remain relatively constant, ~17 μg. Similar to ODP Site 1123, the MD97-2120 *G. bulloides* 300-355 μm record reaches a minimum after Termination 1 but shell weights increase during the recent Holocene. Over Termination 2, the CHAT 16K record follows a pattern similar to that for ODP Site 1123 but covers a narrower range. During glacial stage 6 the *G. bulloides* 300-355 μm shell weights are generally lighter at CHAT 16K than at ODP Site 1123, as observed in glacial stage 2.

The *G. inflata* shell weight record over Termination 1 at CHAT 16K (Fig. 4.12f) ranges from 19 μg at the core top to a maximum of 43 μg in glacial stage 2, a more pronounced weight change than observed at ODP Site 1123. Over Termination 2, a narrower range in *G. inflata* shell weights (from 23 to 35 μg) is seen at CHAT 16K. *G. inflata* are lighter at ODP Site 1123 than at CHAT 16K over Termination 2, again covering a narrower range than over Termination 1. The lighter *G. inflata* shell weights at ODP Site 1123 compared to CHAT 16K are consistent with greater dissolution at the deeper site although some features may reflect picking preferences between thin walled and thicker, encrusted specimens.

Comparison of $\delta^{18}O$ records between size fractions and species shows, for *G. bulloides* 250-300 μm (Fig. 4.13d) progressively lower $\delta^{18}O$ from MD97-2120 through ODP Site 1123 to CHAT 16K during glacial Stages 2 and 6. Across both Terminations and during subsequent interglacials the ODP Site 1123 and CHAT 16K records are similar, whereas higher $\delta^{18}O$ values are found at site MD97-2120. The *G. bulloides* 300-355 μm $\delta^{18}O$ records (Fig. 4.13e) show consistently lower values at CHAT 16K than at ODP Site 1123. Very similar *G. bulloides* 300-355 μm records are observed at MD97-2120 and ODP Site 1123 across Termination 1. The *G. inflata* $\delta^{18}O$ records at ODP Site 1123 and CHAT 16K (Fig. 4.13f) follow similar trends to the respective Mg/Ca records shown in Figure 4.11f.

4.5 Processes controlling Mg/Ca and shell weight of planktonic foraminiferal calcite

The Mg/Ca, shell weight and $\delta^{18}O$ records described in the Section 4.4 reflect a combination of the parameters as initially recorded, potentially modified by carbonate dissolution over time. Differences in calcification depths of foraminifera populations, season of growth and water column stratification may all influence the initial records. Post depositional carbonate dissolution, a function of the depth of the sites and bottom water [CO_3^{2-}] together with the pore water chemistry also can affect the records.

4.5.1 Foraminiferal habitat and hydrography

Studies of the abundance over time and in different hydrographic regimes [King and Howard 2001; Sautter and Thunell, 1991] have shown that populations of *G. bulloides* are sensitive to regional and temporal differences in water properties. The abundance of *G. bulloides* can vary substantially in the Southern Ocean, both geographically and temporally [Mortyn and Charles, 2003]. Different size fractions may reflect calcification at different depths in the water column and the abundance, size and weight of *G. bulloides* are closely tied to water stratification. Food sources may be sharply defined with depth, restricting the occurrence of *G. bulloides* to a narrow range of temperatures. The onset of upwelling can dramatically affect phytoplankton populations and food availability is a strong control on foraminiferal abundance. Shell chemistry may be closely linked to water column stratification. McConnell and Thunell [2005] found a strong seasonal component to *G. bulloides* Mg/Ca recorded in a time series study of sediment trap samples from the Guaymas Basin. If this is typical of other oceanic regions, *G. bulloides* Mg/Ca in the sedimentary record must reflect an integrated signal of seasonal abundance and depth of calcification.

The contrasting seasonal dependency of foraminifera fluxes in waters north and south of the Subtropical Front reported by King and Howard [2001] suggest that, if applicable over a longer timescale, the *G. bulloides* records shown in Figures 4.9 and 4.11 to 4.13 may reflect different calcification seasons between sites north and south of the Subtropical Front, with a short calcification season occurring during Austral spring south of the Subtropical Front and a longer calcification season, through spring, summer

and autumn, occurring north of the Subtropical Front. If this hypothesis is valid, a possible effect would be for temperature records from sites south of the Subtropical Front to show more sharply defined features than records of comparable sampling resolution from sites located north of the Subtropical Front. A longer calcification season over a wider range of temperatures would produce an average temperature record which would tend to mask features observable in a record covering a shorter calcification season.

The distinctly contrasting features observed in Figures 4.9 and 4.11 to 4.13, between site MD97-2120 south of the Subtropical Front and the shallow CHAT 16K and deep ODP Site1123 to the north suggest a dominant hydrographic control on the records. The longer *G. bulloides* Mg/Ca records at site MD97-2120 and ODP Site1123 (Fig. 4.9a) are, except over Terminations 1 and 2, consistent with what might be expected from a comparison of temperature records between a warmer site north of the Subtropical Front and a colder more southerly site. Except in sections covering Terminations 1 and 2, downcore *G. bulloides* Mg/Ca at ODP Site1123 are generally higher than or comparable to Mg/Ca at site MD97-2120. Any dissolution which may preferentially have occurred at the deeper site has evidently not been sufficient to offset the ODP Site1123 Mg/Ca record to lower values than in the MD97-2120 record. The situation over Terminations 1 and 2, but not Termination 3, is different and must reflect habitat or preservation differences between the two *G. bulloides* size fractions (Fig. 4.11).

Initial shell weight is controlled by $[CO_3^{2-}]$ in the oceans [Barker and Elderfield, 2002]. The ambient carbonate ion concentration changes between glacial and interglacial cycles in response to atmospheric pCO_2. The heavier glacial compared to interglacial shell weights seen for both size fractions of *G. bulloides* and for *G. inflata* at all three sites (Figures 4.9 and 4.12) are consistent with this hypothesis, but the magnitude of the weight changes observed for the 300-355 μm *G. bulloides* and *G. inflata* would imply very large amplitude changes in $[CO_3^{2-}]$ over glacial to interglacial cycles [Barker *et al.*, 2002]. The dominant signal in shell weights may be initial shell weight variability related to changes in water mass stratification, the large amplitude of glacial-interglacial weight changes possibly reflecting changes in upwelling. Mortyn *et al.*, [2002] compared $\delta^{18}O$ and $\delta^{13}C$ records from shallow and deep dwelling species of planktonic

foraminifera and found evidence for changes in water column stratification in the Southern Ocean over the last two glacial terminations, water column structure becoming more stratified during the course of a climate transition. Sautter and Thunell [1991] documented *G. bulloides* weights within a size fraction (300-355 μm) during different months of the year, and found evidence of large seasonal weight changes in modern upwelling areas.

4.5.2 Calcite dissolution

The depth of ODP site 1123 (3290 m) implies that dissolution is likely and this is supported by the scarcity of *G. bulloides* in the 300-355 μm size fraction from interglacial stages 9 and 11. The large variations in shell weight (Figure 4.8) may record both a component of initial weight variability and a bottom water signal as a result of dissolution. Records from the different size fractions may be influenced differently according to their relative susceptibilities to dissolution. The predicted effect of dissolution on measured shell weights is illustrated in Figure 4.14, showing initial shell weight variation on glacial to interglacial timescales and two possibilities for the influence of dissolution, depending on whether dissolution is greater during glacials or interglacials. Dissolution reduces foraminiferal Mg/Ca, by preferential removal of magnesium rich calcite [Brown and Elderfield; 1996, Rosenthal *et al.;* 2000], and increases $\delta^{18}O$, the effect in both cases being to bias records towards artificially cooler temperatures.

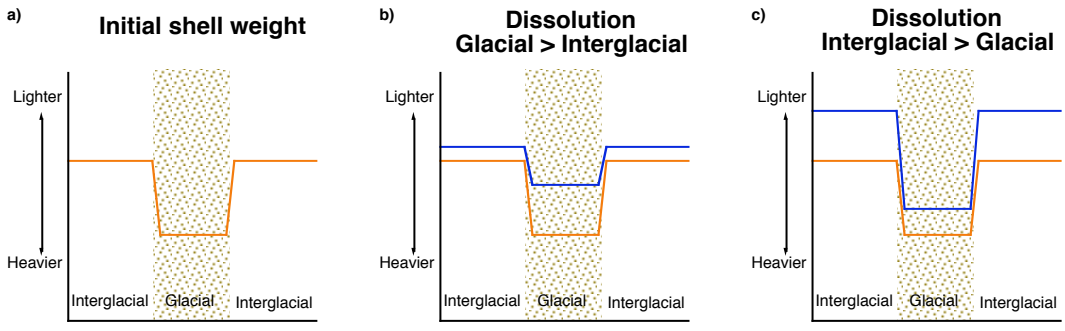

Orange – initial shell weight record.
Blue – record modified by dissolution.

Figure 4.14 Predicted effect of dissolution on initial foraminifera shell weights

The large weight difference between interglacial and glacial *G. bulloides* from the 300-355 μm size fraction at ODP Site 1123 (8μg to 28μg) suggests that significant post-depositional dissolution has occurred with dissolution greater in the interglacial than glacial periods (Figure 4.14c), with dissolution perhaps completely erasing the record from interglacial stages 9 and 11 (Figure 4.7b). However, other arguments contradict this interpretation. It was shown by Howard and Prell [1994], in the Southern Ocean, that increased carbonate dissolution occurred in glacial periods although this is dependent on location and bottom water mass covering a site [Hodell *et al.,* 2001]. There is evidence from fragmentation indices and planktonic/benthic foraminiferal abundance ratios to suggest increased dissolution during glacial periods in this region, particularly during isotope stage 2 to the south of Chatham Rise [Weaver *et al.,* 1998]. Investigation of benthic $\delta^{13}C$ gradients in the deep Pacific during glacial-interglacial cycles has been interpreted to record increased ventilation during glacials [Hall et al., 2001] which would imply less corrosive deepwater during glacials. Comparison of the *G. bulloides* 300-355 μm shell weight records at ODP Site 1123 and CHAT 16K (Figure 4.12e), except for samples immediately following Termination 1, does not suggest greater dissolution at the deeper site.

Site MD 97–2120, located south of the Subtropical Front (Figure 4.1), is overlain by Antarctic Intermediate Water (Figure 4.4) and its shallow depth (1210 m) implies that records from this site are unlikely to be influenced by significant post-depositional dissolution. Pahnke *et al.,* [2003] discussed potential carbonate dissolution and concluded that any effect of dissolution on their *G. bulloides* Mg/Ca record was minor. In comparison, site CHAT 16K is located north of the Subtropical Front at a similar depth (1408m) but is overlain by a mixture of Antarctic Intermediate Water and Circumpolar Deep Water (Figure 4.4). The susceptibility to dissolution at these sites may be different because of the influence of the different bottom waters. Weaver *et al.,* [1997], in an examination of foraminferal assemblages and fragmentation indices of core top samples, recognised corrosion at sites in shallow depths north of Chatham Rise, incuding site CHAT 16K.

4.5.3 Summary

The similar Mg/Ca and $\delta^{18}O$ records observed for the two *G. bulloides* size fractions at site MD97-2120 indicate that these data sets are reliable indicators of the same environmental conditions. In contrast, Mg/Ca and $\delta^{18}O$ records from CHAT 16K and ODP Site1123 may reflect calcification at different depths or in different seasons.

Dissolution at the sea floor must have influenced the geochemical and shell weight variability at ODP Site 1123 and there is evidence for dissolution influencing the records at CHAT 16K. The large variability in shell weights at ODP Site 1123 across Terminations 1 and 2 (Figure 4.12e), and CHAT 16K across Termination 2, could record the sensitivity of regional upwelling to glacial-interglacial conditions. The low shell weights of interglacial foraminifera tests would make them more prone to dissolution, enhancing glacial-interglacial contrasts. The lack of *G. bulloides* during interglacial stages 9 and 11 probably reflects both low initial shell weights and intense dissolution during these interglacials. The *G. bulloides* shell weight record needs to be interpreted as an initial shell weight signal, but affected by post-depositional dissolution sufficient to erase the record from interglacial stages 9 and 11.

4.6 Mg/Ca - temperature calibrations and $\delta^{18}O_{seawater}$ calculation

An advantage of Mg/Ca palaeothermometry, compared to alkenone unsaturation ratios or faunal abundances as palaeotemperature proxies, is that paired measurements of Mg/Ca and $\delta^{18}O$ permit $\delta^{18}O_{seawater}$ to be calculated from $\delta^{18}O_{carbonate}$ [Mashiotta *et al.,* 1999; Elderfield and Ganssen, 2000; Lea *et al.,* 2000, 2002; Lear *et al.,* 2000]. Measurement of Mg/Ca and $\delta^{18}O_{carbonate}$ on splits of the same shells ensures a common source for these signals, recorded from the same season and depth habitat and influenced by the same post depositional conditions, thereby minimizing uncertainties in $\delta^{18}O_{seawater}$ reconstruction. Samples for this study were crushed and split before cleaning. However, cleaning procedures affect both Mg/Ca and $\delta^{18}O$ and splitting of foraminifera samples after cleaning would ensure that both records were affected by the

same process. The calculated $\delta^{18}O_{seawater}$ provides an estimate of salinity from the linear $\delta^{18}O_{seawater}$ salinity relationship [Schmidt *et al.,* 1999; Bigg & Rohling, 2000] but accuracy is critically dependent on the assumptions made and the errors involved [Schmidt, 1999; Rohling, 2000].

4.6.1 Mg/Ca – temperature calibrations for *G. bulloides* and *G. inflata*

Temperature calibrations of the form:

$$Mg/Ca = A \exp (B \times T)$$

where T is temperature in ºC, have been produced for planktonic foraminifera from culture [Nürnberg *et al.,* 1996; Lea *et al.*,1999; Mashiotta *et al.*,1999], core tops [Elderfield and Ganssen, 2000; Lea *et al.,* 2000; Dekens *et al.*, 2002] and sediment traps [Anand *et al.,* 2003; McConnell and Thunell, 2005]. The exponential constant, B, gives the temperature sensitivity while the pre-exponent, A, (the Mg/Ca intercept at T = 0 ºC) determines the absolute temperature. Published temperature calibrations for *G. bulloides* and *G. inflata* are listed in Table 4.2.

The foraminifera culture calibration of Lea *et al*. [1999], the combined core top and culture calibration of Mashiotta *et al*. [1999] and the sediment trap calibration of McConnell and Thunell [2005] are tied to sea surface temperatures, whereas the core top calibration of Elderfield and Ganssen [2000] and the sediment trap calibration of Anand *et al,* [2003] relate Mg/Ca to foraminifera calcification temperatures. Core top calibrations include implicitly any post depositional effects at the calibration sites whereas these are excluded by culture and sediment trap calibrations. The Mashiotta *et al*. [1999] and Elderfield and Ganssen [2000] calibrations were recalculated by Anand *et al*. [2003] using the geometric mean method (Table 4.2), applied in situations where both variables contain significant errors and there is no independent variable.

The sediment trap calibrations of Anand *et al*. [2003] and McConnell and Thunell [2005] cover warm waters from the Sargasso Sea and the Gulf of California respectively. The culture calibration of Lea *et al*. [1999] also covers warm waters

(Table 4.2). Temperatures calculated using *G. bulloides* and *G. inflata* calibrations for colder waters are compared in Figure 4.15.

Species	Source	T range (ºC)	Mg/Ca = A exp (BT) A	B	Reference
G. bulloides	Culture	16 - 25	0.53	0.102	Lea *et al.*, 1999
G. bulloides	Coretop/culture	10 - 25	0.474	0.107	Mashiotta *et al.*, 1999
G. bulloides	Coretop/culture	10 - 25	0.47	0.108	Mashiotta *et al.*, 1999 [c]
G. bulloides	Coretop	8 - 15	0.56	0.10	Elderfield & Ganssen, 2000
G. bulloides	Coretop	8 - 15	0.81	0.081	Elderfield& Ganssen, 2000[c]
G. bulloides	Sediment trap	16 - 31	1.20	0.057	McConnell & Thunell, 2005
G. inflata	Coretop	8 - 15	0.49	0.10	Elderfield & Ganssen, 2000
G. inflata	Sediment trap	17 - 21	0.299	0.090	Anand *et al.*, 2003
Mixed [a]	Coretop	0 - 19	0.52	0.10	Elderfield & Ganssen, 2000
Mixed [a]	Coretop	0 - 19	0.65	0.085	Elderfield& Ganssen, 2000[c]
Mixed [b]	Sediment trap	13 - 28	0.38	0.090	Anand *et al.*, 2003

[a] 8 planktonic species including *G. bulloides* and *G. inflata*.
[b] 10 planktonic species including *G. inflata*.
[c] Recalculated using geometric mean method [Anand *et al.*, 2003]

Table 4.2 Published *G. bulloides* and *G. inflata* Mg/Ca temperature calibrations.

Over the 0.9 to 2.6 mmol/mol Mg/Ca range measured in *G. bulloides* at ODP Site 1123 and MD97-2120, the equations of Mashiotta *et al.* [1999], Elderfield and Ganssen [2000] and Mashiotta *et al.* [1999] as recalculated by Anand *et al.* [2003] yield temperatures that are in agreement within 1.0 ºC (Figure 4.15). The recalculation by Anand *et al.* [2003] of the Elderfield and Ganssen [2000] eight species calibration is more sensitive to changes in Mg/Ca and produces progressively lower temperatures for Mg/Ca < 1.75 mmol/mol, giving a temperature of 5.1 ºC at Mg/Ca = 1.0 mmol/mol compared to 6.5 – 7.0 ºC from the other three calibrations. In their original forms, the species specific *G. bulloides* and *G. inflata* calibrations of Elderfield and Ganssen [2000] give temperatures close to the combined eight species calibration, but in their recalculated forms lower temperatures, by up to 3 ºC, are produced (Figure 4.15). Temperatures calculated using the equation of Mashiotta *et al.* [1999] maintain

consistency with other studies [Pahnke *et al*., 2003; Nürnberg and Groeneveld, 2006] and this equation is used in this work.

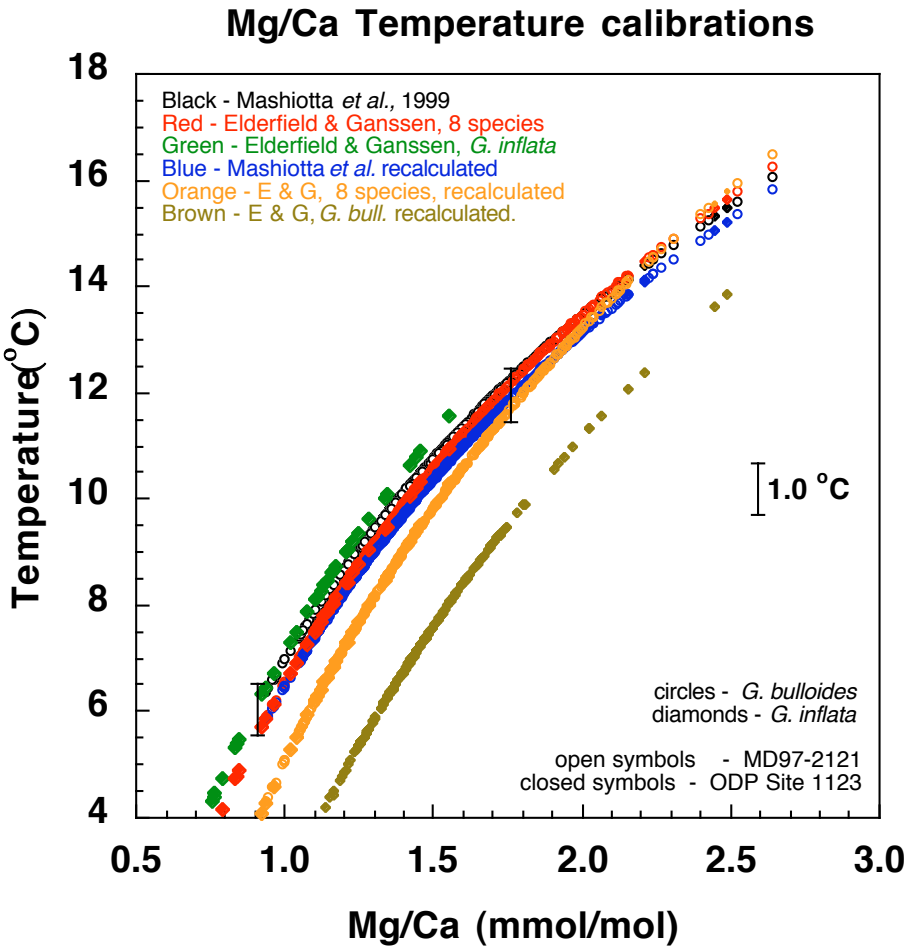

Figure 4.15 Comparison of Mg/Ca temperature calibration equations for *G. bulloides* and *G. inflata* at ODP Site 1123 and MD97-2120.

Corrections to temperature calibrations for the effects of dissolution have been developed from depth transects of core-top foraminiferal Mg/Ca on the assumption that, if surface waters over a series of sites have similar properties, shells with similar initial compositions are deposited and differences observed reflect differences in dissolution between the sites. Rosenthal *et al*. [2000] and Rosenthal and Lohmann [2002] used the relationship between dissolution and size-normalised shell weight to provide dissolution corrected calibrations for *Globigerinoides ruber* and *Globigerinoides sacculifer*. Dekens *et al*. [2002] quantified Mg/Ca loss in *G. ruber, G. sacculifer* and *Neogloboquadrina dutertrei* from four core-top depth transects using both core depth

and ΔCO_3^{2-} as dissolution parameters. These authors observed also that different species showed varying responses to dissolution. A depth transect of Caribbean core tops was used by Regenberg *et al*. [2006] to assess the effect of dissolution on seven species of tropical to sub-tropical planktonic foraminifera over a depth range from ~900 to 4700m. However, all of these studies were from sites at low latitudes and included neither *G. bulloides* nor *G. inflata*.

4.6.2 Calculation of $\delta^{18}O_{seawater}$ from calcification temperature and $\delta^{18}O_{carbonate}$

The palaeotemperature equation:

$$T = a + b(\delta^{18}O_{carbonate} - \delta^{18}O_{seawater}) + c(\delta^{18}O_{carbonate} - \delta^{18}O_{seawater})^2$$

relates the the difference between $\delta^{18}O_{carbonate}$ and $\delta^{18}O_{seawater}$ to the calcification temperature T (°C) of the foraminifera. Values for the coefficients a, b and c are available from a number of studies, from inorganic calcite precipitation [O'Neil *et al*., 1969; Kim and O'Neil, 1997] and foraminifera [Shackleton, 1974; Bemis *et al*., 1998; Mulitza *et al*., 2003] using either the quadratic or linear (c = 0) forms of the equation. Spero and Lea [1996] determined the relationship between $\delta^{18}O_{carbonate}$ and the number of chambers, and hence shell size, in cultured *G. bulloides* and found an increase in $\delta^{18}O_{carbonate}$ of ~0.11 ‰ between 10 chamber (239 μm) and 11 chamber (296 μm) shells. Bemis *et al*., [1998] developed size dependent linear palaeotemperature equations for 11, 12 and 13 chambered *G. bulloides* shells over the temperature range 15 – 25 °C. Field based calibrations for *G. bulloides, G. ruber, G. sacculifer and N. pachyderma* collected from plankton tows and pumped surface seawater samples were established by Mulitza *et al*., [2003]. The relationship obtained by these authors for *G. bulloides,* size range between 150 and 400 μm, over the temperature range 1 to 25 °C was indistinguishable from the relationship found by Bemis *et al*., [1998] for 13 chambered shells over the temperature range 15 to 25 °C.

Similar slopes among the different calibrations (Table 4.3) act to yield calculated temperatures in agreement for relative temperature changes, but absolute temperatures are governed by the intercepts and, therefore, culture and field based calibrations produce noticeably lower temperatures than calibrations derived from inorganic studies.

Consequently, on rearrangement of the palaeotemperature equation to calculate $\delta^{18}O_{seawater}$, significantly higher values of $\delta^{18}O_{seawater}$ are produced by the culture and field based calibrations than by calibrations based on inorganic calcite precipitation.

Source	Size (μm)	$T = a + b(\delta_c - \delta_w) + c(\delta_c - \delta_w)^2$			Reference
		a	b	c	
Inorganic		16.9	-4.38	0.1	O'Neil *et al*. 1969
Uvigerina		16.9	-4.0		Shackleton, 1974
Inorganic		16.1	-4.64	0.09	Kim &O'Neil,1997
G. bulloides:					
Culture -11 chambers	301 ± 25	12.6	-5.07		Bemis *et al*. 1998
Culture -12 chambers	369 ± 30	13.2	-4.89		Bemis *et al*. 1998
Culture -13 chambers	414 ± 39	13.6	-4.77		Bemis *et al*. 1998
Plankton tow	150 to 400	14.62	-4.70		Mulitza *et al*. 2003

Table 4.3 Published palaeotemperature equations applied to *G. bulloides*.

Changes in $\delta^{18}O_{carbonate}$ and temperature operate in the same direction on calculated $\delta^{18}O_{seawater}$ as a consequence of the negative slope, b, of the palaeotemperature equation (Table 4.3) but, because post depositional dissolution increases $\delta^{18}O_{carbonate}$ and reduces Mg/Ca and Mg/Ca derived temperatures, the effect of carbonate dissolution is cancelled to some extent in the calculation of $\delta^{18}O_{seawater}$. The outcome of this process depends on the relative effect of dissolution on $\delta^{18}O_{carbonate}$ compared to Mg/Ca.

4.6.3 Comparison of core top Mg/Ca temperatures and calculated $\delta^{18}O_{seawater}$ with modern hydrography

Where foraminifera have calcified under modern conditions, comparison of calculated temperatures and $\delta^{18}O_{seawater}$ with modern hydrography can verify results and may provide evidence about the depth and season of calcification or evidence for post depositional dissolution. The cores studied here were not collected with the specific intention of sampling the latest Holocene. Nevertheless, it is useful to compare calculated temperatures for the Holocene with modern hydrography to asses the effects of dissolution on foraminifera samples from coretops at these sites.

The Mg/Ca records from the sites in this study (Figs. 4.7, 4.9 & 4.11) show maxima close to Termination 1 with values decreasing through the Holocene. Therefore, modern conditions can be assumed only for the most recent samples. Coretop ages are constrained by ^{14}C dates at site MD97-2120, where the topmost sample was dated at 2ka, but by the age model alone at the other sites.

At site MD97-2120 a maximum of 2.4 mmol/mol Mg/Ca is observed in the *G. bulloides* 250-300 μm size fraction record at 10.7 ka following Termination 1 (Fig. 4.9a) with Mg/Ca decreasing through the Holocene to 1.67 mmol/mol for most recent sample. The temperature of ~12 ºC calculated for this sample using the equation of Mashiotta *et al.* [1999] is consistent with modern hydrography (Fig. 4.16a) and with calcification of *G. bulloides* during late spring [King and Howard, 2001].

Samples younger than 6 ka were not analysed from ODP Site1123 and coretop samples from nearby core CHAT 1K were used to compare calculated temperatures with modern hydrography. Core top Mg/Ca of 1.45, 1.32 and 0.81 mmol/mol (Fig. 4.11c) give temperatures of 10.4, 9.6 and 5.0 ºC for *G. bulloides* 250-300 μm, *G. bulloides* 300-355 μm and *G. inflata* 300-355 μm respectively (Fig. 4.16b). Estimated calibration errors are 1.1 to 1.4 ºC [Dekens *et al.,* 2002; Anand *et al.,* 2003] although here temperatures are quoted to 0.1 ºC to demonstrate the relative effect from differences in Mg/Ca. These calculated temperatures are well below those expected from modern hydrography and indicate significant calcite dissolution in the core top at this site. The greater depth of CHAT 1K (3556 m) compared to ODP Site 1123 (3290 m) also may be significant when comparing these two sites.

Core top Mg/Ca at the shallower CHAT 16K site are respectively 1.84, 1.76 and 1.27 mmol/mol (Fig. 4.11b), giving temperatures of 12.7, 12.3 and 9.2 ºC for *G. bulloides* 250-300 μm, *G. bulloides* 300-355 μm and *G. inflata* 300-355 μm (Fig. 4.16c). Calculated temperatures are lower than expected from modern hydrography and calcification during spring [King and Howard, 2001]. Dissolution has affected the Mg/Ca record at CHAT 16K (1408 m) but is not as intense as at the deeper CHAT 1K.

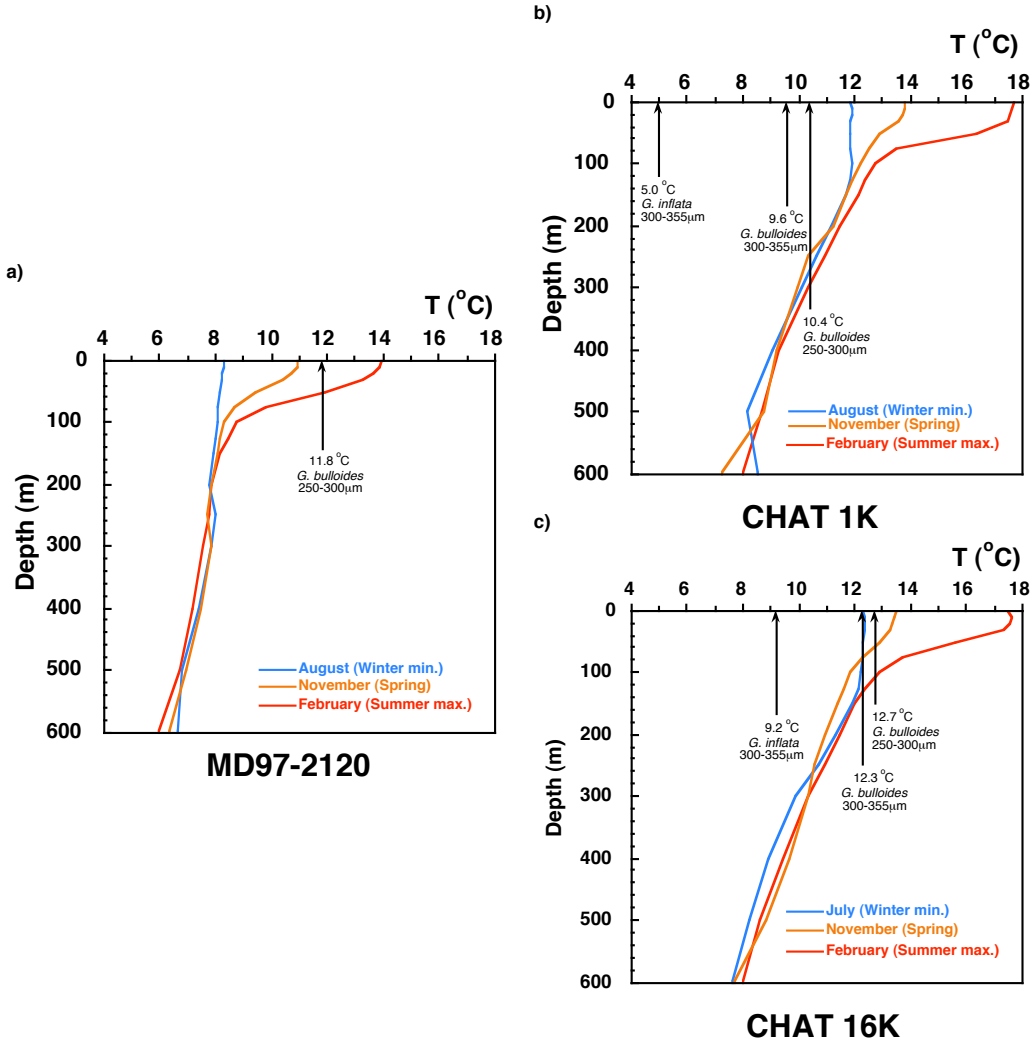

Figure 4.16 Holocene Mg/Ca temperatures and modern hydrography.

In comparison, using foraminiferal abundances, Weaver *et al*. [1998] predicted winter surface water temperatures over CHAT 16K (core R657 in their study) and CHAT 1K of 13 – 14 ºC, and summer sea surface temperatures of ~ 20 ºC, close to the temperatures expected from modern hydrography. These authors estimated dissolution from foraminiferal fragmentation ratios and percent benthic foraminifera, and found increasing dissolution through the Holocene at CHAT 16K and CHAT 1K, with dissolution reaching a maximum in the core top samples.

Calculated $\delta^{18}O_{seawater}$ and inferred salinity also may be compared to modern hydrography, but here the uncertainties are much greater than for the calculation of temperature alone. In the absence of measured $\delta^{18}O_{seawater}$ data for the sites in this study,

$\delta^{18}O_{seawater}$ must be estimated from regional $\delta^{18}O_{seawater}$ salinity relationships [Legrande & Schmidt, 2006]:

South Pacific $\delta^{18}O_{seawater} = 0.45S - 15.29$ ($r^2 = 0.936$, n = 19)

The 19 measurements from the South Pacific are GEOSECS data covering longitudes approximately180 to 120 °W [Schmidt *et al.,* 1999] and the principal uncertainty in applying this relationship is the lack of data from the Chatham Rise region of the Southwest Pacific Ocean. This relationship estimates $\delta^{18}O_{seawater}$ from 0.19 to 0.46 ‰ for salinity in the range 34.4 to 35.0 appropriate to surface waters over these sites (Figure 4.3).

Calculation of $\delta^{18}O_{seawater}$ from coretop $\delta^{18}O_{carbonate}$ and Mg/Ca temperatures shown in Figure 4.16, using the quadratic form of the palaeotemperaure equation [O'Neil *et al*., 1969; Shackleton, 1974] gives, over CHAT 16K $\delta^{18}O_{seawater}$ values of 0.22, 0.34 and 0.11 ‰ from *G. bulloides* 250-300 μm, *G. bulloides* 300-355 μm and *G. inflata* 300-355 μm respectively, close to values expected from the above regional $\delta^{18}O_{seawater}$ salinity relationships. In comparison, the linear palaeotemperature equation of Mulitza *et al*. [2003] gives higher $\delta^{18}O_{seawater}$ values of 0.79, 0.93 and 0.80 ‰ respectively.

Over ODP Site 1123, a value of $\delta^{18}O_{seawater}$ of 0.21 ‰ is obtained from *G. bulloides* 300-355 μm using the quadratic palaeotemperature equation [O'Neil *et al*., 1969; Shackleton, 1974] compared to 0.93 ‰ calculated from the Mulitza [2003] palaeotemperature equation.

South of the Subtropical Front at site MD97-2120, the much higher coretop *G. bulloides* 250-300 μm $\delta^{18}O_{carbonate}$ of 2.15 ‰ (Fig. 4.13d) produces correspondingly higher $\delta^{18}O_{seawater}$ of 1.21 ‰, calculated using the quadratic palaeotemperaure equation [O'Neil *et al*., 1969; Shackleton, 1974], well outside the range expected from the South Pacific $\delta^{18}O_{seawater}$ salinity relationship. Even higher $\delta^{18}O_{seawater}$ of 1.81 ‰ is given if the Mulitza [2003] equation is applied.

The regional $\delta^{18}O_{seawater}$ salinity relationship for the Southern Ocean [Legrande & Schmidt, 2006]:

$\delta^{18}O_{seawater} = 0.24S - 8.45$ ($r^2 = 0.374$, n = 503)

predicts lower $\delta^{18}O_{seawater}$ than the South Pacific relationship, -0.19 for salinity of 34.4 but, with $r^2 = 0.374$ this relationship is poorly constrained and none of the data are from sites close to Chatham Rise [Schmidt *et al.*, 1999]. Clearly, better coverage of modern $\delta^{18}O_{seawater}$ measurements is required.

4.6.4 Downcore $\delta^{18}O_{seawater}$ records

Downcore records of $\delta^{18}O_{seawater}$ (Figures 4.17 and 4.18) were calculated using the Mashiotta *et al*. [1999] Mg/Ca temperature calibration (see section 4.6.1) and the quadratic palaeotemperature equation, after O'Neil *et al*. [1969] and Shackleton [1974]. This palaeotemperature equation was selected because better agreement between calculated $\delta^{18}O_{seawater}$ from coretop samples and modern $\delta^{18}O_{seawater}$ was obtained using this equation compared to alternative palaeotemperature equations (sections 4.6.2 and 4.6.3).

Figure 4.17 shows calculated $\delta^{18}O_{seawater}$ records across Terminations 1 and 2, plotted using the same format as Figures 4.11 to 4.13. The $\delta^{18}O_{seawater}$ records obtained from the two size fractions of *G. bulloides* across Termination 1 at site MD97-2120 (Figure 4.17a) are similar to one another, as expected from the agreement between *G. bulloides* size fractions observed for both Mg/Ca and $\delta^{18}O_{carbonate}$ at this site (Figures 4.11a and 4.13a). Both records give a $\delta^{18}O_{seawater}$ change of 2 ‰ across Termination 1, reflecting changes in ice volume and local salinity [Pahnke *et al.*, 2003]. Calculated modern $\delta^{18}O_{seawater}$ is significantly heavier over this site south of the Subtropical Front than over sites CHAT 16K and ODP Site 1123 to the north and, as noted in section 4.6.3, is heavier than predicted from modern $\delta^{18}O_{seawater}$ salinity relationships.

At CHAT 16K (Figure 4.17b) calculated $\delta^{18}O_{seawater}$ values for the three available records are in agreement across both Termination 1 and Termination 2, implying that the populations analysed occupied waters of similar salinities. All three records show a change in $\delta^{18}O_{seawater}$ of 1.7 ‰ across Termination 2 but across Termination 1 the 250-

300 µm *G. bulloides* record changes by 1.4 ‰, the 300-355 µm record by 1.5 ‰ and a 2.0 ‰ change was calculated from the *G. inflata* record.

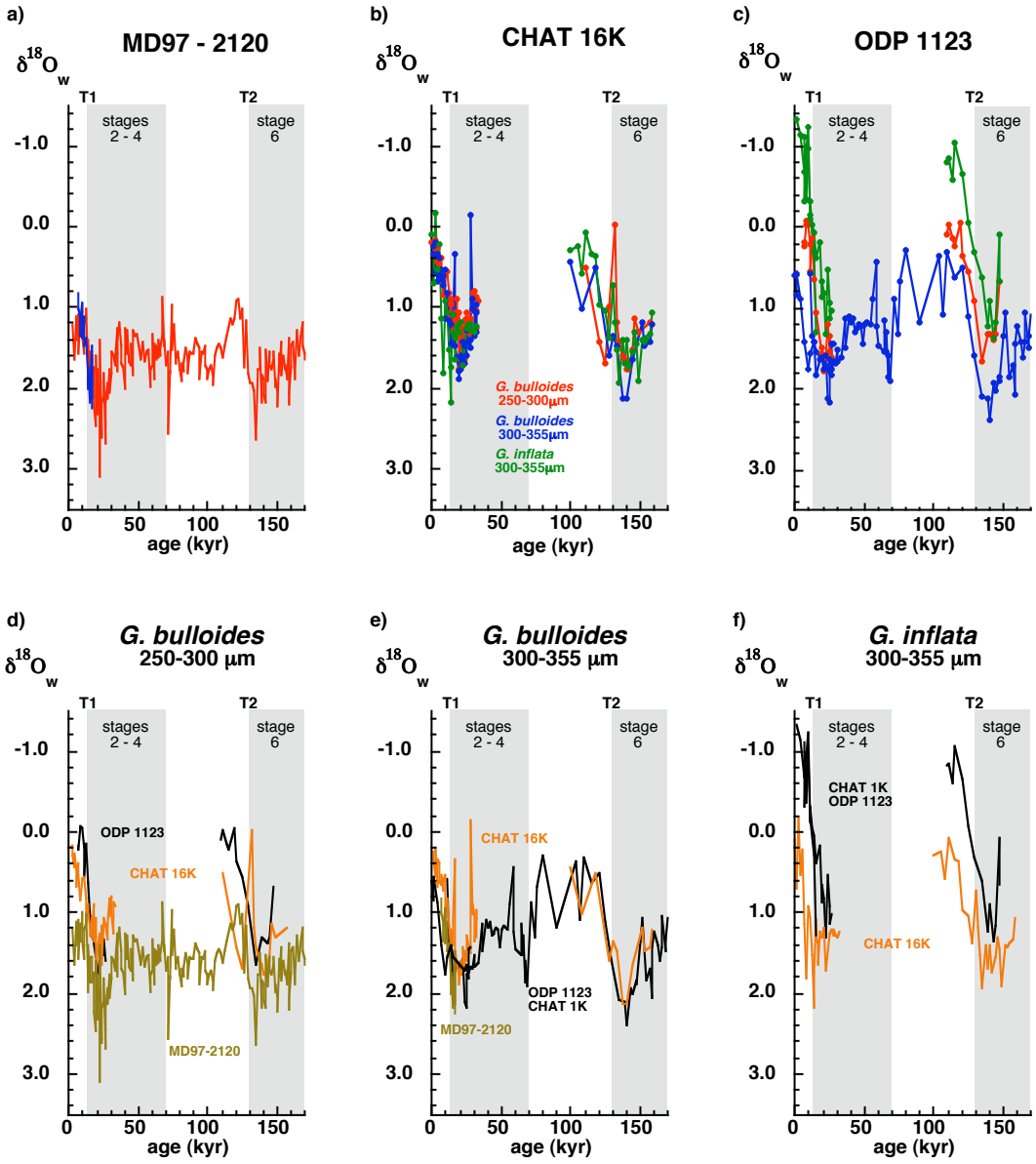

a) MD97-2120, b) CHAT 16K, c) ODP Site 1123, CHAT 1K
G. bulloides - 250-300 µm (red), 300-355 µm (blue), *G. inflata* (green)

d) *G. bulloides* 250-300 µm, e) *G. bulloides* 300-355 µm, f) *G. inflata* 300-355
ODP 1123, CHAT 1K (black), CHAT 16K (orange), MD97-2120 (brown)

Figure 4.17 Calculated seawater oxygen isotopic composition $\delta^{18}O_w$ (V-SMOW) records across Terminations 1 and 2

The offsets between calculated $\delta^{18}O_{seawater}$ values at ODP Site 1123 (Figure 4.17c) suggest that *G. bulloides* in the 300-355 μm calcified in waters with higher $\delta^{18}O$ and consequent higher salinity than the 250-300 μm *G. bulloides*. Across Termination 2, records for both *G. bulloides* size fractions exhibit a 1.6 ‰ shift, whereas across Termination 1 the 250-300 μm *G. bulloides* changes by 1.8 ‰. The *G. inflata* record at ODP Site1123 shows lower calculated $\delta^{18}O_{seawater}$ values than both of the *G. bulloides* size fractions, consistent with calcification of this species in deeper, less saline water.

Comparison of calculated $\delta^{18}O_{seawater}$ records for the same species and size fractions between sites shows noticeably lower values for *G. bulloides* in the 250-300 μm (Figure 4.17d) at both CHAT 16K and ODP Site 1123 than at site MD97-2120. However, the $\delta^{18}O_{seawater}$ records calculated from the *G. bulloides* 300-355 μm size fraction (Figure 4.17e) are similar at all three sites, suggesting a dominant hydrographic control. In contrast, $\delta^{18}O_{seawater}$ records across both Termination 1 and Termination 2 calculated from *G. inflata* demonstrate the effects of different controls on this species between CHAT 16K and ODP Site 1123 (Figure 4.17f). The differences between the $\delta^{18}O_{seawater}$ records at CHAT 16K and ODP Site 1123 may be a consequence of greater dissolution affecting the *G. inflata* record at the deeper site, whereas agreement between the $\delta^{18}O_{seawater}$ records at CHAT 16K suggests hydrographic rather than dissolution control.

The long term $\delta^{18}O_{seawater}$ records calculated from the 250-300 μm *G. bulloides* size fraction at site MD97-2120 and the 300-355 μm *G. bulloides* size fraction at ODP Site 1123 are compared in Figure 4.18.

Differences between the $\delta^{18}O_{seawater}$ records (Fig. 4.18) predominantly reflect differences between the $\delta^{18}O_{carbonate}$ records at the two sites (Fig. 4.9c). The record from the 300-355 μm *G. bulloides* size fraction at ODP Site 1123 shows lower $\delta^{18}O_{seawater}$ values than the 250-300 μm *G. bulloides* record from site MD97-2120. The records are more similar in glacial than in interglacial stages, converging during the later sections of all three glacial stages covered by both records. The most striking differences are observed during interglacial stages 5 and 7 where the 300-355 μm ODP Site1123 record is consistently lower, by up to 1.0 ‰, than the 250-300 μm MD97-2120 record. The most likely explanation is that these records represent differences in hydrography and

foraminiferal habitat between the two sites. The alternative explanation, that dissolution at depth has preferentially affected the $\delta^{18}O_{seawater}$ record from the 300-355 μm *G. bulloides* size fraction at ODP Site 1123, appears less likely because the relative effects of dissolution on $\delta^{18}O_{carbonate}$ and Mg/Ca (section 4.6.2) operate in opposite directions on calculation of $\delta^{18}O_{seawater}$.

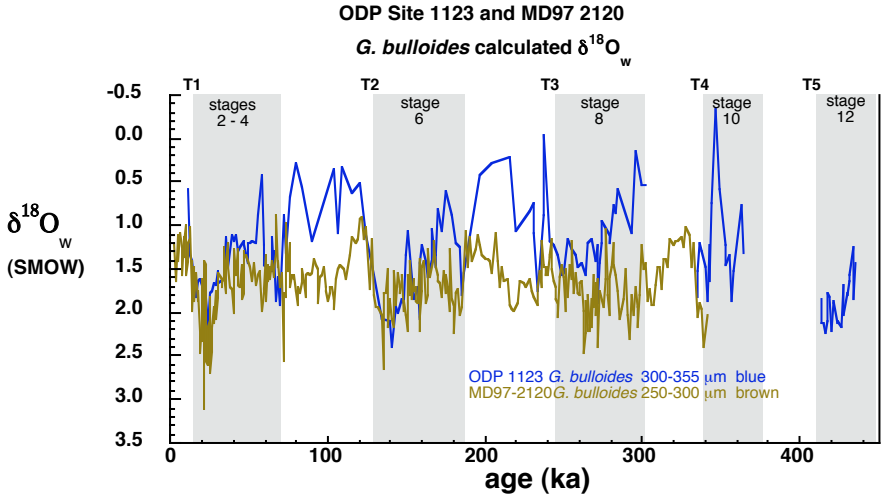

Figure 4.18 $\delta^{18}O_w$ (V-SMOW) records at ODP Site1123 and MD97-2120, calculated from *G. bulloides* Mg/Ca temperatures and $\delta^{18}O_{carbonate}$

4.7 Summary and Conclusions

In order to constrain past changes in surface water hydrography over Chatham Rise, records of Mg/Ca, $\delta^{18}O$ and shell weight of *G. bulloides* and *G. inflata* were investigated at three sites located north and south of the Subtropical Front. Comparison of Mg/Ca records for two different size fractions of *G. bulloides* at site MD97-2120 indicates that these are reliable indicators of temperatures at the same depths, whereas records at CHAT 16K and ODP Site1123 may reflect calcification at different depths or times of year but also are influenced by dissolution. Large variations in shell weight over glacial interglacial cycles are a consequence of initial shell weight variability, modified by post depositional dissolution.

The large differences in Mg/Ca, shell weight and $\delta^{18}O$ records found between two narrow size fractions of *G. bulloides* (300-355 μm and 250-300 μm) at the same site has

implications which must be considered when selecting samples for analysis and comparing records from different sources. A lack of $\delta^{18}O_{seawater}$ measurements in the study area and uncertainty in the regional $\delta^{18}O_{seawater}$ salinity relationship compounds systematic errors in palaeosalinity estimates, but comparison of calculated $\delta^{18}O_{seawater}$ records permits investigation of relative differences in hydrography.

Differences between records mainly reflect hydrographic differences between the sites, linked to vertical stratification of the upper water column and may be due to different calcification depths and/or seasons of growth for different foraminifera populations. Food availability and seawater density can become more sharply defined with depth across frontal boundaries in the Southern Ocean, resulting in different habitats being occupied by various populations of *G. bulloides* [Mortyn and Charles, 2003]. Variable upwelling histories between the sites also would exert a strong control on Mg/Ca, $\delta^{18}O$ and shell weight. Enhanced dissolution during early interglacial conditions may be partly responsible for the lower Mg/Ca ratios recorded at ODP Site1123 relative to CHAT 16K.

Chapter 5

Determination of cadmium in foraminifera by ID-TIMS

5.1 Introduction

The material presented in this chapter describes my contribution to method development work performed in collaboration with Rosalind Rickaby, published by Rickaby, Greaves and Elderfield [2000], and subsequent developments to this method which are applied in Chapter 6.

The relationship between Cd and P in the oceans permits Cd/Ca ratios in foraminifera to be used as a proxy for deepwater phosphate and deep ocean circulation [Boyle, 1981, 1988, 1992]. The determination of foraminiferal Cd/Ca ratios was established by Boyle [1981] and Boyle and Keigwin [1985/86], using graphite furnace atomic absorption spectrophotometry to determine Cd, combined with flame atomic absorption spectrophotometry for Ca determination. More recently, methods using inductively coupled plasma mass spectrometry have been described, employing either isotope dilution [Lea and Martin, 1996] or element intensity ratios [Rosenthal et al. 1999]. In this chapter, a method for Cd determination in foraminifera using isotope dilution thermal ionisation mass spectrometry (ID-TIMS) is developed and described. The established method is automated, reliable, precise and very sensitive. It therefore permits routine analyses of Cd in planktonic foraminifera, a possible tracer of surface water hydrography, and analyses of small samples of benthic foraminifera. It follows that smaller species or individual shells may be analysed, for example to examine phytodetrital species, or zones where benthic foraminifera are extremely sparse, or to investigate factors controlling shell chemistry. The main objective of this work was to exploit the sensitivity of ID-TIMS rather than its high precision; measurement precision is not usually the limiting factor in interpretation of foraminiferal Cd/Ca data [Boyle, 1995]. Published applications of the method include investigation into the

temperature sensitivity of the partition coefficient (D_{Cd}) for incorporaton of Cd into planktonic foraminiferal calcite [Rickaby and Elderfield, 1999], and a study of microhabitat effects on Cd/Ca and $\delta^{13}C$ of benthic foraminifera [Tachikawa and Elderfield, 2002].

5.2 Mass spectrometry method development

Successful determination of Cd by ID-TIMS requires the development of a stable ion beam from a small amount of Cd, together with a low analytical blank from the chemical procedures. There have been previous ID-TIMS determinations of Cd, in residues of the Allende meteorite [Loss et al., 1990], aerosols [Radlein and Heumann, 1995] and ice cores [Matsumoto and Hinkley, 1997]. These studies worked with nanogram quantities of Cd whereas for foraminiferal Cd/Ca determinations picogram levels need to be analysed. Previous analyses of Cd/Ca in benthic foraminifera have concentrated on sample sizes of an average of 10 individuals or >0.2mg of initial crushed foraminifera, containing typically ~100 pg Cd.

5.2.1 Cadmium isotopes and isobaric interferences

Cadmium has eight stable isotopes covering the mass range 106 – 116 amu (Table 5.1). Elemental isobaric interferences exist from palladium, indium and tin, ^{111}Cd being the only isotope free from this effect. Molecular interference is possible from molybdenum oxides, with potential interference on all cadmium isotopes except ^{106}Cd. Interference from $CaPO_2$ must also be considered when samples are loaded with phosphoric acid, $^{40}Ca^{31}P^{16}O_2$ occuring at 103 amu and $^{48}Ca^{31}P^{16}O_2$, with a signal amounting to 0.2% of the intensity at mass 103, at 111 amu. Scans of the Cd mass spectrum confirmed the presence of $^{40}Ca^{31}P^{16}O_2^+$, $^{48}Ca^{31}P^{16}O_2^+$ and $^{40}Ca^{31}P^{16}O_3^+$ at 103, 111 and 119 amu respectively, but Mo and Sn were not observed, presumably because of their low ionisation efficiency under TIMS conditions. The situation for Sn is in marked contrast to ICPMS where Sn is a significant interfering element in Cd determination.

Mass	105	106	107	108	109	110	111	112	113	114	115	116	117
$Mo^{16}O$				15.0		9.4	14.8	16.6	9.6	24.0		9.7	
Pd	22.3	27.3		26.5		11.7							
Ag			51.8		48.2								
Cd		1.25		0.89		12.49	12.80	24.13	12.22	28.73		7.49	
In									4.3		95.7		
Sn								1.0		0.7	0.3	14.5	7.7

Table 5.1 Natural abundances (%) of cadmium isotopes and potential isobaric interferences.

5.2.2 Cadmium determination by isotope dilution

The basis of isotope dilution mass spectrometry is the measurement of the ratio of two isotopes of an element after adding a tracer, or spike, artificially enriched in one or more isotopes. The measured isotope ratio falls on a linear mixing line between the natural and spike values of this ratio and the amount of the natural element is calculated from these values and the amount of spike added [Faure, 1986]. ^{116}Cd was selected as enriched spike isotope (98.14% enrichment, AEA Technology, Harwell, UK) because of its low natural abundance and ^{114}Cd, the most abundant isotope, was chosen for quantification. The minor isotopes ^{106}Cd and ^{108}Cd were rejected as spikes because they are isobaric with Pd which had significant potential for contamination, being used in high concentration in the laboratory as a modifier for atomic adsorption spectrophotometry. ^{111}Cd, despite being free of elemental isobaric interference, was not chosen as the enriched spike isotope after preliminary tests found significant molecular interference.

A stock ^{116}Cd spike solution was prepared in ~0.1M HNO_3 and diluted such that samples containing 0.5 pmol Cd (i.e., a typical sample) could be spiked with 0.1 g of a solution containing 0.25 pmol ^{116}Cd to give the optimum $^{114}Cd/^{116}Cd$ ratio of 0.23; this being the geometric mean of the natural and spike $^{114}Cd/^{116}Cd$ ratios and possessing the minimum error magnification factor for isotope dilution (Figure 5.1). The ^{116}Cd spike has a wide useable range with error magnification factor < 2.0 for $^{114}Cd/^{116}Cd$ ratios in

the range 0.03 to 1.90 (Figure 5.1), equivalent to 0.01 to 3.4 pmol Cd for a sample spiked with 0.25pmol ^{116}Cd. In addition, a more concentrated ^{116}Cd spike (Cd-1) was prepared from the stock solution such that a 0.5 μl aliquot containing 40pg Cd, equivalent to a typical sample size, could be loaded directly onto the filament and run in parallel with samples to check the mass-spectrometer running procedures and the loading blank. Each spike solution was calibrated using Cd standards diluted gravimetrically from a 1000 μg/ml plasma emission standard.

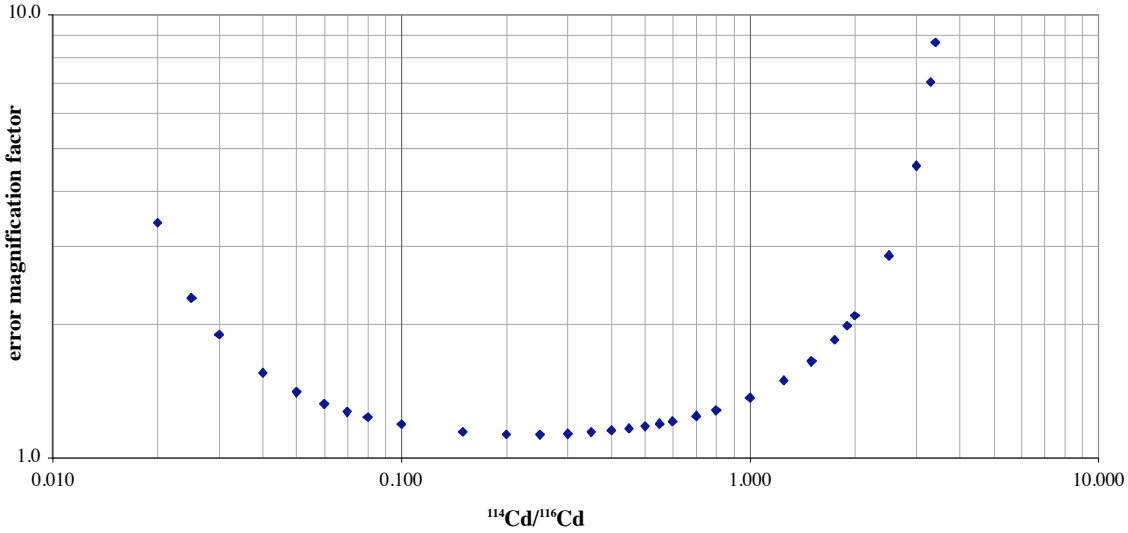

Figure 5.1 ^{114}Cd/^{116}Cd error magnification curve.

5.2.3 Cadmium ionisation by TIMS

The high first ionisation potential of Cd (867.6 kJ mol^{-1}) requires an optimisation of ion formation if picogram quantities are to be analysed. The silica gel activator technique, developed by Cameron et al. [1969] for running small quantities of lead which is similarly difficult to ionise, was therefore adopted. In this technique samples are loaded onto single rhenium filaments with silica gel and phosphoric acid, both to maximise ionisation and to minimise isotopic fractionation on evaporation from the filament.

Initially, silica gel was prepared by the addition of silicon (IV) chloride to ultrapure water and made up in 0.25M H_3PO_4 to maximise the ionisation efficiency and to minimise the Cd loading blank. The dried sample was dissolved in 1μl of 0.2M HNO_3

to form hydrated Cd cations, added to 1μl Si gel/ 0.25M H_3PO_4 solution on the filament and dried slowly, aiming to produce a clear glassy deposit to maximise ionisation. This method worked well for some samples but did not give consistently good cadmium ionisation. Reproducibility of loading was improved by mixing the dissolved sample with 1μl silica gel/ 0.25M H_3PO_4 in the vial before loading onto the filament. A similar technique of adding the activator ingredients to samples was used by Chisholm et al. [1995] in the determination of Pb isotopes in snow and ice. As current is applied to the adsorbed sample in the mass spectrometer, the silica gel becomes molten [Huett et al., 1995] and the Cd cations can migrate freely through the lattice to the surface towards the accelerating potential. It is necessary to regulate the emission of these ions to prevent rapid loss of sample. Lukes et al. [1994] showed that on heating silica gel with H_3PO_4 an ester is formed, the yield of which is improved by continuous water removal as would occur when drying a filament during loading. Therefore, the final stage of the loading process was to add an additional 1μl of 0.25M H_3PO_4 to the adsorbed cadmium sample. As a result, the migration of ions through the silica gel as it is heated is slowed and, in particular, the surface-bonded esters help to regulate the ion emission process. This loading procedure permitted a ^{116}Cd ion beam of 3 - 5 x 10^{-14}A to be maintained for approximately 2 hours from a clean 40 pg Cd load on the filament, equivalent to approximately 1% Cd ionisation efficiency.

The subsequent introduction of the silica gel preparation procedure of Gerstenberger & Haase [1997] led to improved Cd ionisation and more reliable sample analyses. These authors investigated silica gel products and preparation procedures, seeking a very dispersed silica gel to produce a more effective emitter for Pb ionisation. They concluded that an optimum mixture of 2g commercial colloidal silicic acid (Merck Art. No. 12475) in 200 ml ~0.05M H_3PO_4 resulted in more constant Pb ion currents at slightly lower filament temperatures, with a significantly higher ion yield by a factor of 4 to 5 compared to previous silica gel preparations. Their procedure was modified to optimise the relative proportions of silicic acid to H_3PO_4 for Cd ionisation. The mixture, in slightly different proportions to the above, was prepared in small quantities on the day of use by adding 20 µl colloidal silicic acid to1ml 0.1M H_3PO_4 while agitating in an ultrasonic bath. Samples were loaded by dissolving in 1 µl 0.2M HNO_3, adding 1 µl silica gel/ 0.1M H_3PO_4 and mixing in the vial, as previously, before loading

onto the filament. The addition of extra H_3PO_4 to the filament was found to be no longer necessary. This loading procedure gave a similar ^{116}Cd ion beam to that previously obtained but using a slightly lower filament current. However, the principal advantage was not the improvement of ionisation efficiency for the best samples, which had run well using the previous method, but improvement in the consistency of loading, leading to a much greater proportion of good sample runs which maintained a ^{116}Cd ion beam $>10^{-14}$A for sufficient time to reproducibly measure the $^{114}Cd/^{116}Cd$ ratio.

The presence of more easily ionisable elements suppresses the ionisation of elements with higher first ionistion potential in the mass spectrometer. Thus, for Cd (1st ionisation potential 867.6 kJ mol^{-1}) the presence of Ca from foraminiferal calcite (1st ionisation potential 589.7 kJ mol^{-1}) leads to serious suppression of the Cd ion beam. Where poor separation of Cd from Ca occurred, investigation of the spectra of samples showed $^{40}Ca^{31}P^{16}O_2^+$ at 103 amu and $^{40}Ca^{31}P^{16}O_3^+$ at 119 amu with consequent suppression of the Cd ion beam. However, loading 100pg Cd together with 100pg Ca on the filament confirmed that at this level Ca did not suppress the Cd ion beam significantly, with a 2 x 10^{-14}A ^{116}Cd beam maintained compared to only 1 x 10^{-16}A $CaPO_3^+$ beam at 119 amu. Thus, an efficient chemical separation procedure is necessary to isolate Cd following foram cleaning so that Cd can be run in the mass spectrometer without ion-beam suppression by Ca.

5.3 Chemical separation of Cd from Ca

Experiments in the mass spectrometer showed that to maximise Cd ionisation and obtain the most stable Cd beam it was necessary to reduce Ca to a level similar to that of Cd, a more than six orders of magnitude reduction of Ca relative to its concentration in foraminiferal calcite (see Chapter 1, Figure 1.1). Cation exchange in hydrochloric acid provides a good separation of Cd from Ca, with minimum manipulation required and easily purified reagents available. Separation was optimised based on equilibrium distribution coefficients (K_d) on cation exchange resin (AG 50W-X8) in hydrochloric acid [Strelow, 1960]. The maximum separation factor for Ca from Cd occurs using 1.0M HCl, with K_d values of 42.3 and 1.54 respectively (Table 5.2).

HCl (M)	Cd (K_d)	Ca (K_d)	Ca/Cd (K_d ratio)
3.0	0.6	7.3	12
2.0	1.0	12.2	12
1.0	1.54	42.3	27
0.5	6.5	151	23
0.2	84	790	9.4
0.1	510	3200	6.3

Table 5.2 AG 50W-X8 cation exchange resin, K_d values at different molalities of hydrochloric acid. [Strelow, 1960]

Miniature ion exchange columns (3.2mm ID, 3.7cm resin bed, Savillex PFA) were designed to enable Ca to be loaded from typical foraminifera samples (200 μg Ca after cleaning) and Cd to be eluted quantitatively, without risk of premature Ca breakthrough. The columns were calibrated by loading a solution containing 200 μg Ca and 150 pg Cd, with 100% Cd recovery obtained after eluting 1.15ml 1.0M HCl. Ca did not appear in the eluate until more than 5.0ml 1.0M HCl were eluted. However, Ca retained on the column after eluting Cd made it necessary to discard the resin after use. The large Ca load, relative to Cd, risks contaminating subsequent samples with residual Ca and suppressing Cd ionisation should any resin cleaning process not reduce Ca to picogram levels.

5.4 Experimental Procedure

5.4.1 Reagents and Apparatus

All containers were rigorously cleaned according to procedures that have been described for trace metal analyses in seawater [Greaves *et al*., 1989]. A Class 100 clean air hood was used for all steps subsequent to the crushing process. Trace element precautions were employed throughout according to Boyle and Keigwin [1985/86]. Reagents were prepared following trace metal clean procedures using water from a reverse osmosis/ion exchange unit (Elga, UK), redistilled in a quartz sub-boiling still. Hydrochoric and nitric acids were purified from analytical grade reagents by sub-

boiling distillation in a quartz still. Sample evaporations were carried out under teflon hoods, swept with filtered air and heated using infrared lamps.

5.4.2 Preparation and cleaning of foraminifera samples

Foraminifera samples (0.1 - 0.5 mg benthic or 0.8 - 1.2 mg planktonic) were cleaned following the technique established by Boyle [1981], Boyle and Keigwin [1985/86], Boyle [1995] and modified by Rosenthal *et al*. [1997] who reversed the order of the reduction/oxidation stages. Gentle crushing of foraminifera samples between glass plates to break open the tests was followed by: (i) mechanical cleaning by ultrasonication in distilled water and methanol to remove clays, (ii) reductive cleaning using hydrazine (NH_2NH_2) in a hot citric acid / ammonia buffer solution to remove trace metal enriched ferromanganese oxide coatings, (iii) oxidative removal of organic matter with hot alkali buffered H_2O_2 solution and (iv) a series of leaching steps with 0.001 M HNO_3 to remove adsorbed contaminants and any manganese carbonate coating. If preparation of a single foraminifer is required, the cleaning procedure is modified for small samples according to Boyle [1995]. The cleaned foraminifera fragments were dissolved by ultrasonicating in 250 – 500 µl of 0.075 M HNO_3 and centifuged to remove any remaining undissolved non-carbonate particles.

5.4.3 Subsampling and spiking

Dissolved samples were split into two unequal fractions; one (80-90%) for Cd determination by ID-TIMS and the other (20-10%) for Ca, Mn, Mg/Ca and Sr/Ca determinations by ICP-OES. The solutions were pipetted into clean pre-weighed 7ml Savillex PFA vials (Cd fraction) and clean pre-weighed 0.5ml microcentrifuge tubes (Ca, Mn etc fraction) taking 50 µl for the Ca, Mn fraction and the remaining 200-450 µl for Cd determination. Both sets of vials and solutions were weighed using a 4 decimal place analytical balance (0.1 mg resolution).

The Ca fraction was diluted (by weight) for accurate determination of Ca by ICP-OES together with Mn/Ca, Mg/Ca and Sr/Ca [de Villiers *et al*., 2002] following procedures detailed in Chapter 2. Any samples with Mn/Ca >100 μmol/mol were rejected on the basis that FeMn coatings had not been sufficiently removed by the cleaning procedure.

The Cd fraction was spiked (by weight) with 0.25 pmol ^{116}Cd spike (100 μl 2.5 pmol g^{-1} ^{116}Cd solution) and evaporated ready for column chemistry.

5.4.4 Separation of Cd

AG50W-X8 200-400 mesh resin was rinsed 5 times in QD (quartz distilled) H_2O to remove the fine fraction, followed by a 24hr soak in QD 6M HCl. Savillex PFA columns (3.2mm ID, 4.0cm length, 5ml reservoir) with polyethylene frits were filled with the cleaned resin. 12 ml of 6M HCl was applied to further clean the resin before conditioning with 1 ml 1M HCl. The dried, spiked samples were dissolved in 50 μl of 1M HCl and added to the columns, under which were placed clean 7 ml Savillex vials. The 50 μl sample was washed in with 2 aliquots of 50 μl 1M HCl and Cd eluted with 1 aliquot of 1ml 1M HCl. The 1.15 ml sample was then evaporated to dryness (~1hr). The samples may be stored at this point. After use the columns were washed free of resin and soaked in hot 10% HNO_3 ready for re-use. It is important to use new resin for each sample so as to avoid any carry over of Ca from a previous sample which can occur despite rigorous cleaning of the resin.

5.4.5 Cd sample loading

Re filaments were outgassed at 3.5A for 40 minutes and removed immediately prior to loading. Fresh loading solution was prepared by adding 20 µl colloidal silicic acid to 1 ml 0.1M H_3PO_4 while agitating in an ultrasonic bath. 1 μl 0.2M HNO_3 was added to the vial containing the Cd sample to dissolve it. Next, 1 µl silica gel in 0.1M H_3PO_4 was added to adsorb the dissolved sample. The mixture was applied in two 1 µl aliquots to the Re filament, preheated by a current of 0.8 A, and allowed to dry at 0.8 A between each application. The filament current was then increased at a rate of ~0.1 A/min to 1.1 A and the sample allowed to dry for 2 minutes before decreasing the current to zero and mounting the filament in the mass spectrometer turret.

5.4.6 Mass spectrometry

The TIMS analysis was performed on a VG Sector 54 mass spectrometer. The filament was degassed by heating with a current of 1.1 A before the current was increased slowly

to 1.9 A over 23 min to warm the sample. The ^{116}Cd ion beam was focused to a targetted ^{116}Cd ion beam of initially 5 x 10^{-15} A and then 1 x 10^{-14} A. The $^{114}Cd/^{116}Cd$ ratio was measured over 3 cycles of 10 ratios and 5 cycles of 10 ratios, respectively, with a maximum filament current set to 2.5A. The silca gel loading technique minimises isotopic fractionation during sample evaporation from the filament and no correction was applied. Precision on the measured $^{114}Cd/^{116}Cd$ ratio was typically <0.1% S.E. on 50 ratios.

5.5 Blanks and method reproducibility

5.5.1 The analytical blank

The range of blanks for the reagents and the complete procedure measured by direct determination is detailed in Table 5.3. The principal contribution to the total blank comes from the HCl reagent. A mean blank of 1.5 pg was obtained for the complete procedure, determined on 18 occasions during a three year period. Where the procedure blank was significant relative to sample size a correction was applied to the results.

Type of Blank	**Determination Method**	**Cd blank (pg)** Mean ± s.d.	n
Reagent			
Si Gel	ID-TIMS on 2 μl	0.37	1
QD 0.2M HNO_3	ID-TIMS on 1 ml	0.23	1
QD H_2O	ID-TIMS on 1 ml	0.27	2
QD 1M HCl	ID-TIMS on 1 ml	1.19 ± 0.31	3
Loading	Routine analysis of Cd-1 Spike	0.20 ± 0.37	164
Column	1.15ml QD 1M HCl passed through columns	1.10 ± 1.10	26
Procedure	Empty vial through the complete procedure	1.54 ± 1.17	18
	Intercept of Cd at zero Ca (planktonic analyses)	1.18 ± 0.30	3

Table 5.3 The Cd blank in various stages of the procedure.

The results of an alternative measure of the total Cd blank, derived from the extrapolation of experimental Cd vs Ca measurements back to zero Ca, are also given in Table 4.3. The sensitivity of the method was investigated by analysing samples of varying size, ranging from 20 to 70 individuals of *G. bulloides* and *N. pachyderma* (dextral) from the 300-350 μm size fraction of the same samples, taken from two box core tops in the North Atlantic. Estimates of the procedure blank were obtained from the intercept at Ca = 0 of the linear best fit lines of the mass of Cd recovered when plotted against mass of Ca (Fig. 5.2). This method estimates the average blank contribution for each set of analyses, the slopes of the lines giving the mean Cd/Ca of each sample. Uncertainty in the blank estimate, as defined by the uncertainty in the intercept, is a function of the variation in the blank, the precision of the individual analyses and the slope of the mixing line.

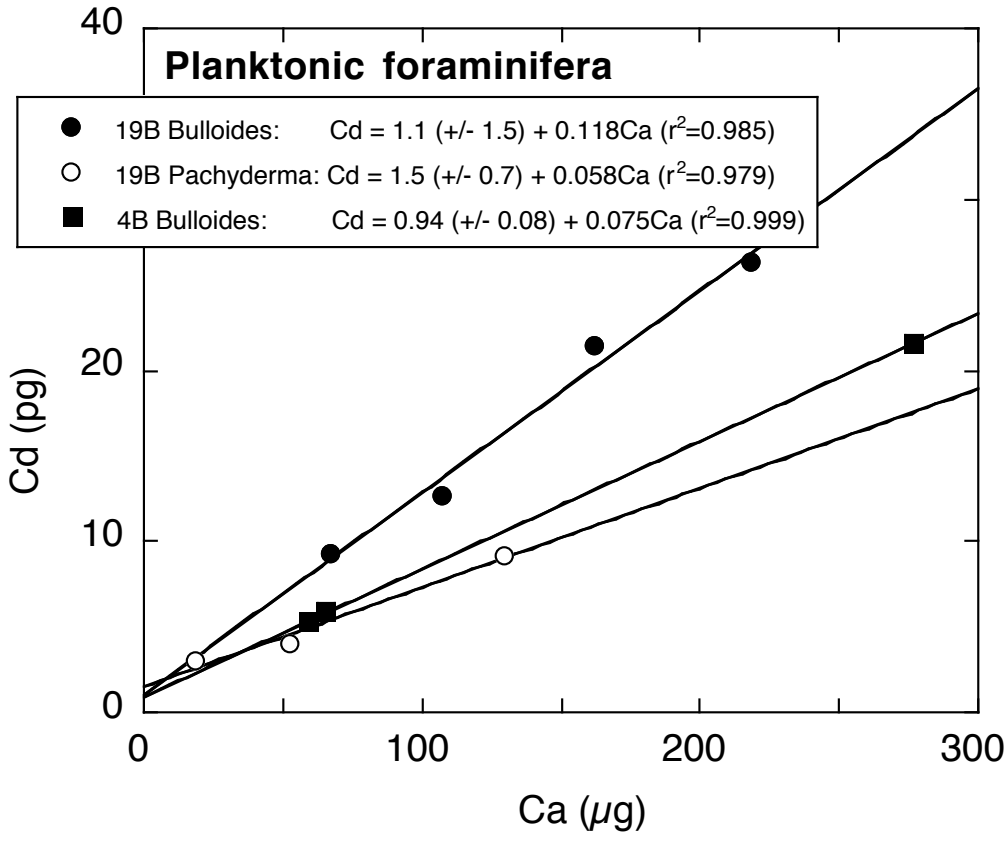

Figure 5.2 Cd (pg) v Ca (μg) for varying sized samples of *G. bulloides* (closed symbols) and *N. pachyderma* (dextral) (open circles). Estimated uncertainty on each intercept is shown in parentheses. [reproduced from Rickaby *et al*. 2000]

5.5.2 Reproducibility

Reproducibility of the method as demonstrated by the replicate analyses of consistency standards is shown in Table 5.4. Two consistency standards, CS1 and CS3, each containing ~800 ppm Ca and respectively benthic and planktonic foraminifera Cd/Ca ratios, were analysed by processing aliquots through the method along with batches of samples. The relative standard deviations of 1.2% and 3.4% on Cd/Ca ratios reflect the increase in r.s.d resulting from the lower Cd in the planktonic foraminifera analogue; the weights of Cd loaded were typical for benthic and planktonic foraminifera Cd/Ca determinations.

Analysis	solution mass (g)	Cd pmol/g	pg	Ca µmol/g	Cd/Ca µmol/mol
CS1 Benthic standard					
1	0.198	5.46	122	19.6	0.279
2	0.198	5.49	123	19.3	0.284
3	0.101	5.62	64	19.6	0.288
4	0.200	5.48	123	19.3	0.284
mean		5.51		19.4	0.284
s.d.		0.07		0.2	0.003
r.s.d. (%)		1.3		0.8	1.2
CS3 Planktonic standard					
1	0.200	0.996	22.4	19.8	0.0504
2	0.200	0.990	22.2	19.2	0.0515
3	0.198	0.955	21.3	19.7	0.0485
4	0.200	0.947	21.3	19.8	0.0479
mean		0.972		19.6	0.0496
s.d.		0.025		0.3	0.0017
r.s.d. (%)		2.5		1.4	3.4

Table 5.4 Reproducibility of consistency standards.

The reproducibility and reliability of the method when analysing foraminifera samples were demonstrated by Rickaby *et al*. [2000] where seawater cadmium concentrations calculated from foraminiferal Cd/Ca determined by the ID-TIMS method were compared with results of previously published studies. A benthic Cd/Ca depth transect was obtained from a series of cores between 52°N and 61°N in the N. Atlantic over depths from 1510 to 3275 m, for both the Holocene and Stage 2 Glacial Maximum (LGM). Foraminiferal Cd/Ca derived using the ID-TIMS method and previously published North Atlantic data [Boyle, 1992; Bertram *et al*., 1995] were converted to seawater Cd concentrations (Cd_{sw}) using the $D_{depth\text{-}dependent}$ described by Boyle [1992]. A comparison of Cd_{sw} versus depth for the Holocene and Glacial and the consistency of the ID-TIMS data with those of the previous studies for a large range of Cd/Ca ratios regardless of sample size demonstrated the flexibility and reliability of the method. An initial study was made of Cd/Ca in planktonic foraminifera from the North Atlantic, demonstrating the capability of the method to resolve small differences in Cd/Ca of the order of 0.01 μmol/mol.

5.6 Conclusions

An ID-TIMS method was developed for the analysis of picogram quantities of cadmium found in the shells of benthic and planktonic foraminifera. The method permits analysis of the Cd/Ca ratio both of small amounts of cleaned benthic foraminiferal calcite (0.06 mg or ~1 foraminifer) and of more typically sized samples to a high precision and accuracy on a routine basis. The precision of the method permits detailed studies of processes affecting shell chemistry to be carried out on individual benthic foraminifera and allows precise down core studies of multi-species planktonic foraminifera to be made at low Cd/Ca ratios.

Chapter 6

Calibration of planktonic foraminiferal Cd/Ca as a palaeoceanographic tracer for surface water nutrients.

6.1 Introduction

The palaeoceanographic application of Cd/Ca ratios in benthic foraminifera is well established as a proxy for deepwater phosphate and deep ocean circulation [e.g. Boyle, 1981, 1988, 1992; Bertram *et al.,* 1995; Beveridge *et al.,* 1995; Marchitto *et al.,* 1998, 2002; Marchitto and Broecker, 2006]. The use of Cd/Ca ratios in planktonic foraminifera for reconstruction of surface ocean phosphate utilisation is complicated by reported evidence of a temperature dependence in the incorporation of cadmium into planktonic foraminiferal calcite [Rickaby and Elderfield, 1999] and by non-linearity of the cadmium:phosphate relationship in surface waters [Elderfield and Rickaby, 2000]. Application of cadmium in planktonic foraminifera as a proxy for surface water nutrients depends critically on knowledge of the partition coefficient D_{Cd} between foraminiferal calcite and seawater which in turn depends on a thorough understanding of the relationship between cadmium and phosphate in seawater [de Baar *et al.*, 1994; Yeats, 1998; Elderfield and Rickaby, 2000].

Cadmium substitutes for calcium in foraminiferal carbonate with an empirical partition coefficient D_{Cd} and, because the cadmium distribution in ocean waters resembles that of phosphate [Boyle *et al.*, 1976; Boyle, 1988; de Baar *et al.*, 1994; Elderfield and Rickaby, 2000], D_{Cd} can be interpreted in terms of seawater phosphate concentrations $[PO_4]_{sw}$:

$$D_{Cd} = \frac{\left(\frac{Cd}{Ca}\right)_{foram}}{\left(\frac{Cd}{Ca}\right)_{sw}} = \frac{\left(\frac{Cd}{Ca}\right)_{foram}}{\left(Cd/P\right)_{sw} \frac{[PO_4]_{sw}}{[Ca]_{sw}}} \quad (6.1)$$

where $(Cd/Ca)_{foram}$ is the measured ratio in foraminifera shells, $(Cd/P)_{sw}$ is the seawater cadmium:phosphate ratio (slope of the oceanic cadmium versus dissolved phosphate relationship) and $[Ca]_{sw}$ is the seawater calcium concentration which can be assumed to be constant. Experimental determinations of D_{Cd} for Cd incorporation into planktonic foraminifera have been performed using culture studies, giving estimated D_{Cd} = 2 to 4 [Delaney, 1989] and D_{Cd} = 1.9 [Mashiotta *et al.*, 1997]. In a study of Cd/Ca in *Globigerinoides bulloides* collected from core tops on a latitudinal transect in the North Atlantic Ocean, Rickaby and Elderfield [1999] found a temperature dependence of D_{Cd}. The partition coefficient was shown to increase over the temperature range 8 to 15 ºC by ~ 15 % per ºC with the relationship:

$$D_{Cd} = 0.637 \exp 0.15T \quad (6.2)$$

This calibration was revised subsequently by Elderfield and Rickaby [2000] taking into account the systematics of Cd and P in surface waters to give:

$$D_{Cd} = 0.75 \exp 0.16T \quad (6.3)$$

Over the 8 to 15 ºC temperature interval investigated by Rickaby and Elderfield [1999], D_{Cd} values for *G. bulloides* ranged from 1.5 to 6.9.

Marchitto [2004] investigated the incorporation of cadmium into the tests of benthic foraminifera and found no evidence for a significant temperature influence on the partition coefficients of six calcitic foraminifera taxa, or the aragonitic species *Hoeglundina elegans*, over the temperature range 4 to 18 ºC.

This study uses records of planktonic foraminiferal Cd/Ca, Mg/Ca and oxygen isotopes from seven species of planktonic foraminifera, *Neogloboquadrina pachyderma (d), Globigerinoides ruber (w)*, *Globigerinoides sacculifer*, *Globigerinella siphonifera, Globorotalia hirsuta*, *Globorotalia inflata* and *Globorotalia truncatulinoides (d)*, from

the same North Atlantic transect used by Rickaby and Elderfield [1999], in a multispecies investigation of temperature influence on planktonic foraminiferal Cd/Ca ratios.

6.1.1 Cadmium and phosphorus in seawater

The cadmium:phosphate relationship in seawater is governed by the incorporation of cadmium into organic matter in the surface ocean and its regeneration on the breakdown of organic matter at depth. The non-linear global cadmium:phosphate relationship (Figure 6.1) was interpreted by Elderfield and Rickaby [2000] to reflect preferential incorporation of cadmium relative to phosphorus into particulate organic matter during photosynthesis. The curvature in the cadmium:phosphorus relationship was modelled using a Rayleigh model and a constant fractionation factor

$$\alpha_{Cd/P} = (Cd/P)_{POM} / (Cd/P)_{SW} \quad (6.4)$$

where the subscripts POM and SW represent respectively particulate organic matter and seawater [Elderfield and Rickaby, 2000]. The preferential incorporation of cadmium into particulate organic matter is reflected in $\alpha_{Cd/P} > 1$ with a global $\alpha_{Cd/P}$ of ~2 (Figure 6.1). Oceanic cadmium can be related to phosphorus by the equation:

$$Cd = 1.2 / (\alpha_{Cd/P}(3.3/P - 1) + 1) \quad (6.5)$$

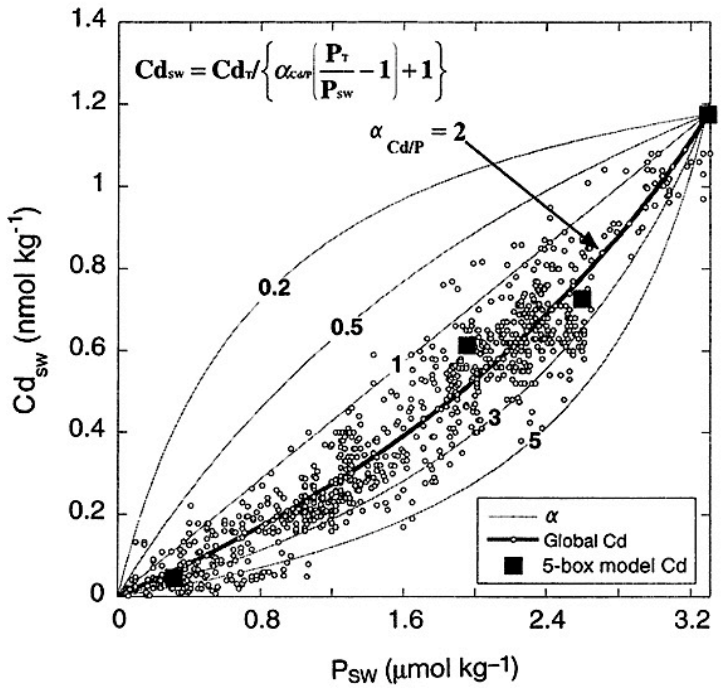

Figure 6.1 Global dissolved cadmium versus phosphate, reproduced from Elderfield and Rickaby [2000]. Curves show solutions to the fractionation equation for discrete values of $\alpha_{Cd/P}$. Bold line is best fit to the global data set, using $\alpha_{Cd/P} = 2$ with average total Cd and P, $Cd_T = 1.2$ nmol kg^{-1} and $P_T = 3.3$ µmol kg^{-1}.

Approximation of the global seawater cadmium:phosphate relationship by a single value of the fractionation factor $\alpha_{Cd/P} = 2$ includes variations within and between the oceans. Surface seawaters are depleted in cadmium relative to phosphate whereas deep waters are relatively enriched by the regeneration of particulate matter containing high Cd/P. The cadmium:phosphate relationship for surface and nutrient depleted deep waters of the North Atlantic Ocean is shown in Figure 6.2 where the best fit curve is given by $\alpha_{Cd/P} = 2.5$ [Elderfield and Rickaby, 2000].

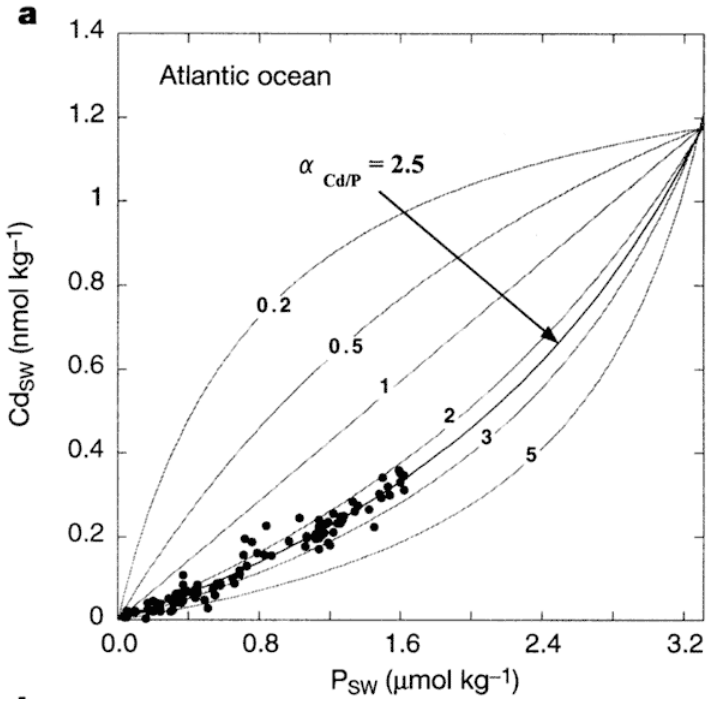

Figure 6.2 Dissolved cadmium versus phosphate for surface and deep waters of the Atlantic Ocean, reproduced from Elderfield and Rickaby [2000].

The compilation of Cd/P in global surface seawater by Elderfield and Rickaby [2000] shows an increase in surface seawater Cd/P from low to high latitudes. Higher phosphorus concentrations and high Cd/P ratios occur at high latitudes whereas at low latitudes lower phosphorus concentrations and low Cd/P ratios are found.

Cadmium is thought to be removed from surface seawater by phytoplankton through the production of a cadmium carbonic anhydrase during inorganic carbon acquisition, providing a mechanism which may regulate the Cd/P ratio of surface seawater [Cullen *et al.*, 1999]. The marine diatom *Thalassiosira weissflogii* was shown by Lane *et al.* [2005] to contain cadmium carbonic anhydrase as a native enzyme, giving a possible biological explanation for the nutrient like behaviour of cadmium in the oceans.

6.2 Materials and methods

6.2.1 Locations of cores

A suite of box core tops, collected between 30º and 60ºN in the North Atlantic during the Actuomicropaleontology Paleoceanography North Atlantic Project (APNAP) (Table 6.1 and Figure 6.3) was used to investigate the variability of D_{Cd} into seven species of planktonic foraminifera, *Neogloboquadrina pachyderma (d), Globigerinoides ruber (w)*, *Globigerinoides sacculifer*, *Globigerinella siphonifera, Globorotalia hirsuta*, *Globorotalia inflata* and *Globorotalia truncatulinoides (d)* spanning a range of temperatures from 6º to 19ºC (Table 6.2). These core tops have been used in a number of previous studies taking advantage of systematic changes in surface water hydrography along this latitudinal transect [Rickaby and Elderfield, 1999; Elderfield and Ganssen, 2000; Elderfield *et al.,* 2000; Ganssen and Kroon, 2000; Barker and Elderfield, 2002; Yu *et al.,* 2007]. Radiocarbon dating verified that the core tops sampled were < 3 ka [Rickaby and Elderfield, 1999; Ganssen and Kroon, 2000].

Core	Latitude (°N)	Longitude (°W)	Depth (m)
T88 1B	59.7	27.4	2010
T90 1B	58.5	20.5	2911
T88 2B	57.9	26.0	2767
T88 3B	56.4	27.8	2819
T88 4B	55.0	28.3	2821
T88 5B	53.6	27.1	2812
T86 1B	53.4	27.5	2580
T90 2B	53.1	20.8	2731
T88 6B	51.4	25.8	3381
T88 7B	50.5	26.5	3013
T86 3B	50.2	27.0	3113
T88 9B	48.4	25.1	3074
T90 3B	47.7	20.8	4479
T90 15B	47.6	20.9	4177
T90 4B	47.2	21.4	3945
T86 5B	46.9	25.4	3121
T90 8B	46.2	23.7	3393
T90 5B	46.0	23.8	3069
T88 11B	45.4	25.4	2741
T90 11B	45.0	24.7	3208
T88 12B	44.1	24.9	3052
T86 7B	43.9	25.0	2664
T88 13B	42.9	25.3	3133
T86 8B	42.3	25.7	3232
T86 9B	40.8	27.5	2026
T88 14B	40.4	25.8	2858
T88 15A	38.9	25.0	2738
T88 15B	38.6	25.0	2585
T86 10B	37.1	30.0	2610
T86 11B	35.6	32.6	2220
T88 17B	35.4	29.4	2934

Table 6.1 Locations and depths of cores sampled

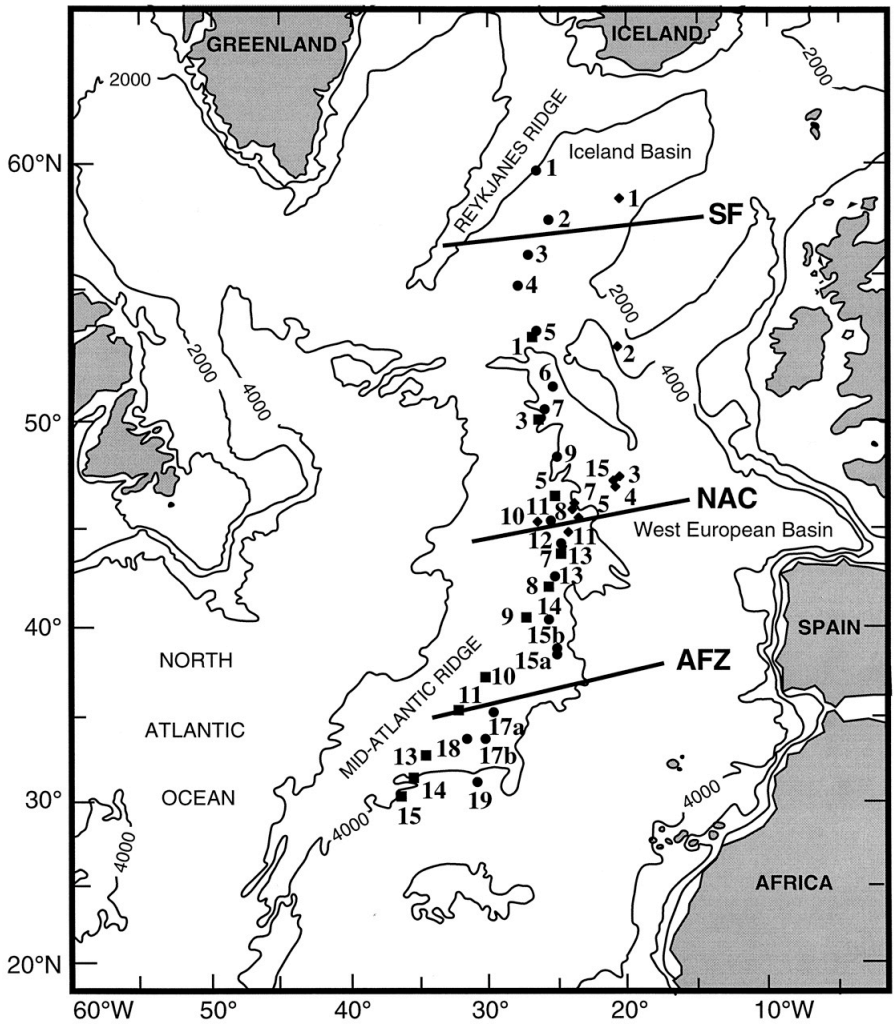

Figure 6.3 Locations of box cores collected during the Actuomicropaleontology Paleoceanography North Atlantic Project (APNAP). Symbols show cores collected in 1986 ■, 1988 ● and 1990 ◆. The main hydrographic fronts [after Ottens 1991] are indicated: SF, Subpolar Front; NAC, North Atlantic Current; AFZ, Azores Frontal Zone. Bathymetric contours of 1000 m, 2000 m and 4000 m also shown. [reproduced from Ganssen & Kroon, 2000]

6.2.2 Modern Hydrography

A large latitudinal and seasonal range in temperature and phosphate is observed in the surface waters of the Northeast Atlantic Ocean, illustrated by monthly data at 27 ºW [Garcia *et al.,* 2006; Locarnini *et al.,* 2006] (Figure 6.4). The north to south transect crosses environments ranging from subpolar to subtropical with surface water masses separated by a series of fronts [Ganssen and Kroon, 2000]. Cold, subpolar water is

separated from the North Atlantic Current by the Subarctic Front at about 57 °N (Figure 6.3). The southernmost extent of the North Atlantic Current occurs at approximately 45 °N with North Atlantic Transitional Water present to the South of this latitude until the Azores Frontal Zone, located at about 35 °N, separates North Atlantic Transitional Water from warmer waters of the subtropical gyre [Ottens 1991]. Temperature and carbonate ion concentration [CO_3^{2-}] are highly correlated in the surface waters of the North Atlantic Ocean [Barker and Elderfield, 2002] increasing from North to South along the latitudinal transect of this study.

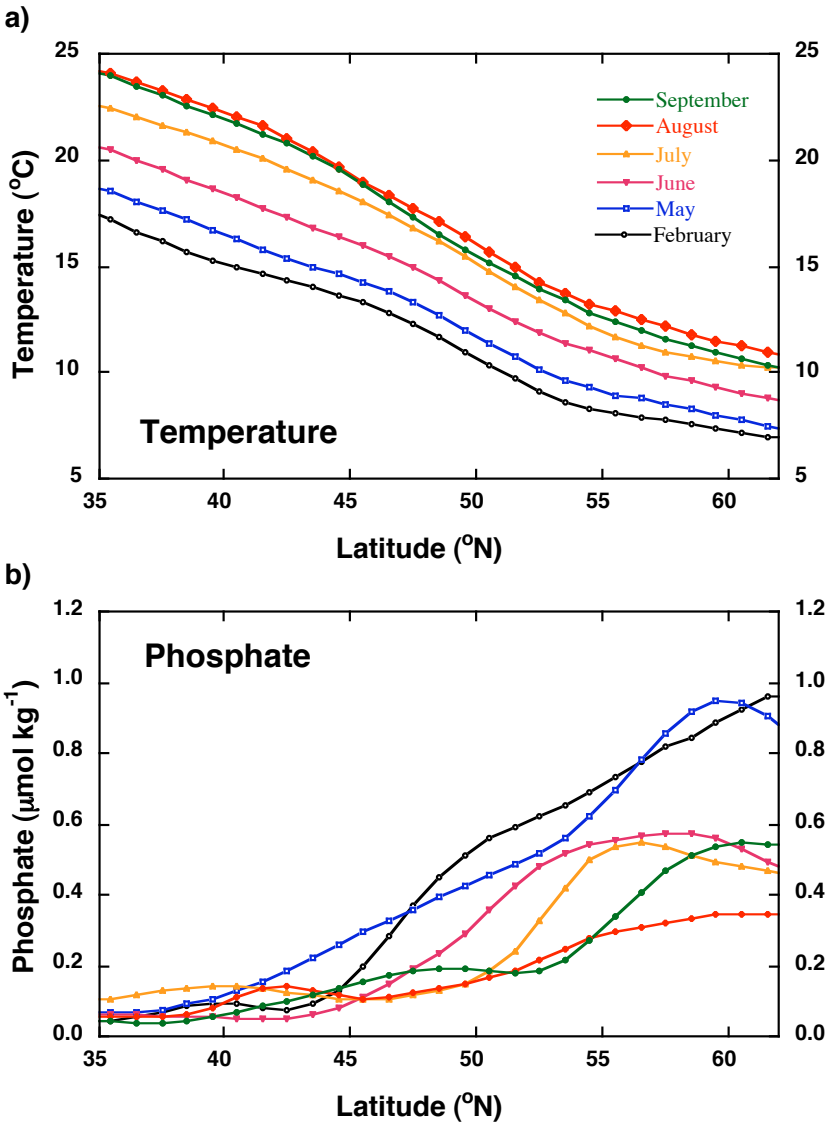

Figure 6.4 (a) Sea surface temperature [Locarnini *et al.*, 2006], (b) Surface water phosphate [Garcia *et al.*, 2006] versus latitude at 27 °W in the Northeast Atlantic Ocean.

6.2.3 Analytical methods

Samples of the species listed in Table 6.2 were picked from the 250-355 μm size fractions of the washed sediment. Analyses of *G. ruber (w)*, *G. sacculifer* (without sac-like final chamber), *G. siphonifera, G. inflata* and *G. truncatulinoides (d)* were performed using approximately 50 individuals. Larger samples of ~70 tests were taken for *N. pachyderma (d)* and smaller samples, ~36 individuals, were used for *G. hirsuta*. The cleaning procedure and instrumental method for foraminiferal Cd/Ca determination are discussed in detail in Chapter 5, a brief summary is given here.

The traditional reductive, oxidative and dilute acid leach cleaning steps developed by Boyle and Keigwin [1985/86], as modified by Rosenthal *et al*. [1997] were followed. Cd/Ca ratios were determined by the ID-TIMS method for low level Cd determination [Rickaby et al. 2000] described in Chapter 5. The Cd/Ca results were corrected for the cadmium blank determined during the procedure. Mn/Ca, Mg/Ca and Sr/Ca ratios were determined by ICP-OES [de Villiers *et al*., 2002] following procedures detailed in Chapter 2. A value of Mn/Ca >100 μmol/mol was used to identify analyses as suspect on the basis that FeMn coatings had not been sufficiently removed by the cleaning procedure.

Species	Latitude range (ºN)			Temperature range (ºC) *		
Neogloboquadrina pachyderma (d)	35.4	-	59.7	9.2	-	15.1
Globorotalia inflata	35.4	-	59.7	7.0	-	14.5
Globorotalia hirsuta	35.4	-	58.5	6.4	-	14.4
Globorotalia truncatulinoides (d)	35.4	-	53.1	8.6	-	13.8
Globigerinella siphonifera	35.4	-	47.7	12.9	-	16.2
Globigerinoides ruber (w)	35.4	-	47.7	16.3	-	18.9
Globigerinoides sacculifer	35.4	-	46.2	17.0	-	19.3

* calcification temperatures of the foraminifera calculated from $\delta^{18}O$.

Table 6.2 Foraminifera species analysed

6.3 Latitudinal variations in foraminiferal Cd/Ca from a core top transect in the North Atlantic Ocean

Planktonic foraminiferal Cd/Ca and Mg/Ca ratios determined in the seven species picked from core tops are compared with the Cd/Ca results for *G. bulloides* obtained by Rickaby and Elderfield [1999] in Figure 6.5. The majority of the samples analysed contained < 10 μmol/mol Mn/Ca and only a single analysis contained > 30 μmol/mol, confirming a negligible effect on measured Cd/Ca from coatings. The data are tabulated in Appendix 3. Mg/Ca and Sr/Ca results presented in this chapter, obtained after reductive cleaning, were compared in Chapter 2 to the Mg/Ca and Sr/Ca data from Elderfield and Ganssen [2000] and Elderfield *et al.* [2000] for the same samples analysed after cleaning without the reductive step.

Cd/Ca in *N. pachyderma (d)*, one of two species occurring over the full latitudinal range of the transect (Table 6.2), shows a latitudinal variation similar to, but less pronounced than, the relationship for *G. bulloides* found by Rickaby and Elderfield [1999]. With the exception of an anomalously high data point at each end of the transect, a south to north latitudinal decrease in *N. pachyderma (d)* Cd/Ca of ~ 0.03 μmol mol^{-1} is observed (Figure 6.5b) compared to ~ 0.05 μmol mol^{-1} for *G. bulloides* (Figure 6.5a). The latitudinal trend in *N. pachyderma (d)* Cd/Ca resembles the Mg/Ca trend (Figure 6.5b) suggesting that the same controls influence both element ratios.

The globigerinids, *G. ruber (w)* and *G. sacculifer,* and also *G. siphonifera* occurred in the coretops up to about 47 ^{o}N (Table 6.2). All three species show an increase in Cd/Ca with latitude over the transect, opposite to the trend observed for *G. bulloides* and *N. pachyderma (d)* and in marked contrast to the Mg/Ca trends (Figure 6.5c-e). The largest range in Cd/Ca, ~0.05 μmol mol^{-1}, occurs in *G. ruber (w)* (Figure 6.5c) and the smallest, ~0.02 μmol mol^{-1}, in *G. sacculifer* (Figure 6.5d), with *G. siphonifera* showing an intermediate range (Figure 6.5e). A large range in Mg/Ca is observed for all three species, Mg/Ca decreasing with increasing latitude in accordance with surface water temperature (Figure 6.4a).

The deeper dwelling globorotaliids, *G. hirsuta*, *G. inflata* and *G. truncatulinoides* (Figure 6.5 f-h) show generally higher Cd/Ca ratios which may be related to water stratification. In mid latitudes, between about 45 ^{o}N and 50 ^{o}N, *G. hirsuta* (Figure 6.5f) contains high Cd/Ca of approximately 0.09 μmol mol^{-1} with lower Cd/Ca ratios found at both low and high latitudes. *G. inflata* (Figure 6.5g) also shows higher Cd/Ca at mid latitudes but over a much smaller range than *G. hirsuta*. In contrast, the latitudinal trend in *G. truncatulinoides* Cd/Ca (Figure 6.5h) is similar to that seen for *G. ruber (w), G. sacculifer* and *G. siphonifera* (Figure 6.5c-e). Cd/Ca ratios of *G. truncatulinoides* increase with latitude from 35 ^{o}N to 53 ^{o}N, the most northerly occurrence of this species. Mg/Ca ratios in *G. hirsuta*, *G. inflata* and *G. truncatulinoides* decrease with latitude along the transect. Measured values are similar to those found in *N. pachyderma (d)* and, as expected, much lower than Mg/Ca observed in the warm surface water dwelling globigerinids (Figure 6.5c-e).

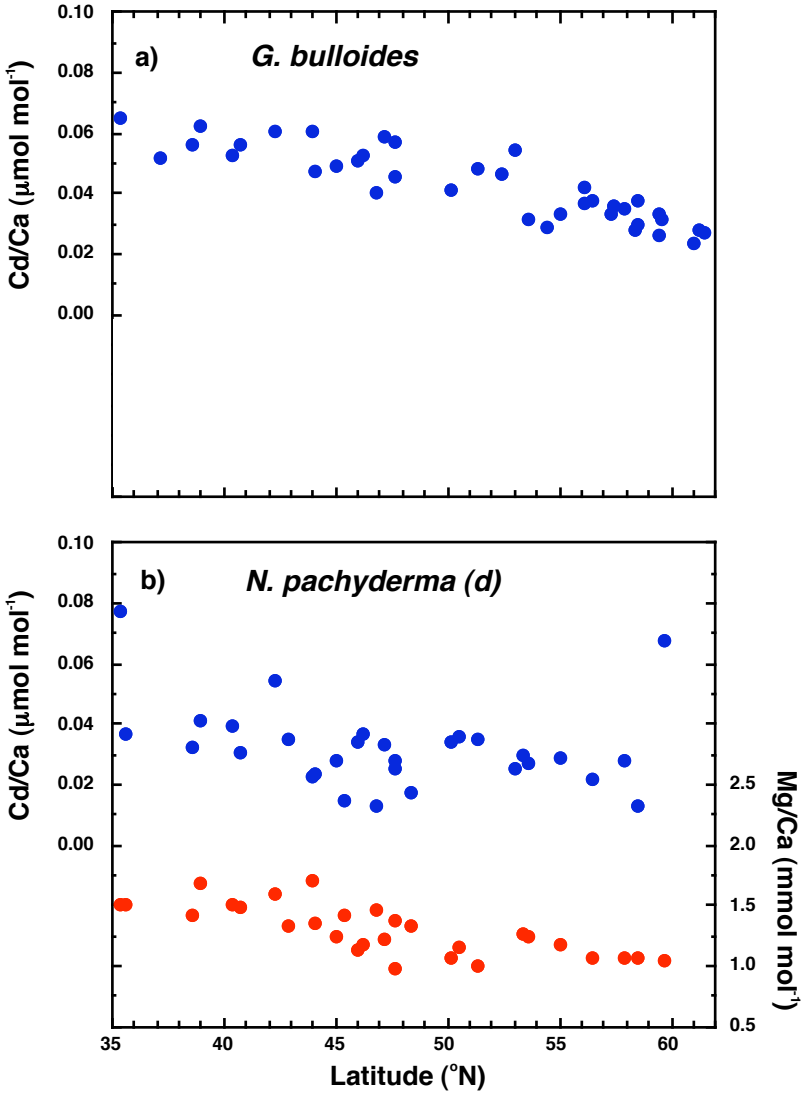

Figure 6.5 Planktonic foraminiferal Cd/Ca (blue) and Mg/Ca (red) versus latitude from the N. Atlantic box core transect (a) *G. bulloides* (Cd/Ca data from Rickaby & Elderfield, 2000), (b) *N. pachyderma (d)*, (c) *G. ruber (w)*, (d) *G. sacculifer*, (e) *G. siphonifera*, (f) *G. hirsuta,* (g) *G. inflata*, (h) *G. truncatulinoides*

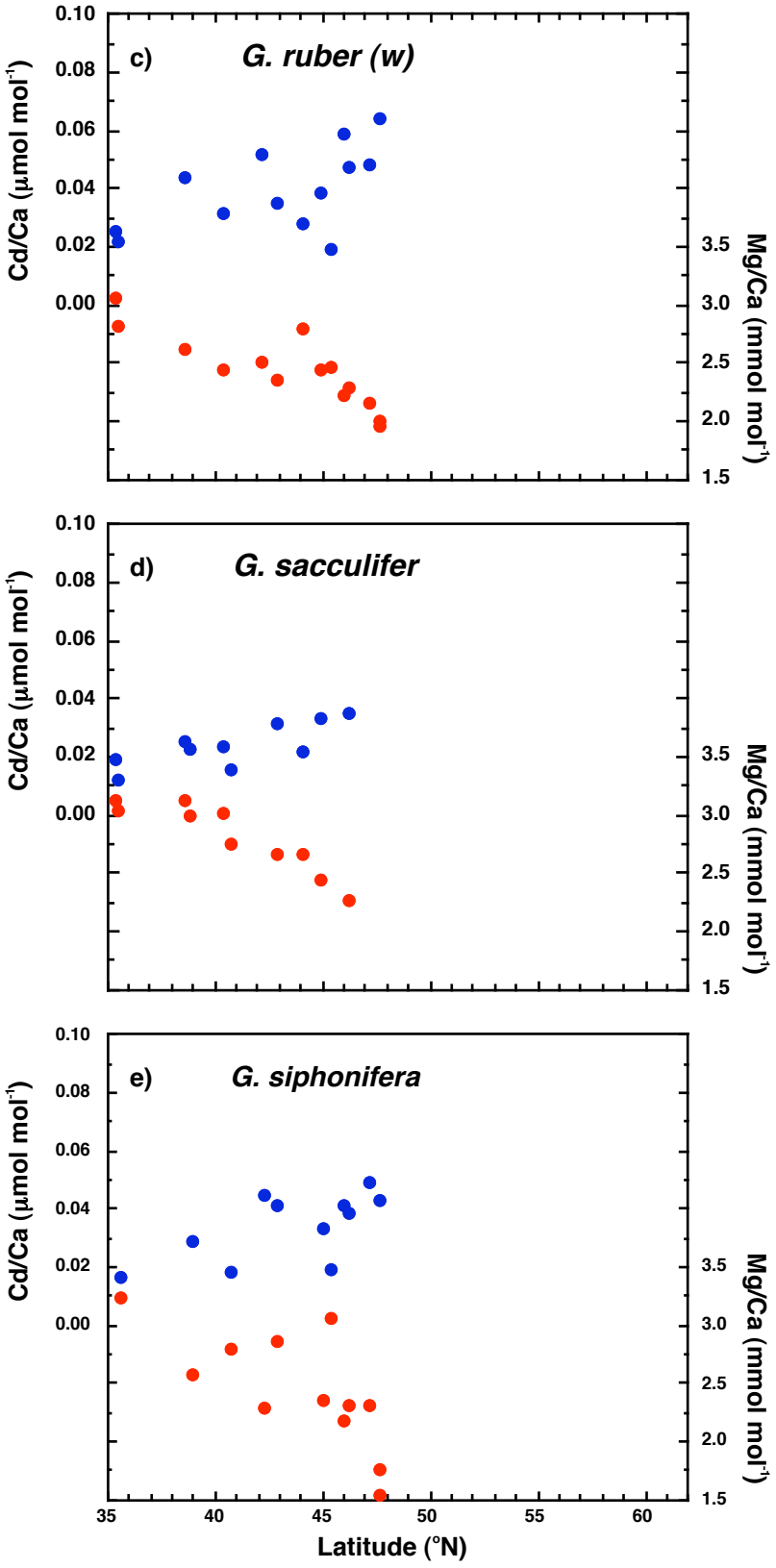

Figure 6.5 Planktonic foraminiferal Cd/Ca (blue) and Mg/Ca (red) versus latitude from N. Atlantic box core transect (c) *G. ruber (w)*, (d) *G. sacculifer*, (e) *G. siphonifera*

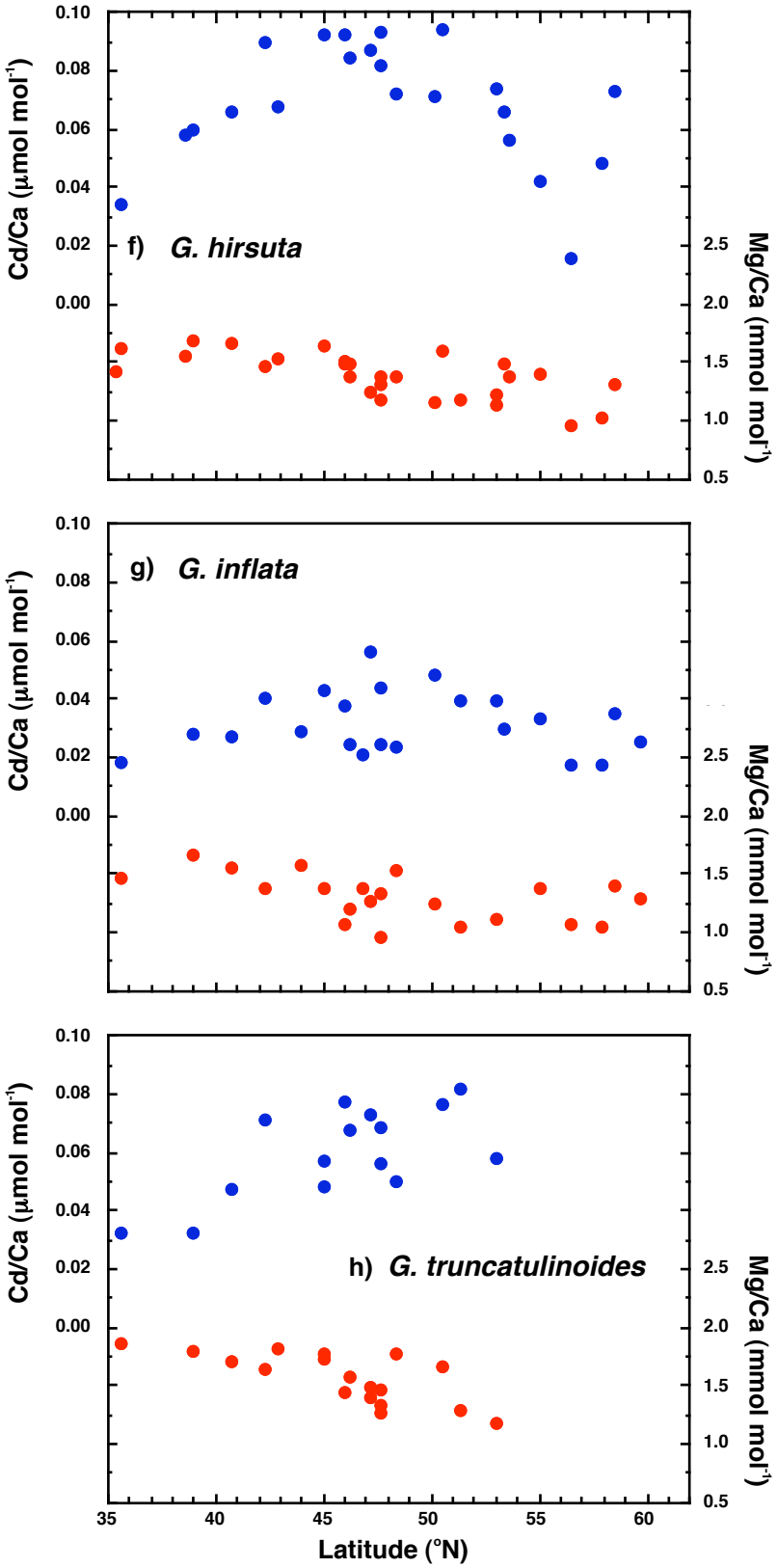

Figure 6.5 Planktonic foraminiferal Cd/Ca (blue) and Mg/Ca (red) versus latitude from the N. Atlantic box core transect (f) *G. hirsuta*, (g) *G. inflata*, (h) *G. truncatulinoides (d)*

Evidence for water stratification can be obtained from the difference in oxygen isotopic composition between surface and deeper dwelling planktonic foraminifera [Mulitza *et al.,* 1997]. Ganssen and Kroon [2000] used the isotopic temperature difference between *G. bulloides* and *G. inflata* as an indicator of stratification in the upper waters above this transect, illustrated in Figure 5 of their paper and reproduced below (Figure 6.6). Their results showed the strongest stratification coincident with the southernmost extent of the North Atlantic Current at about 45 ºN, with stratification decreasing northwards and deep mixing occurring in waters north of 57 ºN, the latitude of the Subarctic Front. The similarity between the pattern observed in Figure 6.6 and the latitudinal trend for Cd/Ca in *G. hirsuta* (Figure 6.5f), provides strong evidence that Cd/Ca in this species is linked to nutrient structure and stratification in the water column.

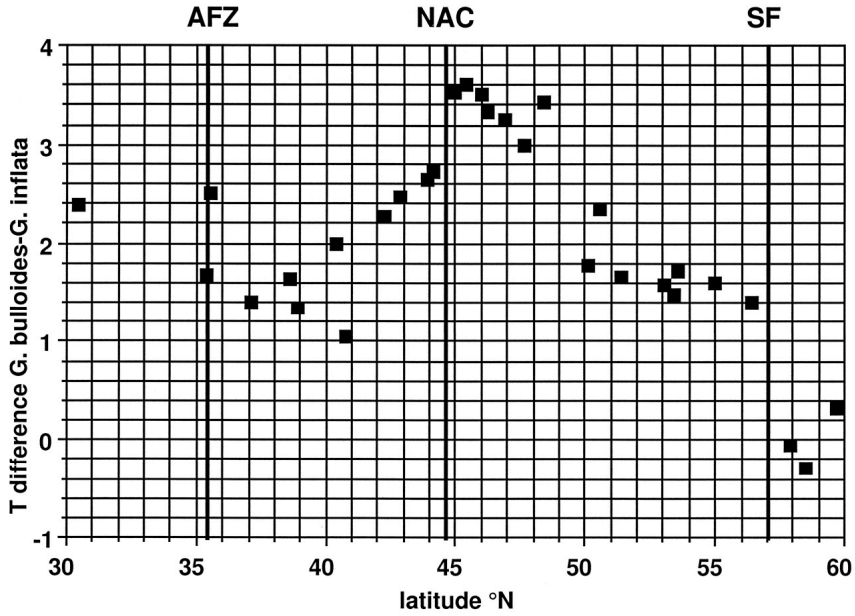

Figure 6.6 Isotope temperature difference between *G. bulloides* and *G. inflata* as a measure for water stratification. [reproduced from Ganssen & Kroon, 2000]. The main water-mass boundaries are indicated; Subarctic Front (SF), southern extent of the North Atlantic Current (NAC) and the Azores Frontal Zone (AFZ).

6.4 Processes controlling Cd/Ca of planktonic foraminiferal calcite

Planktonic foraminiferal Cd/Ca and Mg/Ca records are controlled by the calcification depths and seasons of growth of the foraminifera populations and by water column hydrography. Initial records may be modified by post depositional dissolution, a function of the depth of the sites (Table 6.1), bottom water [CO_3^{2-}] and chemistry of the pore waters. The effects of dissolution depend on the relative susceptibility of individual species.

6.4.1 Foraminiferal habitat and hydrography

Seasonal and depth distributions of planktonic foraminifera over this transect were established by Elderfield and Ganssen [2000] and Ganssen and Kroon [2000] from comparisons of calculated calcification temperatures with modern hydrography. The temperature of calcification for each sample was derived from its $\delta^{18}O_{calcite}$ using the palaeotemperature equation of Shackleton [1974] and $\delta^{18}O$ of modern seawater along the transect.

Hydrographic data, temperature, salinity, phosphate and $\delta^{18}O_{seawater}$ were measured on the 1988 APNAP II cruise [Ganssen and Kroon, 2000]. The $\delta^{18}O_{seawater}$ (V-SMOW) relationship versus salinity derived by Ganssen and Kroon [2000]

$$\delta^{18}O_{seawater} = 0.55602S - 19.448 \quad (r^2 = 0.938) \qquad (6.6)$$

was used to estimate $\delta^{18}O_{seawater}$ over the individual core sites from the 1986 and 1990 cruises (Figure 6.3). The relationship is close to the regional $\delta^{18}O_{seawater}$ salinity relationship for the North Atlantic [Legrande & Schmidt, 2006]:

$$\delta^{18}O_{seawater} = 0.55S - 18.98 \quad (r^2 = 0.951, n = 743)$$

The relationships between oxygen isotopic composition and seawater temperature for *G. bulloides, G. ruber, G. trilobus* (*G. sacculifer* without a sac-like final chamber), *G. inflata and G. truncatulinoides* were discussed in detail by Ganssen and Kroon [2000]. Here, foraminifera calcification temperatures are compared with hydrographic data

from the World Ocean Circulation Experiment (WOCE) and additional species, *G. siphonifera* and *N. pachyderma,* have been included. The seasons and/or depths of calcification were inferred by fitting calcification temperatures to plots of modern monthly seawater temperatures from the World Ocean Atlas 2005 [Locarnini *et al.,* 2006], at discrete depths versus latitude at 27 °W (Figure 6.7). Results are generally consistent with those of other studies using multispecies $\delta^{18}O$ to determine calcification depths and growth seasons [Cleroux *et al.,* 2007; Farmer *et al.,* 2007].

G. ruber (w) reflects surface water conditions with calcification temperatures coinciding with April to June surface water temperatures (Figure 6.7a), calcifying later in the summer further northwards [Ganssen and Kroon, 2000]. Calcification of *G. ruber (w)* occurs between the surface and about 30 m depth [Farmer *et al.,* 2007]. At 30 m depth, calcification temperatures correspond to temperatures between May and July (Figure 6.7b).

G. sacculifer is a mixed layer species believed to live in slightly deeper water than *G. ruber*, calcification occurring predominantly in the depth range 20 to 40 m [Farmer *et al.,* 2007]. Along this transect, *G. sacculifer* calcification temperatures are slightly higher than those of *G. ruber (w)*, corresponding with calcification later in the summer, during June and July for temperatures at 30 m depth (Figure 6.7b).

G. siphonifera also occurs in the mixed layer but may continue to grow while sinking to water deeper than 100 m [Hemleben 1989]. Calcification temperatures of *G. siphonifera* correspond well with seawater temperatures at 75 m along this transect (Figure 6.7c) but also may reflect temperatures at shallower depths in spring (Figure 6.7a, b) whereas at lower latitudes, < 40° N, calcification appears to occur deeper in the water column.

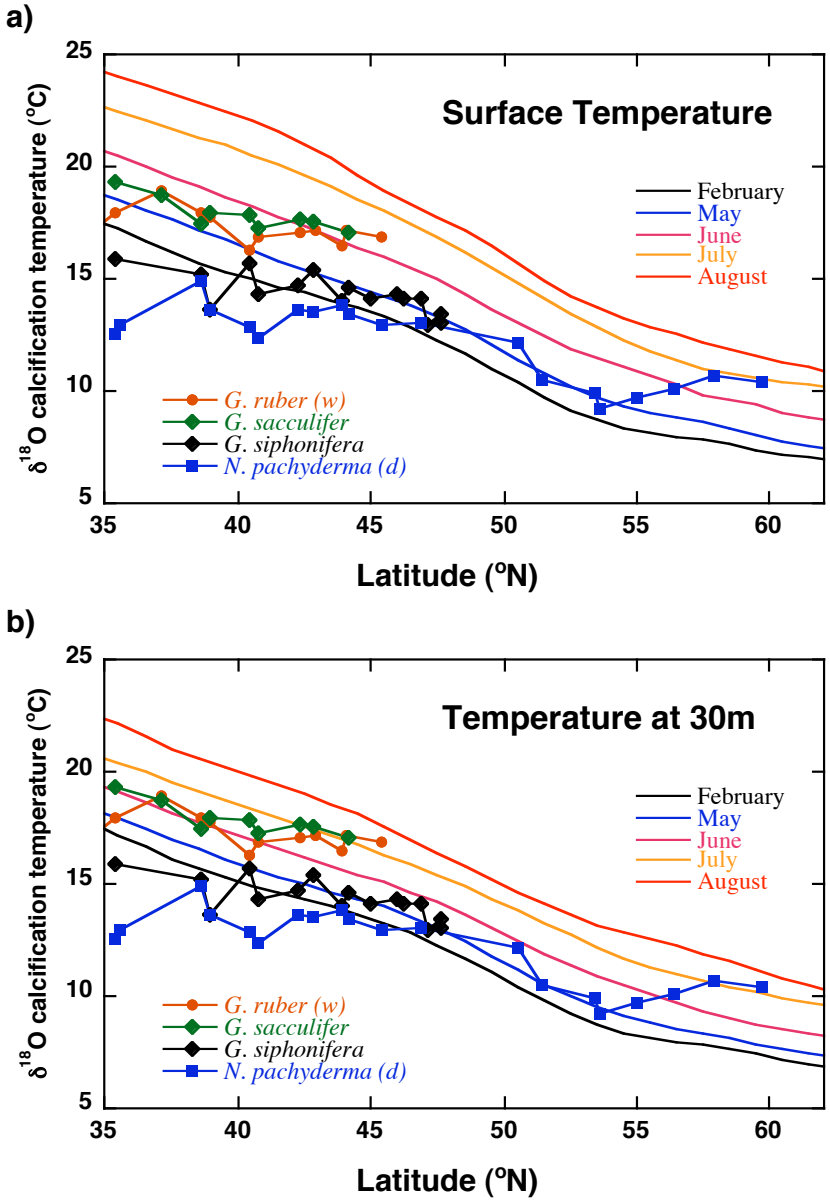

Figure 6.7 Calculated isotopic temperatures for the different species of planktonic foraminifera compared with seawater temperatures [Locarnini *et al.*, 2006] versus latitude at 27 °W in the Northeast Atlantic Ocean (a) Seasonal sea surface temperature (b) Seasonal temperatures at 30 m depth (c) Seasonal temperatures at 75 m depth (d) Annual temperatures at discrete depths from 100 to 500 m.

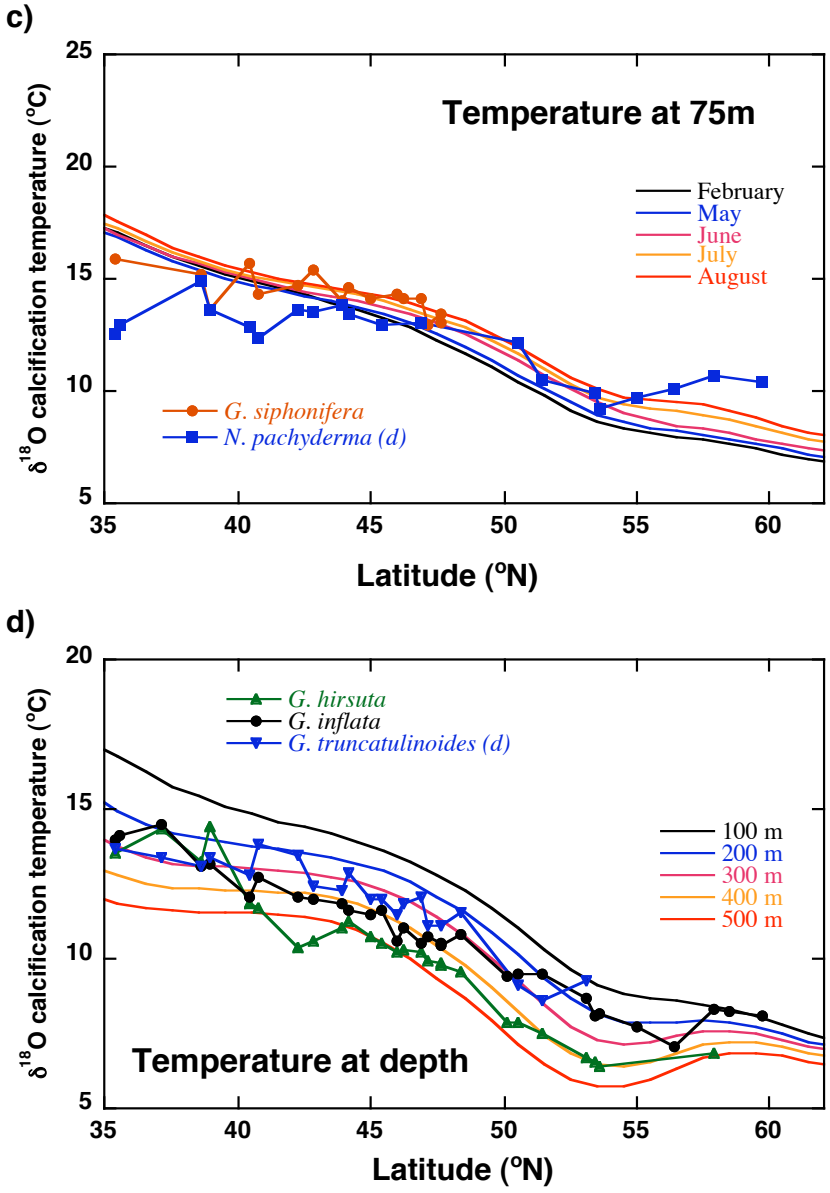

Figure 6.7 Calculated isotopic temperatures for the different species of planktonic foraminifera compared with seawater temperatures [Locarnini *et al.*, 2006] versus latitude at 27 °W in the Northeast Atlantic Ocean (a) Seasonal sea surface temperature (b) Seasonal temperatures at 30 m depth (c) Seasonal temperatures at 75 m depth (d) Annual temperatures at discrete depths from 100 to 500 m.

The behaviour of *N. pachyderma (d)* is more complicated, maintaining a narrow range of calcification temperatures, between 9 and 15 ºC, over a wide latitudinal range. *N. pachyderma (d)* is a mixed layer species typically found at depths between ~30 m and 100 m and calcification temperatures along this transect can be fitted to a range of depths and seasons. At high latitudes from about 50 to 60 ºN calcification temperatures reflect seasonal water temperatures between the surface and 30 m depth (Figure 6.7a,b). At mid latitudes, approximately 42 to 55 ºN, calcification temperatures match seawater temperatures at 75 to 100 m (Figure 6.7c) while at lower latitudes, 35 to 47 ºN, calcification temperatures correspond to water temperatures at depths of 100 m or greater.

The globorotaliids *G. inflata* and *G. truncatulinoides* grow in deeper waters with calcification temperatures corresponding to water depths between 100 and 400 m, depending on latitude [Ganssen and Kroon, 2000]. *G. inflata* calcification temperatures coincide with annual seawater temperatures between 200 and 300 m depth at latitudes < 40 ºN (Figure 6.7d) and with temperatures in deeper waters, close to 400 m, in mid latitudes, until approximately 48 ºN. Further northwards, *G. inflata* calcification temperatures reflect progressively shallower seawater temperatures, until North of 57 ºN temperatures equivalent to those at 100 m are found (Figure 6.7d). A narrower depth range is observed for *G. truncatulinoides (d)*. Calcification temperatures of *G. truncatulinoides (d)* are equivalent to seawater temperatures between 200 and 400 m, frequently close to 300 m, along the entire transect, except for the single most northerly sample (Figure 6.7d).

In comparison, an average calcification depth of ~250 m was determined for *G. truncatulinoides* by Mulitza *et al.* [1997]. Cleroux *et al.* [2007] showed that for temperatures lower than 16 ºC, applicable to this study (see Table 6.2), isotopic temperatures of *G. inflata* and *G. truncatulinoides* corresponded to the temperature at the base of the summer thermocline, defined by Cleroux *et al.* [2007] as the depth where winter and summer temperature profiles coincide. In contrast to the findings of Cleroux *et al.* [2007], along this transect, *G. truncatulinoides* does not appear to occupy a deeper habitat than *G. inflata* (Figure 6.7d). An additional observation made by Cleroux *et al.* [2007] was that *G. inflata* followed the 0.3 to 0.4 μmol kg^{-1} seawater PO_4 concentration line along their North Atlantic longitudinal sections.

The deepest dwelling species studied in this work was *G. hirsuta*, descending below 400 m [Hemleben *et al*., 1989; Elderfield and Ganssen, 2000]. Figure 6.7d suggests that the shallowest depth habitat for *G. hirsuta* occurs at low latitudes, < 40 ºN, where calcification temperatures correspond to seawater temperatures at depths between 200 and 300 m. In mid latitudes, from 40 to 46 º N, *G. hirsuta* calcification temperatures coincide with the deepest seawater temperatures, at depths of 500 m and below. Further northwards, *G. hirsuta* calcification temperatures reflect a progressively shallower depth habitat, in a similar manner to *G. inflata,* although *G. hirsuta* remains deeper than 400 m.

6.4.2 Dissolution effects on foraminiferal Cd/Ca

Post depositional carbonate dissolution affects foraminiferal Mg/Ca and Sr/Ca because of heterogeneity within the shells; preferential dissolution of high Mg and high Sr calcite produces lower Mg/Ca and Sr/Ca ratios [Lohmann, 1995; McCorkle *et al.,* 1995; Brown and Elderfield, 1996; Rosenthal *et al*., 2000; Dekens *et al*., 2002; Regenberg *et al*., 2006]. Strong decreases in benthic (*Cibicidoides wuellerstorfi*) foraminiferal Cd/Ca, Ba/Ca and Sr/Ca ratios with increasing water depth have been observed at water depths greater than about 2.5 km. [McCorkle *et al*.,1995; Elderfield *et al*.,1996]. Elderfield *et al*. [2000], in analyses of planktonic foraminifera from this North Atlantic transect, observed decreases in Sr/Ca with depth for the globorotaliid species (*G. hirsuta*, *G. inflata* and *G. truncatulinoides*) but not for other species (*G. ruber (w)*, *G. bulloides, N. pachyderma (d), G. sacculifer*, *G. siphonifera)*. Decreases in Sr/Ca with depth were attributed to either depth dependent dissolution or a greater temperature sensitivity of the globorotaliids compared to the other species. The effect of post depositional carbonate dissolution on $\delta^{18}O_{calcite}$ is to increase $\delta^{18}O_{calcite}$, biasing both isotopic and Mg/Ca temperatures towards cooler conditions.

Along this North Atlantic transect, the effects of depth dependent dissolution will be greatest in mid-latitudes, between about 42 ºN and 52 ºN where the deeper core sites, at depths greater than 3000 m are located (Figure 6.8).

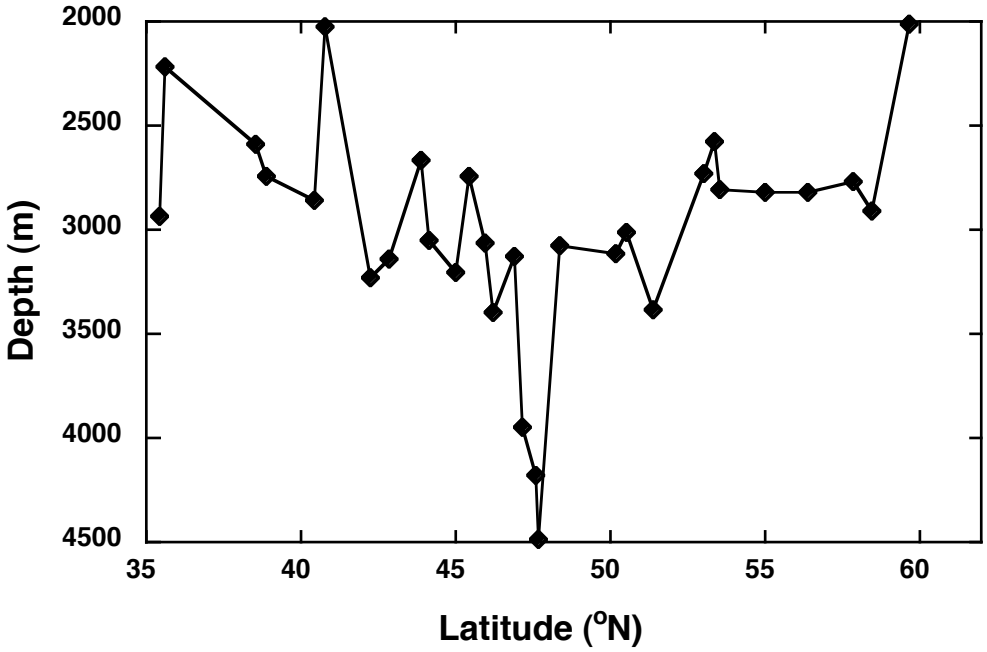

Figure 6.8 Depths of core sites versus latitude along the transect

Comparisons of foraminiferal Cd/Ca, Mg/Ca and Sr/Ca with water depths at the core sites are shown in Figure 6.9. Decreasing Mg/Ca with bottom water depth demonstrates that partial dissolution affects all of the planktonic species analysed at water depths below 2000 m, in accordance with the results of previous studies [Rosenthal *et al.*, 2000; Dekens *et al.*, 2002]. The largest change in Mg/Ca occurs in *G. siphonifera* (Figure 6.9d) where Mg/Ca decreases by 50%, from 3 mmol mol^{-1} to 1.5 mmol mol^{-1}, over the 2.0 to 4.5 km depth range. A 30% decrease in Mg/Ca occurs in *G. ruber (w)* and *G. sacculifer* (Figure 6.9b-c). The lower Mg/Ca ratios of *N. pachyderma (d)* (Figure 6.9a) and of the globorotaliids (Figure 6.9e-g) also decrease by about 30% between 2.0 and 4.5 km depth. The observed Mg/Ca ratios reflect a combination of temperature variability along the transect and depth dependent dissolution at the individual core sites. There is little evidence in these results for species specific critical water depths for the onset of dissolution between ~2500 and 3000 m, proposed by Regenberg *et al.* [2006].

Cd/Ca in *N. pachyderma (d)* has a similar trend to that observed for Mg/Ca (Figure 6.9a), suggesting that depth dependent dissolution influences *N. pachyderma (d)* Cd/Ca

although the scatter in the data between 2500 and 3500 m, where the majority of cores are located, shows that the dominant control must be from other factors.

G. ruber (w), G. sacculifer, and *G. siphonifera* (Figure 6.9b-d) all show increasing Cd/Ca with bottom water depth. Any effect of depth dependent dissolution on Cd/Ca is completely masked by other factors. Similarly, the globorotaliids, *G. hirsuta*, *G. inflata* and *G. truncatulinoides* (Figure 6.9e-g) show increasing Cd/Ca with depth of core, except for the deepest sites at depths > 4000 m where some effect of dissolution may be apparent.

The Sr/Ca trends for the globorotaliids (Figure 6.9e-g) confirm the results of Elderfield *et al.* [2000] as does the negligible change in Sr/Ca with core depth found for *N. pachyderma (d)* (Figure 6.9a). The globigerinids, *G. ruber (w)* and *G. sacculifer,* and also *G. siphonifera* (Figure 6.9b-d) show Sr/Ca decreasing slightly with depth, not observed by Elderfield *et al.* [2000]. These differences may be attributable to improved instrumental procedures since that study [see Chapter 2] or could be a result of the more corrosive reductive cleaning used in this work.

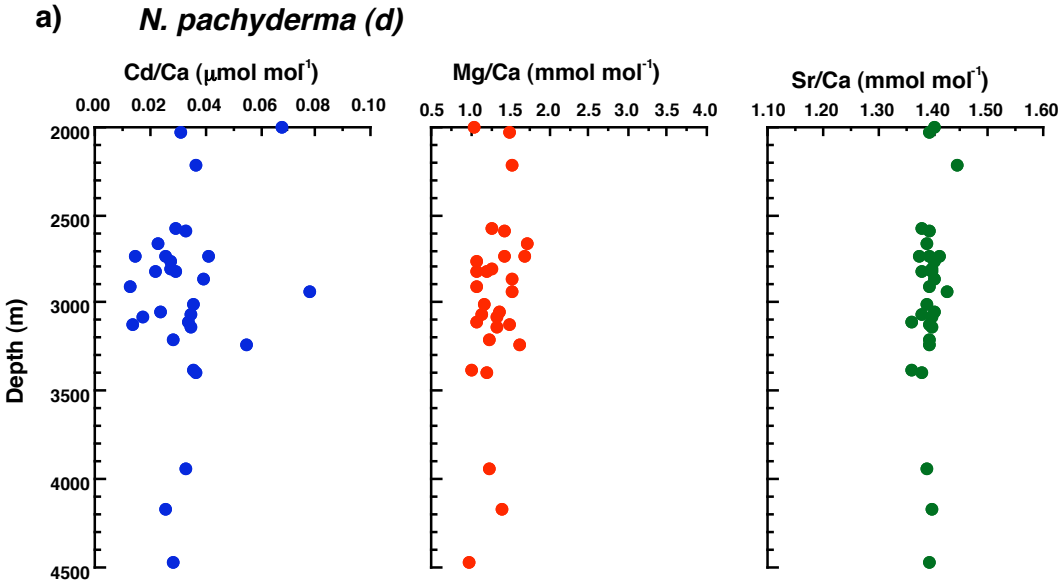

Figure 6.9 Planktonic foraminiferal Cd/Ca (blue), Mg/Ca (red) Sr/Ca (green) versus seafloor water depth on the North Atlantic box core transect (a) *N. pachyderma (d)*, (b) *G. ruber (w)*, (c) *G. sacculifer*, (d) *G. siphonifera*, (e) *G. hirsuta,* (f) *G. inflata*, (g) *G. truncatulinoides*

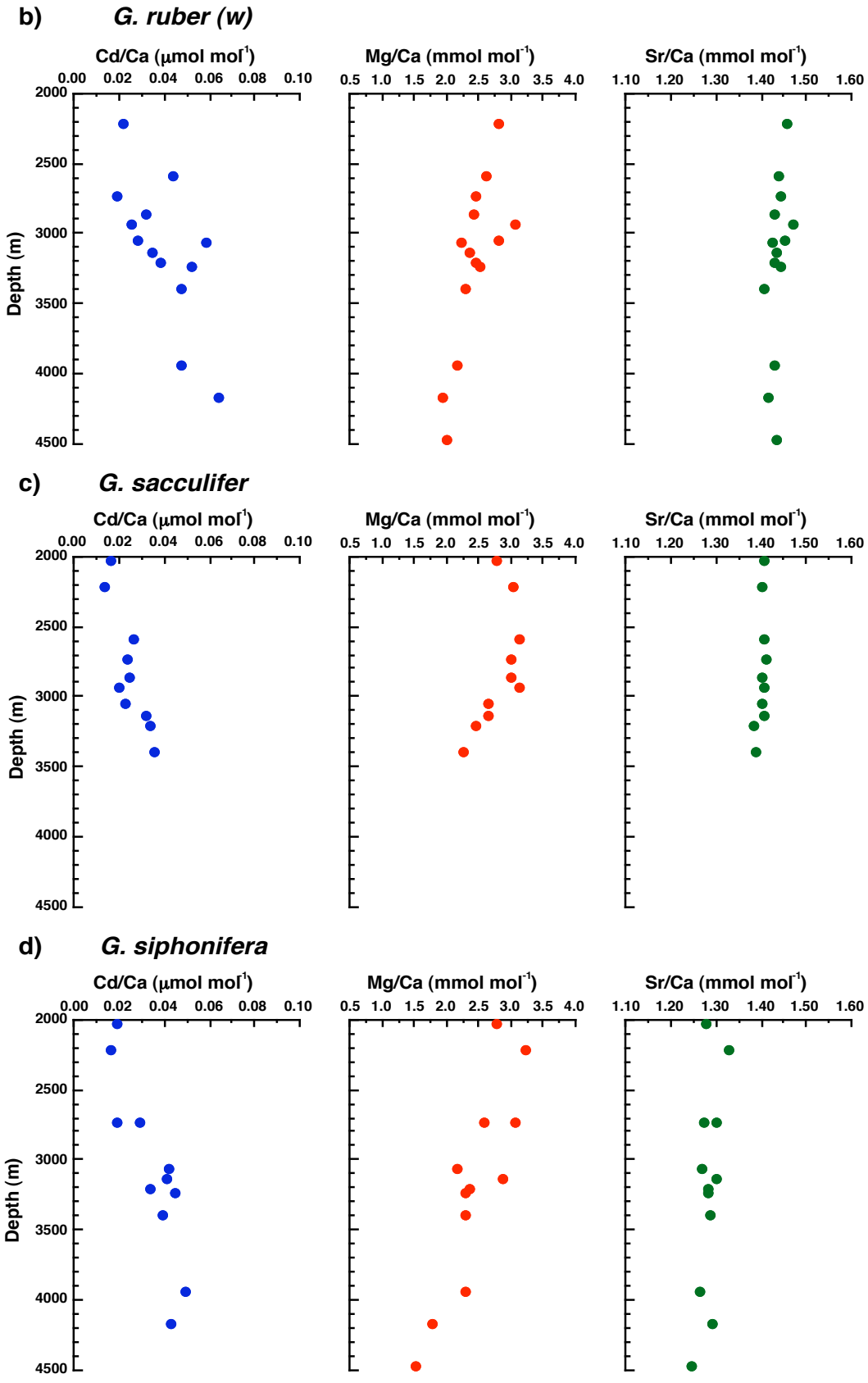

Figure 6.9 Planktonic foraminiferal Cd/Ca (blue), Mg/Ca (red) Sr/Ca (green) versus seafloor water depth on the North Atlantic box core transect (b) *G. ruber (w)*, (c) *G. sacculifer*, (d) *G. siphonifera*

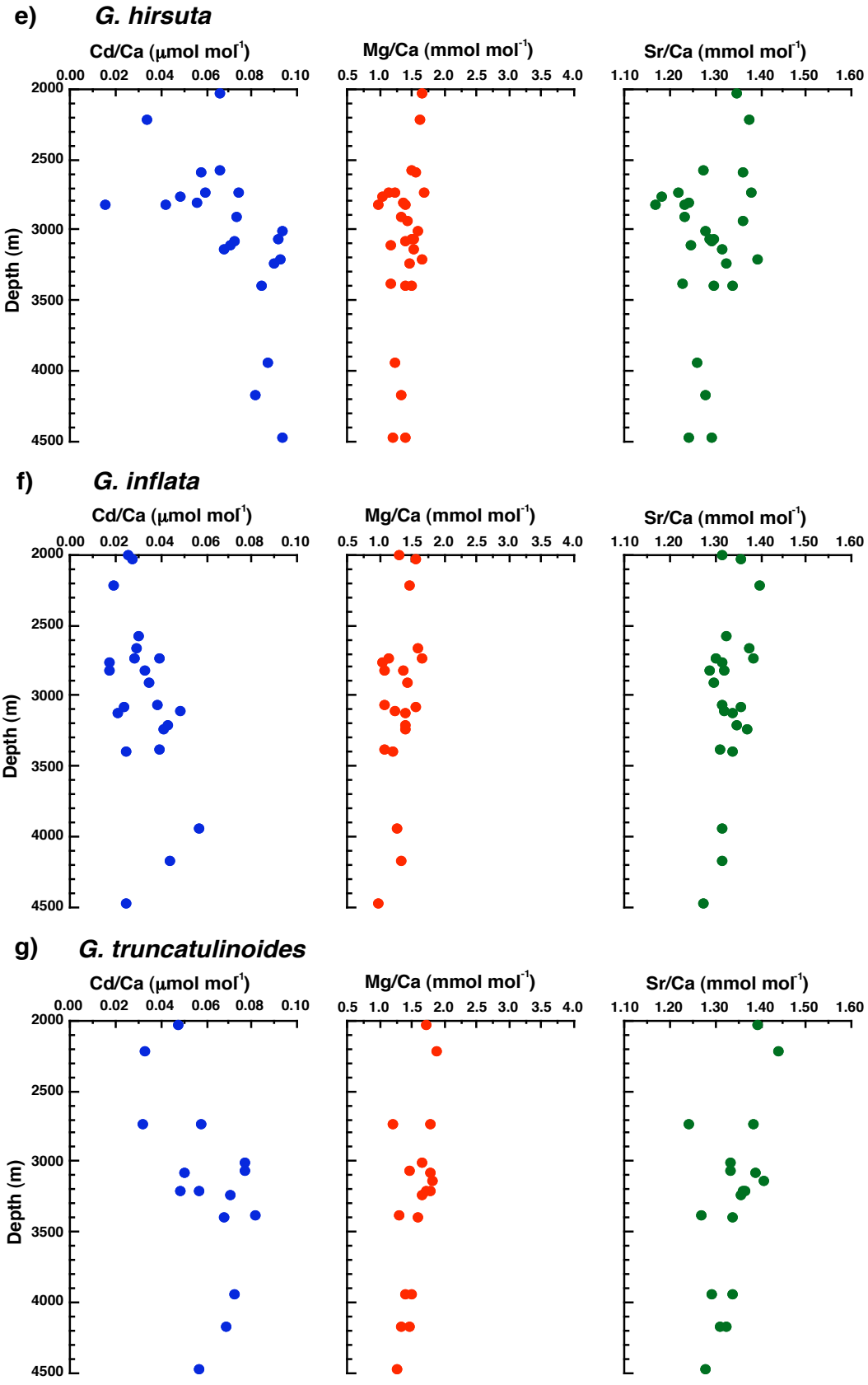

Figure 6.9 Planktonic foraminiferal Cd/Ca (blue), Mg/Ca (red) Sr/Ca (green) versus seafloor water depth on the North Atlantic box core transect (e) *G. hirsuta*, (f) *G. inflata*, (g) *G. truncatulinoides*

The Cd/Ca depth profiles indicate that dissolution represents only a minor control on planktonic foraminiferal Cd/Ca from these North Atlantic core tops. The effects of dissolution on Cd/Ca ratios appear to be insignificant for all except the three deepest core sites (T90 3B, T90 15B, T90 4B), located at depths > 3900 m between latitudes 47 °N and 48 °N (Figure 6.8, Table 6.1).

6.5 Determination of Cd partition coefficient

In principle, the partition coefficient, D_{Cd}, can be estimated from directly determined seawater Cd concentrations. However, $Cd_{seawater}$ concentrations were not measured on this longitudinal transect and large uncertainties would be involved in matching inferred calcification depths and seasons to water column cadmium concentrations. Seawater cadmium concentrations need to be estimated from the cadmium phosphate relationship at the depths and/or seasons of calcification.

Modern monthly phosphate values from the World Ocean Atlas 2005 [Garcia *et al.*, 2006] at discrete depths versus latitude at 27 °W were matched to the calcification depths and seasons determined in section 6.4.1. Seawater cadmium concentrations were estimated from Equation 6.5 using a value of $\alpha_{Cd/P} = 2.5$, appropriate for the nutrient depleted waters of the North Atlantic Ocean [Elderfield and Rickaby, 2000]. The partition coefficient, D_{Cd}, was calculated for each sample according to Equation 6.1, with $[Ca]_{sw}$ assumed constant at 10 mM [Boyle, 1992]. An average value of D_{Cd} was calculated for each sample over the estimated range of $[Cd]_{sw}$ for the seasons and depths of calcification shown in Figure 6.7. The data are tabulated in Appendix 3. Overall mean values of the partition coefficients for each species are shown in Table 6.3 together with parameters for fitting exponential equations to the data, of the form

$$D_{Cd} = A \exp BT \qquad (6.6)$$

The results are plotted against calcification temperatures and compared with the exponential D_{Cd} versus temperature calibration for *G. bulloides* of Elderfield and Rickaby [2000] in Figure 6.10.

Species	D_{Cd} average	s.d.	n	A	B	r^2
G. ruber (w)	26.5	10.4	14	0.91	0.19	0.03
G. sacculifer	19.6	4.6	11	8.98	0.04	0.01
G. siphonifera	8.81	3.13	12	0.51	0.20	0.35
N. pachyderma (d)	4.22	1.78	31	1.28	0.093	0.07
G. hirsuta	4.80	1.79	23	1.54	0.12	0.55
G. inflata	2.39	0.78	23	0.91	0.088	0.17
G. truncatulinoides (d)	5.47	1.65	15	3.47	0.036	0.07

Table 6.3 Average values of the partition coefficient, D_{Cd}, for each species and parameters for the equation $D_{Cd} = Ae^{BT}$

Calculated partition coefficients, D_{Cd}, for *G. ruber (w)* and *G. sacculifer* (Figure 6.10a,b) include large uncertainties because of proportionately large errors in estimating $[Cd]_{sw}$ in low nutrient surface waters (Figure 6.4b). Seasonal phosphate concentrations between latitudes 35 and 45 ºN, from the surface to a depth of 30m, are in the range 0.05 to 0.20 μmol kg^{-1} [Garcia *et al.,* 2006]. These low phosphate concentrations give calculated $[Cd]_{sw}$ of 0.008 to 0.029 nmol kg^{-1}, producing both high values and large errors on estimation of D_{Cd}, with no significant correlation between D_{Cd} and temperature (Table 6.3). Values are much larger than the range of 2 to 4 estimated for D_{Cd} in *G. sacculifer* from culture experiments [Delaney, 1989]. To obtain D_{Cd} in the range 2 to 4, phosphate concentrations between 0.2 and 0.4 μmol kg^{-1} would be required, an order of magnitude greater than found in surface waters at these latitudes in the North Atlantic [Garcia *et al.,* 2006].

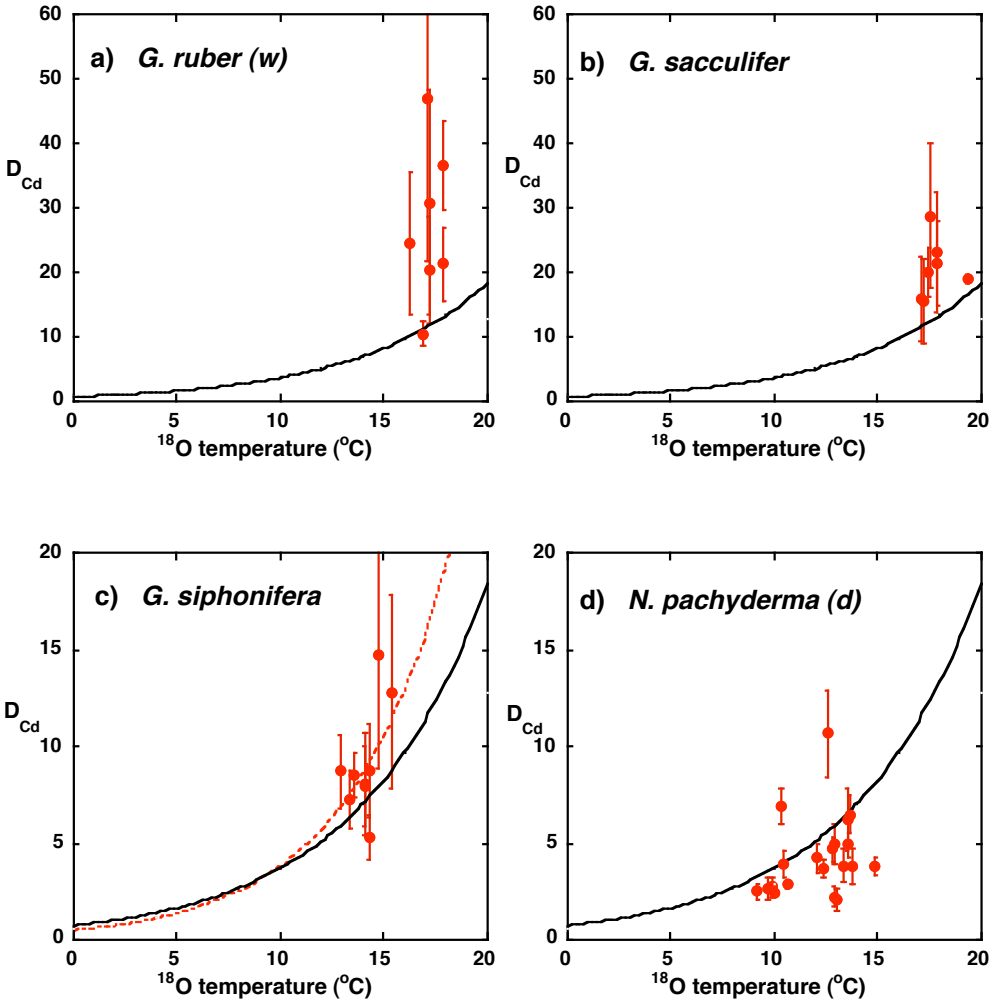

Figure 6.10 Cd partition coefficients versus temperature for planktonic foraminifera from North Atlantic box core tops a) *G. ruber (w)*, b) *G. sacculifer*, c) *G. siphonifera*, d) *N. pachyderma (d)*, e) *G. hirsuta*, f) *G. inflata*, g) *G. truncatulinoides (d)*, h) all species. Error bars are the standard deviation of the estimated D_{Cd} for each sample (see text). Black curve shows the exponential equation for *G. bulloides* from Elderfield and Rickaby [2000], $D_{Cd} = 0.75 \exp 0.16T$. Red curves are the exponential fit to the data for two species (Table 6.3).

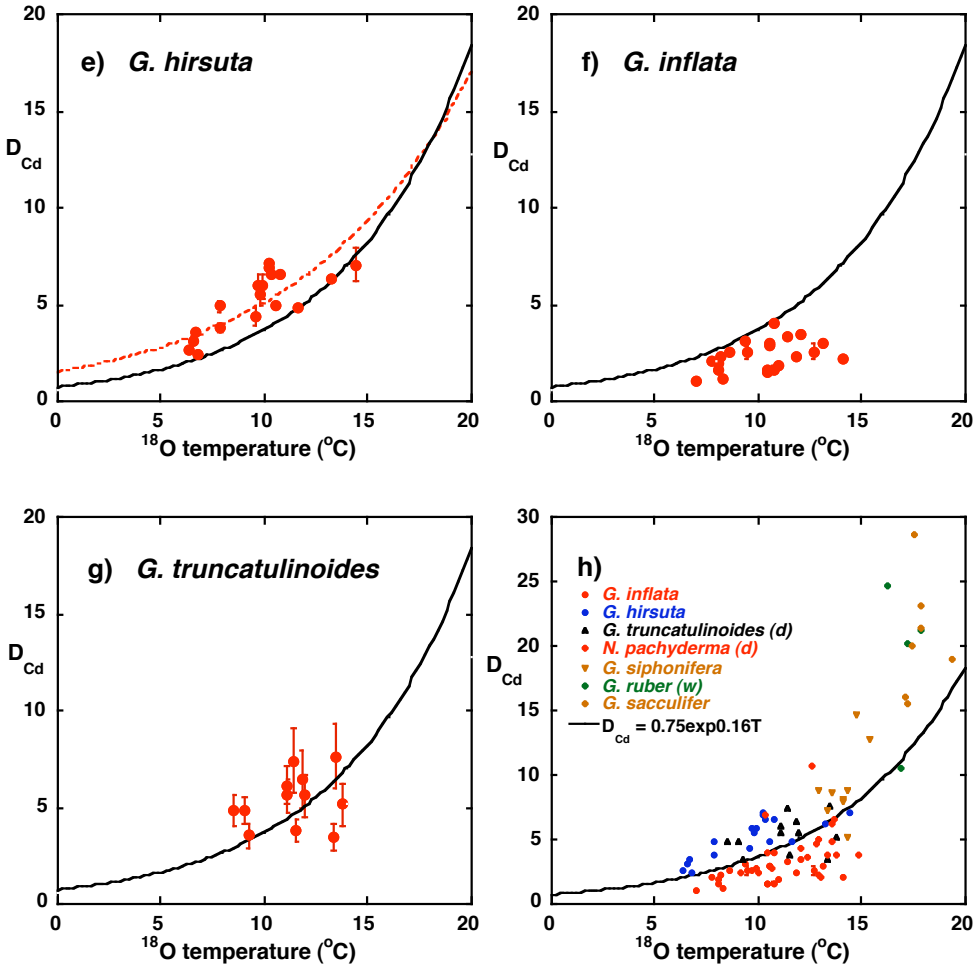

Figure 6.10 Cd partition coefficients versus temperature for planktonic foraminifera from North Atlantic box core tops e) *G. hirsuta*, f) *G. inflata*, g) *G. truncatulinoides (d)*, h) all species. Error bars are the standard deviation of the estimated D_{Cd} for each sample (see text). Black curve shows the exponential equation for G. bulloides from Elderfield and Rickaby [2000], DCd = 0.75 exp 0.16T. Red curves are the exponential fit to the data for two species (Table 6.3).

D_{Cd} in *G. siphonifera* (Figure 6.10c) shows a weak correlation with temperature (r^2 = 0.35, Table 6.3) not anticipated from the Cd/Ca versus latitude plot (Figure 6.5d). Higher phosphate concentrations, from 0.1 to 0.5 μmol kg^{-1}, at the depth and season of calcification of *G. siphonifera* (Section 6.4.1) translate to correspondingly higher $[Cd]_{sw}$ and lower D_{Cd} (Table 6.3) compared to *G. ruber* and *G. sacculifer*. Large uncertainty exists in the calculated D_{Cd} values because of uncertainty in the estimation of calcification season and depth.

Despite the similarity between the Cd/Ca trend versus latitude of *N. pachyderma (d)* and that of *G. bulloides* (Figure 6.5a,b), no significant temperature dependence in calculated D_{Cd} was found for *N. pachyderma (d)* (Table 6.3, Figure 6.7d). Phosphate concentrations at the seasons and depths of calcification estimated for *N. pachyderma (d)* (Section 6.4.1) range from 0.3 to 0.8 μmol kg^{-1}, giving average $D_{Cd} = 4.2$, close to values determined for planktonic foraminifera from culture studies [Delaney, 1989; Mashiotta *et al.*, 1997].

Estimation of D_{Cd} for the deeper dwelling globorotaliids, *G. hirsuta*, *G. inflata* and *G. truncatulinoides,* is less complicated than for surface dwelling species because of the higher and less seasonally variable phosphate concentrations in deeper waters. Similar to *N. pachyderma (d)*, average values of D_{Cd} calculated for *G. hirsuta*, *G. inflata* and *G. truncatulinoides* (Table 6.3) fall within or close to the range for planktonic foraminifera determined from culture studies [Delaney, 1989; Mashiotta *et al.*, 1997]. *G. hirsuta* (Figure 6.10e) shows the most significant correlation with temperature of the species studied, with $r^2 = 0.55$ and a 12% change in D_{Cd} per ºC temperature change (Table 6.3). In contrast, D_{Cd} in *G. inflata* and *G. truncatulinoides* show no obvious trend with temperature (Figure 6.10f,g, Table 6.3). Phosphate concentrations at the estimated calcification depths of *G. inflata* (Section 6.4.1) along this North Atlantic transect range from 0.4 to 1.0 μmol kg^{-1}, compared to 0.3 to 0.4 μmol kg^{-1} phosphate associated with the depth habitat of *G. inflata* in the study by Cleroux *et al.* [2007].

Calculated D_{Cd} for all species are compared in Figure 6.10h where the considerable scatter in D_{Cd} versus calcification temperature is evident. Uncertainties in the depth and season of calcification lead to large errors in estimation of $[PO_4]_{sw}$ and produce much of the uncertainty in D_{Cd}.

6.6 Summary and conclusions

Analyses of multiple species of planktonic foraminifera, covering a range of calcification temperatures, depths and seasons of calcification and associated phosphate

concentrations, were used in an investigation into factors controlling Cd/Ca of planktonic foraminifera and possible temperature dependence of the partion coefficient, D_{Cd}.

The transect of Cd/Ca in planktonic foraminifera from North Atlantic coretops shows a latitudinal variation for Cd/Ca in *N. pachyderma (d)* similar to that previously observed for *G. bulloides* by Rickaby and Elderfield [1999]. Other mixed layer species, *G. ruber (w), G. sacculifer,* and *G. siphonifera* display the opposite latitudinal Cd/Ca trend. There is evidence that Cd/Ca in the deeper dwelling globorotaliid species, *G. inflata*, *G. truncatulinoides* and particularly *G. hirsuta*, is linked to stratification in the water column.

Foraminiferal habitat and hydrography represent the dominant controls on Cd/Ca in planktonic foraminifera with, over this North Atlantic transect, evidence of only a minor influence from post depositional dissolution.

The major uncertainty in determination of the partition coefficient, D_{Cd}, for the incorporation of cadmium into planktonic foraminifera from core tops comes from uncertainty in estimation of the depth and season of calcification of the foraminifera, and consequent uncertainty in estimation of phosphate concentrations.

An alternative method for the determination of calcification depths would be to exploit Mg/Ca ratios. In principle, this should be the preferred technique for core top samples because Mg/Ca gives both temperature and $\delta^{18}O_{seawater}$ [Mashiotta *et al.,* 1999; Elderfield and Ganssen, 2000; Lea *et al.,* 2000, 2002; Lear *et al.,* 2000] and results can be verified by comparison with modern hydrography. There are two reasons why this technique was not used here. Firstly, samples in this work come from the same core tops used for Mg/Ca temperature calibration by Elderfield and Ganssen [2000], with the consequent risk of circular calculation. Secondly, although there is little evidence for a significant dissolution effect on Cd/Ca in these samples, there is a noticeable effect of depth dependent dissolution on Mg/Ca. It would be necessary to develop dissolution corrections to Mg/Ca temperatures for each species to enable them to be used to establish and verify calcification depths.

This study was unable to confirm a temperature dependence of D_{Cd} in the planktonic foraminifera species used, but at the same time it was not possible to conclusively rule out such a temperature influence on D_{Cd}. Further investigation would be required, using either core top material or water column samples, and ideally a combination of both, to determine D_{Cd} in planktonic foraminifera linked to seawater cadmium concentrations at the depths and seasons of calcification of the foraminifera.

Chapter 7

Conclusions and future work.

7.1 Development and verification of analytical methods

7.1.1 Mg/Ca and Sr/Ca determination in foraminiferal calcite

The development and optimisation of methods for the efficient cleaning of foraminiferal calcite and determination of Mg/Ca and Sr/Ca ratios by ICP-OES is described in Chapter 2. Cleaning procedures were investigated and a significant contribution to Mg/Ca ratios from the analytical blank was traced to contamination from Mg in polypropylene. At low Mg/Ca ratios, or for determinations at low concentration, the analytical blank is the limiting factor to obtaining accurate results. The ICP-OES instrumental procedure uses measured intensity ratios of emission lines, calibrated against element ratios of standard solutions at constant Ca concentration, to determine Mg/Ca and Sr/Ca element ratios. Long term precision, determined by routine analyses of consistency standards, is better than 0.5% (r.s.d.) without requiring normalisation of results, either for within run instrumental drift correction or to correct for calibration differences between runs.

7.1.2 Accuracy, standardisation and interlaboratory calibration standards for foraminiferal Mg/Ca thermometry

Differences in instrumental calibrations, attributed to errors involved in the preparation of accurate calibration standards, represent a significant contribution to interlaboratory analytical precision for Mg/Ca and Sr/Ca determinations in foraminiferal calcite. To improve accuracy and minimise systematic errors in the preparation of mixed standards, initial single element standard solutions were prepared starting from primary solid standards. Commercial reference materials were investigated to determine whether existing carbonate standards of appropriate composition are available for use as

reference materials for Mg/Ca determinations in foraminiferal calcite. ECRM 752-1, a limestone CRM containing Mg/Ca within the range of typical planktonic foraminifera is a suitable solid standard for interlaboratory calibration. Homogeneity of this material was demonstrated within the precision of daily instrumental Mg/Ca determinations over a range of sample weights from 10 - 1000 mg, with Mg/Ca = 3.75 mmol/mol (0.015 s.d., 0.41% r.s.d.) on 118 determinations of the material, taken from two bottles. The reproducibility of Mg/Ca ratios confirms the potential of ECRM 752-1 as a reference material for Mg/Ca determinations in foraminiferal calcite, provided that care is taken to remove undissolved contaminant silicate phases before analysis [Greaves *et al.*, 2005].

7.1.3 An ID-TIMS method for Cd determination

A highly sensitive ID-TIMS method was developed for determination of the picogram quantities of cadmium found in the shells of benthic and planktonic foraminifera. The method permits analysis of the Cd/Ca ratio of small amounts of cleaned foraminiferal calcite (0.06 mg). Efficient separation of cadmium from calcium and optimisation of the filament loading technique enabled the production of a stable ion beam, despite the high first ionisation potential of cadmium. Reproducibility of the method, determined by replicate analyses of consistency standards, is 3.4% for the determination of Cd/Ca ratios at abundance levels typical of planktonic foraminifera.

7.1.4 Developments in the determination of foraminiferal trace element ratio proxies

Considerable interest in foraminiferal trace element proxies has provided the impetus, and modern ICPMS instruments the capability, to develop multiple element ratio methods for the determination of trace element proxies in foraminiferal calcite [Yu *et al.*, 2005; Harding *et al.*, 2006; Marchitto, 2006]. The fast scanning feature of ICPMS allows multiple trace element ratios to be determined on the same foraminifera samples, although not the simultaneous determination of element ratios. For elements with sufficiently high abundance (e.g. Mg, Na, Sr), determination by simultaneous ICP-OES provides better precision on element/calcium ratios than does ICPMS because of the elimination of plasma noise and the stability of ICP-OES during a run [Chapter 2].

Where precision is paramount, such as for the determination of Sr/Ca in corals, the precision of ICPMS can be optimised by restricting the number of element ratios measured [Rosenthal *et al.,* 1999], or by using isotope dilution in combination with sector-field ICPMS [e.g. Ripperger and Rehkämper, 2007].

The determination of multiple element ratios on a single sample raises both instrumental and calibration issues because of the different susceptibilities of elements to instrumental interferences and contamination during the cleaning process. In addition, a foraminifera cleaning procedure developed for one trace element proxy is not necessarily appropriate for others. An investigation by Yu *et al.,* [2007] demonstrated the effect of preferential dissolution during reductive cleaning on trace element/calcium ratios in benthic foraminiferal calcite, with implications for the determination of multiple trace element proxies.

An increasing number of laboratories are performing trace element determinations in foraminifera and, consequently, intercalibration and comparison of results within and between laboratories has become an important issue. This was addressed in the interlaboratory comparison study of Mg/Ca and Sr/Ca measurements in planktonic foraminifera by Rosenthal *et al.,* [2004]. The work described in Chapter 3 represents a significant step towards establishing an intercalibration standard for foraminiferal Mg/Ca and Sr/Ca determinations.

7.2 Planktonic foraminiferal Mg/Ca, oxygen isotope and shell weight records across the subtropical front over Chatham Rise

Comparisons of *G. bulloides* Mg/Ca, shell weight and oxygen isotope records from ODP Site 1123 and CHAT 16K, located north of the Subtropical Front on Chatham Rise, with records from site MD97-2120, south of the Subtropical Front, demonstrate the effects of hydrography, foraminiferal habitat and dissolution susceptibility as controls on Mg/Ca. Records were obtained from two size fractions (250-300 μm and 300-355 μm) of *G. bulloides* at these locations north and south of the Subtropical Front.

At site MD97-2120 two size fractions of *G. bulloides* display almost identical Mg/Ca and $\delta^{18}O$ values. This finding is consistent with the two populations being influenced by the same calcification temperatures and preservation history at this site. North of the Subtropical Front, at ODP Site 1123 and CHAT 16K, the records of Mg/Ca and $\delta^{18}O$ differ between the same two *G. bulloides* size fractions. These differences may reflect calcification at different depths or in different seasons. Across glacial Terminations 1 and 2, the 250-300 μm *G. bulloides* Mg/Ca record at ODP Site 1123 shows the anticipated temperature changes, whereas the 300-355 μm *G. bulloides* Mg/Ca record does not. However, across Termination 3 the Mg/Ca records from both size fractions of *G. bulloides* analysed at ODP Site 1123 and MD97-2120 closely match the anticipated temperature excursion.

The geochemical and shell weight records at ODP Site 1123 are affected by dissolution and there is evidence for dissolution affecting the records at CHAT 16K despite its shallow depth (1408m), probably because of the influence of corrosive bottom water over this site.

The large differences between Mg/Ca, shell weight and $\delta^{18}O$ records found for the two narrow size fractions of *G. bulloides* (300-355 μm and 250-300 μm) has implications for the analysis and comparison of records from different sources. A lack of $\delta^{18}O_{seawater}$ measurements in the Southwest Pacific and the consequent uncertainty in the regional $\delta^{18}O_{seawater}$ salinity relationship compounds systematic errors in palaeosalinity estimates. Further investigation into the influence of foraminifera size fraction on Mg/Ca, and other proxies, is needed to improve understanding of trace element proxy records. A depth transect of core tops, collected using box cores to adequately sample the recent Holocene, would enable the influence of dissolution on different size fractions of *G. bulloides, G. inflata* and other foraminifera species from colder waters to be more fully investigated. This would facilitate the development of reliable dissolution corrections for Mg/Ca ratios and calculated temperatures from these species. Measurement of $\delta^{18}O_{seawater}$ in the associated water column would verify salinity estimates derived from core top foraminiferal $\delta^{18}O_{carbonate}$ and Mg/Ca temperatures which, in turn, would contribute to improved palaeosalinity estimation.

7.3 Planktonic foraminiferal Cd/Ca as a palaeoceanographic tracer for surface water nutrients.

The empirical partition coefficient, D_{Cd}, for cadmium incorporation into calcite, in an ideal solid solution relative to seawater, is predicted to be ~7 at thermodynamic equilibrium. For a divalent element such as cadmium, present in calcium carbonate in trace amounts, it is anticipated that the partition coefficient will be only slightly dependent on temperature and pressure. Foraminiferal calcite is precipitated rapidly by biogenic organisms and biochemical and kinetic processes result in trace metal incorporation different from that predicted for thermodynamic equilibrium [Boyle, 1988].

D_{Cd} in benthic foraminiferal calcite varies with water depth, from 1.3 at depths < 1150 m to 2.9 for depths > 3000 m, [Boyle, 1992] but no significant temperature influence has been found [Marchitto, 2004]. In contrast, a strong temperature dependence of D_{Cd} has been proposed for the planktonic foraminifera *G. bulloides,* with $D_{Cd} = 0.75 \exp 0.16T$ [Rickaby and Elderfield, 1999; Elderfield and Rickaby, 2000].

Chapter six reports the results of a study of Cd/Ca in seven species of planktonic foraminifera, *N. pachyderma (d), G. ruber (w)*, *G. sacculifer*, *G. siphonifera, G. hirsuta*, *G. inflata* and *G. truncatulinoides (d)*, from the same North Atlantic transect as used by Rickaby and Elderfield [1999]. This study shows little convincing evidence for a temperature dependence of D_{Cd} in planktonic foraminiferal calcite. A latitudinal variation similar to that observed for *G. bulloides* by Rickaby and Elderfield [1999] is seen for Cd/Ca in *N. pachyderma (d)* but the mixed layer species, *G. ruber (w), G. sacculifer,* and *G. siphonifera* display the opposite trend. Cd/Ca in the deeper dwelling globorotaliid species, *G. inflata*, *G. truncatulinoides* and *G. hirsuta*, may be linked to stratification in the water column.

The dominant controls on Cd/Ca in planktonic foraminifera are confirmed to be from foraminiferal habitat and hydrography, with evidence of only a minor influence of post depositional dissolution. The major uncertainty in determination of D_{Cd} comes from uncertainty in the knowledge of the depths and seasons of calcification of planktonic foraminifera, with consequent uncertainty in estimation of phosphate concentrations.

Calculated partition coefficients, D_{Cd}, for *G. ruber (w)* and *G. sacculifer* contain large uncertainties from proportionately large errors in estimated $[Cd]_{sw}$ in low nutrient surface waters. Values of D_{Cd} in the range 19.6 to 26.5 were obtained for these species, much larger than the range of 2 to 4 estimated from culture experiments [Delaney, 1989].

Despite a similarity between the Cd/Ca trend versus latitude of *N. pachyderma (d)* and that of *G. bulloides* [Rickaby and Elderfield [1999], no significant temperature dependence in calculated D_{Cd} is evident for *N. pachyderma (d)*. The difference in behaviour between *N. pachyderma (d)* and *G. bulloides* is attributed to differences in habitat between these species.

Estimation of D_{Cd} for the deeper dwelling globorotaliids, *G. hirsuta*, *G. inflata* and *G. truncatulinoides,* are believed to be more reliable than for surface dwelling species because of higher and less seasonally variable phosphate concentrations in deeper waters. Average values of D_{Cd} for these species fall within or close to the range of 2 to 4 determined for planktonic foraminifera from culture studies [Delaney, 1989; Mashiotta *et al.*, 1997].

Only two of the species studied, *G. siphonifera* and *G. hirsuta,* show significant evidence for a temperature influence on D_{Cd}, with correlation coefficients, $r^2 = 0.35$ and 0.55 respectively, found for an exponential D_{Cd} versus temperature relationship.

Uncertain knowledge of depth habitats and seasons of calcification lead to order of magnitude errors in estimation of $[PO_4]_{sw}$ and produce most of the uncertainty in determination of D_{Cd} from core top samples. A future investigation, combining a study of core top material and associated water column samples, linked to seawater cadmium concentrations at the depths and seasons of calcification, would improve the determination of D_{Cd} in planktonic foraminifera. Such a study, in combination with the investigation of Mg/Ca as described in Section 7.2 and including other trace elements, would lead to improved understanding of trace element proxy relationships and consequent benefits for palaeoceanographic interpretation.

Appendix 1

Stepwise cleaning procedure for the preparation of foraminiferal calcite for elemental analysis.

(from Barker, Greaves and Elderfield 2003, with subsequent modifications)

The procedure assumes moderately difficult (e.g. *G. bulloides*), cold (< 2 mmol/mol Mg/Ca) samples and includes transfer to low Mg blank vials before stages involving acid.

N.B. It is important to assess the cleaning requirements of each particular set of samples and modify the stages in the procedure accordingly. e.g. for high Mg/Ca samples with little clay in fill it may be appropriate to shorten some stages, whereas for cold samples containing Ice Rafted Debris it will be necessary to be more rigorous.

Clean in batches of about 10 samples at a time. Expect to take about 4 hours for the complete procedure.

Weighing:

The method is sensitive enough to analyse as few as one or two forams but for best statistics use at least 20 individuals per sample. Select clean tests and try to keep all the samples approximately the same size. Record details of core, depth, species, size fraction, number of tests and the sample weight.

Weigh samples using the 6 or 7 place microbalance. Transfer the forams to a stainless steel weighing boat, record the weight and number of individuals. Transfer back to the picking slide after weighing . *It is very important to accurately count the number of individuals weighed; an incorrect count of 1 in 20 represents a 5% weighing error.*

Crushing:

Foraminifera tests are gently crushed between two clean glass plates - *the aim here is to allow any chamber fill to escape during subsequent cleaning stages*.

1. Place the tests in a single layer on the lower glass slide. Keep the sample moist with excess water.

2. In a controlled manner, lower the second plate onto the sample and apply gentle pressure in order to open every shell chamber. *Take care not to over-crush the sample; this will lead to excessive loss of sample during cleaning*.

3. Remove the upper glass plate and transfer all particles to the lower plate.

4. Place a piece of light coloured paper beneath the sample under the microscope. This will reveal the presence of any larger silicate grains that may not be removed during the following clay removal steps. ***It is not necessary to remove such grains at this stage*** but only to note their presence so that action may be taken later on.

Steps (5) to (7) should be followed if the sample is intended for paired analyses of trace metals and stable isotopes or similar.

5. Add water to the sample in order to bring the shell particles into suspension.

6. Mix particles thoroughly with a brush with the aim of homogenizing the sample as far as possible.

7. Remove any excess water and divide into the desired proportions.

8. Using a moistened brush, transfer the crushed sample to an acid cleaned 500µl micro-centrifuge tube or relevant sample tube.

Clay removal:

During this stage, all samples should be treated individually in order to maximize cleaning effectiveness (batch treatment for ultrasonication is appropriate). It is important to use separate pipette tips for adding and removing reagents.

Having opened the test chambers during crushing, much of the test fill will be loosened and easily brought into suspension.

1. Squirt 500µl of UHQ H_2O onto the crushed sample (trapped air bubbles may be freed by flicking the tube end with a fingernail)

2. Allow the sample to settle for 30 seconds or so.

3. Remove the overlying solution (supernatant) with a separate pipette – *the size of a 1000µl pipette tip is suitable for removing most of the overlying liquid from the tube without risk of sample loss.*

At this stage, all tubes should still contain about 10-20µl of H_2O.

4. Place the sample rack in an ultrasonic bath for 1-2 minutes - *this will encourage separation of more tightly bound clays from the test surfaces.*

Suspended clays will appear as a milky residue in the liquid just above the sample.

5. Squirt 500µl of UHQ H2O onto each sample - *this will agitate the sample and bring loose clays into suspension.*

6. ***Briefly*** allow the sample to settle ***(minimal settling technique)*** - sufficient settling will only take a number of seconds (long enough for the distinct carbonate grains to reach the bottom). *After this period the remaining settling material will mainly comprise unwanted silicate particles.*

7. Remove the overlying solution.

8. Repeat steps (4) to (7) a further 4 times. More repetitions may be necessary for as long as clays are being visibly brought into suspension by ultrasonication.

After the water cleaning steps, methanol is used for further clay removal - *the lower viscosity of this reagent should dislodge material still attached to the carbonate tests*.

9. Add 250µl of Aristar methanol to each tube.

10. Ultrasonicate the tubes for 1-2 minutes.

11. Treating each tube individually, lift the methanol off the sample with a pipette and squirt straight back in to bring clays into suspension.

12. Allow sample to settle for a few seconds and remove the methanol.

13. Repeat steps (9) to (12).

14. Repeat steps (5) to (7) in order to remove any remaining methanol. (further ultrasonication may be applied if desired).

Removal of organic matter:

1. Add 250µl of alkali buffered 1% H_2O_2 solution to each tube and secure the rack with a lid to prevent tubes popping open whilst under pressure.

2. Place the sample rack in a boiling water bath for 10 minutes. At 2.5 and 7.5 minutes remove the rack momentarily and rap on the bench top to release any gaseous build-up. At 5 minutes place the rack in an ultrasonic bath for a ***few seconds*** and return to the water bath after rapping on the bench – *the aim of these interim steps is to maintain contact between reagent and sample*.

3. Flick the sample tubes to remove gas bubbles and ensure the samples have settled then remove the oxidizing reagent using a pipette.

4. Repeat steps (1) to (3).

5. Remove any remaining oxidizing reagent by filling the tube with UHQ H_2O and removing after settling. This step should be repeated 1-2 times.

Removal of coarse-grained silicates:

This step is necessary if silicates were observed in the sample after crushing. It is a good idea to follow this step even if no larger particles were seen; any foreign body that has entered the sample during the preceeding steps might bias the desired measurement.

Particulate removal at this stage is less time consuming than straight after crushing as the clay treatment and oxidation steps will have broken down and removed some particles already.

If silicate particles were observed on crushing then a glass slide or microbeaker should be used for their removal, otherwise transfer directly to a clean tube and examine under a microscope.

Later centrifuging will remove particles not removed at this stage, but because centrifuging occurs after sample dissolution there remains the risk of contamination from leaching of any remaining particles by the dissolution acid.

A 100µl pipette is used to transfer the sample into either a clean 0.5ml low Mg blank microcentrifuge tube or into a 1ml glass micro-beaker or a microscope slide for examnination under the microscope.

Label a set of clean tubes ready for the sample transfer. Include a blank tube at this stage if not already included.

1. Squirt 100µl of UHQ H_2O into the sample and immediately transfer avoiding settling.

2. Repeat step (1) 3-4 times ensuring that the entire sample is transferred.

3. Remove excess H_2O leaving approximately 100µl overlying the sample.

4. View the sample under a microscope using a dark and light background in turn. If unwanted particles are observed then transfer to a 1ml glass microbeaker or microscope slide for removal, otherwise continue from step (7).

5. Remove any particles that are not apparently carbonate using a fine brush. Strongly discolored carbonate should also be removed.

6. Transfer the sample into a clean (low Mg blank) micro-centrifuge tube using the technique in step (1)

7. Remove excess H_2O.

NB if particles are not removed using the technique outlined above, it is still necessary to transfer the samples to clean vials to minimise contamination. *Polypropylene contains Mg which will be leached on addition of acid and which contributes significantly to the analytical blank.*

To minimise contamination, all stages involving addition of acid should be performed in clean low Mg blank thin-walled polypropylene or polystyrene vials.

Dilute acid leach:

Dilute acid is used to remove any adsorbed contaminants from the test fragments.

1. Add 250µl of 0.001M HNO_3 to each sample.

2. Ultrasonicate all samples for 30 seconds.

3. Remove acid from each sample.

4. Squirt UHQ H_2O into each tube.

It is important to replace the leach acid with H_2O as soon as possible for all samples in order to prevent excess dissolution.

5. Remove the overlying H_2O.

6. Repeat steps (4) and (5).

7. Using a 10µl pipette, carefully remove any remaining solution from each sample.

Samples should be stored after this stage, then dissolved and diluted on the day they are to be run.

Dissolution:

Dissolution should be performed with consideration given to any non-carbonate particles that may still be present in the sample. The following steps act to reduce the risk of contamination from such phases.

In order to ensure accurate dilutions, it is important that all volumes are accurately pipetted from this stage onwards.

1. Add 350µl of 0.075M HNO_3 to the sample (for large samples 500µl may be used).

2. Place the sample rack in an ultrasonic bath to promote reaction.

3. Momentarily remove each tube in turn and flick with a fingernail to allow any buildup of CO_2 to escape and the reaction to continue.

4. As soon as production of CO_2 ceases in any sample tube, remove that tube from the ultrasonic bath, shake to mix then leave to settle.

5. Centrifuge (5000 rpm for 5 mins) to settle any remaining small silicate particles.

6. Immediately transfer 300µl of solution to a clean sample tube, leaving any particles to be discarded in the residual 50µl.

If the dissolution acid is left on a sample containing any silicate or other non-carbonate material for longer than is necessary to dissolve the sample, there is a high risk of contamination by elemental leaching.

Mg/Ca and Sr/Ca determination by ICP-OES:

After cleaning and dissolution, 20 planktonic forams should give Ca concentrations in the range 100 – 200 ppm Ca depending on the species and sample loss during cleaning.

The method for Mg/Ca & Sr/Ca determinations using the Vista ICP-OES requires, for best precision and accuracy, solutions containing known Ca concentrations of typically either 60 or 100 ppm and uses ~250µl solution per analysis.

Two runs of each sample are required; an initial concentration determination followed by a second run at optimum Ca concentration for Mg/Ca and Sr/Ca determinations.

Dilutions:

For samples in 300µl of 0.075M HNO_3 after centrifuging, a 5 fold dilution should be done for the initial concentration determination, followed by dilution of the remaining concentrate as required.

1. Set up a series of clean 0.5ml thin walled vials for the dilutions.

2. Add 200µl of 0.075M HNO_3 to each.

3. Add 50µl sample to give a 5 fold dilution.

It is important that volumes are accurately pipetted at this stage to ensure correct concentration calculations and subsequent dilutions.

Run the diluted samples on the Vista ICP-OES to determine Ca concentrations. Calculate dilutions required to give optimum [Ca] (100 ppm if Mg/Ca < 2 mmol/mol, otherwise 60 ppm) for the intensity ratio calibration of Mg/Ca & Sr/Ca ratios.

Dilute the remaining 250µl of sample concentrates as calculated and run on the Vista using the intensity ratio calibration at the appropriate Ca concentration.

Reagents:

Tip rinse:

Acid - 10% HNO_3 in Elga UHQ water.

Water - Elga UHQ H2O

Removal of fine clays:

Elga UHQ H2O

Methanol (Aristar)

Oxidising reagent: (to remove organic matter)

Alkali buffered 1% H_2O_2 solution.

250 µl oxidising solution used per sample.

Prepare fresh mixture for each batch of samples.

Prepared from:-

Hydrogen peroxide 30% w/v Aristar grade.

0.1M sodium hydroxide (Aristar grade) in Elga UHQ water

Add 100 µl H_2O_2 to ~10 ml 0.1 M NaOH (sufficient for ~ 20 samples).

Dilute acid leach:

QD 0.001 M HNO_3 - 250 µl used per sample.

Prepared by 75 fold dilution of 0.075 M HNO_3

6ml 0.075M HNO_3 in 450ml UHQ H_2O

Dissolution acid:

QD 0.075 M HNO_3 - 500 µl used per sample.

Prepared by 200 fold dilution of sub-boiling quartz distilled (QD) 15M HNO_3

5ml conc HNO_3 in 1 litre UHQ H_2O

Micro Centrifuge Tube Cleaning:

Cold acid cleaning procedure used for Mg, Sr (& also Cd).

Clean the micro centrifuge tubes in a 500ml Nalgene polypropylene screw top jar.

Rinse jar x 2 with purified water. (Elga Option 3)

Fill ~ 3/4 full with 10% HNO_3. (1 + 9 mixture of Analar HNO_3 & Elga H_2O).

Add 10% HNO_3 individually to the 0.5ml micro centrifuge tubes to ensure there are no air bubbles (use a pipette or a washbottle).

Place vials in the jar of 10% HNO_3 with their lids open; they will float.

Add acid into the lids.

Screw the lid onto the jar and allow to stand for 24 hours.

Decant off the 10% HNO_3 to waste.

Rinse x 3 with Elga UHQ H_2O

Give a final rinse with Elga UHQ H_2O, individually from a wash bottle.

Dry the vials in the clean drying cabinet.

Appendix 2

Planktonic foraminifera data from Chatham Rise

ODP Site 1123 *G. bulloides* 300 – 355 μm

Hole	Core	C	Sct	Top (cm)	Bot (cm)	Mcd	Age (ka)	Shell wt (μg)	Mg/Ca (mmol/mol)	$\delta^{18}O$ (‰)	T (^{o}C)	$\delta^{18}O_w$ (SMOW)
C	1	H	1	4	6	0.04	6.3	14.3				
C	1	H	1	14	16	0.14	8.4	14.0	1.549		11.1	
C	1	H	1	25	27	0.25	10.6	15.3	1.610	1.60	11.4	0.58
C	1	H	1	33	35	0.33	12.3	20.8	1.622	2.35	11.5	1.35
C	1	H	1	40	42	0.40	13.7	19.9	1.597	2.46	11.4	1.42
C	1	H	1	49	51	0.49	15.6	22.0	1.567	2.90	11.2	1.82
C	1	H	1	60	62	0.60	17.8	21.0	1.372	3.01	9.9	1.63
C	1	H	1	66	68	0.66	19.0	24.3	1.345	3.05	9.7	1.62
C	1	H	1	69	71	0.69	19.7	24.4		3.38		
C	1	H	1	76	78	0.76	21.0	24.2	1.454	3.00	10.5	1.76
C	1	H	1	80	82	0.80	21.7	21.1	1.252	3.18	9.1	1.58
C	1	H	1	90	92	0.90	23.6	21.0	1.606	3.15	11.4	2.12
C	1	H	1	94	96	0.94	24.4	22.8	1.612	3.19	11.4	2.17
C	1	H	1	100	102	1.00	25.5	18.5	1.396	3.12	10.1	1.78
C	1	H	1	103	105	1.03	26.1	22.7	1.373	3.13	9.9	1.75
C	1	H	1	109	111	1.09	27.2	23.4	1.457	2.91	10.5	1.67
C	1	H	1	120	122	1.20	29.3	18.1	1.458	2.94	10.5	1.69
C	1	H	1	123	125	1.23	29.9	20.4	1.399	2.86	10.1	1.52
C	1	H	1	128	130	1.28	30.8	14.9	1.429	2.96	10.3	1.67
C	1	H	1	140	142	1.40	33.1	19.3		2.78		
C	1	H	1	143	145	1.43	33.7	18.2	1.496	2.80	10.7	1.62
C	1	H	2	3	5	1.53	35.6	21.7	1.222	2.78	8.9	1.13
C	1	H	2	9	11	1.59	36.7	23.7	1.443	2.76	10.4	1.49
C	1	H	2	20	22	1.70	38.8	18.9	1.508	2.27	10.8	1.10
C	1	H	2	22	24	1.72	39.2	20.9	1.266		9.2	
C	1	H	2	29	31	1.79	40.5	17.1	1.722	2.05	12.1	1.18
C	1	H	2	37	39	1.87	42.0	15.2	1.597	2.16	11.4	1.12
C	1	H	2	40	42	1.90	42.6	19.8	1.531	2.42	11.0	1.29
C	1	H	2	49	51	1.99	44.3	22.2	1.364	2.65	9.9	1.25
C	1	H	2	52	54	2.02	44.8	19.9	1.567	2.32	11.2	1.24
C	1	H	2	60	62	2.10	46.4	24.7	1.527	2.32	10.9	1.19
C	1	H	2	62	64	2.12	46.7	17.7	1.715	2.09	12.0	1.22
C	1	H	2	75	77	2.25	49.2	25.7	1.539	2.56	11.0	1.44
C	1	H	2	77	79	2.27	49.6	22.4	1.375	2.59	10.0	1.21
C	1	H	2	80	82	2.30	50.2	26.1	1.333	2.67	9.7	1.21
C	1	H	2	90	92	2.40	52.0	23.4	1.330	2.63	9.6	1.17
C	1	H	2	100	102	2.50	53.9	24.4	1.442	2.47	10.4	1.21
C	1	H	2	109	111	2.59	55.6	19.9	1.401	2.23	10.1	0.89
C	1	H	2	120	122	2.70	57.7	19.6	1.432		10.3	
C	1	H	2	123	125	2.73	58.3	14.7	1.374	1.81	9.9	0.43
C	1	H	2	128	130	2.78	59.2	16.8	1.548	2.33	11.1	1.23
C	1	H	2	130	132	2.80	59.6	19.2	1.517	2.61	10.9	1.46
C	1	H	3	3	5	3.03	64.0	19.1	1.419	2.83	10.2	1.53
C	1	H	3	6	8	3.06	64.5	17.5	1.347	2.56	9.8	1.14
C	1	H	3	9	11	3.09	65.1	20.6	1.531	2.66	11.0	1.53
C	1	H	3	13	15	3.13	65.9	19.4	1.385	2.65	10.0	1.29
C	1	H	3	20	22	3.20	67.2	19.7	1.414	3.17	10.2	1.86
C	1	H	3	23	25	3.23	67.8	19.7	1.692	2.49	11.9	1.59
C	1	H	3	29	31	3.29	68.9	19.1	1.650	2.87	11.7	1.91
C	1	H	3	40	42	3.40	71.5	20.8	1.241	2.49	9.0	0.88
C	1	H	3	49	51	3.49	73.6	21.2	1.321	2.78	9.6	1.31
C	1	H	3	60	62	3.60	76.2	18.3	1.257	2.26	9.1	0.67

Hole	Core	C	Sct	Top (cm)	Bot (cm)	Mcd	Age (ka)	Shell wt (μg)	Mg/Ca (mmol/mol)	$\delta^{18}O$ (‰)	T (^{o}C)	$\delta^{18}O_w$ (SMOW)
C	1	H	3	66	68	3.66	77.6	14.2	1.279		9.3	
C	1	H	3	69	71	3.69	78.3	11.3		1.05		
C	1	H	3	76	78	3.76	79.9	11.7	1.725	1.15	12.1	0.29
C	1	H	3	80	82	3.80	80.9	11.5		0.97		
C	1	H	3	90	92	3.80	83.2	11.6	2.067	1.01	13.8	0.55
C	1	H	3	98	100	3.98	85.1	13.0	1.475		10.6	
C	1	H	3	100	102	4.00	85.5	17.7		2.37		
C	1	H	3	107	109	4.07	87.2	12.5				
C	1	H	3	120	122	4.20	90.2	17.2	1.661	2.13	11.7	1.18
C	1	H	3	130	132	4.30	92.6	19.6	1.472		10.6	
C	1	H	3	137	139	4.37	94.2	14.1	1.445		10.4	
C	1	H	4	3	5	4.53	98.0	11.4		1.38		
C	1	H	4	9	11	4.59	99.4		2.301		14.8	
C	1	H	4	9	11	4.59	99.4	10.6				
C	1	H	4	11	13	4.61	99.8	9.7				
C	1	H	4	20	22	4.70	102.0		1.694		11.9	
C	1	H	4	20	22	4.70	102.0	12.6		1.66		
C	1	H	4	22	24	4.72	102.4	13.6				
C	1	H	4	29	31	4.79	104.1	14.6	1.641	1.33	11.6	0.36
C	1	H	4	40	42	4.90	106.6	17.6	1.575	2.16	11.2	1.09
C	1	H	4	49	51	4.99	108.8	8.7	1.804	1.08	12.5	0.32
C	1	H	4	60	62	5.10	114.2	15.5		1.35		
C	1	H	4	62	64	5.12	115.2	11.9	1.659	1.57	11.7	0.63
C	1	H	4	70	72	5.20	119.2		1.700		11.9	
C	1	H	4	70	72	5.20	119.2	13.2		1.58		
C	1	H	4	72	74	5.22	120.2	15.8	1.581	1.57	11.3	0.51
C	1	H	4	80	82	5.30	124.2	19.8	1.568	2.19	11.2	1.11
C	1	H	4	89	91	5.39	128.6	24.2	1.515	2.73	10.9	1.58
C	1	H	4	100	102	5.50	134.1	26.6	1.572	3.15	11.2	2.08
C	1	H	4	110	112	5.60	139.1	25.1	1.472	3.33	10.6	2.11
C	1	H	4	120	122	5.70	140.8	23.5	1.781	3.18	12.4	2.39
C	1	H	4	130	132	5.80	142.6	24.0	1.537	3.05	11.0	1.93
C	1	H	4	140	142	5.90	144.4	26.8	1.559	3.11	11.1	2.02
C	1	H	5	3	5	6.03	146.6	23.5	1.556	2.93	11.1	1.84
C	1	H	5	9	11	6.09	147.7	23.6	1.684	2.81	11.8	1.89
C	1	H	5	20	22	6.20	149.6	14.4	1.705	2.24	12.0	1.35
C	1	H	5	29	31	6.29	151.2	15.2	1.741	1.90	12.2	1.06
C	1	H	5	40	42	6.40	153.2	16.8	1.729		12.1	
C	1	H	5	49	51	6.49	154.7	19.9	1.518	3.00	10.9	1.85
C	1	H	5	60	62	6.60	156.7	23.4	1.457	2.94	10.5	1.70
C	1	H	5	70	72	6.70	158.4	20.8	1.607	3.09	11.4	2.07
C	1	H	5	72	74	6.72	158.8	17.7	1.506	2.60	10.8	1.43
C	1	H	5	80	82	6.80	160.2	27.9	1.249	2.83	9.1	1.23
C	1	H	5	90	92	6.90	162.0	25.0	1.275	2.96	9.2	1.41
C	1	H	5	100	102	7.00	163.7	28.2	1.362	3.00	9.9	1.60
C	1	H	5	110	112	7.10	165.5	25.3	1.275	2.97	9.2	1.42
B	2	H	3	144	146	7.12	165.8	22.9	1.268	2.61	9.2	1.05
B	2	H	4	4	6	7.22	168.2	23.6	1.486	2.68	10.7	1.48
B	2	H	4	6	8	7.24	168.7	20.3	1.534	2.47	11.0	1.34
B	2	H	4	14	16	7.32	170.5	19.6	1.415	2.12	10.2	0.81
B	2	H	4	24	26	7.42	172.9	14.1	1.940	1.65	13.2	1.06
B	2	H	4	31	33	7.49	174.5	14.8	1.359	2.00	9.8	0.60
B	2	H	4	34	36	7.52	175.2	13.5		1.54		
B	2	H	4	46	48	7.64	178.0	11.5		1.60		
B	2	H	4	50	52	7.68	178.7	13.8	1.662	1.81	11.7	0.87
B	2	H	4	58	60	7.76	180.1	11.8		1.93		
B	2	H	4	64	66	7.82	181.1	21.6	1.351	2.62	9.8	1.21
B	2	H	4	77	79	7.95	183.3	22.6	1.351	2.67	9.8	1.25
B	2	H	4	84	86	8.02	184.5	22.7	1.597	2.84	11.4	1.81
B	2	H	4	94	96	8.12	186.2	20.9	1.491	2.73	10.7	1.54
B	2	H	4	144	146	8.62	196.9	11.3	1.807	1.18	12.5	0.43
B	2	H	5	14	16	8.82	201.4		2.163		14.2	
B	2	H	5	14	16	8.82	201.4	10.4		0.94		

Hole	Core	C	Sct	Top (cm)	Bot (cm)	Mcd	Age (ka)	Shell wt (μg)	Mg/Ca (mmol/mol)	$\delta^{18}O$ (‰)	T (^{o}C)	$\delta^{18}O_w$ (SMOW)
B	2	H	5	24	26	8.92	203.6	12.9	2.026	0.80	13.6	0.29
B	2	H	5	34	36	9.02	209.6	13.2	1.970	0.68	13.3	0.11
B	2	H	5	44	46	9.12	215.5	12.4	2.027	0.71	13.6	0.21
B	2	H	5	51	53	9.19	219.7	13.9	1.921	1.68	13.1	1.06
B	2	H	5	70	72	9.38	228.6	21.1	1.185	2.56	8.6	0.83
B	2	H	5	81	83	9.49	230.8	21.8	1.192	2.45	8.6	0.74
B	2	H	5	84	86	9.52	231.4	19.7	1.397	2.43	10.1	1.09
B	2	H	5	94	96	9.62	233.4	21.1	1.668	2.70	11.8	1.76
B	2	H	5	104	106	9.72	235.5	21.2	1.428	2.48	10.3	1.18
B	2	H	5	111	113	9.79	236.9	17.3	1.437	2.15	10.4	0.88
B	2	H	5	114	116	9.82	237.5	13.4	1.747	0.79	12.2	-0.04
B	2	H	5	124	126	9.92	239.5	14.1				
B	2	H	5	125	127	9.93	239.7		2.153		14.1	
B	2	H	5	125	127	9.93	239.7	13.8		1.47		
B	2	H	5	131	133	9.99	240.9	12.4	2.486	1.24	15.5	1.18
B	2	H	5	134	136	10.02	241.5		2.444		15.3	
B	2	H	5	134	136	10.02	241.5	12.7		0.86		
B	2	H	5	141	143	10.09	242.9	15.8	2.210	1.53	14.4	1.22
B	2	H	5	144	146	10.12	243.5		2.212		14.4	
B	2	H	5	144	146	10.12	243.5	15.2		1.90		
B	2	H	6	4	6	10.22	245.8		1.460		10.5	
B	2	H	6	4	6	10.22	245.8	22.4		2.81		
B	2	H	6	7	9	10.25	246.5	21.8	1.406	2.67	10.2	1.34
B	2	H	6	14	16	10.32	248.0	22.5	1.380	2.95	10.0	1.58
B	2	H	6	24	26	10.42	250.3	20.7	1.419	2.85	10.2	1.54
B	2	H	6	34	36	10.52	252.6	21.9	1.200	2.86	8.7	1.16
B	2	H	6	44	46	10.62	254.8	19.4	1.331	2.73	9.6	1.27
B	2	H	6	54	56	10.72	257.1	20.6	1.438	2.62	10.4	1.35
B	2	H	6	64	66	10.82	259.4	20.8	1.411	2.80	10.2	1.48
B	2	H	6	74	76	10.92	261.6	18.2	1.474	2.65	10.6	1.43
B	2	H	6	84	86	11.02	263.9	23.0	1.250	3.16	9.1	1.56
C	2	H	2	85	87	11.08	265.2	20.0	1.154	3.00	8.3	1.21
C	2	H	2	97	99	11.20	268.0	19.8	1.214	2.82	8.8	1.15
C	2	H	2	105	107	11.28	269.8	17.2	1.281	2.94	9.3	1.40
C	2	H	2	111	113	11.34	271.1	18.3	1.353	2.64	9.8	1.22
C	2	H	2	115	117	11.38	272.0	20.8	1.423	3.20	10.3	1.90
C	2	H	2	119	121	11.42	272.7	18.4	1.491	2.62	10.7	1.43
C	2	H	2	125	127	11.48	273.7	16.8	1.435	2.48	10.4	1.20
C	2	H	2	129	131	11.52	274.4	19.3	1.204	2.65	8.7	0.96
C	2	H	3	5	7	11.78	278.9	18.2	1.306	2.60	9.5	1.10
C	2	H	3	7	9	11.80	279.2	21.2	1.354	2.62	9.8	1.21
C	2	H	3	18	20	11.91	281.1	18.8	1.256	2.36	9.1	0.77
C	2	H	3	30	32	12.03	283.2	20.0	1.297	2.36	9.4	0.85
C	2	H	3	38	40	12.11	284.5	14.7	1.637	1.57	11.6	0.59
C	2	H	3	88	90	12.61	293.1	13.8	1.604	2.11	11.4	1.09
C	2	H	3	102	104	12.75	295.5	12.6	1.364	1.55	9.9	0.15
C	2	H	3	115	117	12.88	297.7		1.347		9.8	
C	2	H	3	125	127	12.98	299.4		1.258		9.1	
C	2	H	3	127	129	13.00	299.8	18.4	1.302	2.05	9.4	0.54
C	2	H	3	138	140	13.11	301.7	11.8	1.366	1.92	9.9	0.53
C	2	H	3	147	149	13.20	303.2	20.8	1.166		8.4	
C	2	H	4	12	14	13.35	305.8	20.1				
C	2	H	4	15	17	13.38	306.3		1.412		10.2	
C	2	H	4	25	27	13.48	308.0		1.456		10.5	
C	2	H	5	7	9	14.80	333.1	13.3		1.46		
C	2	H	5	15	17	14.88	334.7	20.2	1.617	2.83	11.5	1.82
C	2	H	5	19	21	14.92	335.6	20.7	1.255	3.11	9.1	1.52
C	2	H	5	23	25	14.96	336.4	18.3	1.161	2.97	8.4	1.20
C	2	H	5	25	27	14.98	336.8	23.1		3.43		
C	2	H	5	32	34	15.05	338.2	21.9	1.137	3.11	8.2	1.29
C	2	H	5	35	37	15.08	338.9	21.9		3.32		
C	2	H	5	42	44	15.15	340.3	21.7	1.296	3.00	9.4	1.49
C	2	H	5	45	47	15.18	340.9	21.2	1.364	3.26	9.9	1.86

Hole	Core	C	Sct	Top (cm)	Bot (cm)	Mcd	Age (ka)	Shell wt (μg)	Mg/Ca (mmol/mol)	$\delta^{18}O$ (‰)	T (^{o}C)	$\delta^{18}O_w$ (SMOW)
C	2	H	5	52	54	15.25	342.4	17.2	1.282	2.76	9.3	1.22
C	2	H	5	55	57	15.28	343.0	17.9	1.434	2.93	10.3	1.65
C	2	H	5	62	64	15.35	344.4	15.4	1.236	2.36	9.0	0.74
C	2	H	5	65	67	15.38	345.0	18.9		3.04		
C	2	H	5	72	74	15.45	346.5	10.4	1.117	1.53	8.0	-0.33
C	2	H	5	82	84	15.55	348.5	10.7	1.343	2.01	9.7	0.58
C	2	H	5	93	95	15.66	350.8	10.3		1.89		
B	3	H	1	114	116	15.72	352.0	13.0		2.16		
B	3	H	1	117	119	15.75	352.6	12.2	1.414	2.54	10.2	1.23
B	3	H	1	121	123	15.79	353.5	20.0	1.387	2.80	10.0	1.45
B	3	H	1	124	126	15.82	354.1		1.387		10.0	
B	3	H	1	131	133	15.89	355.5	21.7	1.298	2.86	9.4	1.35
B	3	H	1	134	136	15.92	356.1	18.0	1.693	2.76	11.9	1.86
B	3	H	1	141	143	15.99	357.6	21.8	1.465	2.76	10.5	1.53
B	3	H	1	144	146	16.02	358.2		1.408		10.2	
B	3	H	2	7	9	16.15	360.9	12.0		2.02		
B	3	H	2	18	20	16.26	363.1	14.9	1.406	2.10	10.2	0.77
B	3	H	2	21	23	16.29	363.8	13.0	1.905	1.95	13.0	1.31
B	3	H	2	31	33	16.39	365.8	18.6	1.381		10.0	
B	3	H	2	40	42	16.48	367.7	15.7		2.28		
B	3	H	2	57	59	16.65	371.2	10.0				
B	3	H	2	82	84	16.90	376.3	11.2				
B	3	H	3	90	92	18.48	408.8	15.0				
B	3	H	3	100	102	18.58	410.9	15.9		2.09		
B	3	H	3	112	114	18.70	413.3	20.1	1.491	3.03	10.7	1.84
B	3	H	3	114	116	18.72	413.8	18.9	1.507	3.29	10.8	2.12
B	3	H	3	121	123	18.79	415.2	21.2	1.651	3.08	11.7	2.12
B	3	H	3	124	126	18.82	415.8	20.4	1.474	3.46	10.6	2.24
B	3	H	3	131	133	18.89	417.3	22.5	1.482	3.29	10.7	2.09
B	3	H	3	134	136	18.92	417.9	20.3	1.294	3.31	9.4	1.79
B	3	H	3	141	143	18.99	419.3	21.4	1.471	3.05	10.6	1.82
B	3	H	3	144	146	19.02	419.9	23.3	1.523	3.36	10.9	2.21
B	3	H	4	2	4	19.10	421.6	20.3	1.432	3.18	10.3	1.90
B	3	H	4	4	6	19.12	422.0	20.0	1.324	3.34	9.6	1.87
B	3	H	4	12	14	19.20	423.6	19.7	1.596	3.17	11.3	2.13
B	3	H	4	14	16	19.22	424.1	21.1	1.416	3.40	10.2	2.09
B	3	H	4	24	26	19.32	426.1	21.8	1.470	3.38	10.6	2.16
B	3	H	4	32	34	19.40	427.8	20.4	1.419	2.99	10.2	1.69
B	3	H	4	34	36	19.42	428.2	20.7	1.445	3.30	10.4	2.04
B	3	H	4	42	44	19.50	429.8	20.5	1.424	3.07	10.3	1.78
B	3	H	4	44	46	19.52	430.2	22.5	1.375	3.18	10.0	1.80
B	3	H	4	53	55	19.61	432.1	23.4	1.495	2.84	10.7	1.65
B	3	H	4	54	56	19.62	432.3	22.2	1.395	2.91	10.1	1.56
B	3	H	4	62	64	19.70	433.9	20.5	1.248	2.86	9.0	1.26
B	3	H	4	64	66	19.72	434.3	22.9	1.478	3.06	10.6	1.85
B	3	H	4	71	73	19.79	435.8	19.6	1.434	2.72	10.3	1.44
B	3	H	4	82	84	19.90	438.0	16.2				

Sct – section of core

Mcd - metres composite depth

Temperatures calculated from Mg/Ca using the equation of Mashiotta *et al.*, [1999]

$\delta^{18}O_W$ calculated using the equation of O'Neil *et al.*, 1969

ODP Site 1123 *G. bulloides* 250 – 300 μm

Hole	Core	C	Sct	Top (cm)	Bot (cm)	Mcd	Age (ka)	Shell wt (μg)	Mg/Ca (mmol/mol)	$\delta^{18}O$ (‰)	T (^{o}C)	$\delta^{18}O_w$ (SMOW)
C	1	H	1	3	5	0.03	6.1	8.5	2.058	0.64	13.72	0.18
C	1	H	1	4	6	0.04	6.3	8.1	2.034	0.72	13.61	0.23
C	1	H	1	9	11	0.09	7.4	9.7	1.643	0.94	11.62	-0.04
C	1	H	1	14	16	0.14	8.4	8.3	1.784	0.70	12.39	-0.08
C	1	H	1	20	22	0.20	9.6	9.2	1.866	0.65	12.81	-0.04
C	1	H	1	25	27	0.25	10.6	10.4	1.870	0.89	12.83	0.20
C	1	H	1	29	31	0.29	11.5	9.8	1.848	1.26	12.72	0.55
C	1	H	1	33	35	0.33	12.3	10.6	1.695	1.05	11.91	0.15
C	1	H	1	40	42	0.40	13.7	12.0	1.610	1.65	11.43	0.64
C	1	H	1	49	51	0.49	15.6	11.2	1.657	2.00	11.70	1.05
C	1	H	1	60	62	0.60	17.8	12.4		2.20		
C	1	H	1	66	68	0.66	19.0	12.2	1.432	2.84	10.33	1.56
C	1	H	1	69	71	0.69	19.7	12.3	1.673	2.41	11.79	1.48
C	1	H	1	76	78	0.76	21.0	13.2	1.467	3.00	10.56	1.77
C	1	H	1	80	82	0.80	21.7	12.2	1.679	2.52	11.82	1.60
C	1	H	1	90	92	0.90	23.6	12.3	1.516	2.37	10.87	1.21
C	1	H	1	94	96	0.94	24.4	10.7	1.742	2.37	12.17	1.53
C	1	H	1	100	102	1.00	25.5	12.7	1.437	2.62	10.37	1.34
C	1	H	1	103	105	1.03	26.1	11.7	1.610	2.61	11.43	1.60
C	1	H	4	44	46	4.94	107.6	9.5	1.308		9.48	
C	1	H	4	49	51	4.99	108.8	7.6	1.695	1.00	11.91	0.09
C	1	H	4	52	54	5.02	110.2	8.2	1.779	0.77	12.36	-0.02
C	1	H	4	60	62	5.10	114.2	9.6	1.916	0.77	13.05	0.14
C	1	H	4	62	64	5.12	115.2	9.1	1.913	0.86	13.04	0.23
C	1	H	4	70	72	5.20	119.2	8.5	2.021	0.46	13.55	-0.05
C	1	H	4	70	72	5.20	119.2	8.7	2.055	0.83	13.71	0.36
C	1	H	4	72	74	5.22	120.2	9.6	2.264	0.80	14.61	0.55
C	1	H	4	80	82	5.30	124.2	10.7	1.991	1.46	13.41	0.92
C	1	H	4	89	91	5.39	128.6	10.7	1.925	2.26	13.10	1.65
C	1	H	4	100	102	5.50	134.1	11.1	1.564	2.40	11.15	1.31
C	1	H	4	110	112	5.60	139.1	12.1	1.548	2.43	11.06	1.33
C	1	H	4	120	122	5.70	140.8	10.9	1.610	2.41	11.43	1.39
C	1	H	4	130	132	5.80	142.6	10.9	1.761	2.13	12.27	1.31
C	1	H	4	140	142	5.90	144.4	10.5	1.625	1.67	11.51	0.67
C	1	H	5	3	5	6.03	146.6	9.7	1.626	1.66	11.52	0.67

Sct - Core Section
Mcd – composite depth in metres
Temperatures calculated from Mg/Ca using the equation of Mashiotta *et al.*, [1999]
$\delta^{18}O_W$ calculated using the equation of O'Neil *et al.*, 1969

ODP Site 1123 *G. inflata* 300 – 355 μm

Hole	Core	C	Sct	Top (cm)	Bot (cm)	Mcd	Age (ka)	Shell wt (μg)	Mg/Ca (mmol/mol)	$\delta^{18}O$ (‰)	T (^{o}C)	$\delta^{18}O_w$ (SMOW)
C	1	H	1	3	5	0.03	6.1	20.2	0.933	1.185	6.33	-1.11
C	1	H	1	4	6	0.04	6.3	18.2	1.249	1.285	9.06	-0.32
C	1	H	1	9	11	0.09	7.4	20.2	1.017	1.097	7.13	-0.99
C	1	H	1	14	16	0.14	8.4	20.5	1.163	1.418	8.39	-0.35
C	1	H	1	20	22	0.20	9.6	21.5	1.076	0.968	7.66	-0.98
C	1	H	1	25	27	0.25	10.6	20.9	1.336	1.337	9.68	-0.11
C	1	H	1	29	31	0.29	11.5	22.6	1.159	1.452	8.36	-0.32
C	1	H	1	33	35	0.33	12.3	25.6	1.229	1.598	8.90	-0.04
C	1	H	1	40	42	0.40	13.7	21.9	1.143	1.867	8.23	0.06
C	1	H	1	49	51	0.49	15.6	25.0	0.960	2.614	6.59	0.39
C	1	H	1	60	62	0.60	17.8	31.3	0.765	2.955	4.48	0.18
C	1	H	1	66	68	0.66	19.0	34.6	0.787	3.578	4.74	0.87
C	1	H	1	69	71	0.69	19.7	31.6	0.707	3.633	3.73	0.66
C	1	H	1	76	78	0.76	21.0	32.2	0.718	3.756	3.89	0.82
C	1	H	1	80	82	0.80	21.7	33.0	0.759	4.122	4.40	1.32
C	1	H	1	90	92	0.90	23.6	29.2	0.753	3.349	4.32	0.53
C	1	H	1	94	96	0.94	24.4	29.4	0.835	3.491	5.29	0.93
C	1	H	1	100	102	1.00	25.5	30.3	0.849	3.652	5.44	1.13
C	1	H	1	103	105	1.03	26.1	32.0	0.840	3.579	5.34	1.03
C	1	H	4	49	51	4.99	108.8	19.0	1.102	1.08	7.88	-0.81
C	1	H	4	52	54	5.02	110.2	20.9	1.121	1.01	8.05	-0.85
C	1	H	4	60	62	5.10	114.2	20.2	1.207	1.09	8.73	-0.59
C	1	H	4	62	64	5.12	115.2	24.4	1.037	1.00	7.32	-1.05
C	1	H	4	70	72	5.20	119.2	20.8		0.93		
C	1	H	4	70	72	5.20	119.2	21.6	1.173	1.08	8.47	-0.66
C	1	H	4	72	74	5.22	120.2	25.7	1.458	1.18	10.50	-0.06
C	1	H	4	80	82	5.30	124.2	27.6	1.556	1.41	11.11	0.32
C	1	H	4	89	91	5.39	128.6	25.2	1.109	2.50	7.94	0.62
C	1	H	4	100	102	5.50	134.1	18.7	1.442	2.49	10.40	1.23
C	1	H	4	110	112	5.60	139.1	34.9	1.342	3.55	9.73	2.12
C	1	H	4	120	122	5.70	140.8	22.3	1.210	2.58	8.76	0.90
C	1	H	4	130	132	5.80	142.6	21.8	1.421	2.66	10.26	1.36
C	1	H	4	140	142	5.90	144.4	26.0	1.133	3.00	8.14	1.17
C	1	H	5	3	5	6.03	146.6	22.9	0.921	2.41	6.20	0.08
C	1	H	5	9	11	6.09	147.7	17.9	1.283	2.19	9.31	0.66

Temperatures calculated from Mg/Ca using the equation of Mashiotta *et al.,* [1999]
$\delta^{18}O_W$ calculated using the equation of O'Neil *et al.,* 1969

CHAT 1K *G. bulloides* 300 – 355 μm

Depth (cm)	Age (ka)	Shell wt (μg)	Mg/Ca (mmol/mol)	$\delta^{18}O$ (‰)	T (^{o}C)	$\delta^{18}O_w$ (SMOW)
0	0.0	20.5	1.318	2.08	9.56	0.60
1	0.6	20.8	1.459	2.08	10.51	0.84
2	1.3	23.4	1.301	2.08	9.44	0.57
3	1.9	24.8	1.348		9.77	
4	2.5	26.9	1.441		10.39	
5	3.1	23.4	1.420		10.25	
6	3.8	24.6	1.384	2.24	10.02	0.88
7	4.4	26.4	1.463		10.53	
8	5.0	22.5	1.140		8.20	
9	5.6	20.9	1.343		9.74	
14	8.8	20.0	1.495	2.95	10.73	1.76
18	11.3	26.2	1.365	2.96	9.88	1.56
22	13.8	26.4	1.374	2.79	9.95	1.41
26	15.2	28.7	1.396	2.88	10.09	1.54
30	16.5	24.3		3.06		
34	17.9	23.3		3.08		
38	19.2	24.4		3.21		
42	20.6	23.5		3.21		
46	21.9	23.6		3.25		
50	23.3	24.8	1.290	3.25	9.36	1.72
54	24.6	22.7	1.358	3.05	9.83	1.64
58	26.0	22.8	1.403	3.16	10.14	1.83
62	27.0	19.6	1.409	2.77	10.18	1.45
66	28.0	19.4	1.288	2.96	9.34	1.43
70	29.0	17.8		3.13		
74	30.0	24.0		3.22		

Temperatures calculated from Mg/Ca using the equation of Mashiotta *et al.,* [1999]
$\delta^{18}O_W$ calculated using the equation of O'Neil *et al.,* 1969

CHAT 1K *G. bulloides* 250 – 300 μm

Depth (cm)	Age (ka)	Shell wt (μg)	Mg/Ca (mmol/mol)	$\delta^{18}O$ (‰)	T (^{o}C)	$\delta^{18}O_w$ (SMOW)
0	0.0	10.6				
1	0.6	10.1	1.447		10.43	
2	1.3	10.1	1.557		11.11	
3	1.9	10.7	1.567		11.17	
4	2.5	10.0	1.640		11.60	
5	3.1	13.8	1.479		10.63	
6	3.8	10.9				
7	4.4	9.4	1.698		11.93	
8	5.0	12.8	1.471		10.59	
9	5.6	9.7	1.634		11.56	
10	6.3	8.9	1.501		10.77	
14	8.8	8.6	1.787		12.40	
18	11.3	10.6				
22	13.8	10.5	1.636		11.58	
26	15.2	11.9	1.486		10.68	
30	16.5	12.5				
34	17.9	11.8				
38	19.2	11.8				
42	20.6	12.5				

Temperatures calculated from Mg/Ca using the equation of Mashiotta *et al.,* [1999]

CHAT 1K *G. inflata* 300 – 355 μm

Depth (cm)	Age (ka)	Shell wt (μg)	Mg/Ca (mmol/mol)	$\delta^{18}O$ (‰)	T (^{o}C)	$\delta^{18}O_w$ (SMOW)
0	0.0	18.9	0.810		5.01	
1	0.6	17.1	0.737		4.13	
2	1.3	18.4	0.997	0.80	6.95	-1.33
3	1.9	19.2	0.948		6.48	
4	2.5	21.0	1.055		7.47	
5	3.1	22.6	0.820		5.12	
6	3.8	23.9	0.803	1.52	4.93	-1.14
7	4.4	21.3	0.749		4.27	
8	5.0	22.7	0.712		3.81	
9	5.6	23.0	0.880		5.78	
10	6.3	23.4	1.121	1.17	8.05	-0.68
14	8.8	25.5	0.804	1.43	4.93	-1.23
18	11.3	25.8	1.111	1.72	7.96	-0.16
22	13.8	28.3	1.035	2.34	7.30	0.30
26	15.2	29.7	1.117	3.15	8.01	1.29
30	16.5	33.2		3.34		
34	17.9	28.1		3.52		
38	19.2	29.5		3.39		
42	20.6	35.2		3.46		
46	21.9	36.2		3.39		
50	23.3	35.3		3.42		
54	24.6	32.9		3.46		
58	26.0	31.2		3.45		
62	27.0	29.9		3.38		
66	28.0	30.7		3.45		
70	29.0	31.7		3.41		
74	30.0	29.8		3.48		

Temperatures calculated from Mg/Ca using the equation of Mashiotta *et al.,* [1999]
$\delta^{18}O_W$ calculated using the equation of O'Neil *et al.,* 1969

CHAT 16K *G. bulloides* 300 – 355 μm

Depth (cm)	Age (ka)	Shell wt (μg)	Mg/Ca (mmol/mol)	$\delta^{18}O$ (‰)	T (^{o}C)	$\delta^{18}O_w$ (SMOW)
0	0.0	21.0				
1	0.7	14.7	1.916	0.87	13.06	0.25
2	1.3	16.4	1.804	1.11	12.49	0.35
3	2.0	16.7	1.704	1.45	11.96	0.56
4	2.6	18.0	1.624	1.20	11.51	0.20
5	3.3	15.7	1.679	1.60	11.82	0.68
6	3.9	16.5	1.793	1.12	12.43	0.34
7	4.6	18.6	1.830	1.11	12.62	0.38
8	5.3	15.7	1.955	1.23	13.24	0.64
9	5.9	18.9	1.877	1.28	12.86	0.60
10	6.6	17.0	1.833	1.38	12.64	0.66
11	7.2	16.3	1.745	1.36	12.18	0.53
12	7.9	17.5	1.929	1.33	13.12	0.72
13	8.5	20.1	1.652	1.56	11.67	0.60
14	9.2	16.7	1.925	1.16	13.10	0.54
15	9.9	17.2	1.981	1.69	13.36	1.14
16	10.5	17.3	1.850	1.54	12.72	0.83
17	11.2	22.8				
18	11.8	16.7	2.028	1.66	13.58	1.16
19	12.5	19.2				
20	13.1	19.8	1.840	2.16	12.68	1.45
21	13.8	19.2				
22	14.1	21.6	1.972	1.78	13.32	1.22

Depth (cm)	Age (ka)	Shell wt (μg)	Mg/Ca (mmol/mol)	$\delta^{18}O$ (‰)	T (^{o}C)	$\delta^{18}O_w$ (SMOW)
24	14.8	19.8	1.890	2.07	12.93	1.41
25	15.2	17.2				
26	15.5	16.7	1.936	1.71	13.15	1.10
27	15.9	22.6				
28	16.2	18.9	1.895	1.01	12.95	0.35
29	16.6	22.4				
30	16.9	24.0	1.735	2.34	12.13	1.49
31	17.2	17.9				
32	17.6	19.3	1.893	2.27	12.94	1.62
33	17.9	17.3				
34	18.3	19.8	1.732	2.48	12.11	1.63
35	18.6	20.9				
36	19.0	22.5	1.750	2.62	12.21	1.79
39	20.0	19.9				
41	20.7	18.8	1.848	2.29	12.72	1.59
43	21.4	22.2	1.542	2.75	11.03	1.64
47	22.8	20.3	1.748	2.27	12.19	1.44
49	23.4	17.6	1.586	2.75	11.29	1.70
51	24.1	18.9	1.506	2.64	10.81	1.47
53	24.8	16.5	1.709	2.49	11.99	1.60
55	25.5	16.6	1.526	2.42	10.93	1.28
57	26.2	19.7	1.619	2.42	11.48	1.42
59	26.8	17.2	1.673	2.35	11.79	1.42
61	27.3	18.9	1.544	2.63	11.04	1.51
63	27.9	19.2	1.690	2.31	11.88	1.40
65	28.5	18.1	1.620	0.86	11.48	-0.14
67	29.0	15.7	1.725	1.87	12.07	1.01
69	29.6	14.7	1.673	1.84	11.79	0.91
71	30.2	14.9	1.717	1.93	12.03	1.05
73	30.7	15.7	1.709	2.23	11.99	1.35
75	31.3	15.1	1.572	2.15	11.21	1.08
77	31.9	15.0	1.847	1.67	12.71	0.96
79	32.4	15.9	1.630	2.29	11.54	1.30
81	33.0		1.813	1.67	12.54	0.92
199	99.9	15.3	1.969	1.00	13.31	0.43
203	104.6	16.1		1.23		
207	107.9	13.2	2.027	1.53	13.58	1.03
211	111.1	14.4		1.12		
215	114.4	15.8	2.059		13.73	
219	117.6	18.3	2.058	0.99	13.72	0.52
223	120.9	21.4	1.814		12.54	
227	124.1	22.5	1.981		13.37	
231	127.4	24.2	1.708	2.48	11.98	1.59
235	129.9	20.0	1.881	2.03	12.88	1.36
239	131.7	18.2	1.897		12.96	
243	133.4	18.5	1.790	2.26	12.42	1.48
247	135.2	19.1	2.148		14.12	
251	137.0	22.4	1.763	2.95	12.28	2.13
255	138.7	21.1	1.921		13.08	
259	140.5	19.8	1.712	3.02	12.00	2.14
263	142.3	22.7	1.560		11.13	
267	144.1	24.9	1.478	2.86	10.63	1.64
271	145.8	23.3	1.722		12.06	
275	147.6	19.4		2.59		
279	149.4	20.9	1.676		11.80	
283	151.1	19.0	1.506	2.37	10.80	1.20
287	152.9	25.7	1.438	2.75	10.37	1.47
291	154.7	17.0		1.83		
295	156.5	15.1	1.934	2.04	13.14	1.43
299	158.2	18.0	1.833	1.95	12.64	1.22

Temperatures calculated from Mg/Ca using the equation of Mashiotta *et al.*, [1999]
$\delta^{18}O_W$ calculated using the equation of O'Neil *et al.*, 1969

CHAT 16K *G. bulloides* 250 – 300 μm

Depth (cm)	Age (ka)	Shell wt (μg)	Mg/Ca (mmol/mol)	$\delta^{18}O$ (‰)	T (^{o}C)	$\delta^{18}O_w$ (SMOW)
0	0.0	10.5	1.707	1.09	11.97	0.20
1	0.7	9.5		0.84		
2	1.3	9.6	1.883	0.87	12.89	0.20
3	2.0	9.1	1.928	0.78	13.11	0.17
4	2.6	11.1	1.859	0.98	12.77	0.29
5	3.3	10.5	2.110	0.86	13.95	0.45
6	3.9	10.4	1.857	0.95	12.76	0.26
7	4.6	12.5	2.079	0.90	13.82	0.46
8	5.3	11.3	2.079	1.13	13.82	0.69
9	5.9	11.4	1.894	1.92	12.95	1.27
10	6.6	11.4	2.042	0.88	13.65	0.39
11	7.2	13.6	2.005	1.05	13.48	0.53
12	7.9	11.7	2.102		13.92	
13	8.5	12.6	2.115	1.26	13.98	0.85
14	9.2	11.6	1.963	1.18	13.28	0.60
15	9.9	11.7	2.093	1.01	13.88	0.58
16	10.5	12.4	1.932		13.13	
17	11.2	14.2	1.939	1.17	13.16	0.57
18	11.8	12.3	1.909	1.47	13.02	0.83
19	12.5	12.0	2.157	1.48	14.16	1.11
20	13.1	12.0	1.953	1.53	13.23	0.95
21	13.8	12.3	1.971	1.45	13.32	0.89
22	14.1	16.2	1.907	1.62	13.01	0.98
23	14.5	12.8	2.072	1.65	13.79	1.19
24	14.8	12.8	1.924		13.09	
25	15.2	12.5	2.051	1.60	13.69	1.13
26	15.5	12.0	2.229	1.58	14.47	1.29
27	15.9	12.4	2.064	1.77	13.75	1.31
28	16.2	11.6	2.132	1.62	14.05	1.23
29	16.6	13.0	2.198	1.39	14.34	1.06
30	16.9	13.5	2.034	1.70	13.61	1.21
31	17.2	12.5	1.878	1.57	12.87	0.90
32	17.6	11.7	1.958		13.25	
33	17.9	11.8	2.079	1.81	13.82	1.37
34	18.3	13.6	1.808	1.90	12.51	1.15
35	18.6	12.1	1.943	1.90	13.18	1.31
36	19.0	11.8	1.789	1.84	12.41	1.06
37	19.3	11.3	2.190	2.09	14.30	1.76
39	20.0	11.6	1.934	2.03	13.14	1.43
41	20.7	11.3	2.133		14.06	
43	21.4	12.1	2.010	1.92	13.50	1.40
45	22.1	11.6	1.924	1.88	13.09	1.27
47	22.8	9.9	2.059	2.20	13.72	1.73
49	23.4	11.8	1.617	2.18	11.47	1.17
51	24.1	10.9	2.065	2.12	13.76	1.66
53	24.8	11.9	1.749	1.98	12.20	1.15
55	25.5	11.5	1.692	1.97	11.89	1.06
57	26.2	11.4	1.716	2.05	12.02	1.17
59	26.8	12.0	1.644	2.14	11.62	1.17
61	27.3	11.6	1.845	2.05	12.70	1.34
63	27.9	12.4	1.664	2.11	11.74	1.17
65	28.5	12.9	1.566	2.21	11.17	1.13
67	29.0	10.8	1.637	1.81	11.59	0.83
69	29.6	10.8	1.718	1.92	12.03	1.05
71	30.2	11.2	1.618	1.81	11.48	0.81
73	30.7	10.3	1.826	1.76	12.60	1.02
75	31.3	9.9	1.926	1.87	13.10	1.26
77	31.9	10.8	1.797	1.82	12.45	1.05
79	32.4	10.6	1.738	1.71	12.15	0.87
81	33.0		1.692	1.83	11.89	0.93

Depth (cm)	Age (ka)	Shell wt (μg)	Mg/Ca (mmol/mol)	$\delta^{18}O$ (‰)	T (^{o}C)	$\delta^{18}O_w$ (SMOW)
199	99.9	10.5	2.050		13.69	
203	104.6	9.9		0.92		
207	107.9	9.8	2.261		14.60	
211	111.1	10.3	2.141	0.89	14.09	0.51
215	114.4	10.7	2.252		14.56	
219	117.6	10.9		0.87		
223	120.9	11.0	2.763	1.26	16.47	1.44
227	124.1	13.0	2.120	2.11	14.00	1.70
231	127.4	11.4	1.971	1.56	13.32	1.00
235	129.9	12.0	1.992		13.42	
239	131.7	13.3	2.156	0.34	14.16	-0.03
243	133.4	12.4	1.891	1.84	12.93	1.18
247	135.2	11.7	1.851	2.14	12.73	1.44
251	137.0	11.7	2.114	2.00	13.97	1.59
255	138.7	12.2	2.087	2.10	13.85	1.66
259	140.5	12.8	2.155	2.13	14.15	1.76
263	142.3	12.2	2.065	2.22	13.76	1.76
267	144.1	12.5	1.867	2.22	12.81	1.53
271	145.8	12.5	1.730	2.01	12.10	1.15
275	147.6	11.4		2.07		
279	149.4	11.6	1.908	1.94	13.02	1.30
283	151.1	11.1		1.76		
287	152.9	11.9	1.871		12.83	
291	154.7	11.0		1.88		
295	156.5	10.8	1.965	1.75	13.29	1.18
299	158.2	11.9		1.63		

Temperatures calculated from Mg/Ca using the equation of Mashiotta *et al.*, [1999]
$\delta^{18}O_W$ calculated using the equation of O'Neil *et al.*, 1969

CHAT 16K *G. inflata* 300 – 355 μm

Depth (cm)	Age (ka)	Shell wt (μg)	Mg/Ca (mmol/mol)	$\delta^{18}O$ (‰)	T (^{o}C)	$\delta^{18}O_w$ (SMOW)
0	0.0	19.0	1.269	1.68	9.20	0.11
1	0.7	20.5	0.998		6.96	
2	1.3	22.2	1.264	2.27	9.17	0.70
3	2.0	21.3	1.044		7.38	
4	2.6	21.7	1.350	1.25	9.79	-0.17
5	3.3	24.1				
6	3.9	23.9	1.353	1.96	9.80	0.54
7	4.6	25.3				
8	5.3	26.8	1.100	2.11	7.87	0.21
9	5.9	29.5				
10	6.6	29.2	1.307	2.64	9.48	1.15
11	7.2	31.9				
12	7.9	30.1	1.300	3.34	9.43	1.83
13	8.5	27.3				
14	9.2	29.9	1.428	2.22	10.31	0.93
15	9.9	28.1				
16	10.5	31.5	1.371	2.45	9.93	1.06
17	11.2	34.2	1.080		7.69	
18	11.8	34.8	1.277	3.08	9.26	1.53
19	12.5	33.6	1.105		7.91	
20	13.1	38.1	1.019	4.26	7.15	2.18
21	13.8	36.2				
22	14.1	35.7	1.099	3.65	7.86	1.75
23	14.5	37.8				
24	14.8	38.8	0.884	3.53	5.82	1.10

Depth (cm)	Age (ka)	Shell wt (μg)	Mg/Ca (mmol/mol)	$\delta^{18}O$ (‰)	T (^{o}C)	$\delta^{18}O_w$ (SMOW)
25	15.2	39.8				
26	15.5	39.6	0.985	3.48	6.83	1.31
27	15.9	40.4				
28	16.2	39.0	0.968	3.59	6.67	1.38
29	16.6	35.8				
30	16.9	36.2	1.148	3.43	8.27	1.64
31	17.2	40.7				
32	17.6	40.1	0.936	3.53	6.35	1.24
33	17.9	39.5				
34	18.3		1.048	3.32	7.42	1.31
35	18.6	37.7				
36	19.0	40.2	0.928	3.63	6.28	1.32
37	19.3	39.0				
39	20.0	38.9	0.897		5.96	
41	20.7	42.3	0.932	3.48	6.32	1.19
43	21.4	40.7	0.965	3.93	6.65	1.72
45	22.1	41.5		3.46		
47	22.8	39.7				
49	23.4	36.9	0.915	3.61	6.14	1.26
51	24.1	35.9				
53	24.8	40.3	0.970	3.40	6.70	1.21
55	25.5	36.9				
57	26.2	38.3	0.930	3.59	6.30	1.29
59	26.8	36.1				
61	27.3	37.9	0.949	3.47	6.49	1.22
63	27.9	34.4				
65	28.5	36.3	1.106	3.18	7.92	1.29
67	29.0	35.1	0.949		6.48	
69	29.6	31.3	1.220	2.98	8.84	1.32
71	30.2	29.5	1.154		8.32	
73	30.7	28.1	1.255	2.83	9.10	1.24
75	31.3	28.8				
77	31.9		1.229	2.28	8.90	0.64
199	99.9	26.6	1.532	1.43	10.97	199
203	104.6	28.0	1.485	1.44	10.67	203
207	107.9	24.3	1.588	1.63	11.30	207
211	111.1	24.6	1.490	1.27	10.70	211
215	114.4	25.1	1.530	1.48	10.95	215
219	117.6	28.0	1.592	1.40	11.32	219
223	120.9	26.7	1.717	1.53	12.03	223
227	124.1	29.4	1.896	1.70	12.96	227
231	127.4	23.9	1.772	2.18	12.32	231
235	129.9	27.1	1.759	1.88	12.26	235
239	131.7	26.6	1.748	2.04	12.19	239
243	133.4	28.7	1.498	2.71	10.75	243
247	135.2	29.4	1.531	3.08	10.96	247
251	137.0	27.7	1.530	2.53	10.95	251
255	138.7	31.6	1.371	3.08	9.93	255
259	140.5	29.8	1.346	2.84	9.75	259
263	142.3	35.3	1.310	3.24	9.50	263
267	144.1	32.8	1.299	3.05	9.42	267
271	145.8	32.2	1.258	2.79	9.13	271
275	147.6	35.3	1.153	3.24	8.31	275
279	149.4	32.6	1.477	3.12	10.62	279
283	151.1	32.6	1.307	2.90	9.48	283
287	152.9	31.4	1.361	2.82	9.85	287
291	154.7	27.2	1.486	2.59	10.68	291
295	156.5	25.9	1.444	2.25	10.41	295

Temperatures calculated from Mg/Ca using the equation of Mashiotta *et al.,* [1999]
$\delta^{18}O_W$ calculated using the equation of O'Neil *et al.,* 1969

Appendix 3

APNAP box core top planktonic foraminifera data

N. Pachyderma (d)

Core Top	Lat. (°N)	Cd/Ca (μmol/mol)	Sr/Ca (mmol/mol)	Mg/Ca (mmol/mol)	Mn/Ca (μmol/mol)	D_{Cd}
T88 1B	59.7	0.0678	1.401	1.041	3.8	7.39
T90 1B	58.5	0.0129	1.392	1.062	6.1	1.39
T88 2B	57.9	0.0276	1.401	1.069	6.8	2.98
T88 3B	56.4	0.0217	1.379	1.072	2.6	2.48
T88 4B	55.0	0.0288	1.397	1.186	4.7	2.65
T88 5B	53.6	0.0275	1.399	1.245	2.3	2.50
T86 1B	53.4	0.0294	1.379	1.266	1.7	2.73
T90 2B	53.1	0.0257	1.393		31.2	2.45
T88 6B	51.4	0.0355	1.362	0.996	2.7	3.92
T88 7B	50.5	0.0359	1.389	1.159	2.5	4.25
T86 3B	50.2	0.0338	1.360	1.075	2.7	4.10
T88 9B	48.4	0.0175	1.399	1.334	1.9	2.51
T90 3B	47.7	0.0279	1.391	0.982	3.7	4.38
T90 15B	47.6	0.0256	1.398	1.387	4.0	4.08
T90 4B	47.2	0.0332	1.388	1.213	2.7	5.54
T86 5B	46.9	0.0131	1.394	1.475	2.3	2.07
T90 8B	46.2	0.0369	1.380	1.180	3.0	5.27
T90 5B	46.0	0.0346	1.381	1.125	3.3	5.04
T88 11B	45.4	0.0146	1.376	1.425	3.5	2.24
T90 11B	45.0	0.0280	1.392	1.234	2.2	4.41
T88 12B	44.1	0.0233	1.404	1.354	3.0	3.87
T86 7B	43.9	0.0228	1.388	1.719	2.5	3.82
T88 13B	42.9	0.0351	1.396	1.327	2.4	6.23
T86 8B	42.3	0.0547	1.393	1.601	3.0	6.52
T86 9B	40.8	0.0309	1.395	1.477	4.8	3.69
T88 14B	40.4	0.0397	1.400	1.513	2.5	4.72
T88 15A	38.9	0.0414	1.412	1.696	5.2	4.91
T88 15B	38.6	0.0324	1.394	1.430	3.2	3.84
T86 10B	37.1					
T86 11B	35.6	0.0369	1.443	1.506	4.2	4.98
T88 17B	35.4	0.0778	1.424	1.509	3.6	10.67

G. ruber (w)

Core Top	Lat. (°N)	Cd/Ca (μmol/mol)	Sr/Ca (mmol/mol)	Mg/Ca (mmol/mol)	Mn/Ca (μmol/mol)	D_{Cd}
T90 3B	47.7		1.433	2.009		
T90 15B	47.6	0.0646	1.418	1.949	1.4	23.36
T90 4B	47.2	0.0479	1.432	2.156	2.1	18.58
T86 5B	46.9					
T90 8B	46.2	0.0476	1.406	2.295	0.9	22.25
T90 5B	46.0	0.0588	1.425	2.219	2.4	28.55
T88 11B	45.4	0.0192	1.443	2.460	1.6	10.55
T90 11B	45.0	0.0383	1.428	2.448	1.3	22.83
T88 12B	44.1	0.0282	1.451	2.804	1.4	20.29
T86 7B	43.9					
T88 13B	42.9	0.0350	1.434	2.355	1.0	30.82
T86 8B	42.3	0.0521	1.445	2.509	1.1	47.18
T86 9B	40.8					
T88 14B	40.4	0.0315	1.431	2.434	2.0	24.65
T88 15A	38.9					
T88 15B	38.6	0.0437	1.440	2.621	2.4	36.62
T86 10B	37.1					
T86 11B	35.6	0.0221	1.456	2.810	1.2	18.40
T88 17B	35.4	0.0254	1.470	3.068	0.7	21.29

G. sacculifer

Core Top	Lat. (°N)	Cd/Ca (μmol/mol)	Sr/Ca (mmol/mol)	Mg/Ca (mmol/mol)	Mn/Ca (μmol/mol)	D_{Cd}
T90 8B	46.2	0.0353	1.390	2.262	0.7	16.49
T90 5B	46.0					
T88 11B	45.4					
T90 11B	45.0	0.0335	1.386	2.449	0.9	19.97
T88 12B	44.1	0.0223	1.403	2.660	0.9	16.04
T86 7B	43.9					
T88 13B	42.9	0.0317	1.405	2.664	1.0	28.72
T86 8B	42.3					
T86 9B	40.8	0.0160	1.406	2.762	0.6	15.61
T88 14B	40.4	0.0240	1.402	3.012	0.7	23.21
T88 15A	38.9	0.0229	1.411	3.005	1.0	21.40
T88 15B	38.6	0.0258	1.408	3.119	4.1	20.13
T86 10B	37.1					
T86 11B	35.6	0.0125	1.404	3.032	0.3	12.06
T88 17B	35.4	0.0196	1.408	3.127	0.6	19.10

G. siphonifera

Core Top	Lat. (°N)	Cd/Ca (μmol/mol)	Sr/Ca (mmol/mol)	Mg/Ca (mmol/mol)	Mn/Ca (μmol/mol)	D_{Cd}
T90 3B	47.7		1.247	1.533		
T90 15B	47.6	0.0432	1.290	1.762	1.2	7.27
T90 4B	47.2	0.0492	1.263	2.303		8.76
T86 5B	46.9					
T90 8B	46.2	0.0389	1.289	2.303	0.4	7.95
T90 5B	46.0	0.0417	1.268	2.170	2.9	8.77
T88 11B	45.4	0.0188	1.299	3.054	0.8	4.28
T90 11B	45.0	0.0337	1.283	2.349	0.9	8.07
T88 12B	44.1					
T86 7B	43.9					
T88 13B	42.9	0.0415	1.302	2.859	1.5	12.83
T86 8B	42.3	0.0445	1.283	2.291	1.9	14.74
T86 9B	40.8	0.0186	1.279	2.791	2.0	5.27
T88 14B	40.4					
T88 15A	38.9	0.0291	1.274	2.570	1.9	8.58
T88 15B	38.6					
T86 10B	37.1					
T86 11B	35.6	0.0165	1.328	3.235	1.7	6.59

G. truncatulinoides (d)

Core Top	Lat. (°N)	Cd/Ca (μmol/mol)	Sr/Ca (mmol/mol)	Mg/Ca (mmol/mol)	Mn/Ca (μmol/mol)	D_{Cd}
T90 2B	53.1	0.0580	1.239	1.188	9.1	3.53
T88 6B	51.4	0.0818	1.267	1.291	12.5	4.85
T88 7B	50.5	0.0766	1.332	1.663	13.6	4.85
T86 3B	50.2					
T88 9B	48.4	0.0504	1.389	1.765	9.3	3.80
T90 3B	47.7	0.0564	1.279	1.265	9.3	4.54
T90 15B	47.6	0.0690	1.324	1.461	10.2	5.60
T90 4B	47.2	0.0727	1.293	1.401	9.8	6.12
T86 5B	46.9					
T90 8B	46.2	0.0675	1.340	1.569	10.0	6.45
T90 5B	46.0	0.0775	1.333	1.454	12.6	7.42
T88 11B	45.4					
T90 11B	45.0	0.0568	1.359	1.778	8.9	5.61
T88 12B	44.1					
T86 7B	43.9					
T88 13B	42.9		1.408	1.810		
T86 8B	42.3	0.0709	1.355	1.651	9.6	7.63
T86 9B	40.8	0.0477	1.392	1.719	9.5	5.16
T88 14B	40.4					
T88 15A	38.9	0.0320	1.386	1.790	10.0	3.45
T88 15B	38.6					
T86 10B	37.1					
T86 11B	35.6	0.0324	1.437	1.859	12.7	3.87

G. hirsuta

Core Top	Lat. (°N)	Cd/Ca (μmol/mol)	Sr/Ca (mmol/mol)	Mg/Ca (mmol/mol)	Mn/Ca (μmol/mol)	D_{Cd}
T88 1B	59.7					
T90 1B	58.5	0.0734	1.234	1.319	6.5	3.80
T88 2B	57.9	0.0481	1.180	1.027	8.7	2.42
T88 3B	56.4	0.0157	1.169	0.955	1.6	0.77
T88 4B	55.0	0.0423	1.232	1.406	7.1	2.05
T88 5B	53.6	0.0561	1.241	1.371	7.0	2.67
T86 1B	53.4	0.0656	1.275	1.496	6.5	3.13
T90 2B	53.1	0.0742	1.220	1.133		3.55
T88 6B	51.4		1.229	1.176	7.7	
T88 7B	50.5	0.0938	1.278	1.589	9.1	4.92
T86 3B	50.2	0.0710	1.244	1.159	8.6	3.80
T88 9B	48.4	0.0723	1.292	1.379	7.1	4.37
T90 3B	47.7	0.0938	1.293	1.385		5.95
T90 15B	47.6	0.0867	1.28	1.32		5.53
T90 4B	47.2	0.0909	1.259	1.239		5.95
T86 5B	46.9					
T90 8B	46.2	0.0844	1.297	1.386		6.87
T90 5B	46.0	0.0926	1.298	1.515		7.10
T88 11B	45.4					
T90 11B	45.0	0.0958	1.394	1.639		6.56
T88 12B	44.1					
T86 7B	43.9					
T88 13B	42.9	0.0677	1.316	1.530	8.0	4.91
T86 8B	42.3	0.0899	1.324	1.467	8.4	6.55
T86 9B	40.8	0.0659	1.349	1.663	8.8	4.81
T88 14B	40.4					
T88 15A	38.9	0.0598	1.380	1.690	11.4	7.09
T88 15B	38.6	0.0580	1.362	1.548	8.7	6.30
T86 10B	37.1					
T86 11B	35.6	0.0340	1.374	1.629	7.7	4.58
T88 17B	35.4		1.363	1.418	7.1	

G. inflata

Core Top	Lat. (°N)	Cd/Ca (μmol/mol)	Sr/Ca (mmol/mol)	Mg/Ca (mmol/mol)	Mn/Ca (μmol/mol)	D_{Cd}
T88 1B	59.7	0.0253	1.316	1.287	8.5	1.61
T90 1B	58.5	0.0349	1.296	1.410	5.1	2.29
T88 2B	57.9	0.0172	1.314	1.047	6.1	1.14
T88 3B	56.4	0.0172	1.288	1.067	2.3	1.06
T88 4B	55.0	0.0332	1.317	1.367	3.4	2.09
T88 5B	53.6					
T86 1B	53.4	0.0301	1.326		9.7	1.98
T90 2B	53.1	0.0391	1.301	1.121	3.4	2.59
T88 6B	51.4	0.0397	1.310	1.051	3.7	2.55
T88 7B	50.5					
T86 3B	50.2	0.0486	1.321	1.237	3.1	3.08
T88 9B	48.4	0.0238	1.354	1.540	3.0	1.66
T90 3B	47.7	0.0243	1.274	0.955	1.8	1.66
T90 15B	47.6	0.0439	1.314	1.335	2.3	3.03
T90 4B	47.2	0.0564	1.314	1.261	2.3	3.99
T86 5B	46.9	0.0207	1.337	1.387	3.5	1.50
T90 8B	46.2	0.0248	1.340	1.203	3.2	1.86
T90 5B	46.0	0.0379	1.315	1.075	3.0	2.88
T88 11B	45.4					
T90 11B	45.0	0.0426	1.345	1.386	3.8	3.37
T88 12B	44.1					
T86 7B	43.9	0.0289	1.376	1.581	3.3	2.37
T88 13B	42.9					
T86 8B	42.3	0.0407	1.372	1.378	2.8	3.44
T86 9B	40.8	0.0269	1.358	1.559	3.3	2.60
T88 14B	40.4					
T88 15A	38.9	0.0280	1.383	1.653	3.6	3.02
T88 15B	38.6					
T86 10B	37.1					
T86 11B	35.6	0.0186	1.396	1.460	3.2	2.15
T88 17B	35.4					

References

Anand, P., H. Elderfield & M.H. Conte, Calibration of Mg/Ca thermometry in planktonic foraminifera from a sediment trap time series. *Paleoceanography* **18,** 1050, 10.1029/2002PA000846, 2003.

Antonov J.I., R.A. Locarnini, T.P. Boyer, A.V. Mishonov & H.E., Garcia. *World Ocean Atlas 2005*, Volume 2: Salinity. S. Levitus, Ed. NOAA Atlas NESDIS 62, U.S. Government Printing Office, Washington, D.C., 182 pp., 2006.

Barker, S., Planktonic foraminiferal proxies for temperature and pCO_2 Ph.D. thesis, Univ. of Cambridge, Cambridge, England, 2002.

Barker S. & H. Elderfield, Foraminiferal Calcification Response to Glacial-Interglacial Changes in Atmospheric CO_2. *Science* **297**, 833-836, 2002.

Barker, S., M.J. Greaves, H. Elderfield, H. Johnstone & I. Hall. Records of planktonic foraminiferal shell weight provide insight into the controls on atmospheric CO_2 variability. *Eos Trans. AGU*, **83** (47), Fall Meet. Suppl., Abstract PP51A-0277, 2002.

Barker, S., M. Greaves & H. Elderfield. A study of cleaning procedures used for foraminiferal Mg/Ca paleothermometry, *Geochem. Geophys. Geosyst.*, **4**, 9, 10.1029/2003GC000559, 2003.

Barker, S., I. Cacho, H. Benway & K. Tachikawa. Planktonic foraminiferal Mg/Ca as a proxy for past oceanic temperatures: a methodological overview and data compilation for the Last Glacial Maximum, *Quaternary Science Reviews*, **24**, 821-834, 2005.

Beck J. W., R. L. Edwards, E. Ito, F. W. Taylor, J.Recy, F.Rougerie, P.Joannot & C.Henin. Sea-surface temperature from coral skeletal strontium/calcium ratios. *Science* **257**, 644-647, 1992.

Bemis, B., H.J. Spero, J. Bijma & D.W. Lea, Reevaluation of the oxygen isotopic composition of planktonic foraminifera : Experimental results and revised paleotemperature equations. *Paleoceanography,* **13**, 150-160,1998.

Bertram C.J., H. Elderfield, N.J. Shackleton & J.A. MacDonald. Cadmium/Calcium and carbon isotopes reconstructions of the glacial northeast Atlantic Ocean. *Palaeoceanography* **10**, 563-578, 1995.

Beveridge, N. A. S., H. Elderfield, and N. J. Shackleton, Deep thermohaline circulation in the low-latitude Atlantic during the last glacial, *Paleoceanography*, **10**, 643 - 660, 1995.

Bigg, G.R. & E.J. Rohling. An oxygen isotope data set for marine water. *J. Geophys. Res.*, **105**, 8527-8535, 2000.

Bijma J., H. J. Spero & D.W. Lea. Reassessing foraminiferal stable isotope geochemistry: Impact of the oceanic carbonate system (experimental results), In *Use of proxies in paleoceanography - Examples from the South Atlantic* (G Fischer, G Wefer, eds) Springer, Berlin, pp. 489-512, 1999.

Boyle E.A., Cadmium, zinc, copper and barium in foraminifera tests. *Earth Planet. Sci. Lett.* **53**, 11-35, 1981.

Boyle, E. A., Manganese carbonate overgrowths on foraminifera tests, *Geochim. Cosmochim. Acta*, **47**, 1815–1819, 1983.

Boyle E.A., Cadmium: chemical tracer of deepwater paleoceanography. *Paleoceanography*, **3**, 471-489, 1988.

Boyle E.A., Oceanic chemical distributions during the stage 2 glacial maximum: cadmium and $\delta^{13}C$ evidence compared. *Ann. Rev. Earth and Planet. Sci.* **20**, 245-287, 1992.

Boyle E.A., Limits on benthic foraminiferal chemical analyses as precise measures of environmental properties. *J. Foram Res.* **25**, 4-13, 1995.

Boyle E.A. & L.D. Keigwin, Comparison of Atlantic and Pacific paleochemical records for the last 250,000 years: changes in deep ocean circulation and chemical inventories. *Earth Planet .Sci. Lett.* **76**, 135-150, 1985/86.

Boyle, E. A., F. R. Sclater & J. M. Edmond, On the marine geochemistry of cadmium, *Nature*, **263**, 42-44, 1976.

Brenner, I. B. and A. T. Zander, Axially and radially viewed inductively coupled plasmas—A critical review, *Spectrochim. Acta Part B*, **55**, 1195–1240, 2000.

Broecker W. S., The Role of the Ocean in Climate Yesterday, Today, and Tomorrow, Eldigio Press, Palisades, N.Y.,176 pp, 2004.

Broecker W. S. & E. Clark, An evaluation of Lohmann's foraminifera weight dissolution index. *Paleoceanography,* **16**, 531-534, 2001a.

Broecker W. S. & E. Clark, Glacial-to-Holocene Redistribution of Carbonate ion in the Deep Sea. *Science*, **294**, 2152-2155, 2001b.

Brown, S.J., & H. Elderfield, Variations in Mg/Ca and Sr/Ca ratios of planktonic foraminifera caused by postdepositional dissolution: Evidence of shallow Mg-dependent dissolution. *Paleoceanography*, **11**, 543-551, 1996.

Cameron A.E., D.H. Smith & R.L. Walker, Mass specrometry of nanogram-size samples of lead. *Analyt. Chem.* **41**, 525-526, 1969.

Carter, L., Currents of change: the ocean flow in a changing world. *N I W A, Water & Atmosphere*, **9**(4), 15–17, 2001.

Carter, L., R. D. Garlick, P. Sutton, S. Chiswell, N. A. Oien, and B. R. Stanton, Ocean circulation New Zealand, Chart Misc. Ser. 76, Natl. Inst. of Water and Atmos. Res., Wellington, New Zealand, 1998.

Carter R.M., I.N. McCave, C. Richter, L. Carter, *et al., Proc. ODP, Init. Rep.* **181**, 1-184, 1999.

Carter, R.M., I.N. McCave and L. Carter, Leg 181 synthesis: fronts, flows, drifts, volcanoes, and the evolution of the southwestern gateway to the Pacific Ocean, eastern New Zealand. *In* Richter, C. (Ed.), *Proc. ODP, Sci. Results*, **181**, 2004a.

Carter, R.M., P.R. Gammon & L. Millwood, Glacial-interglacial (MIS1-10) migrations of the Subtropical Front across ODP Site 1119, Canterbury Bight, southwest Pacific Ocean. *Mar. Geol.,* **205**, 29-58, 2004b.

Chisholm W., K.J.R. Rosman, C.F. Boutron, J.P. Candelone, & S. Hong, Determination of lead-isotopic ratios in Greenland and Antarctic Snow and Ice at picogram per gram concentrations. *Analytica. Chimica. Acta* **311**, 141-151, 1995.

Chiswell, S.M., Variability in sea surface temperature around New Zealand from AVHRR images. *N. Z. J. Mar. Freshwater Res.*, **28**,179-192, 1994.

Chiswell, S.M., Temperature and salinity mean and variability within the Subtropical Front over the Chatham Rise, New Zealand. *N. Z. J. Mar. Freshwater Res.*, **36**,281-298, 2002.

Cléroux, C., E. Cortijo, J.-C. Duplessy, and R. Zahn, Deep-dwelling foraminifera as thermocline temperature recorders, *Geochem. Geophys. Geosyst.*, **8**, doi:10.1029/2006GC001474, 2007.

Conkright, M.E., R. A. Locarnini, H.E. Garcia, T.D. O'Brien, T.P. Boyer, C. Stephens, J.I. Antonov, World Ocean Atlas 2001: Objective Analyses, Data Statistics, and Figures, CD-ROM Documentation. National Oceanographic Data Center, Silver Spring, MD, 17 pp., 2002.

Cullen, J.T., T.W. Lane, F.M.M. Morel & R.M. Sherrell, Modulation of cadmium uptake in phytoplankton by seawater CO_2 concentration. *Nature,* **402**, 165-167, 1999.

de Baar, H.J.W., P.M. Saager, R.F. Nolting & J. van der Meer, Cadmium versus phosphate in the world ocean, *Mar. Chem.* **46,** 261-281, 1994.

de Lange, G. J., B. Vanos & R. Poorter, Geochemical composition and inferred accretion rates of sediments and manganese nodules from a submarine hill in the Madeira Abyssal Plain, Eastern North Atlantic, *Mar. Geol.*, **109**, 171–194, 1992.

de Villiers, S., G.T. Shen & B.K. Nelson, The Sr/Ca temperature relationship in coralline aragonite: Influence of variability in (Sr/Ca) seawater and skeletal growth parameters. *Geochimica et Cosmochimica Acta*, **58**, 197-208,1994.

de Villiers, S., B.K. Nelson, & A.R. Chivas, Biological controls on coral Sr/Ca and $\delta^{18}O$ reconstructions of sea surface temperatures. *Science*, **269**, 1247-1249, 1995.

de Villiers, S., M. Greaves & H. Elderfield, An intensity ratio method for the accurate determination of Mg/Ca and Sr/Ca of marine carbonates by ICP-AES, *Geochem. Geophys. Geosyst.* **3**, 2001GC000169, 2002.

Deer, W.A., R.A. Howie & J. Zussman, *An introduction to the rock forming minerals,* 2nd Edn., Longman Scientific & Technical, Harlow, England, 1992.

Dekens, P. S., D. W. Lea, D. K. Pak, & H. J. Spero, Core top calibration of Mg/Ca in tropical foraminifera: refining paleo-temperature estimation, *Geochemistry, Geophysics, Geosystems,* **3**, 2001GC000200, 2002.

Delaney, M.L., Uptake of cadmium into calcite shells by planktonic foraminifera. *Chem. Geol.*, **78**, 159-165, 1989.

Elderfield, H. & G. Ganssen, Past temperature and $\delta^{18}O$ of surface ocean waters inferred from foraminiferal Mg/Ca ratios, *Nature* **405**, 442-445, 2000.

Elderfield, H. & R.E.M. Rickaby, Oceanic Cd/P ratio and nutrient utilization in the glacial Southern Ocean, *Nature* **405**, 305-310, 2000.

Elderfield, H., C.J. Bertram and J. Erez, A biomineralization model for the incorporation of trace elements in foraminiferal calcium carbonate. *Earth Planet .Sci. Lett.* **142**, 409-423, 1996.

Elderfield, H., M. Cooper & G. Ganssen, Sr/Ca in multiple species of planktonic foraminifera: Implications for reconstructions of seawater Sr/Ca, *Geochem. Geophys. Geosyst.* **1**, 1999GC000031, 2000.

Elderfield, H., M. Vautravers & M. Cooper. The relationship between shell size and Mg/Ca, Sr/Ca, $\delta^{18}O$ and $\delta^{13}C$ of species of planktonic foraminifera. *Geochem. Geophys. Geosyst.* **3**, 2001GC000194, 2002.

Elderfield, H., J. Yu, P. Anand, T. Kiefer & B. Nyland, Calibrations for benthic foraminiferal Mg/Ca paleothermometry and the carbonate ion hypothesis, *Earth Planet. Sci. Lett.* **250**, 633-649, 2006.

Emiliani, C., Pleistocene temperatures, *J. Geol.* **63,** 538-578, 1955.

Farmer, E. C., A. Kaplan, P. B. de Menocal & J. Lynch-Stieglitz, Corroborating ecological depth preferences of planktonic foraminifera in the tropical Atlantic with the stable oxygen isotope ratios of core top specimens, *Paleoceanography*, **22**, PA3205, doi:10.1029/2006PA001361, 2007.

Faure, G., *Principles of isotope geology*. 2nd edition, Wiley, 1986.

Fenner, J., & A. Di Stefano, Late Quaternary oceanic fronts on Chatham Rise indicated by phytoplankton assemblages, and refined calcareous nannofossil stratigraphy for the mid-latitude S.W. Pacific. *Mar. Geol.* **205**, 59-86, 2004.

Fenner, J., L. Carter & R. Stewart, Late Quaternary paleoclimatic and paleoceanographic change over northern Chatham Rise, New Zealand. *Mar. Geol.* **108**, 383-404, 1992.

Ganssen, G.M. & D. Kroon, The isotopic signature of planktonic foraminifera from NE Atlantic surface sediments: implications for the reconstruction of past oceanic conditions, *Journal of the Geological Society*, **157**, 693-699, 2000.

Garcia, H. E., R. A. Locarnini, T. P. Boyer, & J. I. Antonov. *World Ocean Atlas 2005*, Volume 4: Nutrients (phosphate, nitrate, silicate). S. Levitus, Ed. NOAA Atlas NESDIS 64, U.S. Government Printing Office, Washington, D.C., 396 pp., 2006.

Gerstenberger H, & G. Haase, A highly effective emitter substance for mass spectrometric Pb isotope ratio determinations. *Chem. Geol.* **136**, 309-312, 1997.

Graham, D.W., M.L. Bender, D.F. Williams & L.D. Keigwin, Strontium-calcium ratios in Cenozoic planktonic foraminifera, *Geochim. Cosmochim. Acta*. **46**, 1281-1292, 1982.

Greaves, M., S. Barker, C. Daunt & H. Elderfield, Accuracy, standardisation and interlaboratory calibration standards for foraminiferal Mg/Ca thermometry, *Geochem. Geophys. Geosyst.,* **6 ,** Q02D13, doi:10.1029/2004GC000790, 2005.

Greaves, M.J., H. Elderfield, & G.P. Klinkhammer, Determination of the rare-earth elements in natural waters by isotope-dilution mass spectrometry. *Analyt. Chim. Acta,* **218**, 265-280, 1989.

Green D. R. H., M. J. Cooper, C. R. German, P. A. Wilson, Optimization of an inductively coupled plasma–optical emission spectrometry method for the rapid determination of high-precision Mg/Ca and Sr/Ca in foraminiferal calcite, *Geochem. Geophys. Geosyst.*, **4** (6), 8404, doi:10.1029/2002GC000488, 2003.

Hall, I.R., I.N. McCave, N.J. Shackleton, G.P. Weedon, & S.E Harris, Intensified deep Pacific inflow and ventilation in Pleistocene glacial times. *Nature*, **412**, 809-812, 2001.

Harding, D. J., J. W. Arden & R. E. M. Rickaby, A method for precise analysis of trace element/calcium ratios in carbonate samples using quadrupole inductively coupled plasma mass spectrometry, *Geochem. Geophys. Geosyst.*, **7**, Q06003, doi:10.1029/2005GC001093, 2006.

Hastings, D. W., A. D. Russell, & S. R. Emerson, Foraminiferal magnesium in *Globeriginoides sacculifer* as a paleotemperature proxy, *Paleoceanography,* **13**, 161-169, 1998.

Heath, R.A., Oceanic fronts around southern New Zealand. *Deep-Sea Res.* **28**, 547-560, 1981

Heath, R.A., A review of the physical oceanography of the seas around New Zealand-1982. *N. Z. J. Mar. Freshwater Res.*, **19**, 70-124, 1985.

Hemleben, C., M. Spindler & O. R. Anderson. *Modern Planktonic Foraminifera*, Springer, New York, 1989.

Henderson, G.M., New oceanic proxies for paleoclimate. *Earth Planet .Sci. Lett.* **203**, 1-13, 2002.

Henderson, G. M., D.J. Martel, R.K. O'Nions & N.J. Shackleton, Evolution of seawater $^{87}Sr/^{86}Sr$ over the last 400 ka: the absence of glacial/interglacial cycles. *Earth Planet. Sci. Lett.,* **128**, 643-651, 1994.

Hess, J., M.L. Bender & J.-G. Schilling, Evolution of the ratio of strontium-87 to strontium-86 in seawater from Cretaceous to Present, *Science,* **231**, 979-984, 1986.

Hodell, D. A., Progress and paradox in strontium isotope stratigraphy, *Paleoceanography,* **9**, 395-398, 1994.

Hodell, D. A., P.A. Mueller, J.A. McKenzie & G. A. Mead. Strontium isotope stratigraphy and geochemistry of the late Neogene ocean (9 to 2 Ma), *Earth Planet .Sci. Lett.* **92**, 165-178, 1989.

Hodell, D. A., G. A. Mead & P.A. Mueller, Variation in the strontium isotopic composition of seawater (8 Ma to present): Implications for chemical weathering rates and dissolved fluxes to the oceans. *Chem. Geol. (Isotope Geosci. Sect.)* **80**, 291-307, 1990.

Hodell, D. A., C.D. Charles & F.J. Sierro, Late Pleistocene evolution of the ocean's carbonate system. *Earth Planet .Sci. Lett.* 1**92**, 109-124, 2001.

Horwitz, W., Evaluation of Analytical Methods Used for Regulation of Foods and Drugs, *Analyt. Chem.* **54**, 67A-76A 1982.

Howard, W.R. & W.L. Prell, Late Quaternary surface circulation of the southern Indian Ocean and its relationship to orbital variations. *Paleoceanography*, **7**, 79-117, 1992.

Howard, W. R., and W. L. Prell , Late Quaternary $CaCO_3$ production and preservation in the Southern Ocean: Implications for oceanic and atmospheric carbon cycling, *Paleoceanography*, **9**, 453–482, 1994.

Huett T., J.C. Ingram, & J.E. Delmore, Ion-emitting molten glasses - Silica Gel revisited. *Intern. J. Mass-Spec. Ion Processes* **146**, 5-14, 1995.

International Union of Pure and Applied Chemistry (IUPAC), *Compendium of Analytical Nomenclature: Definitive Rules 1997,* 3rd edn., Blackwell Science, 1998. (http://www.iupac.org/publications/analytical_compendium/)

Kim, S.T. & O'Neil, J.R., Equilibrium and nonequilibrium oxygen isotope effects in synthetic carbonates. *Geochim. Cosmochim. Acta* **61**, 3461-3475, 1997.

King, A.L. & W.R. Howard, Seasonality of foraminiferal flux in sediment traps at Chatham Rise, SW Pacific: implications for paleotemperature estimates. *Deep-Sea Res.* **48**, 1687-1708, 2001.

Lane T.W., M.A. Saito, G.N. George, I.J. Pickering, R.C. Prince, F.M.M. Morel, A cadmium enzyme from a marine diatom, *Nature* **435**, 42, 2005.

Lea, D.W., Constraints on the alkalinity and circulation of glacial Circumpolar Deep Water from benthic foraminiferal barium. *Global Biogeochem, Cycles,* **7,** 695-710, 1993.

Lea, D.W., A trace metal perspective on the evolution of Antarctic Circumpolar Deep Water chemistry, *Paleoceanography*, **10**, 733-747, 1995.

Lea, D.W., Trace elements in foraminiferal calcite. In *Modern Foraminifera* edited by Barun K. Sen Gupta, pp 259-277, Kluwer, 1999.

Lea, D.W., & E.A. Boyle, Barium content of benthic foraminifera controlled by bottom-water composition. *Nature,* **338**, 751-753, 1989.

Lea, D.W., & E.A. Boyle, A 210,000 year record of barium variability in the deep northwest Atlantic Ocean. *Nature,* **347**, 269-272, 1990.

Lea, D.W., & E.A. Boyle, Barium in planktonic foraminifera, *Geochim. Cosmochim. Acta*. **55**, 3321-3331, 1991.

Lea D.W. & P.A. Martin, A rapid mass-spectrometric method for the silmultaneous analysis of barium, cadmium, and strontium in foraminiferal shells. *Geochim. Cosmochim. Acta* **60**, 3143-3149, 1996.

Lea, D.W., T.A. Mashiotta & H.J. Spero, Controls on magnesium and strontium uptake in planktonic foraminifera determined by live culturing, *Geochim. Cosmochim. Acta*. **63**, 2369-2379, 1999.

Lea, D.W., D.K. Pak & H.J. Spero, Climate impact of Late Quaternary equatorial Pacific sea surface temperature variations, *Science*, **289**, 1719-1724, 2000.

Lea, D.W., P.A. Martin, D.K. Pak & H.J. Spero, Reconstructing a 350 ky history of sea level using planktonic Mg/Ca and oxygen isotope records from a Cocos Ridge core, *Quaternary Science Reviews* **21**, 283–293, 2002.

Lea D. W., D. K. Pak, & G. Paradis, Influence of volcanic shards on foraminiferal Mg/Ca in a core from the Galápagos region, *Geochem. Geophys. Geosyst.*, **6**, Q11P04, doi:10.1029/2005GC000970, 2005.

Lean, C.M.B. & I.N. McCave, Glacial to interglacial mineral magnetic and palaeoceanographic changes at Chatham Rise, SW Pacific Ocean, *Earth Planet Sci. Lett.* **163**, 247-260, 1998.

Lear, C.H., H. Elderfield & P.A. Wilson, Cenozoic deep sea temperatures and global ice volumes, *Science*, **287**, 269-272, 2000.

Lear, C. H., Y. Rosenthal & N. Slowey, Benthic foraminiferal Mg/Ca-paleothermometry: A revised core-top calibration. *Geochim. Cosmochim. Acta*. **66**, 3375-3387, 2002.

Lear, C.H., H. Elderfield & P.A. Wilson, A Cenozoic seawater Sr/Ca record from benthic foraminiferal calcite and its application in determining global weathering fluxes, *Earth Planet Sci. Lett.* **208**, 69-84, 2003.

LeGrande A.N. & G.A. Schmidt, Global gridded data set of the oxygen isotopic composition in seawater, *Geophys. Res. Lett.*, **33**, L12604, doi:10.1029/2006GL026011, 2006.

Locarnini, R. A., A.V. Mishonov, J. I. Antonov, T. P. Boyer & H. E. Garcia. *World Ocean Atlas 2005*, Volume 1: Temperature. S. Levitus, Ed. NOAA Atlas NESDIS 61, U.S. Government Printing Office, Washington, D.C., 182 pp., 2006.

Lohmann, G.P. A model for variation in the chemistry of planktonic foraminifera due to secondary calcification and selective dissolution. *Paleoceanography*, **10**, 445-457, 1995.

Loss R.D., K.J.R. Rosman & J.R. Delaeter, The isotopic composition of zinc, palladium, silver, cadmium, tin, and tellurium in acid-etched residues of the Allende Meteorite. *Geochim. Cosmochim. Acta* **54**, 3525-3536, 1990.

Lukes, I., M. Borbaruah, & L.D. Quin, Direct reaction of phosphorus-acids with hydroxy of a silanol and on the silica-gel surface. *J. Amer. Chem. Soc.* **116**, 1737-1741, 1994.

Marchitto, T. M., Lack of a significant temperature influence on the incorporation of Cd into benthic foraminiferal tests, *Geochem. Geophys. Geosyst.*, **5**, Q10D11, doi:10.1029/2004GC000753, 2004.

Marchitto, T. M., Precise multielemental ratios in small foraminiferal samples determined by sector field ICP-MS, *Geochem. Geophys. Geosyst.*, **7**, Q05P13, doi:10.1029/2005GC001018, 2006.

Marchitto, T. M. & W. S. Broecker, Deep water mass geometry in the glacial Atlantic Ocean: A review of constraints from the paleonutrient proxy Cd/Ca, *Geochem. Geophys. Geosyst.*, **7**, Q12003, doi:10.1029/2006GC001323, 2006.

Marchitto, T. M., W. B. Curry, and D. W. Oppo, Millennial-scale changes in North Atlantic circulation since the last glaciation, *Nature*, **393**, 557-561, 1998.

Marchitto, T.M., W.B. Curry, & D.W. Oppo, Zinc concentrations in benthic foraminifera reflect seawater chemistry, *Paleoceanography*, **15**, 299-306, 2000.

Marchitto, T. M., Jr., D. W. Oppo, and W. B. Curry, Paired benthic foraminiferal Cd/Ca and Zn/Ca evidence for a greatly increased presence of Southern Ocean Water in the glacial North Atlantic, *Paleoceanography*, **17**(3), 1038, doi:10.1029/2000PA000598, 2002.

Martin, P. A. & D. W. Lea, A simple evaluation of cleaning procedures on fossil benthic foraminiferal Mg/Ca, *Geochem. Geophys. Geosyst.* ,**3**(10), 8401, doi:10.1029/2001GC000280, 2002.

Martin, P.A., D.W. Lea, T.A. Mashiotta, T. Papenfuss & M. Sarnthein, Variation of foraminiferal Sr/Ca over Quaternary glacial-interglacial cycles: Evidence for changes in mean ocean Sr/Ca?, *Geochem. Geophys. Geosyst.*, **1**, 1999GC000006, 1999.

Martin, P.A., D.W. Lea, Y. Rosenthal, N.J. Shackleton, M. Sarnthein & T. Papenfuss, Quaternary deep sea temperature histories derived from benthic foraminiferal Mg/Ca, *Earth Planet Sci. Lett.* **198**, 193-209, 2002.

Mashiotta, T.A., D.W. Lea & H.J. Spero, Experimental determination of cadmium uptake in shells of the planktonic foraminifera *Orbulina universa* and *Globigerina bulloides*: Implications for surface water paleoreconstructions. *Geochim. Cosmochim. Acta* **61**, 4053-4065, 1997.

Mashiotta, T.A., D.W. Lea & H.J. Spero, Glacial-interglacial changes in Subantarctic sea surface temperature and δ^{18}O-water using foraminiferal Mg, *Earth Planet Sci. Lett.* **170**, 417-432, 1999.

Matsumoto A. & T.K. Hinkley, Determination of lead, cadmium, indium, thallium, and silver in ancient ices from Antarctica by isotope dilution thermal ionization mass-spectrometry. *Geochemical Journal* **31**, 175-181, 1997.

Masuda, T., H. Makio & A. Miyashita. Olefin polymerisation by Ziegler-Natta catalysts. In. *Catalysis in Precision Polymerisation*. (S. Kobayashi. Ed.) J. Wiley & Sons, Chichester, England, 18-54, 1997.

McConnell, M.C. & R.C. Thunell, Calibration of the planktonic foraminiferal Mg/Ca paleothermometer: Sediment trap results from the Guaymas Basin, Gulf of California, *Paleoceanography*, **20**, PA2016, doi: 10.1029/2004PA001077, 2005.

McCorkle, D. C., P. A. Martin, D. W. Lea & G. P. Klinkhammer, Evidence of a dissolution effect on benthic foraminiferal shell chemistry: δ^{13}C, Cd/Ca, Ba/Ca, and Sr/Ca results from the Ontong Java Plateau, *Paleoceanography*, **10**, 699-714, 1995.

McCulloch M.T, M. Gagan, G.E. Mortimer, A.R. Chivas & P.J. Isdale. A high resolution Sr/Ca and δ^{18}O coral record from the Great Barrier Reef, Austraila, and the 1982-1983 El Nino. *Geochim. Cosmochim. Acta*, **58**, 2747-2754, 1994.

Mermet, J. M., Use of magnesium as a test element for inductively coupled plasma atomic emission spectrometry diagnostics, *Anal. Chim. Acta*, **250**, 85–94, 1991.

Miller, JC and Miller JN, *Statistics for analytical chemistry*, Ellis Horwood, London,3rd ed., 233pp., 1993.

Mitsuguchi, T., E. Matsumoto, O. Abe, T. Uchida & P.J. Isdale. Mg/Ca thermometry in coral skeletons. *Science*, **274**, 961-963, 1996.

Moody, J.R. & R. Lindstrom, Selection and Cleaning of Plastic Containers for Storage of Trace Element Samples. *Analyt. Chem.* **49**, 2264-2267, 1977.

Moody J.R., R.R. Greenberg, K.W. Pratt and T.C. Rains, Recommended Inorganic Chemicals for Calibration. *Analyt. Chem.*, **60**, 1203A - 1218A, 1988.

Mortyn, P.G. & C.D. Charles, Planktonic foraminiferal depth habitat and $\delta^{18}O$ calibrations: Plankton tow results from the Atlantic sector of the Southern Ocean, *Paleoceanography*, **18**, 1037, doi:10.1029/2001PA000637, 2003.

Mortyn, P.G., C.D. Charles & D.A. Hodell, Southern Ocean upper water column structure over the last 140 kyr with emphasis on the glacial terminations, *Global Planet. Change,* **34**, 241-252, 2002.

Mortyn, P.G., H.Elderfield, P. Anand & M.J. Greaves, An evaluation of controls on planktonic foraminiferal Sr/Ca: comparison of water column and core top data from a North Atlantic transect, *Geochem. Geophys. Geosyst.*, **6**, 2005GC001047, 2005.

Mucci, A., Influence of temperature on the composition of magnesian calcite overgrowths precipitated from seawater. *Geochim. Cosmochim. Acta*, **51**, 1977-1984, 1987.

Mulhaupt, R. Ziegler-Natta catalysts and propylene polymerization. In. *Polypropylene : an A-Z reference* (J.Karger-Kocsis Ed.), Dordrecht ; London : Kluwer, 896-920, 1999.

Mulitza, S., A. Dürkoop, W. Hale & G. Wefer, Planktonic foraminifera as recorders of past surface-water stratification. *Geology,* **25**, 335-338, 1997.

Mulitza, S., D. Boltovskoy, B. Donner, H. Meggers, A. Paul & G. Wefer, Temperature:$\delta^{18}O$ relationships of planktonic foraminifera collected from surface waters, *Palaeogeography, Palaeoclimatology, Palaeoecology,* **202**,143-152, 2003.

Nelson, C.S., P.J. Cooke, C.H., Hendy & A.M. Cuthbertson. Oceanographic and climatic changes over the past 160,000 years at Deep Sea Drilling Project Site 594 off southeastern New Zealand, southwest Pacific Ocean. *Paleoceanography*, **8**, 435-458, 1993.

Nürnberg, D. & J. Groeneveld, Pleistocene variability of the Subtropical Convergence at East Tasman Plateau: Evidence from planktonic foraminiferal Mg/Ca (ODP Site1172A), *Geochem. Geophys. Geosyst.*, **7**, Q04P11, doi:10.1029/2005GC000984, 2006.

Nurnberg, D., J. Bijma, & C. Hemleben, Assessing the reliability of magnesium in foraminiferal calcite as a proxy for water mass temperatures, *Geochim. Cosmochim. Acta*, **60**, 803-814, 1996.

Ohde, S., M. Greaves, T. Masuzawa, H.A. Buckley, R. Van Woesik, P.A. Wilson, P.A. Pirazzoli & H. Elderfield, The chronology of Funafuti Atoll: revisiting an old friend. *Proc. R. Soc. Lond. A*, **458**, 2289–2306, 2002.

O'Neil, J.R., R.N. Clayton & T.K. Mayeda, Oxygen isotope fractionation in divalent metal carbonates. *J. Chem. Phys.* **51**, 5547-5558, 1969.

Oomori, T., H. Kaneshima & Y. Maezato. Distribution coefficient of Mg^{2+} ions between calcite and solution at 10-50ºC. *Mar. Chem.* **20,** 327-336, 1987.

Ottens, J.J., Planktic foraminifera as North Atlantic water mass indicators. *Oceanologica Acta* **14**, 123-140, 1991.

Pahnke, K., R. Zahn, H. Elderfield & M. Schultz. 340,000-Year Centennial-Scale Marine Record of Southern Hemisphere Climatic Oscillation. *Science* **301**, 948-952, 2003.

Palmer, M.R. & H. Elderfield, Sr isotope composition of seawater over the past 75 Myr., *Nature,* **314**, 526-528, 1985.

Palmer, M.R. & P.N. Pearson, A 23,000-year record of surface water pH and PCO_2 in the western equatorial Pacific Ocean, *Science*, **300**, 480-482, 2003.

Pattan, J. N., Manganese micronodules: A possible indicator of sedimentary environments, *Mar. Geol.*,**113**, 331–344, 1993.

Pederson, T. F., and N. B. Price, The geochemistry of manganese carbonate in Panama Basin sediments, *Geochim. Cosmochim. Acta*,**46**, 59–68, 1982.

Radlein N. & K.G. Heumann, Size-fractionated impactor sampling of aerosol-particles over the Atlantic-Ocean from Europe to Antartica as a methodology for source identification of Cd, Pb, Tl, Ni, Cr, and Fe. *Fresenius J. Anal. Chem.* **352**, 748-755, 1995.

Ramsey, M. H. & B.J. Coles, Strategies of multielement calibration for maximising the accuracy of geochemical analysis by inductively coupled plasma-atomic emission spectrometry, In *Plasma Spectrometry in theEarth Sciences:* (I.Jarvis & K. E. Jarvis Eds.) *Chem. Geol.,* **95**, 99-112,1992.

Ramsey, M. H., M. Thompson & S. J. Walton, Self-matrix effects as a cause of calibration curvature in inductively coupled plasma atomic emission spectrometry, *J. Anal. Spectrom.*, **2**, 33-38, 1987.

Rathburn, A.E. & P. de Deckker, Magnesium and strontium compositions of Recent benthic foraminifera from the Coral Sea, Australia and Prydz Bay, Antarctica. *Mar. Micropaleontol.*, **32,** 23 l-248, 1997.

Regenberg, M., D. Nürnberg, S. Steph, J. Groeneveld, D. Garbe-Schönberg, R. Tiedemann & W. Dullo. Assessing the effect of dissolution on planktonic foraminiferal Mg/Ca ratios: Evidence from Caribbean core tops, *Geochem. Geophys. Geosyst.*, **7**, Q07P15, 10.1029/2005GC001019, 2006.

Rickaby, R.E.M. & H.Elderfield, Planktonic foraminiferal Cd/Ca: Paleonutrients or paleotemperature?, *Paleoceanography* **14**, 293-323, 1999.

Rickaby, R.E.M., M.J, Greaves, & H.Elderfield, Cd in planktonic and benthic foraminiferal shells determined by thermal ionisation mass spectrometry. *Geochim. Cosmochim. Acta* **64**, 1229-1236, 2000.

Riley, J.P. & R. Chester, *Introduction to Marine Chemistry,* Academic Press, London, 1971.

Ripperger, S & M. Rehkämper, A highly sensitive MC-ICPMS method for Cd/Ca analyses of foraminiferal tests. *J. Anal. At. Spectrom.*, **22**, 1275–1283, 2007.

Roemmich, D. & P. Sutton, The mean and variability of ocean circulation past northern New Zealand: Determining the representativeness of hydrographic climatologies, *J. Geophys. Res.,* **103**(C6), 13,041–13,054, 1998.

Rohling, E.J., Paleosalinity: confidence limits and future applications, *Mar. Geol.* **163**, 1-11, 2000.

Rosenthal, Y. & G.P. Lohmann. Accurate estimation of sea surface temperatures using dissolution-corrected calibrations for Mg/Ca paleothermometry. *Palaeoceanography* **17**, 1044, 2001PA000749, 2002.

Rosenthal Y., E.A.Boyle & L. Labeyrie, Last glacial maximum palaeochemistry and deepwater circulation in the Southern Ocean: Evidence from foraminiferal cadmium. *Palaeoceanography* **12**, 787-797, 1997a.

Rosenthal, Y., E.A. Boyle & N. Slowey, Temperature control on the incorporation of magnesium, strontium, fluorine and cadmium into benthic foraminiferal shells from Little Bahama Bank: Prospects for thermocline paleoceanography, *Geochim. Cosmochim. Acta.* **61**, 3633-3643, 1997b.

Rosenthal Y., R.M. Sherrell & M.P. Field, A novel method for precise determination of element : calcium ratios in calcareous samples using sector field inductively coupled plasma mass spectrometry. *Analyt. Chem.* **71,** 3248-3253, 1999.

Rosenthal, Y., G.P. Lohmann, K. C. Lohmann, & R.M. Sherrell, Incorporation and preservation of Mg in *Globigerinoides sacculifer*: Implications for reconstructing the temperature and $^{18}O/^{16}O$ of seawater, *Palaeoceanography* **15**, 134-135, 2000.

Rosenthal, Y., S. Perron-Cashman, C.H., Lear, E. Bard, S. Barker, K. Billups, M. Bryan, M.L. Delaney, P.D. deMenocal, G.S. Dwyer, H. Elderfield, C.R. German, M. Greaves, D.W. Lea, T.M., Marchitto Jr., D.K. Pak, G.L., Paradis, A.D. Russell, R.R. Schneider, K. Scheiderich, L. Stott, K. Tachikawa, E. Tappa, R. Thunell, M. Wara, S. Weldeab, P.A. Wilson, Interlaboratory comparison study of Mg/Ca and Sr/Ca measurements in planktonic foraminifera for paleoceanographic research. *Geochem. Geophys. Geosyst.,* **5**(4), 10.1029/2003GC000650, 2004.

Rubin, S.I., L.S. King, R.A. Jahnke & P.N. Froelich, Benthic barium and alkalinity fluxes: Is Ba an oceanic paleo-alkalinity proxy for glacial atmospheric CO_2? *Geophys. Res. Lett.,* **30,** 2003GL017339, 2003.

Russell, A.D., S.R. Emerson, B. K. Nelson, J. Erez & D.W. Lea, Uranium in foraminiferal calcite as a recorder of seawater uranium concentrations, *Geochim. Cosmochim. Acta,* **58**, 671-681, 1994.

Russell, A.D., S. Emerson, A.C. Mix & L.C. Peterson, The use of foraminiferal uranium/calcium ratios as an indicator of changes in seawater uranium content, *Palaeoceanography* **11**, 649-663, 1996.

Sautter, L.R. & R.C. Thunell, Seasonal variability in the $\delta^{18}O$ and $\delta^{13}C$ of planktonic foraminifera from an upwelling environment: sediment trap results from the San Pedro Basin, Southern California Bight, *Paleoceanography,* **6**, 307-334, 1991.

Schaefer, G., J. S. Rodger, B. W. Hayward, J. P. Kennett, A. T. Sabaa, and G. H. Scott, Planktic foraminiferal and sea surface temperature record during the last 1 myr across the Subtropical Front, southwest Pacific, *Mar. Micropaleontol.*, **54**(3–4), 191–212, 2005.

Schmidt, G. A., Error analysis of paleosalinity calculations, *Paleoceanography*, **14**(3), 422–429, 1999.

Schmidt, G.A., G.R. Bigg & E. J. Rohling, Global seawater oxygen-18 database http://www.giss.gov/data/o18data/ 1999.

Schrag, D.P., Rapid analysis of high-precision Sr/Ca ratios in corals and other marine carbonates, *Paleoceanography*,**14**, 97–102, 1999.

Scott, G.H., & I. Hall, Planktonic foraminiferal evidence on late Pliocene-Quaternary surface water masses at ODP Site 1123B, northern Chatham Rise, east of New Zealand. *Mar. Geol.* **205**, 127-145, 2004.

Shackleton, N.J., Attainment of isotopic equilibrium between ocean water and the benthonic foraminifera genus *Uvigerina* : isotopic changes in the ocean during the last glacial. *Cent. Nat. Rech. Sci. Colloq. Int.* **219**, 203–209, 1974.

Shackleton, N.J., The 100,000 year ice-age cycle identified and found to lag temperature, carbon dioxide, and orbital eccentricity, *Science*, **289**, 1897-1902, 2000.

Shackleton, N.J., M.A. Hall & E. Vincent, Phase relationships between millennial-scale events 64,000-24,000 years ago. *Paleoceanography* **15** , 565, 2000.

Shen, C., T. Lee, C. Chen, C. Wang, C. Dai, & A. Li, The calibration of D[Sr/Ca] versus sea surface temperature relationship for Porites coral. *Geochim. Cosmochim. Acta,* **60**, 3849–3858, 1996.

Shen, C., D.W. Hastings, T. Lee, C. Chiu, M. Lee, K. Wei & R.L. Edwards, High precision glacial-interglacial benthic foraminiferal Sr/Ca records from the eastern equatorial Atlantic Ocean and Caribbean Sea, *Earth Planet Sci. Lett.* **190**, 197-209, 2001.

Sikes, E. L., W.R. Howard, H.L. Neil & J.K. Volkman, Glacial-interglacial sea surface temperature changes across the subtropical front east of New Zealand based on alkenone unsaturation ratios and foraminiferal assemblages. *Paleoceanography,* **17**, 1029/2001PA000640, 2002.

Skinner, L. C., N.J. Shackleton & H. Elderfield. Millennial-scale variability of deep-water temperature and $\delta^{18}O_{dw}$ indicating deep-water source variations in the Northeast Atlantic, 0–34 cal. ka BP. *Geochem. Geophys. Geosyst.,* **4**, 1098, 2003GC000585, 2003

Spero, H.J. & D.W. Lea, Experimental determination of stable isotope variability in Globigerina bulloides : Implications for paleoceanographic reconstructions. *Mar. Micropaleontol.* **28**, 231-246,1996.

Spero, H. J., J. Bijma, D.W, Lea & B.E. Bemis, Effect of seawater carbonate concentration on foraminiferal carbon and oxygen isotopes, *Nature*, **390**, 497-500, 1997.

Stoll, H. M., D. P. Schrag, and S. C. Clemens, Are seawater Sr/Ca variations preserved in Quaternary foraminifera? *Geochimica Cosmochimica Acta,* **63**, 3535-3547, 1999.

Strelow F.W.E, An ion exchange selectivity scale of cations based on equilibrium distribution coefficients. *Analyt. Chem.* **32**, 1185-1188 1960.

Sutton, P., Detailed structure of the Subtropical Front over Chatham Rise, east of New Zealand, *J. Geophys. Res.*, **106**, 31,045–31,056, 2001.

Swart P.K., H. Elderfield & M.J. Greaves, A high-resolution calibration of Sr/Ca thermometry using the Caribbean coral Montastraea annularis. *Geochem. Geophys. Geosyst.,* **3**, 2002GC000306, 2002.

Tachikawa, K. & H. Elderfield, Microhabitat effects on Cd/Ca and $\delta^{13}C$ of benthic foraminifera. *Earth Planet Sci. Lett.* **202**, 607-624, 2002.

Walsh, J.N., Use of multiple internal standards for high-precision, routine analysis of geological samples by inductively coupled plasma-atomic emission spectrometry, In *Plasma Spectrometry in the Earth Sciences:* (I.Jarvis & K. E. Jarvis Eds.) *Chem. Geol.,* **95**,113-121,1992.

Wara, M. W., L. D. Anderson, S. A. Schellenberg, R. Franks, A.C. Ravelo & M.L. Delaney. Application of a radially viewed inductively coupled plasma-optical emission spectrophotometer to simultaneous measurement of Mg/Ca, Sr/Ca, and Mn/Ca ratios in marine biogenic carbonates, *Geochem. Geophys. Geosyst.,* **4**, 8406, 2003GC000525, 2003.

Weaver, P.P.E., H. Neil & L. Carter, Sea surface temperature estimates from the southwest Pacific based on planktonic foraminifera and oxygen isotopes. *Palaeogeogr., Palaeoclimatol., Palaeoecol.*, **131,** 241-256, 1997.

Weaver, P.P.E., L. Carter & H.L. Neil, Response of surface water masses and circulation to late Quaternary climate change east of New Zealand. *Paleoceanography*, **13**, 70-83, 1998.

Weedon, G.P., & I.R. Hall, Neogene palaeoceanography of Chatham Rise (Southwest Pacific) based on sediment geochemistry. *Mar. Geol.* **205**, 207-225, 2004.

Wilson, K, B.W. Hayward, A.T. Sabaa, G.H. Scott & J.P. Kennett, A one-million-year history of a north-south segment of the Subtropical Front, east of New Zealand. *Paleoceanography*, **20**, PA2004, 10.1029/2004PA001080, 2005.

Yeats, P.A., An isopycnal analysis of cadmium distributions in the Atlantic Ocean. *Mar. Chem.* **61,** 15-23, 1998.

Yu, J. & H. Elderfield, Benthic foraminiferal B/Ca ratios reflect deep water carbonate saturation state, *Earth Planet Sci. Lett.* **258**, 73-86, 2007.

Yu, J., J. Day, M. Greaves & H. Elderfield, Determination of multiple element/calcium ratios in foraminiferal calcite by quadrupole ICP-MS, *Geochem. Geophys. Geosyst.*, **6**, Q08P01, doi:10.1029/2005GC000964, 2005.

Yu, J., H. Elderfield, M. Greaves & J. Day, Preferential dissolution of benthic foraminiferal calcite during laboratory reductive cleaning. *Geochem. Geophys. Geosyst.*, **8**, 10.1029/2006GC001571, 2007.

Yu, J., H. Elderfield & B. Hönisch, B/Ca in planktonic foraminifera as a proxy for surface seawater pH. *Paleoceanography* **22**, PA2202, doi:10.1029/2006PA001347, 2007.